UNIVERSITEIT VAN PRETORIA
UNIVERSITY OF PRETORIA
YUNIBESITHI YA PRETORIA

Seasonality and mineral, chemical and optical properties of dust storms in the Sistan region of Iran, and their influence on human health

by

Alireza Rashki

Submitted in partial fulfillment of the requirements

for the degree

DOCTOR OF PHILOSOPHY

in the

Faculty of Natural and Agricultural Sciences

University of Pretoria

June 2012

DECLARATION:

I declare that the thesis that I hereby submit for the PhD degree in Geoinformatics at the University of Pretoria has not previously been submitted by me for degree purposed at any other university.

SIGNATURE……DATE…….

Seasonality and mineral, chemical and optical properties of dust storms in the Sistan region of Iran, and their influence on human health

Alireza Rashki

Supervisor: Prof. Hannes Rautenbach

Co-Supervisors: Prof. Patrick Eriksson

Dr. Dimitris Kaskaoutis

Department: Department of Geography, Geoinformatics and Meteorology

Faculty: Faculty of Natural and Agricultural Science

University: University of Pretoria

Degree: Doctor of Philosophy

Summary:

Atmospheric aerosols are suspensions of solid and/or liquid particles in the air from natural and anthropogenic sources. Aerosols are ubiquitous in the air and are often observable as dust, smoke and haze. Dust is considered to be one of the major components of tropospheric aerosols over the globe. Natural and human processes contribute to aerosol emissions. Each year, several billion tons of soil-dust is entrained into the atmosphere playing a vital role in solar irradiance attenuation, and affects marine environments, atmospheric dynamics and weather. Air pollution has recently become a serious environmental problem. Over recent years in the public health domain particulate matter (PM) concentration has become a topic of considerable importance, since epidemiological studies have shown that exposure to particulates with aerodynamic diameters of < 10 µm (PM_{10}) and especially < 2.5 µm ($PM_{2.5}$) induces an increase of lung cancer, morbidity and cardiopulmonary mortality.

Mineral dust plays an important role in the optical, physical and chemical processes in the atmosphere, while dust deposition adds exogenous mineral and organic material to terrestrial surfaces, having a significant impact on the Earth's ecosystems and biogeochemical cycles.

The role of dust aerosols in atmospheric processes, i.e. Earth's radiation balance, cloud microphysics, etc, strongly depends on a variety of physico-chemical parameters, size distribution, dust sources, atmospheric lifetime and mixing processes in the atmosphere.

Analysis of the physical properties and chemical composition of dust aerosols is important to determine aerosol sources, mixing processes, transport pathways and their effects on human health.

Atmospheric aerosols affect the global climatic system in many ways, i.e. by attenuating the solar radiation reaching the ground, modifying the solar spectrum, re-distributing the earth-atmosphere energy budget and influencing cloud microphysics and the hydrological cycle. Satellite remote for sensing provides an important observational means for monitoring dust production and for improving the understanding of the effects of regional-scale atmospheric processes on dust emission and transport.

The Sistan region is located in southeastern Iran, close to the Iranian borders with Pakistan and Afghanistan. The climate is arid, with low annual average precipitation of ~55 mm occurring mainly in the winter (December to February) and evaporation exceeding ~4000 mm.year^{-1}. During summer (June – September), the area is under the influence of a low pressure system attributed to the Indian thermal low that extends further to the west as a consequence of the south Asian monsoon system. These low pressure conditions are the trigger for the development of the Levar northerly wind, commonly known as the "120-day wind", causing frequent dust and sand storms and contributing to the deterioration of air quality. Therefore, one of the main factors affecting the weather conditions over the region is the strong winds rendering Sistan as one of the windiest deserts in the world. Severe droughts during the past decades, especially after 1999, have caused desiccation of the Hamoun lakes which is located in the northern part of Sistan, leaving a fine layer of sediment that is easily lifted by the wind, thus modifying the basin to one of the most active sources of dust in southwest Asia. The strong winds blow fine sand off the exposed Hamoun lake beds and deposit it to form huge dunes that may cover a hundred or more villages along the former lakeshore. Hamoun dry lake beds are mainly composed of quaternary lacustrine silt and clay material as well as Holocene fluvial sand, silt and clay. These materials have been carried to the basin by the rivers, while along their courses neogene fluvial sand, eolian sand, silt and clay are the main constituents.

This thesis analyses the aerosol characteristics, dust loading and air quality over the Sistan region based on first time measurements conducted. The dust loading was measured using dust traps near the Hamoun basin during the period August 2009 to July 2010. Dust loading from the Hamoun basin appears to have a significant contributing influence on the

development of extreme dust storms, especially during the summer days. This influence firstly seems to depend on the intensity and duration of dust storms, and secondarily, on the distance from the source region, the wind speed and altitude. The grain-size distribution of the dust loading is strongly influenced by the distance from the dust source. Furthermore, the particle size distribution exhibited a shift towards lower values as the altitude increases, with this feature found to be more obvious amongst larger sized particles, while the frequency of particles below 2.5 μm seemed not to be affected by altitude. In general, the analysis revealed significant spatio-temporal variability of regional dust loading and characteristics. This finding necessitates more systematic observations at as many locations as possible around the Hamoun basin in order to improve the understanding of force dynamics, transport mechanisms as well as to quantify the dust amounts emitted from the Hamoun basin.

To assess air quality characteristics in two cities of Zabol and Zahedan affected by the Sistan dust storms , systematic airborne PM concentrations were measured during the period September 2010 to September 2011 and July 2008 to March 2010, respectively. The results showed that the PM_{10} concentrations were considerably higher than the corresponding European Union air quality annual standard and the mean $PM_{2.5}$ concentration (32 μgm^{-3}) also overcame the Air Quality Index (AQI) annual $PM_{2.5}$ standards. This poor air quality is affected by dust storms from the Sistan desert. The drainage of the Hamoun wetlands, in association with the intense Levar winds in summer, is the main factor responsible for the frequent and massive dust storms over the Sistan region. Hamoun, as an intense dust source region, caused a dramatic increase in PM_{10} concentrations and a deterioration of air quality (65% of the days were considered unhealthy for sensitive people and 34.9% as hazardous) in Zabol city. The maximum PM_{10} concentrations occurred between 8:00 to 11:00 Local Sidereal Time (LST) in Zabol and between 12:00 and 20:00 LST in Zahedan, indicating that Sistan dust storms reach Zahedan after six to nine hours. The strong correlation between daily $PM_{2.5}$ and PM_{10} concentrations indicated that they have similar sources and an increase of PM_{10} significantly affects $PM_{2.5}$. Considering the air pollution standards defined by the United state Environmental Protection Agency (USEPA), determining that only on one day per year may the AQI be higher than 100 $\mu g.m^{-3}$, it was found that the values of AQI in Zahedan overcame this level for 86 days out of 399, expressing a fraction of 21.5%. It should be noted that on 25 days (6.3%) the atmospheric conditions were very unhealthy or hazardous for the whole population and this requires more attention by officials, managers and urban planners.

Windblown transport and deposition of dust is widely recognized as an important physical and chemical concern to climate, human health and ecosystems. To mitigate the impact of these phenomena, this thesis examines for the first time, the mineralogical and chemical properties of dust over Sistan by collecting aerosol and soil samples. These data were analyzed to investigate the chemical and mineralogical characteristics of dust, relevance of inferred sources and contributions to air pollution. Dust aerosol characterization included chemical analysis of major and trace elements by X-Ray Fluorescence (XRF) and mineral analysis by X-Ray Diffraction (XRD). The results showed that quartz, calcite, muscovite, plagioclase and chlorite are the main mineralogical components of the dust, in descending order, over Sistan, and were present in all the selected airborne dust samples. In contrast, significantly lower percentages for enstatite, halite, dolomite, microcline, gypsum, diopside, orthoclase and hornblende were found, since these elements occurred only in some of the samples. On the other hand, silicone dioxide (SiO_2), Calcium oxide (CaO), Aluminum oxide (Al_2O_3), Sodium oxide (Na_2O), Magnesium Oxide (MgO) and Iron (III) Oxide (Fe_2O_3) were the major elements characterising the dust, while large amounts of Fluorine (F), Chlorine (Cl) and Sulfur (S) were also found as trace elements. The mineralogy and chemical composition of airborne dust at both stations were nearly the same and quite similar to the soil samples collected at several locations downwind. This suggests that the dust over Sistan is locally emitted, i.e. from the Hamoun basin, and in a few cases can also be long-range transported to distant regions. On the other hand, individual dust storms showed significant differences between either evaporite-dominated aerosols or those characterized by deflation from alluvial silts. These possibly reflect either localized climatic cyclicity or desiccation cycles. However, in some cases the soil samples showed poor comparisons with aerosol compositions, suggesting that dynamic sorting, soil-forming processes and climatic influences, such as rainfall, altered the mineralogy and chemistry in these partially eolian deposits. Estimates of Enrichment Factors (EF) for all studied elements show that all of them have very low EF values, suggesting natural origin from local materials. The results suggest that a common dust source region can be inferred, which is the eroded sedimentary environment in the extensive Hamoun dry lakes. Scanning Electronic Microscope (SEM) analyses of the samples indicated that airborne dust has rounded irregular, prismatic and rhombic shapes, with only the finer particles and a few cases of the coarser dust being spherical.

Tis thesis analyses the aerosol patterns over the arid environment of Sistan region by means of multiple satellite platforms aiming to reveal the spatio-temporal and vertical

distribution of dust aerosols. The dataset used includes records of Aerosol Index (AI) from the Total Ozone Mapping Spectrometer (TOMS) on board the Nimbus-7 (1979–92) and the Earth Probe (mid-1996 to 2001) satellites and six-year AI records from OMI aboard Aura. Moreover, the Aerosol Optical Depth (AOD) is analyzed through 11-year records from Multi-angle Imaging SpectroRadiometer (MISR) aboard Terra (2000-2010) and from seven-year Deep Blue records from MODIS aboard Aqua (2002-2011). The main focus is to determine similarities and differences in dust climatology provided by these sensors over the Sistan region and surroundings. The results showed a marked seasonal cycle with high aerosol loading during summer and lower in winter, while MISR, MODIS Deep Blue and OMI climatologies agree in both terms of monthly and seasonally mean spatial and temporal aerosol patterns revealing similar seasonal behavior over the region. After prolonged drought conditions in 1999 at Hamoun lakes (northern of Sistan) the dust-aerosol load over the area has increased. The higher aerosol concentrations during summer are interpreted as a result of the Levar northerly winds and the drying of Hamoun lakes. The satellite monitoring highlights Sistan and Hamoun basin as major dust source regions in south Asia, spreading dust aerosols over Afghanistan, Pakistan and Arabian Sea.

ACKNOWLEDGMENTS

First I have to thanks God for giving me to strength to overcome many obstacles and allowing me to reach my goals. I would like to express my sincere thank to Prof. Hannes Rautenbach (my supervisor) and Prof Patrick Eriksson (my Co-supervisor) for their innumerable ideas and guidance through the development of this work, and for all the support they provided me during of my studies at the University of Pretoria. Without their excellent direction, thoughtful encouragement, and uniform assistance and support, this study would not have been successfully accomplished. I really appreciate their warm-hearted consideration and devotion and these will be deeply engraved in my memory.

I am very grateful to Dr. Dimitris Kaskaoutis (my Co-supervisor) for his valuable comments and advice during this research. Thanks to his careful guidance and keen insight, I was able to carry this study forward on a right track. His amazing ability to review any material I sent to him, usually within a day, gave me the feedback and confidence to complete the study.

I need to express my appreciation to the scientists and technical staff at the Natural and Agricultural Research Centre of Sistan, the Environmental Research Centre of Zahedan and the Zabol Meteorological Station who established, maintained and provided assistance at the two stations used in the Sistan region.

I would like to thank the collaborators, Mojtaba Ganjali and Reza Mirshekar whose hard work in the field contributed to a robust data set of in situ measurements.

Samples were maintained meticulously in laboratories at the University of Pretoria, South Africa, and Lanzhou University, China, and I would like to thank Prof Qiang Mingroui who provided and opportunity at the Lanzhou University, to improve my experiences and do size distribution analysis, also Grote and Dykstra at the Geology laboratory, University of Pretoria, for assisting with XRD and XRF samples analysis. Thanks to my mother for supporting me through this most special part of my life and who made me what I am today.

Finally, I would like to thank my wife, Maryam Derakhshani, who put her career on hold and stayed with me in South Africa and endured me spending most of the time away from home working on my research. She took care of our son and everything else while I focused on my research. Thanks to her for her sharing company, support and positive attitude.

TABLE OF CONTENT

LIST OF TABLES

LIST OF FIGURES

LIST OF ABBREVIATIONS

AERONET	Aerosol Robotic Network
AI	Aerosol Index
AIRS	Atmospheric Infrared Sounder
Al	Aluminum
Al_2O_3	Aluminum oxide
AOD	Aerosol Optical Depth
AQI	Air Quality Index
ARF	Aerosol Radiative Forcing
As	Arsenic
Ba	Barium
BSNE	Big Spring Number Eight
CALIPSO	Cloud-Aerosol Lidar Infrared Pathfinder Satellite Observation
CaO	Calcium oxide
CCN	Cloud Condensation Nuclei
Cl	Chlorine
Co	Cobalt
COPD	Chronic Obstructive Pulmonary Diseases
Cr	Chrome
Cr_2O_3	Dichromium trioxide
Cs	Cesium
Cu	Copper
dp	Particle Size
d0.5	Median grain size
d0.9	90% of the grain size of particles is below this value
EARLINET	European Aerosol Research Lidar Network
EFs	Enrichment Factors
ENSO	El Niño-Southern Oscillation
EPA	Environmental Protection Agency
EPMSP	Enhanced Particulate Matter Surveillance Program
EU	European Union
F	Fluorine
Fe	Iron
Fe_2O_3	Iron III Oxide
g	Asymmetry parameter
GDP	Gross domestic product
HAVA	Helmand-Arghandab Valley Authority
HIRDLS	High Resolution Dynamic Limb Sounder
HNLC	High-Nutrient, Low-Chlorophyll
ICZ	Intertropical Convergence Zone
IDDI	Infrared Difference Dust Index
K_2O	Potassium oxide
LST	Local Sidereal Time
LULC	Land Use Land Cover
MgO	Magnesium Oxide
MISR	Multi-angle Imaging Spectro-Radiometer
MnO	Manganese oxide

MODIS	Moderate Resolution Imaging Spectroradiometer
MWAC	Modified Wilson and Cooke
N7T	Nimbus 7
Na_2O	Sodium oxide
Na_3PO_412H2O	Tri-sodium orthophosphate
NaOH	sodium hydroxide
NASA	National Aeronautics and Space Administration
Ni	Nickel
NiO	Nickel Oxide
OMI	Ozone Monitoring Instrument
P_2O_5	Phosphorus pentoxide
Pb	lead
PM	Particulate matter
PM_{10}	Particulates with aerodynamic diameters of < 10 µm
ppm	Parts per million
r	Correlation coefficient
R^2	Determine coefficient
RH	Relative Humidity,
S	Sulfur
SEM	Scanning Electron Microscopy
Si	silicon
SiO_2	silicone dioxide
SSA	Single scattering albedo
SSDS	Siphon Sand and Dust Sampler
SUSTRA	SUspended Sediment TRAp
Tg	Million tons (Teragram)
TiO_2	Titanium dioxide
TOA	Top-Of-Atmosphere
TOMS	Total Ozone Mapping Spectrometer
U.S	United state
USEPA	United state Environmental Protection Agency
UV	UltraViolet
V_2O_5	vanadium pentoxide
WDFG	Wedge Dust Flux Gauge
WMO	World Meteorological Organization
XRD	X-Ray Diffraction
XRF	X-Ray Fluorescence
Zn	Zinc
ZrO_2	Zirconium oxide

CHAPTER 1

INTRODUCTION

1.1 Atmospheric aerosols

Atmospheric aerosols are suspensions of solid and/or liquid particles in the air from natural and anthropogenic sources. Natural background aerosols are present in the absence of human activity, while urban aerosols are dominated by anthropogenic sources. In both cases, the primary particles are continuously emitted into the atmosphere, while the secondary ones are formed via oxidation, photolysis and mixing processes. Aerosols are ubiquitous in the air and are often observable as dust, smoke and haze (Fig 1). On a global basis, aerosol mass derives predominantly from natural sources, mainly dust and sea salt. However, anthropogenic aerosols, arising primarily from a variety of combustion sources, can dominate in, and downwind of, highly populated and industrialized regions and over areas of intense biomass burning. Atmospheric aerosols might affect the global climatic system in many ways, i.e. by attenuating the solar radiation reaching the ground, by modifying the solar spectrum, by re-distributing the earth-atmosphere energy budget and by influencing cloud microphysics and even the hydrological cycle (IPCC, 2007). Although the optical properties of aerosols are well known, large uncertainties still occur about aerosol-climate interaction due to the variety of aerosol types, their changing optical and physico-chemical properties, the influence of dynamic and synoptic scale meteorology and the mixing (internal and external) processes in the atmosphere.

Table 1.1 summarizes the source strengths, production mechanism and amounts of natural and anthropogenic aerosols over the globe. Anthropogenic aerosols are emitted from densely populated and industrialized regions over the globe due to anthropogenic activities and having the greatest climate effect. These are short-lived and mostly fine particles (size <1µm). The main chemical components of anthropogenic aerosols are sulfate, nitrate, organic and inorganic carbonaceous compounds produced by several physical and chemical processes such as gas-to-particle conversion, biomass burning and fossil fuel burning. A substantial fraction of the organic aerosols is water soluble and

constitute the efficient Cloud Condensation Nuclei (CCN) which is the important sink for organic aerosols. The marine aerosols are composed of both natural and anthropogenic constituents such as liquid sea water drops, dry sea-salt particles, dust and minerals transported from continental origin and from volcanoes, biological particles (bacteria, viruses), sulfate, nitrates, ship exhaust emissions, soot. The marine aerosols can be generated by several processes such as gas-to-particle conversion, nucleation, condensation and their size ranges from nanometers to millimeter. After emission in the atmosphere sea-salt particles can be internally and externally mixed with other aerosols. Sulfate particles are produced by the aqueous phase reaction within cloud droplets by oxidation of SO_2 via gaseous phase reaction with Oxide Hydroxides (OH) and by condensational growth onto pre-existing particles (Penner *et al.*, 2001). The dominant source of sulfate particles is fossil fuel burning with some small contribution from biomass burning. However, sulfate aerosols are also produced by natural sources, such as DiMethyl Sulphide (DMS), marine phytoplankton and volcanoes.

Table 1.1: The sources, source strength, production mechanism, and particle components of the natural and anthropogenic aerosols [Source: d'Almeida *et al.*, (1991) and Hobbs (1993)].

Source	Production mechanism	Aerosol component	Source strength (Tg.yr-1)
Anthropogenic			
Direct-emission	Direct-injection	Dust/soot/water-soluble	10-90
Biomass burning	Combustion	soot	3-150
Gas-to-particle conversion	Nucleation	Sulfate/nitrate/organics	175-325
Natural			
Extraterrestrial	Cosmic dust	Meteoric dust	10
Biosphere	Direct-injection	Pollen/spores	80
Volcanoes	Direct-injection	Water-soluble	15-90
Biomass burning	Combustion	Soot	200-450
Gas-to-particle conversion	Nucleation	Sulfate/nitrate/organics	345-1100
Ocean/fresh water	Bubble bursting	Sea-salt	1000-2000
Crust/cryosphere	Weathering	Soil dust	2000
Cloud processing	Cloud evaporation	Water-soluble	3000

Finally, mineral dust is a mixture of carbonates, sulfates, organic material and soot particles constituting one of the largest sources of tropospheric aerosols with emissions of 2150 $Tg.yr^{-1}$, about 37% of the total production of primary atmospheric aerosols by both natural and anthropogenic sources (Penner *et al.*, 2001). Mineral-dust aerosols are produced

mainly by wind erosion of desert soils, lifted to high altitudes by convection and can be transported over long distances from their source regions and mixed with continental aerosols such as sulfate, nitrate, soot, playing an important role in the heterogeneous chemical reactions (Ginoux *et al*., 2001). Furthermore, Fig. 1.1 provides a schematic presentation of the major aerosol types, their sources as well as climate implications through the attenuating of solar radiation and their influence on microphysical properties of clouds.

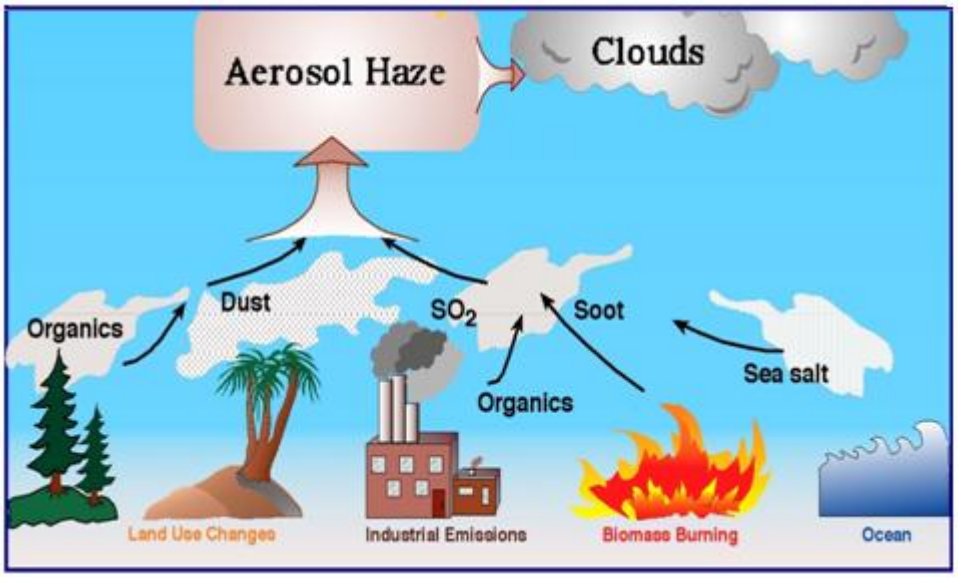

Figure 1.1: Various aerosol particle sources and their formation and removal mechanisms and distribution on the Earth's surface [source: D.G. Kaskaoutis PhD thesis, University of Ioannina, Greece 2008, reproduction with permission].

1.2 Definition of dust events

Dust events, according to the World Meteorological Organization (WMO), are defined by McTainsh and Pitblado (1987) as follows:

(1) *Dust storms* are the result of turbulent winds raising large quantities of dust into the air and reducing visibility to less than 1000 m above the surface.

(2) *Blowing dust* is raised by winds to moderate heights above the ground reducing visibility at eye level (1.8 m) but not to less than 1000 m above the surface.

(3) *Dust haze* is produced by dust particles in suspended transport which have been raised from the ground by a dust storm prior to the time of observation.

(4) *Dust whirls (or dust devils)* are whirling columns of dust moving with the wind and are usually less than 30 m high (but may extend to 300 m or more above the surface) and of narrow dimensions.

There is some confusion in the literature between 'sand storms' and 'dust storms'. Sand storms tend to be low altitude phenomena of limited areal extent, composed of predominantly sand-sized materials. On the other hand, dust storms reach higher altitudes, travel longer distances and are mainly composed of silt and clay. In this thesis, the term dust storm refers to an atmospheric phenomenon in meteorology, where the horizontal visibility at eye level is reduced to less than 1000 m by atmospheric mineral dust. While aerosol in the Earth's atmosphere may be derived from a number of different sources – including cosmic dust, sea salt, volcanic dust and smoke particles from fires – in this thesis I concentrate on the dust emitted from the Sistan desert that originates in Iran from surfaces at low latitudes (25º to 35º North Hemisphere).

1.3 Origin of Dust aerosols

Currently there are limited grain-size data available for dust particles. Bagnold (1941) defines such particles as having diameters of less than 0.08 mm (80 μm), but many others prefer to define them according to the silt/sand boundary (i.e. less than 62.5 μm). Below this cut-off, fine particles are commonly categorized into those of silt and clay sizes, with grain diameters of 4.0 to 62.5 μm and <4.0 μm, respectively (Wentworth, 1922). Whereas inorganic clay-size particles are generally agreed to be derived largely from chemical weathering, the processes responsible for silt formation in the desert environment remain a matter for debate. As Pye (1987) pointed out, many mechanisms of silt formation have been formulated but no clear picture regarding their relative importance has yet emerged. One major hypothesis is that silt can be formed by glacial grinding. This is an attractive theory to explain the great expanses of loess that occur on the margins of the former great Pleistocene ice caps (Smalley, 1966; Smalley and Vita-Finzi, 1968). Abrasion (sometimes called corrasion) during fluvial and aeolian transport may also produce silt. For example, numerous laboratory experiments have shown that abrasion of dune sand releases fines by spalling, chipping and breakage of particles and by the removal of grain surface coatings (Bullard et al., 2004; Bullard and White, 2005).

Moreover, many surfaces in both desert and Polar regions show clear evidence of wind abrasion at a variety of spatial scales. In the latter case, some of the abrasion is achieved by driven snow, though snow abrasion is less efficient than that by quartz grain impacts. The greater kinetic energy of windblown sand compared to water transported sand explains the greater abrasion achieved by wind transport (Kuenen, 1960). Furthermore, of potential importance to silt formation are various types of weathering, including frost action, salt attack, thermal fatigue weathering and chemical weathering (see, for example Goudie *et al*., 1979; Nahon and Trompette, 1982; Smith et al., 2002). For instance, deeply weathered granitoid rocks may contain a quite high silt percentage – up to 37.7% in eastern Australia (Wright, 2002). The role of salt weathering may also be important in producing what is often termed 'rock flour'. Goudie *et al.*, (1979) designed an experiment to test whether silt-sized debris could be produced by salt weathering of aeolian dune sand, and found that it could. Subsequently other successful experimental simulations of salt attack on sands and on rocks were undertaken by Pye and Sperling, (1983); Fahey, (1985); Smith *et al*., (1987) and Goudie and Viles, (1995). In addition, samples of salt-weathered rock collected in the field have shown that appreciable quantities of silt-sized material are produced (Goudie and Day, 1980; Mottershead and Pye, 1994). Although the relative importance of these mechanisms is difficult to assess, the important point to make is that silt can be produced in many ways, either singly, or more likely, in combination. Moreover, such mechanisms allow silt production in many types of environment, whether glacial, periglacial, arid or humid tropical (Wright, 2001a; Smith *et al*., 2002). In addition, complex pathways of silt production and transport may be involved (Wright, 2001b). As Smith *et al*., (2002) remark "Weathering mechanisms coupled with periods of sediment reworking and associated silt production by glacial, fluvial and aeolian systems may provide a feasible explanation for the provenance of a significant majority of total global quartz silt. In addition to releasing silt-size particles directly, weathering may release considerable quantities of partially flawed sand grains. These flaws may then be readily exploited during subsequent periods of transport within glacial, fluvial or aeolian systems".

Some dust may be derived from erosion of organic materials (such as diatomite), which were deposited in pluvial lakes that have now become desiccated. Diatomite is a very light substance that, if abraded, produces fine, easily carried debris. This has been

proposed as a major dust source in the Bodélé Depression in the Central Sahara (Giles, 2005). Other dust may be provided by the winnowing of fines from reactivated sand dunes. Dunes that have long been stable, having been produced under earlier conditions of greater aridity in the late Pleistocene, contain silt and clay contents in reasonably substantial quantities. Such fines may be the result of penecontemporaneous deposition of clay aggregates within the dunes as they were formed, but also important are post-depositional weathering and accretion of dust. Data from Kordofan (Sudan), north-west India, Zimbabwe, Niger and north-west Australia suggest that silt and clay contents of stabilized dunes can range from 7.8% to 32.0% (Goudie *et al*., 1993).

Thus, if such dunes become mobile as a result of climate or land-cover changes, they can release silt and clay for dust storm generation. Given that there are so many mechanisms to produce silt-sized material (Smalley *et al*., 2005), It is not surprising that various geomorphological environments, in addition to old dunes, contain silt-sized material that is available for deflation. These include settings like outwash and alluvial fans, playa basins, weathered or unconsolidated rock exposures and areas of previously deposited loess (Fig. 2.2). Coudé-Gaussen (1984), whose work is largely based on the Sahara, has attempted to categorize desert surfaces that are highly favorable for producing dust:

– Dried-out salt lakes of internal drainage, the surface of which is disrupted and rendered mobile by salt crystallization

– Wadi sediments containing silt and the floodplains of great rivers, like the Niger

– Powdery areas (fech-fech) derived from ancient lake muds or on certain argillaceous rocks

– Desert clay soils (takyrs) with polygonal desiccation cracks

– Outcrops of materials like unconsolidated Neogene fine-grained sediments

Desiccation of lake beds, whether due to drought or to water diversion schemes, as in the Aral Sea in Turkmenistan, or the Hamoun lakes in Iran, can also lead to increased dust storm activity. Thus, some dust may be derived from dried lake beds and can be highly saline, while the finest aerosols can be injurious to health.

1.4 Physical properties of dust aerosols

1.4.1 Size distribution

Size distribution is a key parameter to characterize the aerosol chemical, physical and optical properties. The distributions of dust aerosol properties are shaped by several dynamical processes namely, advection, convection, turbulent mixing, humidification, condensation, cloud contamination, scavenging and long range transport. The power law distribution is valid for monodispersion, i.e. the value representing the concentration of aerosol particles decreases exponentially with the radius and shows narrow size distributions and lower geometric standard deviation values. However, nature does not support monodispersive distribution and, therefore, the aerosols in the atmosphere are polydispersive, i.e. wider size distributions and higher geometric standard deviation values due to wide sources that follow the lognormal distribution.

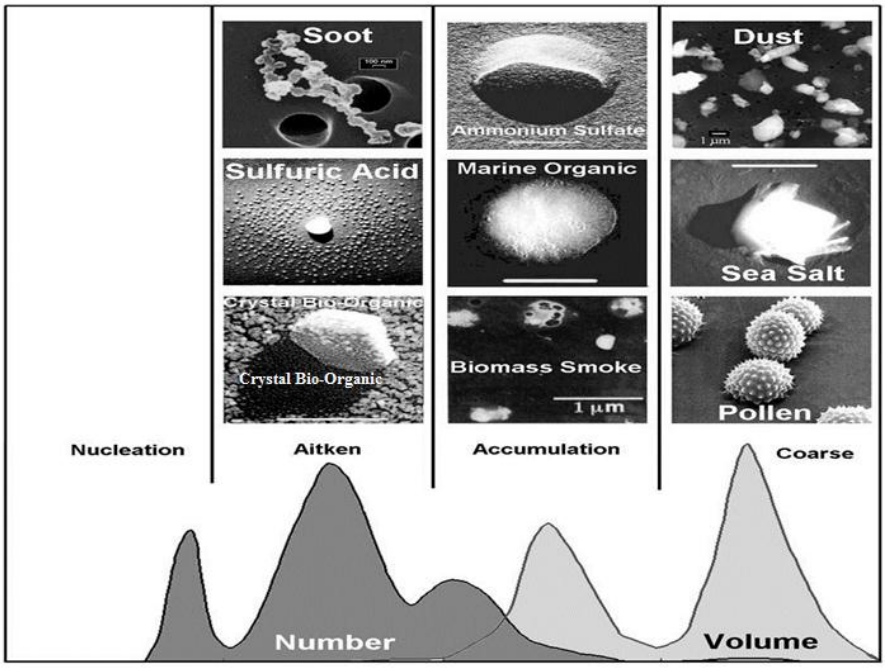

Figure 1.2: Morphology and size classification of aerosol and dust particles [S.N. Singh presentation at the COSPAR aerosol workshop 2011]

The lower and upper size limits of dust aerosols are from a few nanometers to ~100µm and aerosol properties change substantially over this size range. Depending on the size, dust aerosols can be classified into three categories i) Aitken nuclei mode (~0.001 to 0.1 µm), ii) accumulation mode (~0.1 to 1.0 µm) and iii), large mode/giant particle >

1.0 µm; or alternately, fine/sub-micron aerosols < 1 µm and coarse mode aerosols > 1 µm. The aerosol size distribution can be used as a proxy to infer the relative contribution of dust particles from different sources.

1.4.2 Refractive index

The refractive index is a key parameter which determines the scattering, absorption and size distribution of aerosols. The refractive index of hygroscopic aerosols changes with the additional amount of water that is absorbed in response to changing relative humidity. This alters the refractive index, including also the change in specific density, size and mass fraction.

1.5 Optical Properties of Dust

1.5.1 Aerosol Optical Depth (AOD):

Aerosol Optical Depth (AOD) is the degree to which aerosol particles prevent the transmission of light. It is defined as the integrated extinction coefficient over a vertical column of unit cross-section. It is an indirect measurement of the size and number concentrations of aerosol particles present in a given column of air. The spectral dependency of AOD contains information about the dominance of fine and coarse mode particles, the aerosol source regions, the modeling of aerosol radiative effects, the air quality (through monitoring of particulate matter) and the correction for aerosol effects in satellite remote sensing of the Earth's surface.

1.5.2 Extinction coefficient:

The attenuation of intensity (energy) of solar radiation by scattering and absorption of aerosol particles are ubiquitous phenomena in the atmosphere and take out the so called. The measurement of extinction coefficient related to extinction contains information about the particles' number concentrations and their size distribution.

1.5.3 Scattering coefficient:

The scattering coefficient is a significant optical property of aerosols that defines the distribution of scattering light around the particle. Scattering (excitation + re-radiation) is the process that a particle in the path of the electromagnetic wave (em) scatters the incident radiation in all directions around it. The distribution of scattering is a strong function of the size and shape of the particle and, therefore, the geometry of scattering is very different. The effect of particle size on scattering is inferred by a physical term called size parameter (i.e. number of wavelengths that is allowed to fit into a circle of given radius) defined as $x=2\pi r/\lambda$, where r is the particle radius and λ is the incident wavelength. The criteria for Rayleigh (molecular) and Mie (aerosol) scattering are $x < 1$ and $x \sim 1$, respectively.

1.5.4 Absorption coefficient:

The absorption coefficient defines the capability of an aerosol particle to absorb and, then re-emit the energy, i.e. sun light and Thus absorption of light is the process by which sun light is absorbed by the particles, converted into another form of energy and, consequently, heats the atmosphere. The strong increase in atmospheric absorption of solar radiation could be due to the presence of large concentrations of absorbing mineral dust or soot (black carbon aerosols). In general, the aerosol absorption efficiency increases with the imaginary part of the refractive index and size of the particles, while it is a strong function of the aerosol chemical composition.

1.5.5 Single scattering albedo (SSA):

Single scattering albedo (SSA) infers the efficiency of the scattering nature of aerosol particles and is defined as the ratio of scattering optical depth to the total optical depth. It is a key variable for determining the aerosol climatic effects and retrieving the AOD from satellite radiances. The SSA contains valuable information about the chemical composition of aerosols in the atmosphere. An increase of SSA with wavelength can be associated with the dominance of coarse-mode desert dust particles in the aerosol size distribution. The value of SSA may vary from 0.2 for absorbing type aerosols, such as soot, to 1.0 for scattering type aerosols, such as sea salt.

1.5.6 Phase function (scattering function):

The Phase function (scattering function) is defined as the angle at which scattered light is distributed as a function of size, shape of the aerosol particle, wavelength and the incidence angle of the light. It is expressed as:

$$P(\theta) = \frac{\beta(\theta)}{\beta_{sc} / 4\pi} \tag{1.1}$$

Where $\beta(\theta)$ and β_{sc} are the angular and total scattering cross-section of the aerosol particles respectively. Due to diverse sources and strength of atmospheric aerosols and the variety of size modes (nucleation, fine and coarse) and complex refractive index, the phase functions are quite different for different size particles, as clearly shown in Fig. 1.3.

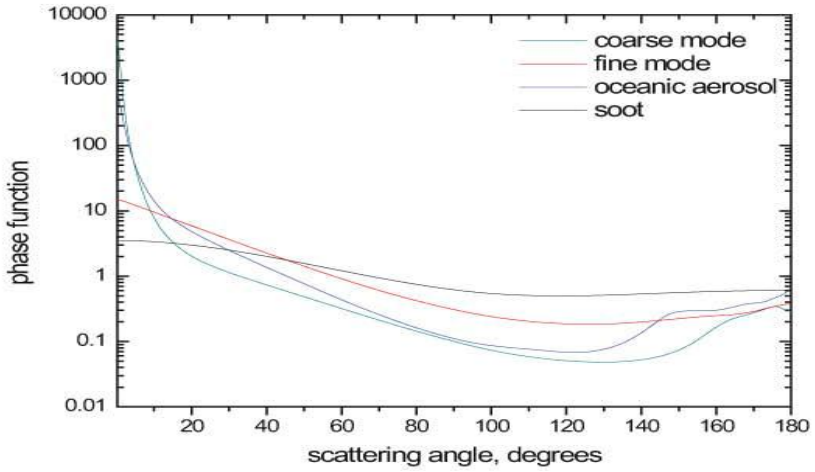

Figure 1.3: Phase function of various aerosol particles (source: Kokhanovsky, 2008).

1.5.7 Asymmetry Parameter:

The asymmetry parameter (g) is defined as the cosine weighted mean of the angular scattering phase function and is a measure of the amount of radiation scattered in the forward versus backward directions. It can be expressed as:

$$g = \frac{\int_{-1}^{1} P(\lambda,\theta)\cos\theta d(\cos\theta)}{\int_{-1}^{1} P(\lambda,\theta) d(\cos\theta)} \tag{1.2}$$

Where g is the asymmetry parameter, P is the phase function and θ the scattering angle. The value of g can vary in the range of -1 (for complete backscattering) to +1 (for complete forward scattering) and it is zero for isotropic or symmetric scattering.

1.6 Dynamics of dust aerosols

1.6.1 Dust emission

The dust emission process is mainly initiated by sand blasting. The mechanism interpreted in empirical formulations is that dust can only be emitted into the atmosphere over dry Earth surfaces when the surface winds exceed a threshold speed of wind erosion.

The formation and evolution of atmospheric aerosols are key processes in describing and determining their dynamics (Kulmala *et al*., 2000). Once the aerosol particles have formed they undergo various physical and chemical processes, namely nucleation, coagulation, transportation and scavenging (Fig. 1.4).

1.6.2 Nucleation

Nucleation is the ubiquitous process in the atmosphere that leads to the formation of freshly-created nanometer-sized particles and subsequent growth to larger size ranges. It plays an important role in several processes, such as cloud radiative properties, cloud lifetime and precipitation rates and, consequently, rain formation and freezing. The transition from one phase to another phase, i.e. from gas to particle during the nucleation processes does not occur instantly due to the enthalpy difference between these two phases. However, as the enthalpy barrier is crossed, the nucleation cluster is formed and it grows very rapidly. The nucleation can be homogeneous or heterogeneous. The homogeneous nucleation takes place by the condensation of precursor gases and creates new aerosol particles in the air with low aerosol concentration at high effective super-saturation. The heterogeneous nucleation takes place when gaseous molecules condense onto pre-existing solid or liquid particles at significantly lower effective super-saturation.

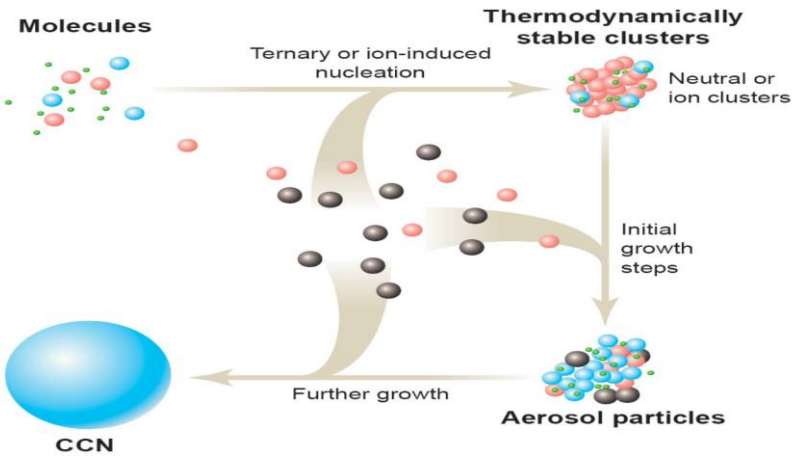

Figure 1.4: Growth of particles (Source: Kulmala *et al*., 2003)

The growth mechanism of aerosol particles, the so-called coagulation, results from the differences in the speed and direction of moment in the atmosphere. The coagulation of aerosol particles significantly modifies their shape and size distribution in the atmosphere and reduces the number concentrations, while the total mass of particles is conserved without changing the chemical compositions. Another important characteristic of coagulation processes is the change of mixing state of particles, since the particles originated from different sources, they often have different sizes and chemical compositions. Therefore, coagulation between unequally-sized particles will externally convert to internally mixed aerosols and to changes in the optical properties and hygroscopic growth characteristics of the particles (Levin and Cotton, 2009). The process of coagulation is the efficient mechanism for the formation of accumulation-mode aerosols in the atmosphere. If the distribution of particles is known, the coagulation rate is a function of the mechanism bringing the particles together. There are several coagulation mechanisms that affect the coagulation rate namely Brownian, gravitational, convective Brownian diffusion enhancement, turbulent inertia and turbulent shear coagulation. Coagulation with larger particles might serve as a significant sink for newly formed nuclei-mode particles.

1.6.3 Dust transportation

Mineral dust is transported in the atmosphere by advection, convection, and turbulent diffusion. The majority of the atmospheric dust falls back to Earth a short time after entrainment and not far from its source. However, intense dust storms are capable of transporting sediments over enormous distances, in many cases over some thousands of

kilometers. In Texas, Sahara dust events with moderate to high fine particulate contents occur on three to six days annually, mainly between June and August, lasting for one to three days after travelling from their source over a period of 10 to14 days. Saharan dust also travels northwards to Europe, eastwards to the Middle East and even as far as China (Tanaka et al., 2005). Dust from Central Asia and China is regularly transported to Korea, Japan, the Pacific and North America (Rahn *et al.*, 1977; McKendry *et al.*, 2001). The distance traveled by dust particles depends upon many factors, including wind speed and turbulence, dust grain characteristics and their settling velocities. The latter is determined by the mass and shape of each particle.

1.6.4 Dust deposition

Atmospheric dust settles to the Earth's surface both through gravitational settling (dry deposition) and through wet deposition with precipitation. Deposition is the most efficient removal pathway for ultrafine (particle size (dp) <0.1 µm) coarse and mode (2.5µm<dp<10µm) particles. Deposition of the particles may be caused by gravitational settling and turbulent deposition. In wet deposition, particles are removed from the atmosphere by rain or fog, and it is the most efficient removal pathway for fine particles, especially particles in the size range 0.1 to 1µm. Wet deposition can occur either below a cloud, when raindrops, snowflakes or hailstones scavenge dust as they fall, or within a cloud when dust particles are captured by water droplets and descend to earth when the precipitation falls. There are two major wet deposition mechanisms, nucleation scavenging i.e. Cloud Condensation Nuclei (CCN), and occult i.e. deposition by the fog and cloud droplets. The removal rate through wet deposition is strongly dependent on the fall velocity, size distribution of the droplets and collision efficiency between droplets and aerosol particles.

Over land, dust is often subject to dry deposition when particles in suspension cross a boundary to terrain with a greater roughness. The presence of vegetation is thought to be important for trapping dust, while rock fragments also perform the same function, although such terrain probably retains less than 20% of settled dust (Goossens, 1995).

1.7 Major desert dust source regions

The largest and most persistent dust sources are located in the northern hemisphere, mainly in the broad "dust belt" that extends from the west coast of north Africa, over the Middle East, central and south Asia, to China. On the other hand, the southern hemisphere is devoid of major dust activity, except for some areas in South America (Atacama) and the Australian desert, north of Lake Eyre. Dust sources, regardless of size or strength, can usually be associated with topographic lows. They are situated in close proximity to mountains and highlands with annual rainfall less than 200 to 250 mm. The largest and most active dust sources are located in remote areas where there is little or no human activity. Dust activity is extremely sensitive to many environmental parameters, such as topography, rainfall, surface winds, regional meteorology, boundary layer height, convective activity, etc. In general, dust mobilization is extremely sensitive to a wide range of factors, including the composition of the soils, their moisture content, and the condition of the surface and wind velocity.

The largest dust source region on earth is a zone that extends from the eastern subtropical Atlantic ocean eastwards through the Sahara Desert to Arabia and southwest Asia. In addition, there is a large zone within central Asia, centered over the Taklamakan Desert in the Tarim Basin. Central Australia has a relatively small zone, located in the Lake Eyre basin, while southern Africa has two zones, one centered on the Mkgadikgadi basin in Botswana and the other on the Etosha Pan in Namibia. In Latin America, there is only one easily identifiable zone. This is in the Atacama and is in the vicinity of one of the great closed basins of the Altiplano – the Salar de Uyuni. North America has only one relatively small zone, located in the Great Basin (Goudie and middleton., 2006).

Dust storms are also widespread in the northern part of the Indian sub-continent and neighboring areas (Léon and Le Grand, 2003; El-Askary *et al*., 2006). Middleton, (1986) used ground station observations to examine the frequency and seasonality of dust storms in southwest Asia. He showed that the highest frequencies occur at the convergence of the common borders between Iran, Pakistan and Afghanistan (Sistan Basin). Other high-frequency areas occur on the Arabian Sea coast of Iran (Makran) and across the Indus Plains of Pakistan (Hussain *et al*., 2005) and the Indo-Gangetic basin (Dey *et al*., 2004).

Figure 1.5: A number of jets of windblown desert dust (light brown plumes) were blowing over the Gulf of Oman and the Arabian Sea on May 2, 2003. Originating from the Arabian Peninsula as well as Iran, Afghanistan, and Pakistan, the dust obscures the surface over much of the region. This image was compiled using data from the MODIS sensors flying aboard NASA's Terra and Aqua satellites at hours apart on the same day.

1.8 Effects of dust storms

According to the Earth Observatory website (*http://earthobservatory.nasa.gov/*) dust storms are considered natural hazards, which affect ecosystems for short time intervals ranging from a few hours to a few days. Dust outbreaks have a significant impact on climate, human health and ecosystems, and numerous studies have been conducted worldwide with different instrumentation and techniques to investigate of such events.

1.8.1 Dust effects on solar radiation and climate

Desert aerosols are probably the most abundant type of aerosol particles that are present in the atmosphere. Dust, which is the most common aerosol type that occurs over deserts (Smirnov *et al.*, 2002a; Masmoudi *et al.*, 2003) or that is emitted from arid and semiarid areas, is considered to be one of the major sources of tropospheric aerosol loading, and constitutes an important key parameter in climate aerosol forcing studies (Kaufman *et al.*, 2002; Christopher and Zhang, 2002). The impact of mineral dust aerosols on the Earth's system depends mainly on particle characteristics such as size, shape and mineralogy (Mahowald *et al.*, 2005), which are initially determined by the terrestrial sources from which the sediments are entrained. Mineral dust is believed to play a crucial

role in climate, with an estimated global planetary radiative forcing in the range of –0.6 to 0.4 $W.m^{-2}$ (IPCC, 2001). Though poorly quantified, the impact of mineral dust on global radiative forcing is expected to be negative (Satheesh and Krishna, 2005), but still have large uncertainties. These uncertainties are mainly attributed to the mineral aerosol shape (Kalashnikova and Sokolik 2002), their spectral optical properties (Sokolik and Toon, 1999), their chemical and mineralogical composition (Claquin et al., 1998), their spatial, vertical and temporal distribution (di Sarra *et al*., 2001), their removal (dry and wet deposition) processes (Alpert *et al*., 2004) as well as the albedo of the underlying surface and the relative height between dust layer and clouds (Kinne and Pueschel, 2001; Abel *et al*., 2005). Dust particles scatter and absorb solar and thermal (outgoing) radiation (direct effect) and also, by acting as cloud condensation nuclei, change the microphysical properties of clouds (see Fig. 1.4), such as brightness, albedo, lifetime, structure, droplet size, precipitation rate and latent heat, thus affecting the hydrological cycle (Haywood and Boucher, 2000; Lohmann and Feichter, 2005).

Desert dust particles attenuate UltraViolet (UV) and visible radiation (Badarinath et al., 2007), thus causing cooling at earth surface (di Sarra *et al*., 2002; Meloni *et al*., 2003). The Sahara dust experiment (SHADE) campaign showed a net radiative forcing of -0.4 $W.m^{-2}$ at the Top-Of-Atmosphere (TOA), thus having a cooling effect (Myhre *et al*., 2003). Badarinath *et al*., (2007) found a 4.77% reduction in solar (0.3 to 3.0 μm) radiation over Hyderabad, India, due to a dust storm that originated from the Thar desert. It has been shown that the extent of solar attenuation is sensitive to the dust particles' source region (Meloni *et al*., 2004) and their vertical distribution and shape (Balis *et al*., 2004), because their optical properties are strongly dependent on their source, as well as through chemical and physical processes occurring along the trajectory. Thus, larger particles scatter solar radiation more. The most absorbing dust particles attenuate more solar radiation above the ground. Balis *et al*., (2004) compared the UV irradiances at 305 nm at Thessaloniki, Greece, for two days (one with and the other without a dust event), but with similar ozone levels and aerosol loading. The UV irradiance during the dust event was almost 5% lower after removing the contribution to the differences caused by small total ozone variation between these two days.

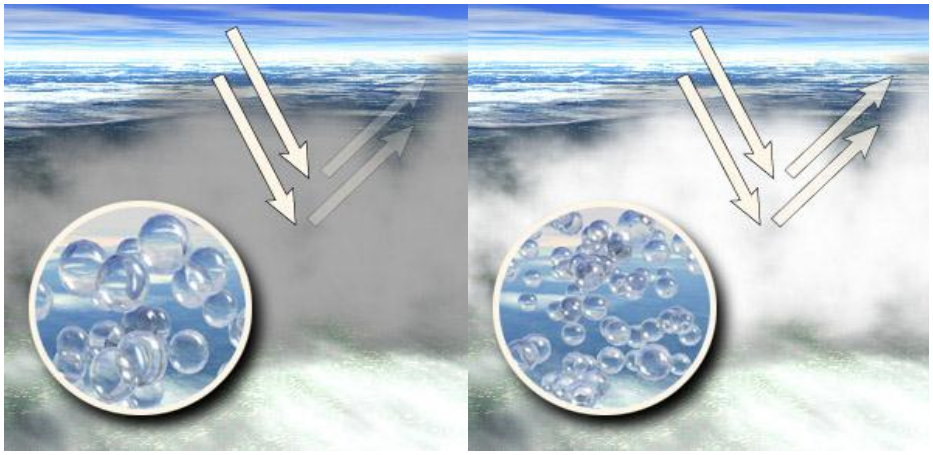

(a) *(b)*

Figure 1.6: The indirect aerosol effect through the modification of the cloud microphysical properties. [Source: *http://terra.nasa.gov/FactSheets/Aerosols/*]

1.8.2 Radiative effects of dust

Atmospheric aerosols play a vital role in the radiation budget of the Earth-atmosphere system by scattering and absorbing part of the incoming solar radiation (called direct effect) and by modifying the cloud droplet size distribution, thereby changing the radiative properties and lifetime of clouds (called indirect effect) (Twomey, 1977; Albrecht, 1989; Charlson *et al*., 1992; Ramanathan *et al*., 2001b; Koren *et al*., 2004). The aerosol direct and indirect effects are associated with the surface area and size of the particles, respectively. Direct scattering of solar radiation by dust aerosol particles may cause a change in the vertical temperature profile, cloud properties and precipitation. In addition, atmospheric heating due to dust can increase the atmospheric temperature and might cause "burning of clouds" i.e. evaporation of clouds, and therefore, absence of precipitation, which is an example of the semi-direct effect of dust aerosols (Ackerman *et al*., 2000). However the sole impacts of aerosols on the Earth radiation budget depend on the types of aerosols (i.e. scattering or absorbing properties), reflecting property of the surface, altitude distribution of aerosols, solar declination, geographical latitude and distribution of clouds.

The change in the amount of total solar radiation reaching the Earth's surface with and without the presence of aerosols is called Aerosol Radiative Forcing (ARF) at the surface. Similarly, the change in the amount of solar radiation going out of the Earth-atmosphere system due to the presence of aerosols is the ARF at the TOA. The difference

between the ARF at the surface and that at the TOA gives the net amount of radiation trapped in the atmosphere due to aerosols, which is the ARF in the atmosphere, which increases with a decrease in the value of the (SSA).

1.8.3 Dust mineralogy, chemistry and environmental impacts

Little information is available about the potential environmental impacts of dust compounds. These impacts depend upon dust composition, application rates and interactions with other environmental components. Potential environmental impacts include: (1) surface and groundwater quality deterioration; (2) soil contamination; (3) toxicity to soil and water biota; (4) toxicity to humans during and after application; (5) air pollution; (6) accumulation in soils; (7) changes in hydrologic characteristics of the soils, and (8) impacts on native flora and fauna populations (Piechota *et al.*, 2002).

Most of the dust mass in the world is composed of illite, kaolinite and montmorillonite minerals (Sokolik and Toon, 1999), as well as of hematite (Quijano *et al.*, 2000). Hematite, which is a strong absorber of light at solar wavelengths, aggregated with the other three clay materials (relatively transparent at solar wavelengths) which results in stronger absorption, particularly at shorter wavelengths. Additionally, since dust particles absorb solar radiation, they heat the lower atmosphere and, as a consequence, for an average dust event, it is estimated that the lower atmosphere (1.5 to 3.5 km) is heated by ~0.2 K per day. For about 30 dust events per year, dust aerosols might lead to a regional atmospheric heating of up to ~6 K per year (Alpert *et al.*, 1998).

Furthermore, it was found that an elevated Saharan dust layer may play a important role in suppressing tropical cyclone activity in the Atlantic ocean (Dunion and Velden, 2004). Several studies have underlined the importance of dust aerosols, not only to the global and regional radiative and energy balance (Satheesh and Krishna Moorthy, 2005 and references therein), but also to weather forecasting (Alpert *et al.*, 1998), rain acidity (Levin *et al.*, 1996), modification of cloud microphysical properties (Twomey, 1959), the hydrological cycle and dynamical processes in the atmosphere (Carlson and Prospero, 1972; Ginoux *et al.*, 2001). Dust aerosols constitute one of the primary sources of minerals for oceanic life and influence the health of coral reefs. Desert-dust aerosols have also been associated with an increase in coral mortality and *Trichodesmium* blooming in the Caribbean (Lenes *et al.*, 2001; Griffin *et al.*, 2003; Shinn *et al.*, 2000). In addition to its

direct radiative effect, dust aerosols mediate ocean carbon uptake and the chemical cycles of other aerosols like sulfates. Trace metals on dust are essential to some marine biological processes. Dust is a source of Iron (Fe), which may be a limiting nutrient for phytoplankton (Falkowski *et al*., 1998; Fung *et al*., 2000). Consequently, dust could modulate the global carbon cycle. Perhaps, the most interesting aspect is the study of dust as a source of iron to High-Nutrient, Low-Chlorophyll (HNLC) oceans, where plankton productivity is limited because of the availability of soluble iron (Lenes *et al*., 2001). It was also found that desert particles carry pathogens from the Sahara desert over the Atlantic Ocean, a fact that may explain the migration of certain types of diseases (Falkowski *et al*., 1998). In addition, certain species of cyanobacteria that utilize Iron (Fe) could play a significant role in the nitrogen chemistry of the ocean. The rate of production of nitrate and ammonium by these organisms could be strongly controlled by the rate of input of mineral dust to the oceans (Falkowski *et al*., 1998).

Dust deposition in the Alps appears to affect the local climate by reducing the albedo of the glaciers, thus contributing to their melting (Franzen *et al*., 1994) and altering the chemistry of Alpine lakes (Psenner, 1999). Furthermore, harmful health effects are caused by elevated concentrations of desert dust particles. These effects have been investigated in several studies (Rodriguez *et al*., 2001; Sultan *et al*., 2005). Dust can serve as a reaction surface for reactive gas species in the atmosphere (Dentener *et al*., 1996) and for moderating photochemical processes (Dickerson *et al*., 1997). Dust also has an important role in paleoclimatic studies. The concentration of windblown mineral dust in deep-sea sediments (Rea, 1994; Kohfeld and Harrison, 2001) and ice cores (Yung *et al*., 1996) is often used as a proxy indicator of paleoclimatic aridity on the continents and of historical changes in global wind systems.

1.8.4 Health effects of dust storms

A number of medical conditions can be traced to the impact of desert dust, and the effects of fine wind-borne particles on human health have recently been the subject of considerable interest (Griffin *et al*., 2001; Garrison *et al*., 2003,). On 9 August 2005, a dust storm in Baghdad led to nearly 1000 cases of suffocation being reported to the city's Yarmuk Hospital, one of whom died (Goudie and Middleton, 2006). The straightforward inhalation of fine particles can cause and/or aggravate diseases such as bronchitis,

emphysema and silicosis. High incidences of silicosis and pneumoconiosis have been reported in Bedouins in the Negev (Bar-Ziv and Goldberg, 1974), while dust blown by the Irifi wind in the Western Sahara is responsible for conjunctivitis that is common among the nomads of the region (Morales, 1946). High concentrations of atmospheric dust in many desert areas often exceed generally recommended health levels for particulate matter (see also Section 1.6 on PM_{10} values). In Mali, for example, Nickling and Gillies, (1993) found that the mean ambient air concentrations during April to June were 1176 $\mu g.m^{-3}$, exceeding the recommended international health standard by an order of magnitude. Similar concentrations can also occur during particularly severe long-range transport events. In certain parts of Spain, the levels of particulate matter associated with frequent incursions of dust from North Africa means that it is not possible to meet European Union (EU) directives on acceptable levels of air pollution (Querol *et al*., 2004). Rodriguez *et al*., (2001) indicated that these Saharan dust events can induce up to 20 days per year in which PM_{10} standards are exceeded in southern and eastern Spain. Intrusions of desert dust from the Hexi Corridor in northern China also make a significant contribution to particulate pollutants in the Lanzhou Valley, an urban area that is among the worst in China for its poor air quality (Ta *et al*., 2004).

Dust may also be otherwise contaminated by organisms, such as bacteria and fungi (Kellogg *et al*., 2004) and by toxic chemicals that can harm people when it settles on the skin, is swallowed or inhaled into respiratory passages. The increase in dust storm activity in Turkmenistan, for example, linked to the desiccation of the Aral Sea, has probably caused severe respiratory problems for children in the area, but the dust from the dry sea bed also happens to contain appreciable quantities of organophosphate particles (O'Hara *et al*., 2000). Dust blown from another former lake bed, that of the desiccated Owens Lake in California, contains arsenic derived from nineteenth-century mining operations (Raloff, 2001). Dust storm material in Saudi Arabia has been found to contain an array of aeroallergens and antigens which could trigger a range of respiratory ailments (Kwaasi *et al*., 1998). Other possible consequences of airborne dust include an increase in asthma incidence (Rutherford *et al*., 1999), as reported for Barbados and Trinidad when Saharan dust outbreaks occur (Monteil, 2002; Gyan *et al*., 2005) and also an increase in the incidence of meningococcal meningitis in the Sahel zone and Horn of Africa (Molesworth *et al*., 2002). The annual meningitis epidemics in West Africa, which affect up to 200 000

people between February and May, are closely related to the Harmattan season in their timing (Sultan *et al*., 2005). Coccidioidomycosis, a disease caused by a soil-based fungus (Coccidioides immitis) transported in airborne dust, is endemic to parts of the southwestern U.S (especially in the San Joaquin Valley of California, southern Arizona, southern New Mexico and west Texas) and northern Mexico (Gabriel *et al*., 1999). In the U.S, where it is known as Valley Fever, an estimated 50 000 to 100 000 people develop symptoms of the disease each year (Leathers, 1981), and a dramatic increase in the incidence of coccidioidomycosis during the early 1990s in California was estimated to have cost more than U.S.$66 million in direct medical expenses and time lost in one county alone (Kirkland and Fierer, 1996). Dust can also contain dried rodent droppings or urine which can cause the spread of Hantavirus Pulmonary Syndrome. In Ladakh and China, dust may contribute to a high silicosis incidence (Derbyshire, 2001). Fungal spores from China reach high ambient levels in Taiwan during dust events and may have health implications (Wu *et al*., 2004). Some recent epidemiological studies indicate that long-range dust transport events are closely associated with an increase of daily mortality in Seoul, Korea (Kwon *et al*., 2002) and Taipei, Taiwan (Chen *et al*., 2004) and have caused cardiovascular and respiratory problems (Kwon *et al*., 2002), including an increased incidence of strokes (Yang *et al*., 2005).

Given the great distances over which dust can be transported, it is not surprising to learn that the intercontinental dispersal of material may include pathogens of crop plants. Long-distance dispersal of fungal spores by the wind can even spread plant diseases across and between continents and reestablish diseases in areas where host plants are seasonally absent (Brown and Hovmøller, 2002). While monitoring aerosols on the Caribbean island of Barbados, Prospero (2004) reported that concurrent detection of bacteria and fungi only occurred in air that contained Saharan dust.

1.8.5 Economic effects of dust storms

The entrainment, transport and deposition of dust can present a variety of problems to inhabitants in arid desert areas, many of which have a deleterious economic impact. Folk (1975), for example, suggests that the ancient Macedonian town of Stobi, which flourished between 400 BC and 400 AD, was abandoned because of the severe effects of dust storms. Another example of the mix of impacts a dust storm can bring is provided for

China by Yang *et al*., (2001): "A major sand-storm on May 5th 1993 caused serious economic loss and was as hazardous as a disaster caused by an earthquake. According to ground observation and investigation made by the expert group of the Ministry of Forestry, a total of 85 people died, 31 people were lost and 264 were injured (most of these victims were children). Agriculture and animal husbandry were most severely hurt. In total, 373,000 ha of crops were destroyed. 16,300 ha of fruit trees were damaged. Thousands of greenhouses and plastic mulching sheds were broken. 120,000animals died or were irrecoverably lost. The fundamental agricultural installations and grassland service facilities were ruined. More than 1,000km of irrigation channels was buried by sand accumulation. Many water resource back-up facilities, such as reservoirs, dams, catchments, underground canals and flood control installations were filled up with sand silts. About 6,021 communication poles and electricity grids were pushed down and electricity transports and communication services in some regions were stopped for several days. Some sections of railway and highway were interrupted due to deflation and sand accumulation."

Another major dust and sandstorm event took place in April 2002 and led to airport closures in Mongolia and Korea. The total damage cost of this event in Korea alone was put at U.S. $ 4.6 billion (or about 0.8% of Gross domestic product (GDP); Asian Development Bank, 2005, pp. 1–5).

In a similar vein, dust storms have regularly been associated with deaths in India. In April 2005, ten people and 50 head of cattle were killed by fires fanned by dust storm winds in Uttar Pradesh. In March 2005, six people were killed and 40 injured in a dust storm in Bihar.

Some progress has been made in identifying the offsite costs of wind erosion. In South Australia, for example, the costs include damage to houses and the need for redecoration, the need to clean power transformers, deaths and damage caused in traffic accidents, road disruption, impacts on the costs of air travel and impacts on human health (especially because of raised asthma incidence(Williams and Young, 1999).

The reduction in visibility caused by dust storms is a hazard to aviation, rail and road transport. The severe pre-frontal storm of 7 November 1988 in South Australia, for example, caused road and airport closures all across the Eyre Peninsula (Crooks and

Cowan, 1993). In the United state (U.S), in November 1991, a series of collisions involving 164 vehicles occurred on Interstate 5 in the San Joaquin Valley in California (Pauley *et al*., 1996), while in Oregon a dust storm in September 1999 set off a chain reaction of 50 car crashes that killed eight people and injured more than 20 (State of Oregon, 2004). The loss of visibility may be very sudden when caused by the arrival of a dust wall associated with a dry thunderstorm. Such Haboob dust walls were responsible for 32 multiple accidents between 1968 and 1975 on Interstate 10 in Arizona (Brazel and Hsu, 1981). The seriousness of the problem inspired the development of a Dust Storm Alert System involving remote-controlled road signs and special dust-alert messages broadcast on local radio (Burritt and Hyers, 1981).

1.8.6 Impact of dust storms in the Sistan region

After the 1999 drought, dust storm activity appears to be increasing in both frequency and severity. Tens of thousands of people have been suffering during the months of devastating dust storms in the Sistan basin, especially in the cities of Zabol and Zahak and surrounding villages. A severe dust storm occurred in Sistan and its 80 surrounding villages on 30 June 2008 that resulted in the closing of schools and businesses. Dust storms lasted about five days and more than 3000 people suffering from allergies and respiratory diseases were admitted to hospital or health centers. Miri *et al*., (2007) showed that 63% of the people in Zabol city suffer from respiratory diseases with the majority coming from the surrounding villages. Miri *et al*., (2007) indicated that 132 people have been considered as patients suffering from respiratory conditions related to dust storms. Information obtained from hospitals indicated that most of the patients who visited hospitals suffered from Chronic Obstructive Pulmonary Diseases (COPD) and asthmatic diseases with the peak of incidences during the summer season (June to September) when the most severe dust storms occur (Rashki *et al*., 2011). It is estimated that ~90% of the population living in the region suffered from respiratory problems in the summer period. The health damages and medical costs for patients for the period 1999 to 2004 exceeded U.S. $166.7 million (Miri *et al*., 2007). According to the Asthma Mortality Map of Iran, the rate of asthma in Sistan is higher than in other regions of the world (Selinus *et al*., 2010).

On the other hand, dust storms affect horizontal visibility, causing accidents. In recent years, many accidents have been reported on dusty and stormy days in the Sistan region resulting in death and injury of travelers. Accidents involving trucks transporting cargo are costly and affect the local economy. A study showed that the greatest number of accidents during one complete 24 hours (day and night) occurred when the dust was at peak intensity. The maximum number of vehicle accidents also takes place in the summer period (Miri *et al.*, 2007).

Particles arising from dust storms affect schools in several ways, causing teachers and pupils to take leave or cause late attendance, disrupting classes due to discomfort, hampering serious study and restricting movement. A total of 623 schools were closed because of dust storms and amounts of damage were about U.S. $ 325 000 during 2000 to 2004. Two hundred and twenty villages are located in the path of dust storms and sand movement in the Sistan region, which need intensive clean-up after dust storms. The cost of evacuating sand from residential areas is estimated at 1.3 to often 1.5 U.S. $/m^3 (Miri *et al.*, 2007).

Table 1.2: Cumulative damage costs of dust storms in the Sistan region during 2000 to 2004 (Source: Miri *et al.*, 2007)

Damage centre	**Damage Percentage (%)**	**Damage costs (×1000 US$)**
Road	4.5	5636
Community health	24.99	31.2
School breaks(enforced holidays)	1.06	1324
Sand aggregation in residential area	8.66	10.789
House cleaning and repairs	60.79	75.9
Total	100	124.849

Dust that is shifted in a dust storm comes down on city surfaces. Some 30 to 40% of the dust that collects on the ground enters into houses which then need regular cleaning. Survey response showed that each person spends roughly four hours cleaning up his/her house after a dust storm, increasing the cost of cleaning by 50%. Some 74% of the

respondents pointed to dust as the cause of decrease in household equipment life and damage to electronic equipment. According to Miri *et al*., (2007), the total damage costs from dust storms during 2000 to 2004 in the Sistan region were estimated at 1213.976 million U.S.$ (Table 1.2).

1.9 Satellite observation of dust storms

The identification of dust aerosol sources, properties and transportation mechanisms over a wide scale is a difficult process, due to the complex natural and anthropogenic processes which are involved in entraining soil particles into the atmosphere during a dust transport event. Ground-based measurements of aerosol optical properties, such as spectral aerosol optical depth and column-mean particle size, are reported by the global sun photometer network AERONET (Aerosol Robotic Network). However, significant limitations of the surface observations are the single point measurements and the intermittency of the reported data. Data coming from surface stations are often unevenly distributed and are generally not available within active dust regions. Nonetheless, visibility measurements have been extensively used for the qualitative and quantitative characterization of dust loadings and transport routes (Sun *et al*., 2001; Zhang *et al*., 2003; Darmenova *et al*., 2005).

Monitoring of dust source region, transport pathways and plume characteristics is only possible from satellites because ground-based measurements are very limited in space and time (Kaskaoutis *et al*., 2008; 2010). Therefore, it is important to identify, also for prognostic purposes, the atmospheric circulation patterns facilitating the transport of dust particles from their source regions over distances of thousands of kilometers downwind. Compared to ground-based measurements, satellite observations offer a more efficient way of determining key characteristics of aerosols at temporal and spatial scales that are needed to study and monitor aerosol impacts upon the climate system. Traditionally, over land and, especially, over bright surfaces such as arid regions, retrieving aerosols from satellite observations is a challenging problem because one needs to separate the signal from the surface from that of aerosols, which requires precise characterization of the surface reflectance or emissivity. In addition, the aerosol products

greatly depend on the correct discrimination between aerosols and clouds, because aerosol retrievals are only possible in cloud-free conditions.

The Total Ozone Mapping Spectrometer (TOMS**)** sensor is able to map the global distribution of the major dust source regions with the aim to identify common environmental characteristics (Prospero *et al.*, 2002). Another satellite product for the detection of dust distributions is the Infrared Difference Dust Index (IDDI), which uses reductions in atmospheric brightness temperatures derived from Meteosat IR-channel measurements (Legrand *et al.*, 2001). Furthermore, Multi-angle Imagining Spectroradiometer (MISR) can retrieve aerosol properties over bright desert areas due to its unique capability of multi-wavelength observations at forward and backward directions (Kahn *et al.*, 2005). Recently, the new algorithm (deep blue) is able to obtain AOD values from Moderate Resolution Imaging Spectroradiometer (MODIS) over desert areas (Hsu *et al.*, 2004). Satellite imagery clearly shows that dust aerosols often cover very large areas. Indeed, the aerosol load associated with dust transport is higher than that attributed to pollution plumes. Furthermore, dust plumes that cover much larger areas, are more persistent, and occur more frequently than those associated with pollutant aerosols (Husar *et al.*, 1997).

However, dust properties are hard to be measured and difficult to be represented realistically by satellite remote sensing because size, shape, composition and regional distribution of dust vary over a wide range of spatial and temporal scales. Therefore, simultaneous measurements of dust chemical, physical, optical properties and related effects on climate are needed in order to support the satellite retrievals (Sokolik *et al.*, 2001; Kohfeld *et al.*, 2005). However, such measurements are very limited and are rarely performed in a coordinated fashion. The bulk of available data originates primarily from ground-based observations (including meteorological stations and short-term field measurements), and short-duration field campaigns that include ground-based measurements, aircraft observations and satellite remote sensing. The dust optical and physical properties (e.g. AOD, Angstrom exponent, size distribution, SSA, asymmetry parameter, refractive index, particle shape) are now well documented via both ground-based and satellite instruments. To this end, except from the experimental campaigns, the standardized networks (e.g. AERONET, European Aerosol Research Lidar Network (EARLINET**)**) have helped in continuing monitoring and analysis of the optical properties

of dust. The National Aeronautics and Space Administration (NASA) website (*http://www.visibleearth.nasa.gov/Atmosphere/Aerosols/*) has an archive of images of spectacular aerosol events, most devoted to dust events. Also, the NASA website (*http://earthobservatory.nasa.gov/NaturalHazards/*) provides several images of the most intense dust events, which are referred to as natural hazards along with floods, forest fires, cyclones, droughts, volcanoes, earthquakes, etc. These images can help the public and the scientists in developing their knowledge of the dust source regions, the dust transport and deposition and its optical properties. In order to improve the scientific knowledge on dust aerosols, their source regions and their effect on global climate, a worldwide effort has been undertaken in the last two decades to produce a global dust aerosol climatology by combining satellite observations (e.g. TOMS, MODIS, MISR) and measurements from ground-based monitoring networks (e.g. AERONET, EARLINET). In this thesis, the satellite monitoring of dust storms over Sistan region is also used along with in-situ measurements to provide deeper knowledge on the dust source region, transport pathways and optical properties of dust.

1.10 Aim, objective and structure of the thesis

The thesis aims at providing knowledge for the first time about the dust events, their source regions, transport pathways, optical properties, mineralogy and effects on human health over Sistan region and Hamoun Basin, located in southeastern Iran close to the Iran-Pakistan-Afghanistan borders. The main objectives of the thesis can be summarized in the followings:

1) Identification and quantification of the grain-size distributions of the dust flux loading over the Sistan region;

2) Identification of the variability of PM_{10} and $PM_{2.5}$ levels and interpretation of their environment and health impacts over the Sistan region;

3) Assessment of the chemical and mineralogical properties of dust particles;

4) Identification of the optical properties of dust storms using satellite observations;

The scientific objectives of the thesis are achieved in seven principal steps (Chapters):

Chapter 1 gives the general introduction and facts about dust storms (i.e. origin, climate implications, and optical properties of dust aerosols), provides some previous results regarding dust in the Middle East, Iran and the Sistan region and highlights the aim, objectives and structure of the thesis.

In Chapter 2, the focus is on the geography, meteorology and climatology of the Sistan Basin based mainly on meteorological data from the Zabol station. In this Chapter firstly, the geography of the Sistan basin is covered. It encompasses large mountains with altitudes of about 5000 m above mean see level in west Afghanistan to an elevation of about 400 m in the Sistan region in the eastern part of Iran. In this Chapter are discussed changes of Hamoun water surface as a main factor affecting of dust storms.

In Chapter 3, the horizontal dust loading of dust events is analyzed via ground-based instruments established in Sistan region. In this Chapter the Hamoun basin is defined as a major dust source region by focusing on the assessment of dust loading at two nearby locations in the Sistan region. The grain size is used to provide useful information regarding the status of Sistan's dust storms.

In order to understand the extent of dust's effects on the atmospheric environment and health and in order to put in place effective remedial policies and strategies, the chemical (composition and mineralogy) characterization of the Sistan aerosols is investigated in Chapter 4. The chemical analysis has been performed in laboratory using airborne and soil dust samples collected in the Sistan region and Hamoun Basin. In this Chapter, an overview of the temporal occurrences and geological-geochemical characteristics of airborne dust in the Sistan region are given. The chemical and mineralogical constituents carried out during major dust storms are analyzed to determine the relationship between the chemical constituents of the dust storms and those of the inferred (Hamoun) source soils, and to investigate atmospheric modifications from anthropogenic causes related to the dust storms in this region.

In Chapter 5, a temporal assessment of PM_{10} and $PM_{2.5}$ concentrations in the atmosphere above the cities of Zabol and Zahedan, which are effected by Sistan dust

storms, is performed. The PM concentrations at both cities were measured from and established dust-pollution monitoring network. This Chapter also includes an examination of the relationship between PM_{10} and $PM_{2.5}$ and the determination of the temporal variability of the Air Quality Index (AQI) over the region. The AQI is used to provide valuable information regarding the status of air quality and the associated health concerns for the public.

In Chapter 6 satellite remote sensing provides observational constraints for monitoring dust production and improving the understanding of the effects of regional-scale atmospheric processes on dust emission and transport over the Sistan as well as south west Asia. This Chapter analyses the aerosol patterns by means of multiple satellite platforms aiming to reveal the spatio-temporal and vertical distribution of dust aerosols. The dataset include records of Aerosol Index (AI) from the TOMS on board the Nimbus-7 (1979–92) and the Earth Probe (mid-1996 to 2005) satellites and 6-year AI records from OMI aboard Aura. Moreover, the AOD is analyzed through 11-year records from MISR aboard Terra (2000-2010) and from Deep Blue records from MODIS Terra (2000-2007) and MODIS Aqua (2002-2011). The main focus is to determine similarities and differences in dust climatology provided by these sensors over the Sistan region and surroundings.

The overall conclusions and future directions of research are summarized in Chapter 7.

CHAPTER 2

GEOGRAPHY, METEOROLOGY AND CLIMATOLOGY OF THE SISTAN BASIN

2.1 Geography of the Sistan Basin

The Sistan basin lies between the Hindu Kush Mountains in Afghanistan and the mountain ranges flanking the eastern border of Iran and is the depression that receives the discharge of the Helmand River in the lower Helmand Basin (Fig. 2.1) and was often described by explorers, military men and natural scientists of the 19th and early 20th centuries as one of the most desolate deserts on the globe**.** It is a large and remote desert basin**,** extremely arid and known for its windstorms, extreme floods and droughts; the lower Helmand Basin in Afghanistan (Fig. 2.1) is considered to be the easternmost extension of the Iranian Highlands. The closed basin receives the waters of the Helmand River, the only major perennial river in western Asia between the Tigris-Euphrates and Indus rivers. The Helmand and its tributary streams drain the southern Hindu Kush Mountains of Afghanistan and flow into an otherwise waterless basin of gravel plains and sandy tracts before terminating in Sistan (also Seistan, British spelling), a depression containing the large delta of the Helmand river and a series of shallow, semi-connected playas at the western edge of the basin (Fig. 2.2).

Extensive archeological ruins in the Helmand valley, on the Helmand delta and around the terminal lakes are evidence that the Helmand River was a major focal point for the development of early civilizations in western Asia. In fact, archeological excavations at Shahr-i Sokhta (Tosi 1973, 1976, Whitney, 2006), located at the edge of the Hamoun Helmand (Hamoun is a lake) (Fig. 2.2), revealed that human societies developed rudimentary irrigation systems and lived in proto-urban settings by 3,200 B.C., several centuries before the great Harappan cities of the Indus valley civilization appeared on the cultural horizon.

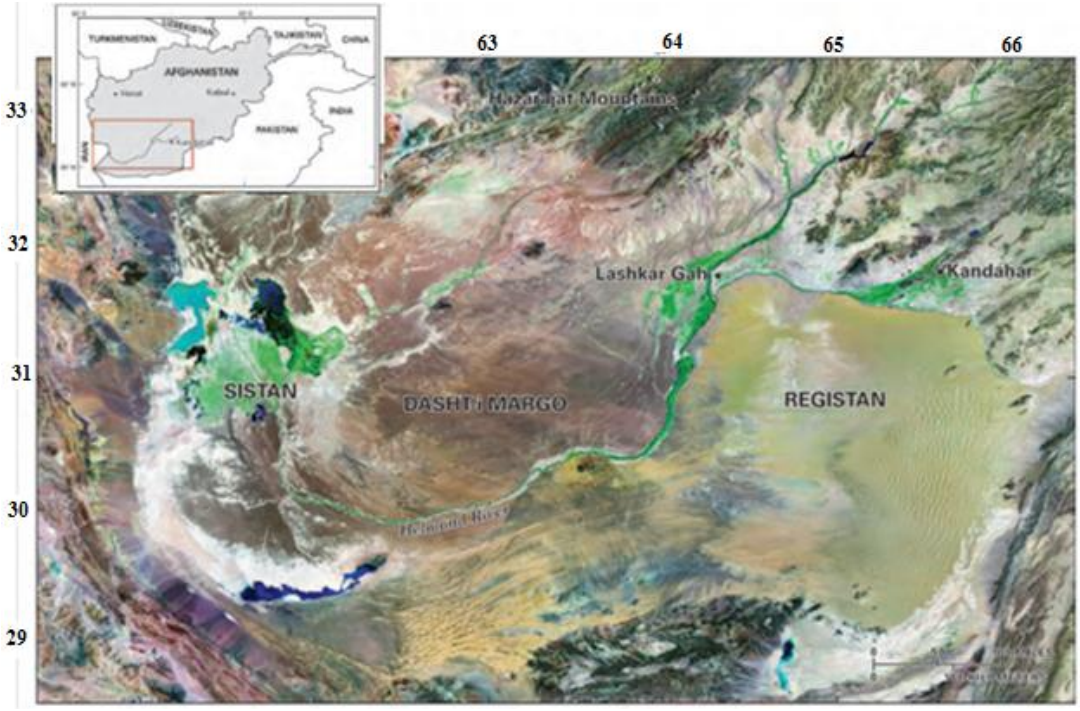

Figure 2.1: Landsat 5 image showing the lower reaches of the Helmand River which terminate in the Sistan Basin, and also the general Sistan region. Note that the Sistan Basin lies between the Hindu Kush ranges in Afghanistan (top right of image) and the mountain ranges flanking eastern Iran (lower left of image) (Sources: Whitney, 2006)

Figure 2.2: Topographic map and hydrological network and of Sistan Basin. The location of Zabol (a city in Sistan region) is indicated by the white circle (30° 57'N, 61° 34'E).

Sistan is also known historically as the "breadbasket of western Asia'' (Goldsmid, 1876). Agricultural civilizations have occupied the deltaic plains in Sistan intermittently and as late as the early 16th century A.D. After the early 16th century, Sistan was not restored to its former prosperity. At present, a large field of active barchan dunes overlies most of the agricultural plain on the Afghan side of the Helmand inland delta. This plain was once the most prosperous and densely populated tract in the delta region.

In 1949 the US initiated a new program for the improvement of underdeveloped areas of the world. The damming of the Helmand River in southern Afghanistan became one of the showcase projects of U.S. foreign aid in the "Third World" after World War II. Set up as the Helmand-Arghandab Valley Authority (HAVA), dams were built on the Helmand River and its main tributary (Arghandab River) during the 1950s. The project goals were to provide hydroelectric power, increased agricultural productivity through irrigation and land reclamation. The Arghandab dam, located northwest of the city of Kandahar, was completed in 1952 with a height of 145 feet (44.2 meters) and storage capacity of 388,000 acre-feet (478.6 million cubic meters). The larger Kajakai dam on the Helmand was completed a year later with a height of 300 feet (91.4 meters) and length of 919 feet (280 meters) and storage capacity of 1,495,000 acre-feet (1,844 million cubic meters). About 300 miles (482.8 kilometers) of concrete-lined canals were built to distribute the reservoir waters (Whitney, 2006)

The Sistan depression is covered by Quaternary sediments with a maximum thickness of about 500 m in the central part of the plain (Lashkaripour and Soloki, 2002). The main source of the Quaternary sediments is weathering of geological formations in the Hindu-Kush Mountains in the eastern part of Afghanistan that have been eroded by fluvial processes and with the detritus deposited in the plain where the topography is smooth with a low slope. The major portion of this sediment is made up of clay and silt. Therefore fine-grained soils including silt and clay as shown in Fig 2.3 are the main surface cover for the Sistan Basin. In view of the Hirmand and the surrounding rivers that supply most of the sediments to Sistan, a brief encapsulation of the relevant geology of the catchment area in Afghanistan is given. Afghanistan has a very complex geology, encompassing two major relatively young orogenies, Triassic and subsequent Himalayan, resulting in amalgamation of crustal blocks and formation of concomitant ophiolites and younger clastic and carbonate sedimentary rocks as well as basaltic lavas and, more recently, extensive

alluvial and eolian detritus (website, British Geological Survey; *http://bgs.ac.uk/*). Fig. 2.3 shows the geological map of the Sistan Basin. The Sistan region and Hamoun dry lake beds are mainly composed of Quaternary lacustrine silt and clay material as well as Holocene fluvial sand, silt and clay. These materials have been carried to the basin by the rivers, while along their courses Neogene fluvial sand, eolian sand, silt and clay are the main constituents. Note also the difference in the soil-dust composition between two major desert areas, Registan and Dasht-i-Margo in Afghanistan. The former is composed of Neogene coarse gravels and the latter of Quaternary eolian sand. This difference causes the different color in Landsat image (Fig. 2.1) between these two arid surfaces that contribute to the material deposited in the Sistan region. However, the Registan area has a pale color that differentiates this region from all the others, while at the Hamoun basin white-colored areas are observed, suggesting a dominance of sand, silt and clay. More details about the geology in the Sistan region can be found in Tirrul et al. (1983).

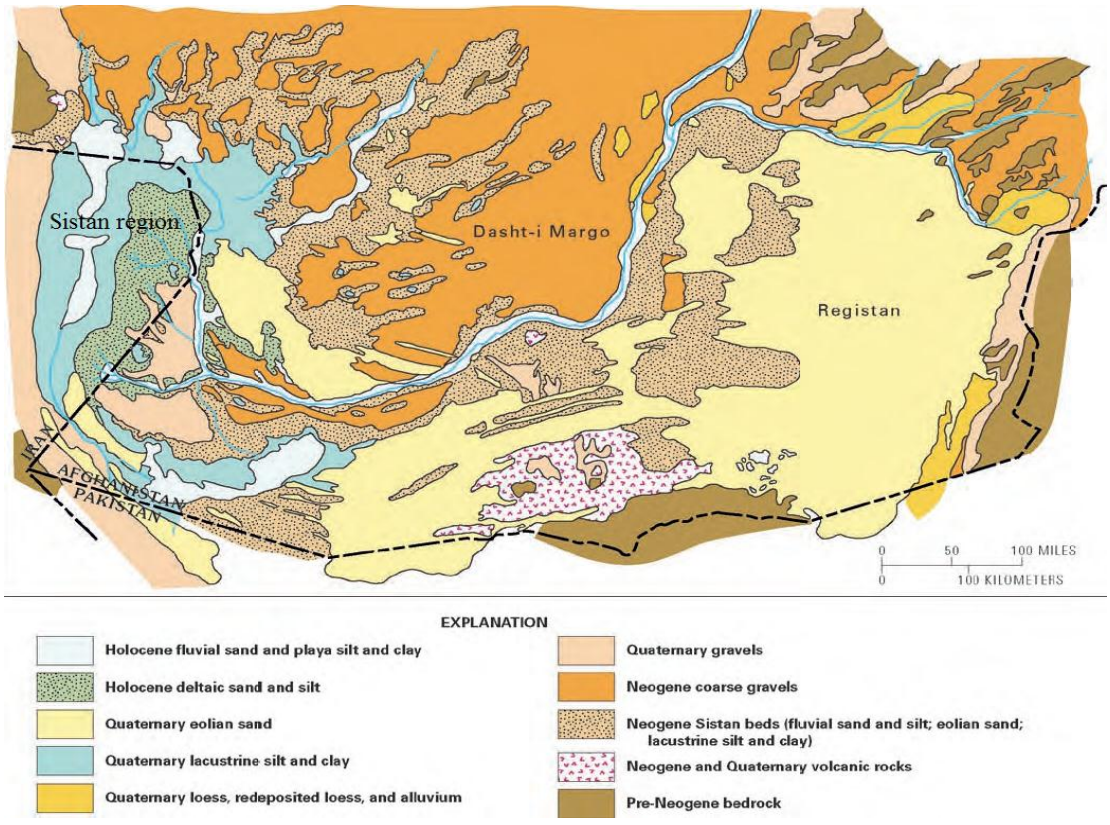

Figure 2.3. Geological map of the Sistan Basin Revised from Wittekind and Weippert (1973) and O'Leary and Whitney (2005a, b).

2.2 The Sistan region in Iran

The Sistan region (30°5' N - 31°28′ N and 61°15' E - 61°50' E), which is the main study area for this thesis is located close to the Iranian border with Pakistan and Afghanistan, in the south-eastern part of Iran in the north of the Sistan and Baluchistan provinces and east of the Sistan basin (Fig. 2.4). It covers an area of approximately 15,197 km^2 and has a population of about 400,000, of which half work in agricultural and animal domesticated fields. The economy is strongly dependent on agriculture and the goods and services provided by the wetlands. The Hirmand River from Afghanistan flows through Sistan Plain and irrigates the Sistan agriculture areas that are about 120,000ha in size, and finally discharges into the natural swamp of Hamoun (Fig. 2.3 to 2.4).

2.3 Hamoun Lakes

The Hamoun lakes (Fig. 2.4) are situated roughly at the termination of the Hirmand river's inland delta. The Hamoun lakes complex (Hamoun Puzak, Hamoun Sabori and Hamoun Hirmand and Baringak) are located in the north of the Sistan region, which is also the largest fresh water ecosystem of the Iranian Plateau and one of the first wetlands in the Ramsar Convention (Moghadamnia *et al*. 2009). Water in the Hamoun lakes is rarely more than 3 meters deep, while the size of the lakes varies both seasonally and from year to year. Maximum expansion takes place in late spring, following snowmelt and spring precipitation in the mountains. In years of exceptionally high runoff, the Hamoun lakes overflow their low divides and create one large lake that is approximately 160 km long and 8 to 25 km wide with nearly 4,500 km^2 of surface area. Overflow from this lake is carried southward into the normally dry Gaud-i Zirreh (Fig. 2.1), the lowest playa (463 meters above mean sea level) in the Sistan depression. Furthermore, mountain runoff varies considerably from year to year. In fact, the Hamoun lakes have completely dried up at least three times in the 20th century (Whitney, 2006). The maximum extent of the Hamoun lakes following large floods is shown in Fig. 2.4, where a continuous large lake has been created covering an extended area of ~4,500 km^2 with a volume of 13000 million m^3. This figure corresponds to spring of 1998 after snowmelt in the Afghanistan mountains that transferred large quantities of water into the Hamoun Basin. As a consequence, livelihoods in the Sistan region are strongly dependent on the wetland

products and services, as well as on agricultural activities in the Sistan plain. Fishing and hunting represent an important source of income for many households and, therefore, the local and regional economy is strongly dependent on weather conditions, precipitation and land use – land cover changes. The political boundary between Iran and Afghanistan splits the Hamoun system, further complicating management possibilities in the area. Most (90%) of the watershed is located in Afghanistan and practically all of the wetlands' water sources originate there. The Iranian part is desert, and produces runoff only in rare cases of significant local rainfall (UNEP, 2006).

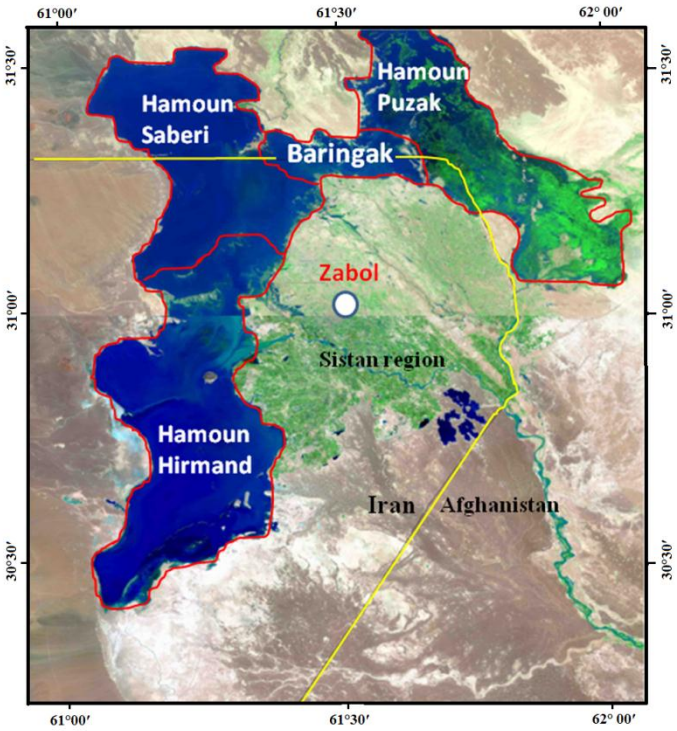

Figure 2.4. Position of the Hamoun Lakes in Iran and Afghanistan, showing a maximum inundation period.

2.4 Droughts in the Sistan Basin

The Sistan Basin has recently experienced an unusually long 10-year drought starting in 2000 (UNEP, 2003, 2006). Combined with war and severe political disruption over the past two decades, the 10-year drought has created conditions of widespread famine that affected many people in eastern Iran and southwestern Afghanistan. A suggested, climatic forcing mechanism has been proposed for the recent drought by

Barlow and others (2002). A prolonged El Niño-Southern Oscillation (ENSO) cold phase (known as La Niña) from 1998 to 2001 and unusually warm ocean waters in the western Pacific appear to have contributed to the prolonged drought. The unusually warm waters (warm pool) resulted in positive precipitation anomalies in the Indian Ocean and negative anomalies over central Afghanistan (Barlow *et al*., 2002), thus contributing to the drying of the Hamoun Basin. The contrast between a relatively wet year in 1976 and the nearly dry Hamoun lakes in 2001 is shown in Fig. 2.5. Millions of fish and unknown number of wildlife and cattle died. Agricultural fields and approximately 100 villages were abandoned, and many succumbed to blowing sand and moving dunes (Partow, 2003).

Most of the Sistan population lives near the Hamoun lakes and is employed in agricultural, fishery, handicrafts and other occupations. To counter the effects of droughts, the Iranian government prepared facilities such as food and flour supplies, medicine and health services and employment in the region to prevent the forced emigration of people, but the continuous and extreme droughts have forced some people to leave the Sistan region. Long droughts at the end of the 1960s, middle of the 1980s, and from 1999 to 2010 affected the Sistan region significantly and resulted in desiccation of the Hamoun lakes, making the surrounding lands saline and disturbing their soil fertility, while some places became barren (see Fig. 2.5). The most important findings in Fig. 2.5 are: (1) in 1976, the Hamoun lakes were still thriving. Dense reed beds appear as dark green, while tamarisk thickets fringing the margins of the upper lakes show up as pink shades in the satellite images (Fig. 2.6). Bright green patches represent irrigated agricultural lands, mainly wheat and barley. The lakes flood to an average depth of half a meter, denoted by lighter shades of blue, while dark blue to black indicates deeper waters, which, however, do not exceed four meters. (2) By 2001, the Hamoun lakes had vanished since central and southwest Asia were hit by the largest persistent drought anywhere in the world (Partow, 2003). The only sign of water in this scorched landscape of extensive salt flats (white) is the Chah Nimeh reservoir in the southern part of Sistan (see Fig. 2.4), which is now only used for drinking water. Degraded reed stands in muddy soil are visible as dark green hues at the southern end of Hamoun Puzak. In 2003 the Hamoun Basin was covered with water again, but with significantly lower coverage than in the mid-1976s (Partow, 2003).

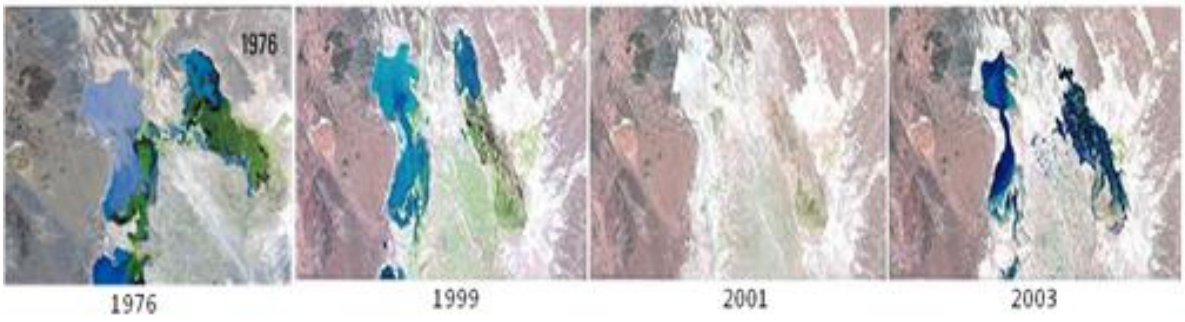

Figure 2.5: Satellite (Landsat) images of the Hamoun Basin in spring of different years. Hamoun lakes are fed primarily by water catchments in neighbouring Afghanistan. In 1976, when rivers in Afghanistan were flowing regularly, the lake's water level was relatively high. Between 1999 and 2011, however, drought conditions caused frequent dryness of the Hamoun lakes that almost disappeared in 2001 after a 3-year intense drought period (Sources: Partow, 2003)

Dust from the area of dry Hamoun lakes can be traced on satellite images moving across Afghanistan and over Pakistan. MODIS true color satellite images of the Sistan basin taken during the recent drought period capture striking evidence of strong aeolian erosion and dust generation in the depression (Fig. 2.6). The dust is silt from the bottom of the Hamoun lakes. Strong winds can easily scoop up the dried silt and carry it for hundreds or thousands of kilometres. Such dust storms appear to be increasing in frequency and severity. When the Hamoun lakes are dry, Sistan becomes a major contributor of global aerosols. The dried bed leaves a fine layer of sediment that is easily lifted by the wind (Ranjbar and Iranmanesh, 2008), thus modifying the basin to one of the most active sources of dust in southwest Asia (Middleton, 1986; Goudie and Middleton, 2000, 2006; Esmailli et al., 2006). Goudie and Middleton Middleton (2000) found that over 30 dust storms per year originate in Sistan, more than from any other area in southwest Asia. Therefore, the Hamoun dry lake beds exhibit large similarities with the other two major dust source regions of the world that comprise of dried lakes and topographic lows, i.e. Bodele depression in Chad (Koren *et al*., 2006) and lake Eyre in Australia (Baddock *et al*., 2009). The strong winds blow fine sand off the exposed Hamoun lake beds and deposit it to form huge dunes that may cover a hundred or more villages along the former lakeshore.

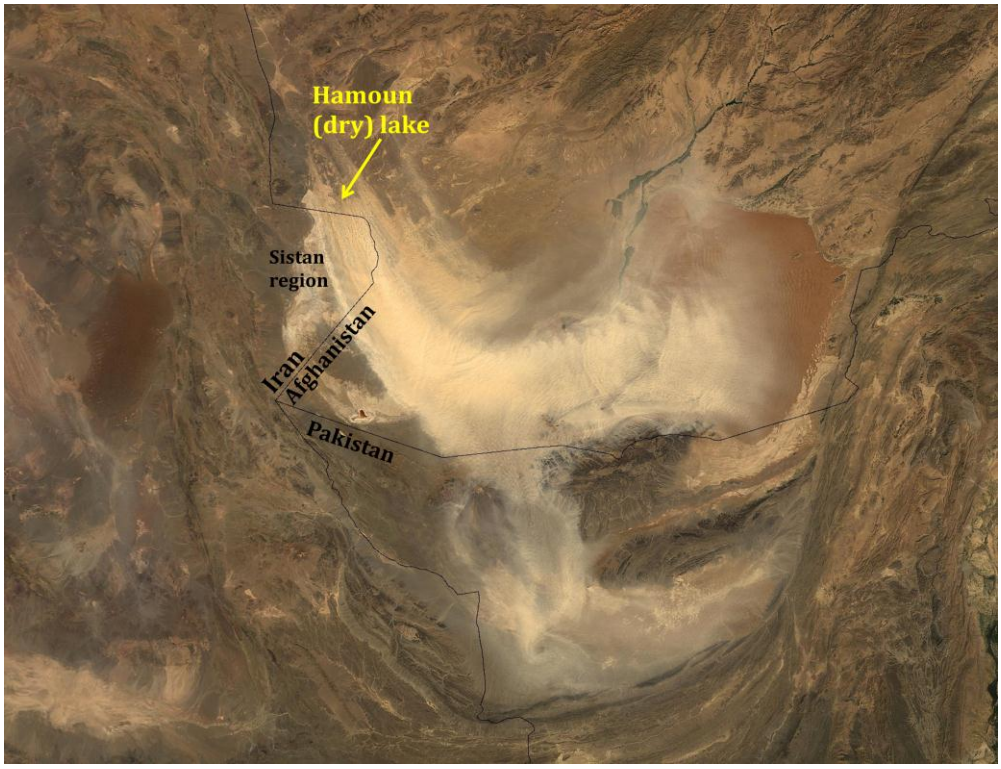

Figure 2.6. MODIS image (weather satellite) of dust deflation from the dry Hamoun lakes in Sistan on August 13, 2004. The intense dust plumes form a giant U shape that extends from Sistan into southern Afghanistan and southwestern Pakistan, and obscures the surface over much of the region. The pale color of the dust plume is consistent with that of dried wetland soils. The dust is blowing off the dry lake beds that become the Hamoun wetlands during wet years

2.5 Climatology of Sistan region

The current research failed to find an extensive study of the climatology of the Sistan region. However the climate of the Sistan region is often classified as totally dry. According to the Koppen and De Martonne methods, the climatology of Sistan is defined as dry, also definable as Saharan and mild desert when applying the Ivanove and Amberge methods, respectively. The mean annual precipitation (1963 to 2010) is 53 mm and in wet years this rate reached 120 mm. However, in some bad years there is almost no precipitation (e.g. 9 mm for 2001 to 2002). This low precipitation makes it impossible for any kind of farming. In these conditions an external water resource is needed and the Hirmand trans-boundary river plays such a role. The annual evaporation is more than 4 meters which underlines the vulnerability of the region to climate change, such as more droughts, or a decreasing flow discharge to the Hamoun lakes. This potential evaporation rate is among the highest rates recorded around the globe (Zawar-Reza *et al.*, 2006).

Sistan is also one of the windiest deserts in the world. In the Sistan depression, active wind erosion and/or sand movement occurs wherever vegetation is not supported by irrigation or ground water. The topography in Sistan has been and continues to be dominated by the interplay of aeolian and fluvial processes in the depression. Wind-eroded yardangs (McCauley *et al*., 1977) and dune fields are common features in Sistan. Active dunes presently cover most of the agricultural fields that supported multiple historical societies over the past 3,000 years (Whitney and Trousdale, 1982, 1984). Sistan inhabitants historically adapted to these winds. Nearly all structures were constructed with their long walls parallel to the north - northwest wind direction and during medieval times, uni-axle windmills were constructed for grinding grain. In modern Iranian Sistan, small wind intakes (bad geres) are built on the top of village houses as a form of air conditioning during the summer. However, summer winds blow steadily from the north and northwest and is locally called the bad-i-sad-o-bist ruz, or "Wind of 120 Days, or "Levar." The Levar wind over Sistan originates from the plains in Turkmenistan via the gap between the Alborz Mountain ranges and the Hindu Kush (Zawar reza *et al*., 2006). This wind has a significant effect on the landscape and the lives of the basin's inhabitants. Eolian erosional and depositional landforms dominate much of the desert basin and drifting sand has been a principal natural determinant in changing irrigation patterns and the location of agricultural endeavours.

The position of the summer low pressure (monsoon) system over the mountains in Pakistan is the principal reason that why high pressure air is drawn into Sistan from the Caspian Sea region (Ganji, 1968; Kendrew, 1961). Sivall (1977) compilation of pressure data in Afghanistan, however, shows that a significant heat low develops over the Dasht-i Margo (fig 2.2) independent of the heat low centered over western Pakistan near the town of Sibi, in the Indus plain. The position of this heat low over the basin explains the pattern and direction of dunes in the basin. Wind stream lines, as observed on Landsat images of south-western Afghanistan, curve in a counter clockwise motion from the Sar-o-Tar area to the Registan (Fig 2.2). Low, and isolated mountains along the southern edge of the basin cannot alone account for such a massive wind deflection. Thus, the wind direction is a direct consequence of the Dasht-i Margo thermal low. In a strict sense, the "Wind of 120 Days" is a trade wind that is accelerated and deflected by a local heat low before the dry, originally polar, air can reach the Intertropical Convergence Zone (ICZ), which is located

over the north-south-striking Sulaiman Mountains of Pakistan (Whitney, 2006). The Sulaiman mountains, and the mountains along the Makran coast, also serve as a southern barrier to the moisture-bearing monsoons. Occasionally, monsoons do invade the high mountainous areas of eastern Afghanistan and cause summer floods (Sivall, 1977). Some of this precipitation may enter Sistan from eastern tributaries of the Helmand River. The "Wind of 120 Days" or Levar is stronger in the Sistan region than over the rest of the Sistan Basin. Stronger winds are concentrated along the western edge of the basin because the wind accelerates along a long, narrow corridor between the mountains of Iran and Afghanistan. The "Levar" is felt further south in Baluchistan. However, its intensity is not as great. The maximum monthly mean wind speed at Nok Kundi, Pakistan, is about 4 $m.s^{-1}$ (Takahashi and Arakawa, 1981).

According to the members of the Sistan Arbitration Commission who have lived in Sistan from 1903 to 1905, the "Wind of 120 Days" blows almost constantly day and night during the hottest months of the year. Sustained, hurricane-force winds of 29 to 36 $m.s^{-1}$ are frequently experienced. One storm in 1905 recorded an average velocity of 39.3 $m.s^{-1}$ for a 16-hour period. During that storm, a maximum velocity of 53.6 $m.s^{-1}$ was recorded (McMahon, 1906). The pebbles, sand, dust and debris carried by the wind, plus its continual noise, make living conditions particularly uncomfortable during summer months

The approach of a windstorm is the same in summer as in winter. The days preceding the arrival of the storm become slightly, but detectably warmer and the air become still, or a slight breeze may blow from the southeast. Less than a day before the gale arrives, small cirrus clouds usually appear in the northwest. Strong winds may arrive suddenly, over a time interval of only a few minutes, or the winds may build strength over half a day. A marked rise in temperature normally accompanies the wind. However, when the strong winds abate, normally after several days, the air temperature is noticeably cooler. Calm days then begin to become more frequent and the temperature begins to rise again, seemingly initiating the next windstorm cycle (Whitney, 2006).

In the summer, daily winds blow on average at speeds of about 9 to 11 $m.s^{-1}$ (20 to 25 miles per hour), with gusts up to 18 to 22 ms^{-1} (40–50 miles per hour) (U.S. Agency for International Development, 1976). Evidence that these strong winds existed in historical times is attested to by dated deposits of eolian sand and by the standing remains of

windmills that are found both in and outside the delta region. The most commonly found windmills were built in the 14th to 15th centuries and were used to grind grain (Whitney and Trousdale, 1982, 1984).

The synoptic weather conditions are a consequence of the Indian thermal low that develops over the whole of south Asia during the summer monsoon, and which have a direct impact on the intensity of the winds over the region, which are as high as 12 ms^{-1} on a monthly mean basis during June and July (Fig. 2.9b), with gusts often above 20 to 25 ms^{-1}. In contrast, during late autumn and winter the wind speed is limited to ~3 to 4 ms^{-1}. Figure 2.7 shows wind roses for Zabol during the period 1963 to 2010. In all seasons, the northwestern flow clearly dominates, being more apparent in summer, while the high percentages for intense winds are also associated with the northwestern direction. In contrast, the possibility for intense winds blowing from other directions is very low. The summer winds are much stronger with ~27% of the wind speeds being above 11 ms^{-1}, while calm conditions are limited to 2.9% for summer against 8.0, 18.8% and 19.6% for Spring, autumn and winter, respectively. The higher frequency and intensity of the northwestern winds is the reason for frequent dust storms affecting Zabol that is located in the downwind direction of the dust storms that originates from the Hamoun lakes.

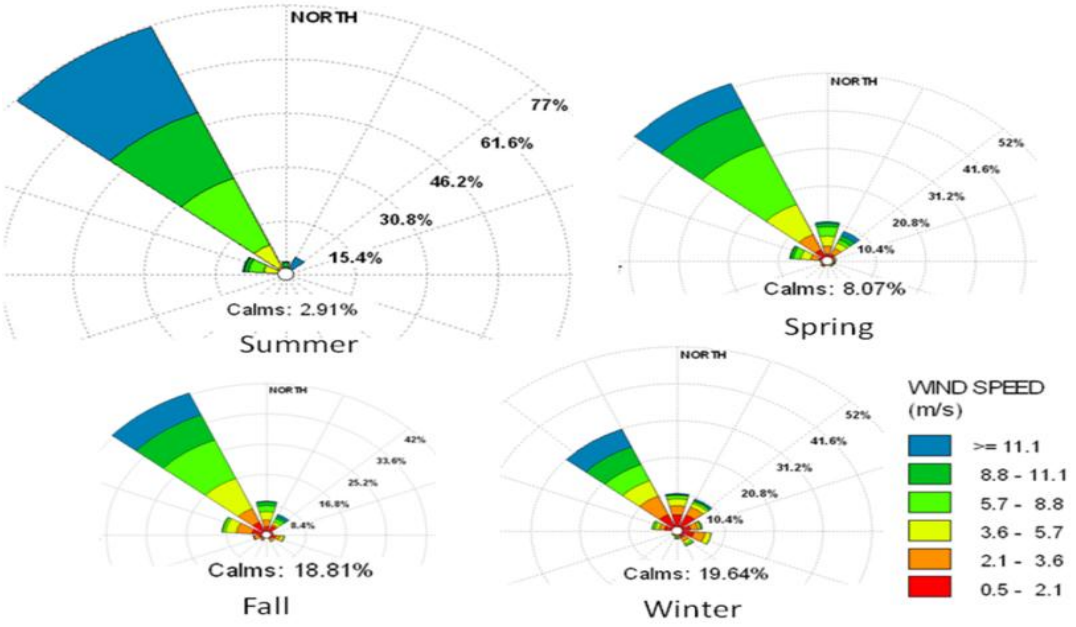

Figure 2.7: Wind roses of the seasonal wind speed and direction in Zabol during the period 1963 to 2010. The percentage of calm events is shown at the bottom of each wind rose. The thickest bar represents wind speeds in excess of 11 ms^{-1}).

The annual cycle of monthly average wind speed exhibits fairly large seasonal variation, with maximum values in summer (June to August) and minimum values during winter (December to February) (Fig 2.8). Continuance of the Levar wind in September also causes a high average wind speed for autumn. The diurnal cycle of the wind speed is high at 12 ms^{-1} at noon and then decreases to a minimum of 7ms^{-1} in the evening.

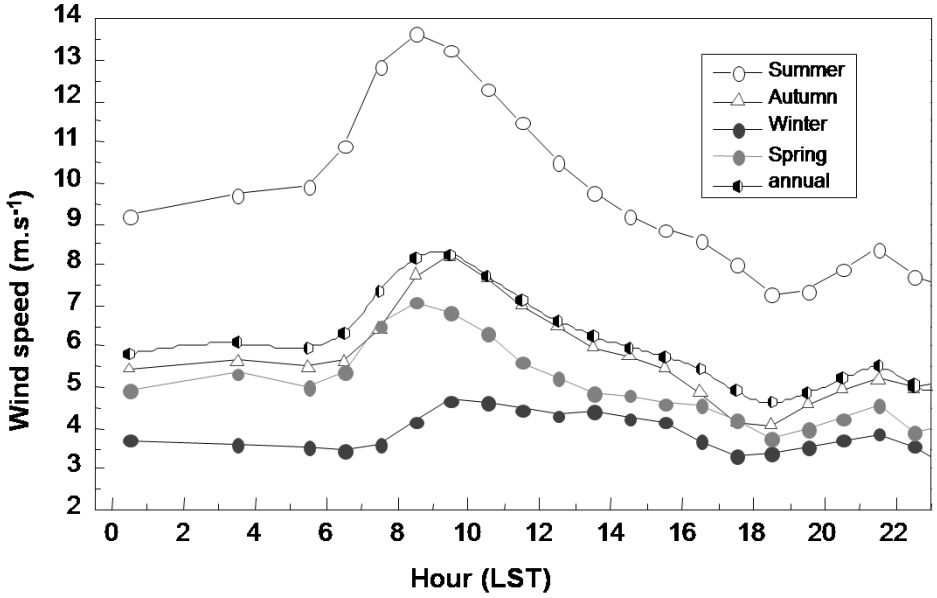

Figure 2.8: Diurnal cycle and seasonal variability in wind speed at Zabol.

Fig. 2.9a presents the annual mean variation of mean Temperature, Relative Humidity (RH) and atmospheric pressure over Zabol for the period 1963-2010. The monthly mean tempreture exhibits a clear annual pattern with low values in winter (9-12 ^{o}C) and high (~35 ^{o}C) in summer following the common pattern found in the northern Mid-latitudes. During the summer period the maximum tempreture often goes up to 46-48 ^{o}C causing an extremely large diurnal variation, characteristic of the desert environment. RH illustrates an inverse annual variation with larger values in winter (50-57%) and very low values in summer (~25%), which are about 10-15% during daytime. In Sistan, the atmospheric pressure presents generally high values in winter (1020-1024 hPa) and is above the mean sea level value of 1013.25 hPa during the period October to April, before starting to decrease during summer (June to August) season (~ 996 hPa in July). There is a considerable gradient between the low pressure system over Pakistan and the high pressure region over the Himalayas (Zawar reza et al., 2006), with flow directed towards

the Sistan basin. The gradient over the Sistan region itself is shallow. The geopotential height distribution over Sistan points to a generally northerly flow.

The annual variation of visibility follows an inverse pattern to that of wind speed (Fig. 2.9b), with large values in winter, usually above 10 km, and very low in summer (<4 km, on average). A decreasing curve relation associated with 93% of the variance holds between wind speed and visibility. This inverse relation indicates that the wind speed does not act as a ventilation mechanism over Zabol, as usually occurs in coastal urban environments with local sea-breeze cells (Adamopoulos *et al*., 2007), but rather as a factor responsible for the deterioration of visibility, since the intense Levar winds are the genetic cause for the dust outbreaks over Sistan.

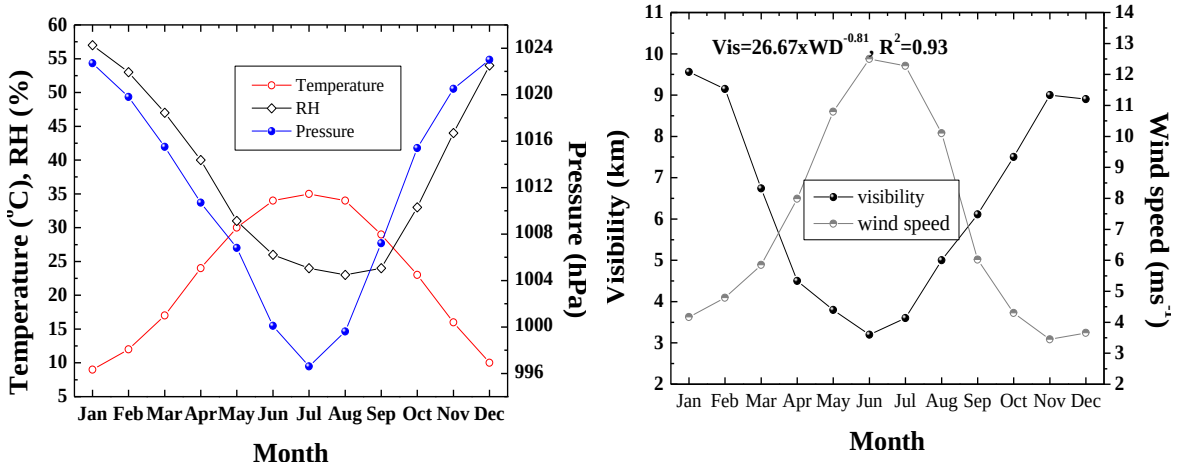

Figure 2.9. Monthly mean variation of air temperature, Relative Humidity (RH) and atmospheric pressure (a), and Visibility and wind speed (b) at Zabol over the period 1963 to 2010. R^2 is determination coefficient of linear regression between Visibility and wind speed.

Although the visibility exhibits a clear annual pattern (Fig. 2.9a), long-term data series over Zabol show that it also presents considerable year-to-year variations (Fig. 2.10b). Focusing on recent years, the days with visibility <= 2 km havingdramatically increased from about 20 during 1995 to 1999 to >100 in 2000 to 2001, following a severe drought period that dried the largest part of the Hamoun wetlands and favored alluvial uplift, the frequency and mass intensity of dust storms that affected the visibility over Sistan. In the 2000s, days with very low visibility seem to have decreased, but remaining above the standards of the climatological mean. Furthermore, except for the intensity, the duration of dust storms over Zabol exhibit a clear annual pattern with a higher duration in

June (about 50 hours on average) (Fig. 2.10a). In further contrast, during the period October to April dust storms are characterized by a low frequency and duration, below 5 hours, although in some cases they may still be intense.

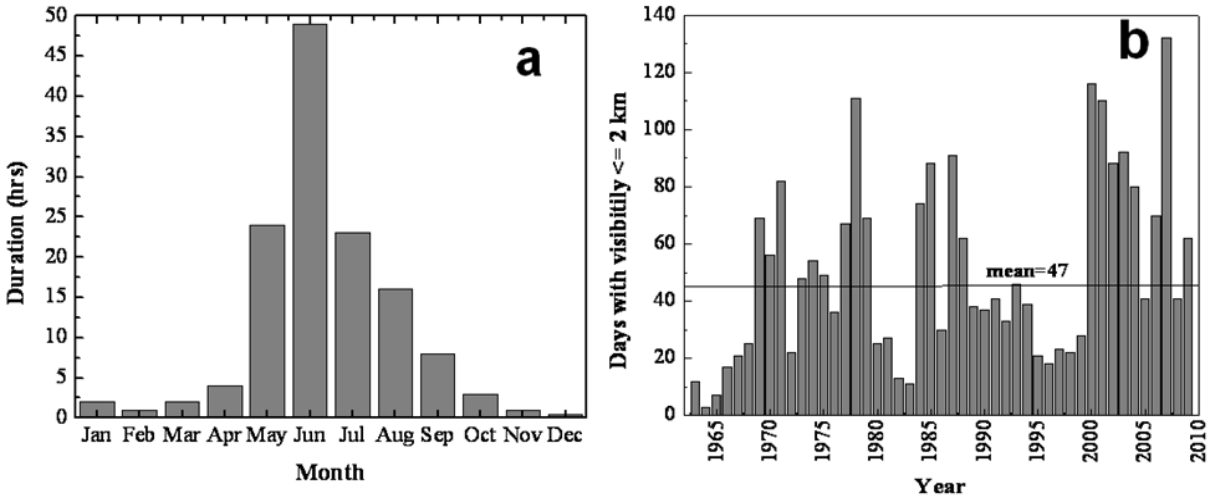

Figure 2.10: (a) Annual variation of the average duration of dust storms (in hours) over the period 1999 to 2010, and (b) year-to-year variation of the visibility recorded at Zabol

2.6 Temporal changes of Hamoun dry lake beds and dust storms

The water levels in the Hamoun lakes change considerably from year to year as has been discussed above. Table 2.1 summarizes the percentage of water surface in July in the Hamoun lakes, as well as the annual precipitation and number of dusty days during the period 1985-2005. Yearly variations of Hamoun lakes water surface identified four periods from 1985 to 2005: (UNEP, 2006):

1. A low-water period from 1985 to 1988: the Hamoun dried out or shrunk to a very small size almost every year, but there was some inflow every year.

2. A high-water period from 1989 to 1993: there was considerable inflow for five years, during which time the Hamoun only shrunk below the previous period's maximum levels for a very short time.

3. A medium-water period from 1994 to 1999: a dynamic balance of inflow and outflow maintained a reasonably high minimum water volume every year.

4. A dry period from 2000 to present: the inflow ceased and a catastrophic drought ensued except for a flood in 2005 that immediately dried up before 2006.

Table 2.1: Yearly variability of percentage of water surface in Hamoun lakes in July, annual precipitation and dusty days (visibility <= 2km) over Sistan region

Year	Baringak	Saberi	Hirmand	Puzak	precipitation	Dusty days
1985	0	30	7	35	25.6	88
1986	35	65	12	53	72.8	30
1987	25	40	2	53	8.7	91
1988	15	50	6	50	69.5	62
1989	90	92	60	54	26.1	38
1990	90	98	70	72	96.1	37
1991	80	95	90	80	85.8	41
1992	80	98	80	93	80.9	33
1993	75	95	70	60	52.4	46
1994	43	60	20	60	116.6	39
1995	48	66	7	62	76.2	21
1996	62	90	47	70	84.3	18
1997	60	85	25	60	76.4	23
1998	80	100	73	60	61.4	22
1999	72	90	25	60	87.7	28
2000	0	12	0	0	26.8	116
2001	0	0	0	0	7.2	110
2002	0	5	0	0	37.5	88
2003	0	0	0	0	32.3	92
2004	0	0	0	0	51.1	80
2005	80	90	18	32	129.5	41

The analysis (Table 2.2) shows that precipitation has a direct effect on water levels (correlation coefficient (r) =0.63 for Hamoun Saberi). That is, in years with high precipitation the lakes had high water surface. Hamoun Saberi is also affected by the Farah river that has a closer watershed, but this correlation is low for both Hamoun Hirmand and Hamoun Puzak (r = 0.35 and r =0.54 respectively). The correlation between dusty days and percentage of dried Hamoun beds (100-percent of water surface) (fig 2.11) shows high correlation coefficient values regarding Hamoun Saberi and Baringak (r =0.88 and r =0.82 respectively) and lower correlation for Hamoun Hirmand (r = 0.63). The high correlation for the Hamoun Saberi and Baringak indicates that Sistan dust storms are directly affected by the north and northwestern winds flowing through the Saberi.

Table 2.2: Correlations between percentage of Hamoun dried beds in July and number of dusty days (1985 to 2005).

Hamoun Lakes	Baringak	Hamoun Saberi	Hamoun Hirmand	Hamoun Puzak	Precipitation	Dusty days
Baringak	1					
Hamoun Saberi	0.96**	1				
Hamoun Hirmand	0.84**	0.80**	1			
Hamoun Puzak	0.80**	0.89**	0.74**	1		
Precipitation	-0.59**	-0.63**	-0.35	-0.54	1	
Dusty days	0.82**	0.88**	0.60**	0.81**	-0.730**	1

**. Correlation is significant at the 0.01 level

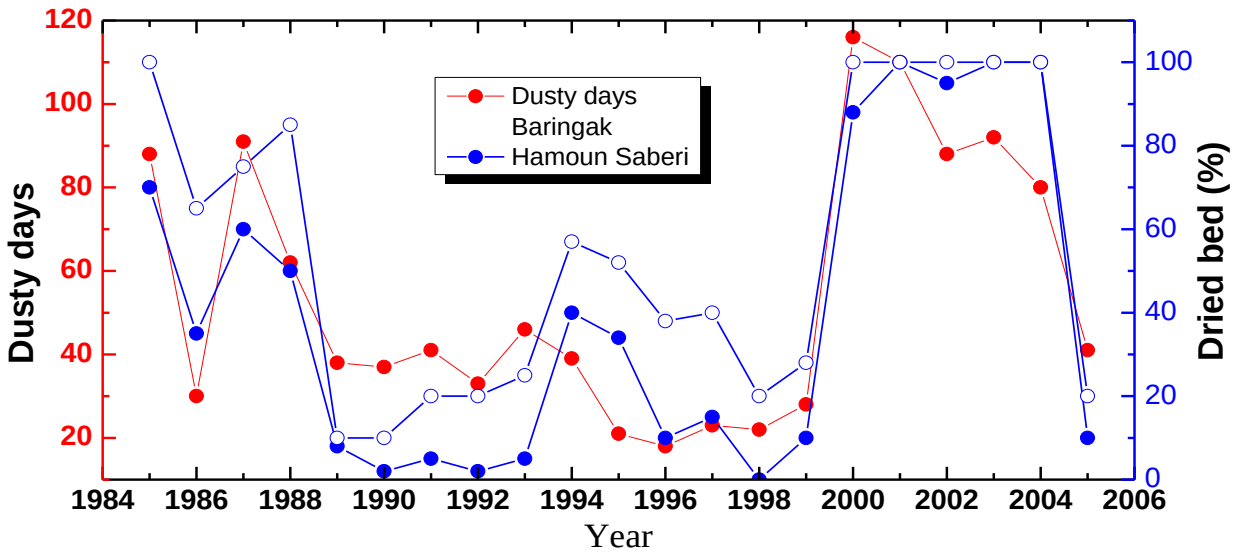

Figure 2.11: Yearly variability of the dusty days (visibility <= 2km) over Sistan region with association to percentage of Hamoun dried beds (1985 to 2005). The lower coverage of the Hamoun Basin by water (high percentage of dried beds) corresponds to higher number of dusty days over Sistan region.

CHAPTER 3

ASSESSMENT OF HORIZONTAL DUST FLUX LOADING OVER SISTAN

3.1 Introduction

Dust storms, as the most important source of mineral aerosols in the atmosphere, frequently occur in arid and semi-arid regions of the world, Dust storms are regarded as a serious environmental hazard (Prospero *et al.*, 2002). Each year, several billion tons of soil-dust is entrained into the atmosphere, playing a vital role in solar irradiance attenuation, and affects marine environments, atmospheric dynamics and even weather (Tegen and Fung, 1994, Tegen *et al.*, 1996; Dunion and Velden, 2004; Prasad *et al.*, 2007; Singh *et al.*, 2008; Patadia *et al.*, 2009).

Desert dust is considered to be a major component of tropospheric aerosols over the globe (Mishchenko and Geogdzhayev, 2007) with global flux estimations of 1500 to 2600 $Tg.yr^{-1}$ (IPCC, 2007). Estimates of dust emissions from the Sahara desert range from 130 to 760 Tg yr^{-1} (Goudie and Middleton, 2001), while another study (Ozer, 2001) estimated the annual Saharan dust emissions to be about 1600 Tg yr^{-1}. For comparison purposes the global dust emissions range from 1000 to 3000 Tg yr^{-1} (Zender *et al.*, 2004). On an annual basis, about 80 to 120 Tg of dust are transported to the Mediterranean area south of Europe (d' Almeida, 1986). Barnaba and Gobbi (2004) found a total seasonal mean value of 119 ktons of desert dust per day to be injected into the Mediterranean atmosphere, corresponding to a total of 4.3×10^4 ktons of dust in 2001. Anthropogenic sources were previously considered as important dust contributors (IPCC, 2001), but more recently (IPCC, 2007) were estimated to contribute only 5 to 7% of total mineral dust. The impact of dust aerosols in the Earth's system depends mainly on particle characteristics such as size, shape and mineralogy (Mahowald *et al.*, 2005), which are initially determined by the terrestrial sources from which the soil sediments are entrained and from their chemical composition (Claquin *et al.*, 1998). On the other hand, particle size distributions provide fundamental information for rock characterization and geological process, including

sedimentology, stratigraphy, structural geology, pedology and volcanology (e.g. Kandler *et al.*, 2009). Although, during recent years, satellite remote sensing of dust has been increasingly available with promising and reliable results, in-situ measurements for dust aerosol characteristics and dust loading are still considered absolutely essential. For this reason, several campaigns have been conducted in the arid areas of the globe, mainly focusing on the Sahara as the largest and most active dust source region. Although the dust activity and plume exposures from the Sahara to both the Atlantic and Mediterranean Oceans have been extensively investigated over the years, significantly fewer studies have been conducted over the Middle East and southwest Asia.

This Chapter aims at defining the Hamoun basin as a major dust source region by focusing on the assessment of dust loading at two nearby locations. The experimental campaign took place from August 2009 to July 2010, a period when the dust loading at different altitudes during major dust events from the Hamoun basin were measured. The grain size is used to provide useful information regarding the status of Sistan's dust storms. Such studies are currently lacking in this region, and the work in this thesis is the very first that examines the evolution of dust sediments over the Sistan arid environment.

3.2 Horizontal dust flux loading measurements

The measurement of amounts of dust flux is one of the most problematic procedures in dust studies. Airborne dust concentration, for example, is usually calculated from horizontal flux data. Also, the rate of deposition of particles on the surface is a direct function of both the vertical and the horizontal dust flux. Vertical dust flux samplers have been extensively described in literature (Clements *et al.*, 1963; Köhler and Fleck, 1963; Clough, 1975; Ganor, 1975; Ralph and Barrett, 1976; Skärby, 1977; Goodman *et al.*, 1979; Bücher, 1986; Hall and Waters, 1986; Hall and Upton, 1988; Goossens and Offer, 1990; Orange *et al.*, 1990; Pye, 1992; Offer *et al.*, 1992; Goossens and Offer, 1993; Littmann, 1997). Vertical samplers are usually passive, i.e., the air is not actively sucked into the trap.

On the other hand, horizontal dust flux samplers have been described by Steen (1977), Wilson and Cooke (1980), White (1982), Fryrear, (1986), Ralph and Hall, (1989), Stout and Fryrear (1989), Janssen and Tetzlaff, (1991), Leys and Raupach, (1991),

Nickling and Gillies (1993), Shao *et al.* (1993) and Hall *et al.*, (1994). These are all passive devices, except for the samplers used by Nickling and Gillies, (1993) and Leys and Raupach, (1991), which use pumping to maintain airflow through a trap.

3.3 Description of the dust samplers

3.3.1 Big Spring Number Eight (BSNE) sampler

The Big Spring Number Eight (BSNE) sampler was developed by Fryrear, (1986). Although it was originally designed to collect airborne dust, it is now also frequently used to collect soil and sand. A picture and a technical diagram is shown in Fig. 3.1. Dust-laden air passes through a vertical 2 cm×5 cm sampler opening. Once inside the sampler, air speed is reduced and the dust settles in a collection pan. Air discharges through a 60-mesh screen. An 18-mesh screen reduces the movement of the deposited material, preventing breakdown of the collected sediment and potential loss of very fine particles out of the top of the screen. A rubber retainer closes any small holes in the back or front of the assembled sampler. A wind vane at the rear insures the sampler is turned to the wind. More details about the sampler can be found in the original description by Fryrear, (1986).

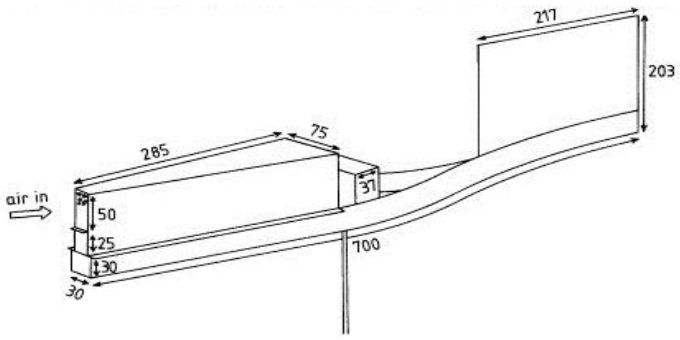

Figure 3.1: Construction of the Big Spring Number Eight (BSNE) sampler. Dimensions are in mm

3.3.2 SUspended Sediment TRAp (SUSTRA) sampler

The SUspended Sediment TRAp (SUSTRA) was developed by Janssen and Tetzlaff, (1991). Similar to the BSNE, it is now used for the collection of different types of sediment (dust, sand and soil). A picture and a technical diagram is shown in Fig. 3.2. The dust-laden air enters the instrument via a horizontal metal tube 5 cm in diameter and rebounds onto a metal plate inside a central vertical pipe. Particles settle onto a plastic dish

placed on top of an electronic balance underneath the pipe, except the finest ones, which may leave the sampler via a small outlet on top of the pipe (together with the air discharging from the instrument). Similar to the BSNE, a wind vane turns the instrument into the wind at all times. To minimise airflow disturbance near the surface, the balance is placed in a metal box dug into the ground. In the original version the horizontal inlet tube is at a height of about 23 cm above the surface, but this value can be adjusted while digging the balance box into the ground. More details on the instrument are described in the original paper by Janssen and Tetzlaff, (1991).

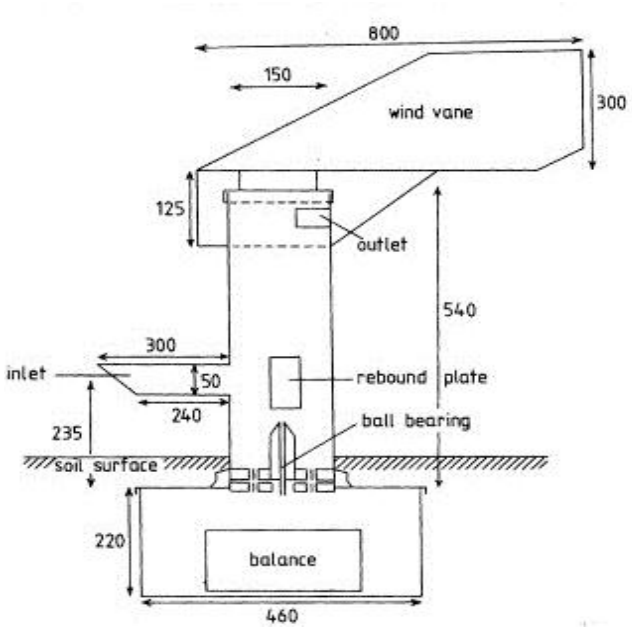

Figure 3.2: Construction of the SUspended Sediment TRAp (SUSTRA) sampler. Dimensions are in mm

3.3.3 Modified Wilson and Cooke (MWAC) sampler

The Modified Wilson and Cooke (MWAC) sampler is based on an original design developed by Wilson and Cooke, (1980). The sampler consists of a plastic bottle, figuring as settling chamber, to which an inlet tube and an outlet tube have been added (Fig. 3.3). The bottle is installed vertically, with the inlet oriented to the wind. Sediment entering the bottle will be deposited due to the pressure drop created by the difference in diameter between the bottle and the inlet and outlet tubes. The clean air then discharges from the bottle via the outlet.

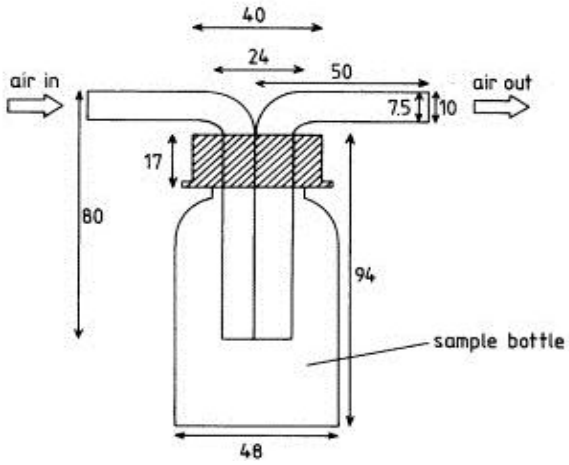

Figure 3.3: Sketch and construction of the Modified Wilson and Cooke (MWAC) sampler. Dimensions is in mm

The original concept was later slightly modified by Kuntze *et al.*, (1990), who attached the bottle in a horizontal (not vertical) position to a mast provided with a wind vane. By attaching several bottles at different levels to the mast, vertical flux profiles can be measured (Sterk, 1993).

3.3.4 Wedge Dust Flux Gauge (WDFG) sampler

The Wedge Dust Flux Gauge (WDFG) was developed by Hall *et al.*, (1994). A picture and a technical diagram is shown in Fig. 3.4. The WDFG consists of a simple, parallel sided box, wedge shaped in elevation and with extended sides towards the rear holding a baffle plate. The flat, horizontal bottom of the box is 18 cm long and 10 cm wide.

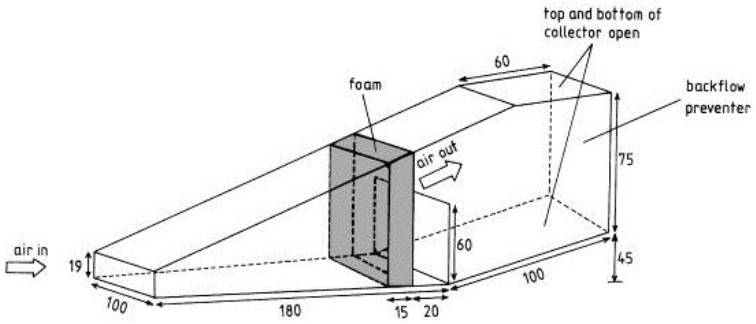

Figure 3.4: Sketch and construction scheme of the Wedge Dust Flux Gauge (WDFG) sampler. Dimensions is in mm

The top slopes upwards at an angle of 24.5°. Sediment-laden air enters the instrument via a 1.9×10.0 cm rectangular slot. The box contains a particle trap made from

10 pores in^{-1} open-celled foam, which is normally sprayed with a thin sticky coating to retain any impacting particle. More details about the WDFG can be found in the original description by Hall *et al*. (1994).

3.3.5 Siphon Sand and Dust Sampler (SSDS) sampler

The Siphon Sand and Dust Sampler (SSDS) was developed by Ekhtesasi (2003), which he later slightly modified (Ekhtesasi *et al*., 2009). The sampler consists of a tube with a diameter of 9 cm. The sediment-laden air passes through a vertical 4 cm x 6 cm sampler opening in the middle. Inside the sampler, air speed is reduced and the particles settle in a collection pan at the bottom, while the air discharges through an outlet with a U shape.

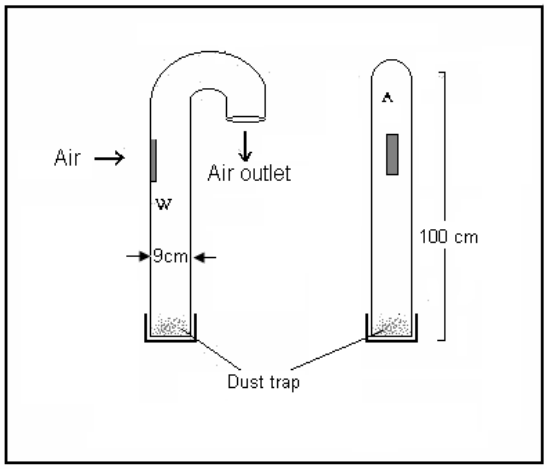

Figure 3.5: Construction of the Siphon Sand and Dust Sampler (SSDS) sampler

3.4 Particle-size analysis

Particle-size distribution is a key parameter determining the entire process of dust storms and wind erosion, from entrainment through transport to deposition. It can be estimated from either a geometric or the dynamic point of view. From the geometric perspective, particle-size distributions can be determined using one of three methods: (a) dry or wet sieving; (b) electro-optical techniques, including Coulter Counter analysis and laser granulometry, and (c) computerised image analysis. From the dynamic perspective, the distribution of the particle terminal velocity can be measured using a settling tube or an elutriator. The choice of the most appropriate method depends largely on the amount of fine material present in the soil sample and the intended applications of the data set.

Samples which contain only small amounts of fine material can be analysed through dry-sieving or settling-tube analysis, whereas Coulter-Counter analysis or laser granulometry are more adequate if the sample contains a significant quantity of dust particles. Image analysis can be employed if both size and shape information is needed.

3.4.1 Dry sieving

Dry sieving is undertaken using a stack of successively-finer sieves, which are mounted on an electrically-powered shaker (Pye and Tsoar, 1990). The shakers have simple vibrating, rotating and tilting actions or have a hammer action. Each sieve consists of a stainless-steel, brass, phosphor-bronze or nylon mesh. The optimum size used for dry sieving depends on the number of sieves and the dimensions of the mesh aperture. Standard permissible sieve-loading according to the British Standards Institution is given in Table 3.1.

Table 3.1: Recommended sieve aperture and maximum permissible sieve loading

Mesh(mm)	20	14	10	6.3	5	3.35	2.0
Load(Kg)	2.0	1.5	1.0	0.75	0.5	0.3	0.2
Mesh(mm)	1.18	0.6	0.425	0.3	0.212	0.15	0.063
Load(Kg)	0.1	0.075	0.075	0.05	0.05	0.04	0.025

3.4.2 Electro-Sensing Methods

One of the instruments used for particle-size analysis is the Coulter Multisizer. The instrument is best suited for handling small samples with a narrow particle-size range. For such samples, the time required for the analysis is short, the resolution is very high, and the reproducibility is good. The Multisizer is less well-suited to samples with a broad particle-size range.

The Coulter Multisizer is based on the Coulter principle (Fig. 3.6). The number and size of particles are measured by suspending the sample in a conductive liquid and measuring the electrical current between two electrodes on either side of a small aperture, through which particles are sucked. As each particle passes through the sensing zone and aperture it changes the impedance of the current between the two electrodes, producing a pulse with a magnitude proportional to the particle volume. These current pulses are

scaled, counted and accumulated in 256 size-related channels from which a particle-size distribution is produced. The Coulter Multisizer produces size distributions in terms of volume, number and particle surface area.

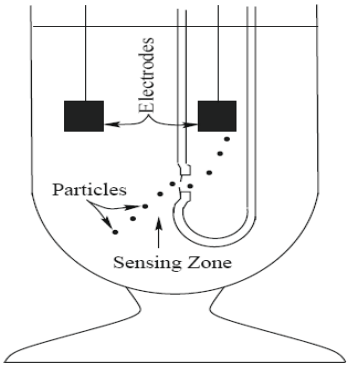

Figure 3.6: Illustration of the electrical sensing zone, showing an aperture tube immersed in an electrolyte with particles passing through the aperture (Redrawn from McTainsh *et al.*, 1997)

The nature of sample pre-treatment has a significant effect on the results of the analyses. As the sample must be analysed in a liquid electrolyte [3% tri-sodium orthophosphate (Na_3PO_412H2O) plus 50% glycerol], the Coulter Multisizer cannot perform undispersed particle-size analyses, i.e., the analyses are always more or less dispersed. If the analysis is done without intentionally dispersing the sample through additional chemical or physical treatments, it is called minimally-dispersed and the resultant particle-size distribution is referred to as the minimally-dispersed particle-size distribution. For most soils, this is probably not too different from the in-situ particle-size distribution or the best approximation to it currently available. For the fully-dispersed analysis, the soil sample receives chemical and vigorous physical dispersions to reduce it to its fundamental particle-size constituents. A typical chemical treatment is to place the sample in a soil dispersant, such as 3% tri-sodium orthophosphate and 1M sodium hydroxide (NaOH). The particle-size analysis of the soil sample after the chemical and physical treatments gives the fully-dispersed particle-size distribution. This particle-size distribution is the best approximation available for that of the sediment during a very strong wind-erosion event. In wind-erosion modelling, the fully-dispersed particle-size analysis is used to estimate the mass fraction of dust in a given soil (Shao, 2010).

One of the advantages of the Coulter Multisizer is its capacity to analyze samples in very small quantities down to about 0.1 g, while other particle-size analysis techniques, such as hydrometer and sieve analyses, require samples up to 30 g. This feature of the

Coulter Multisizer allows the particle-size analysis of sediment samples collected using high-volume samplers. The Coulter Multisizer also produces a relatively-high resolution for particle-size analysis, since particles are sized into 256 classes. The multisizer can measure particles over a size range from 0.45 to 1200µm, but there are practical difficulties with analyses at the coarse end (>150 µm), and the Multisizer appears to underestimate the clay fraction (<2 µm) (McTainsh *et al*., 1997). For the <2 µm fraction, pipette analysis can be performed instead.

3.4.3 Laser granulometry

Laser granulometry is based on the principle that there is a direct relationship between the size of particles and the degree to which they diffract light. In the case of the Malvern Instruments Laser Particle Sizer Type 3600E, a beam of monochromatic light (wave length 633 nm) is passed through a cell containing the sample in suspension and the diffracted light is focused onto a detector which senses the angular distribution of scattered light energy (McCave *et al*., 1986). The size range detected depends on the focal length of the focusing lens, which is placed between the sample cell and the detector. Grains are kept in suspension by a mechanical stirring device. Three lenses are available, each of which divides the distribution into 15 size classes. The 300 mm focal length lens has a range of 5.8 to 560 µm and is therefore most appropriate for sands. However, the coarsest of the 15 class intervals have a very wide range (261 to 264 µm).

3.4.4 Abrasion emitter

The dust-emission potential of a given soil is the mass fraction of dust particles that can be released during the process of wind erosion. It is a key quantity to be determined for dust-emission modelling. This potential is related to the observation that different techniques for particle-size analysis produce different particle-size distributions, depending on the degree of the mechanical and/or chemical destructions applied to the soil sample. To approximate dust-emission potential, Lu and Shao (1999) introduced the concept of minimally-disturbed and fully-disturbed particle-size distributions. However, it is not exactly clear what laboratory methods should be used to determine these two particle-size distributions. Shao (2001) assumed that they can be approximated, respectively by using the minimally-dispersed particle size distribution and fully-dispersed particle-size distribution. This assumption now appears to be questionable, because

evidence suggests that the effect of saltation bombardment, even under strong wind conditions, is likely to be much weaker than that of chemical treatment in the laboratory (Fig. 3.7b).

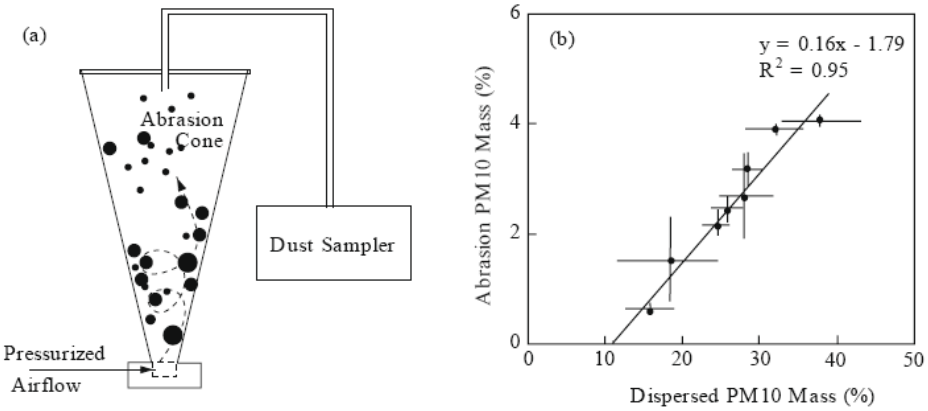

Figure 3.7: (a) A schematic illustration of an abrasion emitter; (b) Emission potential for PM10 for 8 soils plotted against the corresponding PM10 mass fractions determined using a dispersed analysis technique (Redrawn from Chandler *et al*., 2002)

Chandler *et al*. (2002) designed a laboratory technique for measuring dust-emission potential. This technique deserves particular attention. The instrument they used couples an abrasion emitter with a dust sampler, e.g. a Tapered Element Oscillating Microbalance or an Optical Particle Counter (Fig. 3.7a). The abrasion emitter is a stainless steel cone attached to a pressurised airflow which can be regulated. The soil sample is placed in a cup located close to the base of the cone. The top of the cone is closed with a plate, and a tube is inserted through the plate to aspirate air from the cone for monitoring dust emission. The pressured airflow fluidizes the soil sample in the cup and propels the particles upward in a rotating motion inside the cone. Abrasion takes place as the particles tumble and slide along the interior surface of the cone. The dust-emission potential of the tested soil is then determined as the ratio of the mass collected by the dust sampler over a run (about one hour) to the mass of the soil sample (Shao, 2010).

3.5 Data set and experimental methods

3.5.1 Dust loading measurements and mass quantities

The amount of dust loadings during dust storms was measured using passive dust samplers (Fig.3.9a) fixed at two monitoring towers (respectively, at four and eight meters above ground level in altitude), with one meter distance between the adjacent individual traps. The four meters tower had four traps and the eight meters tower had eight traps (Fig. 3.9b). The measurements were done during the period August 2009 to July 2010. The towers were erected at two open locations near Hamoun (31.08^{o}N, 61.54^{o}E and 31.26^{o} N, 61.76^{o}E), which are sufficiently distant from any obstacles which ensured that undisturbed wind flow could enter for taking representative dust samples (station A and station B, denoted by red stars in Fig. 3.8).

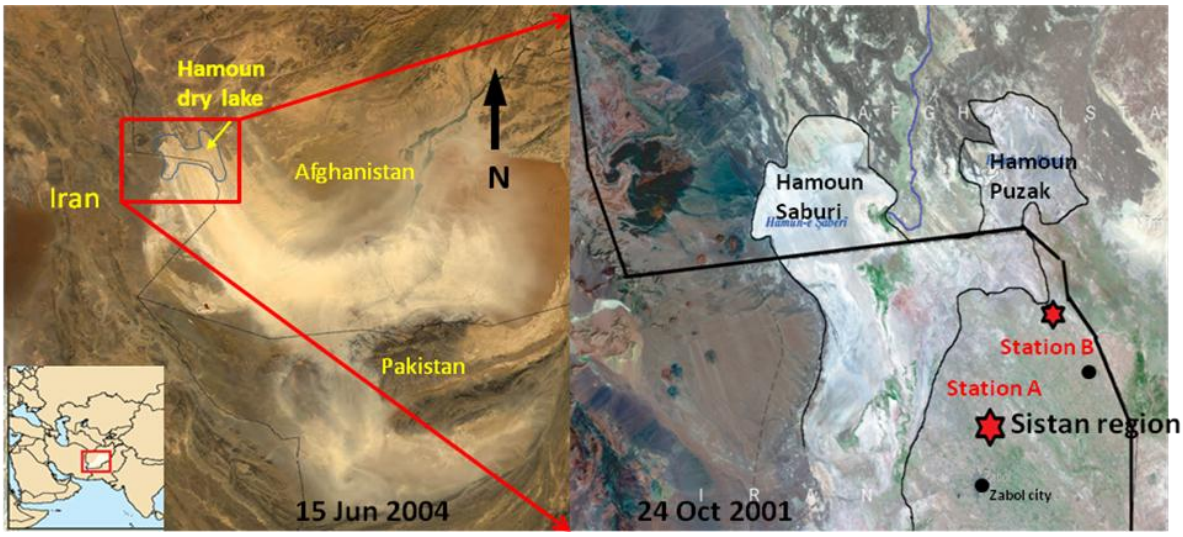

Figure 3.8: Locations of the dust loading measurement stations (stations A and B). The left image shows an intense dust storm that originated from the Hamoun basin on 15 June 2004 (Terra MODIS satellite image), while the right image zooms in on the Hamoun wetlands on 24 October 2004.

The dust sampler used in the campaign was developed by the Agricultural and Natural Research Center of Sistan, and is a modified version of the SUSTRA sampler (Janssen and Tetzlaff, 1991) and the SSDS sampler (Ekhtesasi *et al*., 2006; 2009). At the observation sites, the samplers collect airborne dust sediment. The traps were mounted on a stable bracket parallel to the wind direction. The samplers consist of a tube with a diameter of 12 cm. The sediment-laden air passes through a vertical 2.5 cm x 6 cm

sampler opening in the middle. Inside the sampler, air speed is reduced and the particles settle in a collection pan at the bottom, while the air discharges through an outlet with a U shape. After each measurement, the samplers were evacuated to make them ready for measuring the following dust events. The collected samples were oven dried at 105 ^{o}C for 24 hours, and then, dried samples were weighed using an electronic scale with 0.001 g precision in order to obtain total mass quantities at each sampling height and for each dust storm.

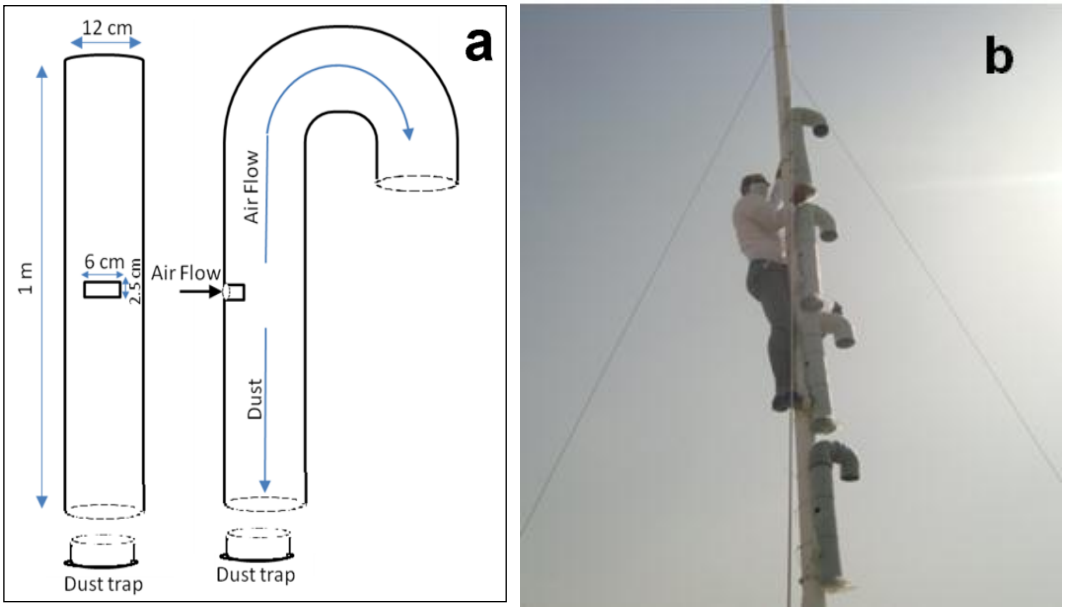

Figure 3.9: Schematic diagram of (a) the dust sampler system and (b) photo of the eight meters dust monitoring tower.

3.5.2 Particle-size analysis

The particle-size distribution of the collected samples was determined with a Malvern Mastersizer 2000 analyzer (Fig 3.10) with a measurement range of 0.02 to 2000 µm at Lanzhou University, China. The samples were pre-treated with 10 to 20 ml of 30% H_2O_2 to remove organic matter and then with 10 ml of 10% Hydrochloric acid (HCl) to remove carbonates. Then, about 2000 ml of de-ionized water was added and the sample solution was kept for about 24 h to rinse acidic ions. The residue sample was finally treated with 100 ml of 0.05 M $(NaPO_3)_6$ on an ultrasonic vibrator for 10 min to facilitate dispersion before grain-size analysis. The Mastersizer 2000 automatically yields the

median diameter and the percentages of the related size fractions of a sample with a relative error of less than 1%.

Figure 3.10: Measurement of dust particle-size using the Malvern Mastersizer 2000 analyzer (Lanzhou University, China).

3.6 Results and discussion

3.6.1 Dust loading measurements

Dust activity is a function of several parameters, such as topography, rainfall, soil moisture, surface winds, regional meteorology, boundary layer height and convective activity (Middleton and Goudie, 2001; Knippertz *et al*., 2009). The dust loading measured at the two stations close to the Hamoun basin for several dust events during the period August 2009 to July 2010 is plotted in Fig. 3.11. In the same graph, meteorological data from the Zabol station that give information about the duration of dust events (for the examined days as well as in the preceding or succeeding days) and daily mean and maximum wind speeds, are also plotted.

The results of the average dust loading measured at eight heights at station B and at four heights at station A reveals considerable variation, ranging from ~0.10 to ~2.5 kgm^{-2}. The average dust loadings for all the examined days were found to be 0.89 $kg.m^{-2}$ (station A) and 0.93 kgm^{-2} (station B), which do not exhibit a statistically significant difference. In general, the highest dust loading is observed for dust events occurring in summer, but

intense dust storms can also take place in winter, since the Hamoun basin is located in an active dust source region throughout the year.

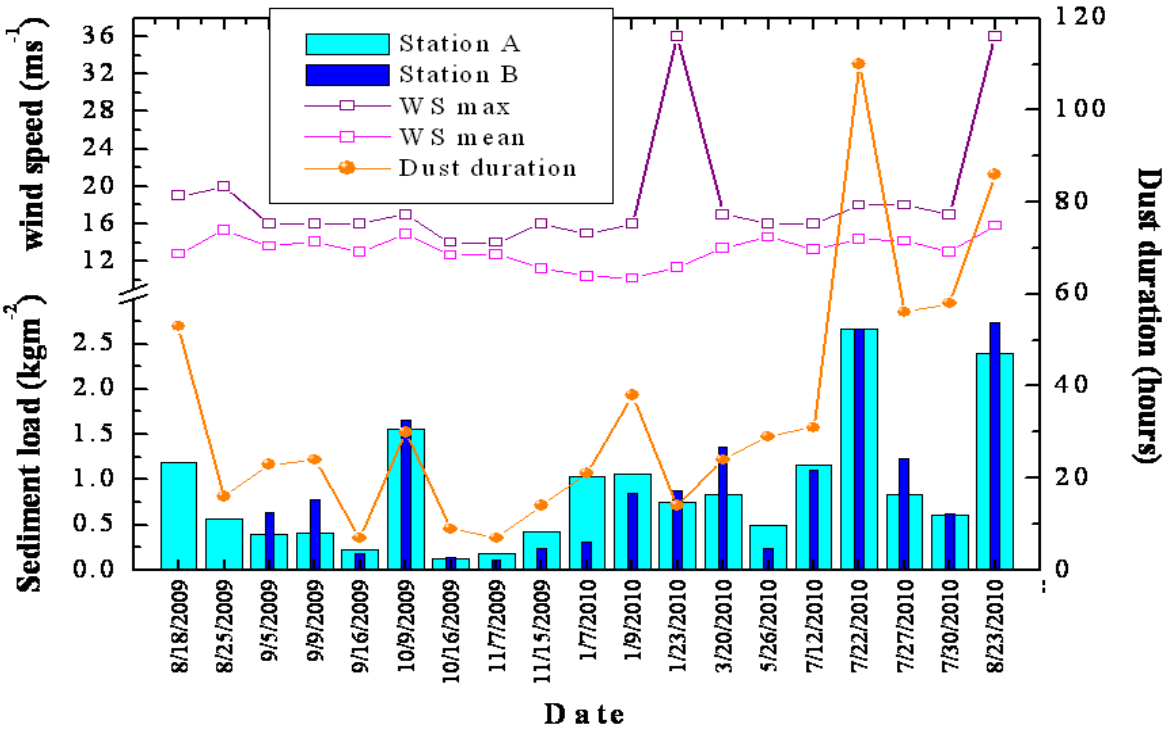

Figure 3.11: Average dust loading (kgm^{-2}) during various dust events in the Sistan region as measured at the 4m (station A) and 8m (station B) monitoring towers. The duration of dust events (hours), as well as the mean and maximum wind speeds on the dusty days were obtained from the Zabol meteorological station.

The dust loading is highly correlated with the duration of the dust storms, as shown from their correlation, with the linear regressions being statistically significant at the 0.99% confidence level (Fig. 3.12). Apart from the strong linke to the duration of dust storms, the dust loading at both stations also seems to have a dependence on the daily mean and maximum wind speeds (Figure not shown). However, this dependence was found to be more intense and statistically significant (at the 95% confidence level) at station B, which is located closer to the dust source, whereas for station A the correlation was not found to be statistically significant. This finding emphasizes the strong effect of the wind speed on dust erosion and transportation, as well as on dust loading, at least for areas close to dust sources. However, the results show that the main factor that controls the dust loading at both stations is the duration of the dust storms, and secondly the wind speed. The role of the wind might have been found to be more critical if measurements were taken at the sampler stations instead of using the meteorological data from Zabol. The total amount of dust loading represents large variation depending on intensity,

duration and particle size distribution for each dust event. The analysis showed that the total dust loading for the 19 events of measurements at station A is 16.9 kg.m^{-2} corresponding to 0.88 kg.m^{-2} per event, whereas at station B the measurements yielded 15.8 kg.m^{-2} (17 events), corresponding to 0.93 kg.m^{-2} per event. The larger dust loading at station B is attributed to the smaller distance from the source region.

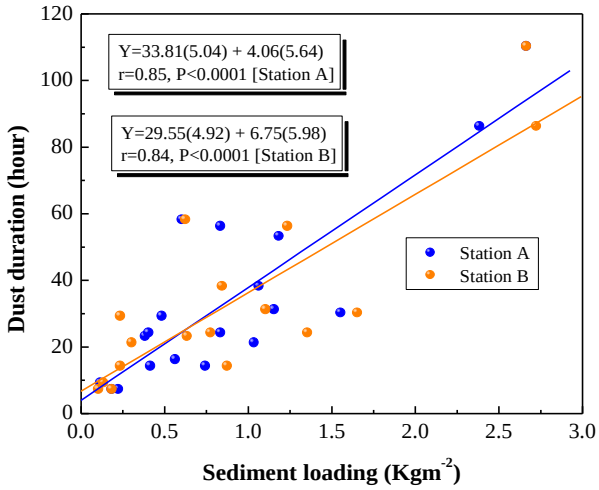

Figure 3.12: Correlation between dust loading measurements and duration of dust storm events for 19 days at station A and 17 days at station B.

Data on dust loading are available at only a few places around the world (e.g. Zhang, 1985; Offer and Goossens, 2001; Dong et al, 2010) and those presented here are the first for the Sistan region. Hence, obtaining measurements of horizontal dust flux will significantly increase our understanding of wind erosion and dust problems. Apart from the natural emissions of dust, Zender et al. (2004) identified two ways in which human activities can influence dust emissions: (a) by changes in land use, which alter the potential for dust emission, and (b) by perturbing local climate that, in turn, alters dust emissions.

Figure 3.13 illustrates the height variation in dust loading during the dust storms measured at station A (19 days, up to 4m in height) and station B (17 days, up to 8m in height). Contrasting height variations measured during intense dust storms occurred between the two stations, while similar variations correspond to moderate and low storm events. More specifically, the dust loading shows an increase (decrease) with height in station A (station B), revealing a difference in the dust transport mechanisms. This finding can be explained by considering the fact that station B is located closer to the Hamoun dust source region,

meaning that uplift and newly transported dust concentration is higher near the surface. On the other hand, at station A that is located about 20 km away, the dust loading presents larger values up to 3 m since the near-ground dust particles have already been deposited near the source, and as the distance increases so does the dust-plume height. The diurnal variability of the dust loading at the two stations (not presented) showed increased mass concentrations during daytime that can be explained by enhanced convection and turbulent mixing in a deepened boundary layer. Furthermore, the local winds are stronger during daytime due to thermal convection.

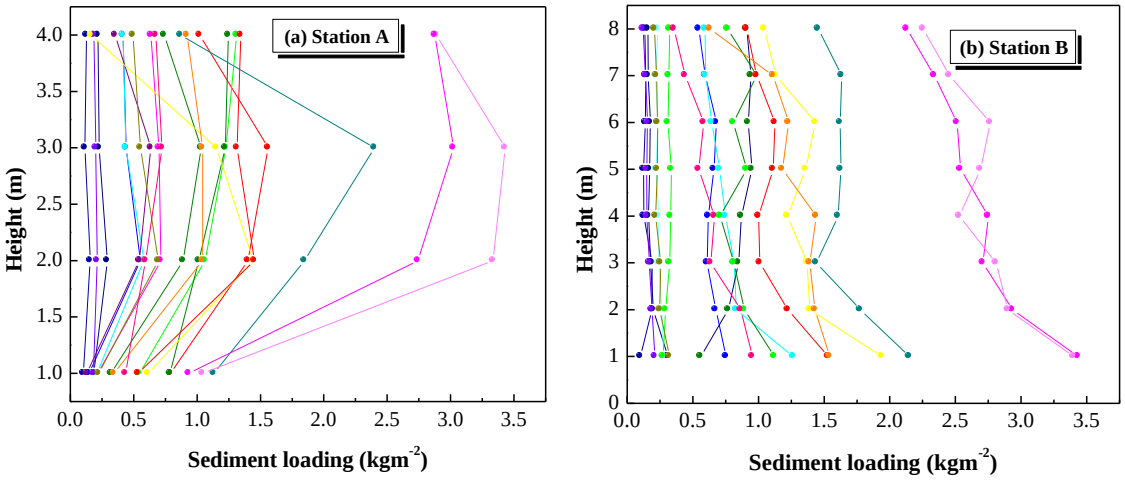

Figure 3.13: Height variation of dust loadings at stations A (a) and at station B (b) for several dust storm days. Green colors are loadings for winter, yellow for spring, red for summer and blue for autumn.

3.6.2 Dust grain-size distribution

Supplementary to the dust loading measurements, the dust grain-size distribution was analyzed for selected samples at stations A and B by means of a Malvern Mastersizer 2000 analyzer. More specifically, the dust grain size was analyzed for 31 samples collected on 12 days at four height levels at station A and for 44 samples corresponding to eight days (eight heights) at station B. The average grain sizes for the selected dust events at stations A and B are summarized in Tables 3.2 and 3.3, respectively. The d(0.5) corresponds to the median grain size (measured in μm) of the particle distribution, while the d(0.9) implies that 90% of the grain size of particles is below this value. The percentages of $PM_{2.5}$ and PM_{10} indicate the fraction of the particles that have diameters of below 2.5 and 10 μm, respectively.

The results in both Tables 3.1 and 3.22 show considerable variation in all grain-sized parameters, depending on the intensity of the dust storms as well as on other factors considering the soil materials. In general, dust storms that occurred during summer present larger grain sizes due to stronger durinal and seasonal winds (fig 2.8 and 2.9b). As a consequence, a smaller fraction of particles is below 10 and 2.5 µm. However, more measurements are needed for evaluating these results. The whole spectrum of grain-size measurements at both stations is analyzed in Figs. 3.14a and b. These figures show box charts for each parameter that allows for a direct comparison between the two stations.

Table 3.2: Variation in average grain size during different dust storms at station A.

Date	d (0.5)	d (0.9)	$PM_{2.5}$ (%)	PM_{10} (%)
19/08/2009	24.1	61.0	8	24
25/08/2009	19.9	56.0	11.0	30.0
05/09/2009	26.1	64.5	9.5	24.0
09/09/2009	28.2	73.8	10.5	26.0
16/09/2009	14.3	46.9	8	38
09/10/2009	23.8	63.4	10.3	27.5
15/11/2009	10.1	36.2	15.3	50.7
07/01/2010	14.8	56.0	11.7	40.8
09/01/2010	12.6	42.6	11.0	51.3
23/01/2010	13.5	45.0	11.0	41.5
08/07/2010	29.9	77.2	9.5	26.0
23/08/2010	31.5	80.6	8.0	20.8

Table 3.3: Variation in average grain size during different dust storms at station B.

Date	d (0.5)	d (0.9)	$PM_{2.5}$ (%)	PM_{10} (%)
05/09/2009	63	163	7	18
09/09/2009	55	149	7	17
16/09/2009	37	115	9	23
09/10/2009	61	159	7	19
16/10/2009	36	102	8	24
15/11/2009	32	96	9	25
07/01/2010	14	54	13	41
08/07/2010	49	147	9	22

The analysis of the dust's grain size reveals large differences between the two stations, especially for the d(0.9). For this parameter, the mean, median as well as the distribution

of the dust diameters are much higher at station B, exhibiting a mean value of 126.2±49.9 µm against that of 58.7±18.0 µm at station A.

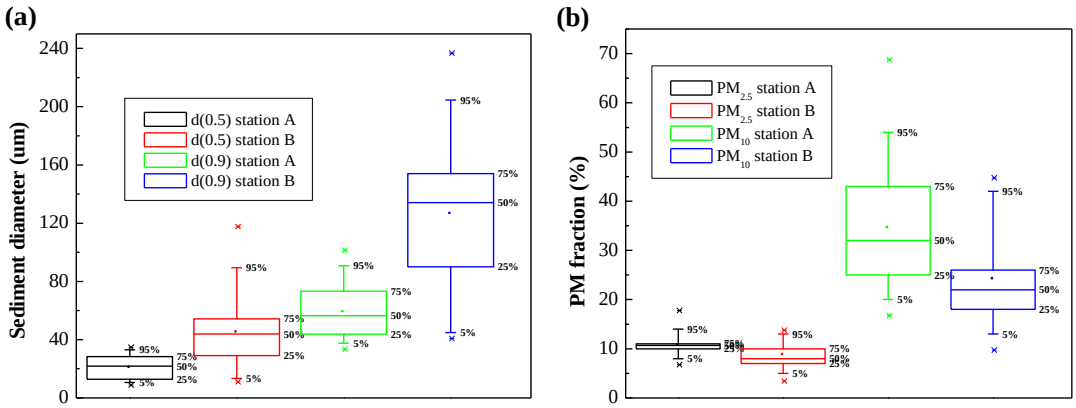

Figure 3.14: Chart boxes for (a) the dust diameters corresponding to d(0.5) and d(0.9) grain sizes and (b) for the fraction (%)lower than $PM_{2.5}$ and PM_{10} particles at both stations A and B.

In general, the median grain size (d0.5) distributions of settled desert dust in Sistan is in the range of ~10–118 µm for both stations, with larger particle sizes and distribution of values at station B (Fig. 3.14a). For example, 50% of the dust particles are below 20.5±8.1 µm at station A, while the same fraction is below 44.8±23.8 µm at station B, implying considerable shift to larger dust particles at station B. This is also clearly observed when plotting the frequency distribution of particle size (Fig. 3.15). In Fig 3.15 the maximum of the mean distribution is around 30 µm for station A, which increases to ~60 to 70 µm for station B. Note also the dominance of higher frequencies of dust particles above 100 µm at station B, while the difference between the distributions is rather low for the small particles. This is particularly valid for particles <2.5 µm, for which the results show fractions of 10.6±2.3% and 8.7±2.5% for stations A and B, respectively (Fig. 3.14b); much larger difference is shown for PM_{10}, which is in the order of 10%. Station B, which is closer to Hamoun, exhibits slightly higher dust loading and significantly higher fraction of large particles than that observed at station A, which is 20 km from B and further from Hamoun. This is indicative of significant spatio-temporal variation in dust sediment loadings and grain-size distribution, which emphasizes the necessity for more systematic measurements, even at some new locations around the Hamoun basin in order to obtain an improved understanding of dust characteristics around the Hamoun lakes.

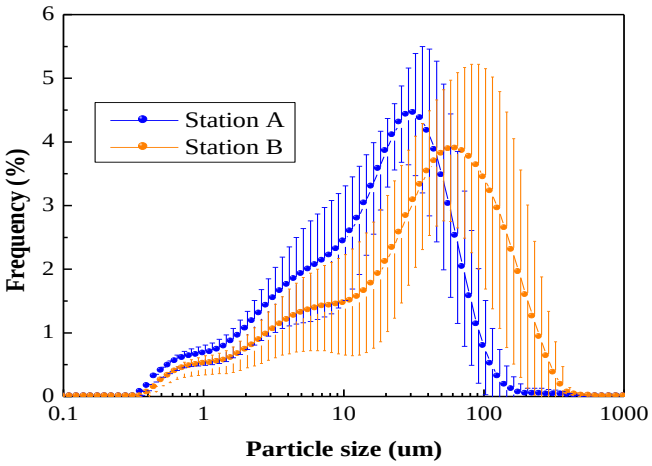

Figure 3.15: Average and standard deviation of the dust samples particle-size distribution at stations A and B.

Finally, Fig. 3.16 provides the mean height variation in grain size parameters at station B. The profiles show a considerable decrease with height, mainly in d(0.9) and secondarily in d(0.5), indicating a shifting of the size-distribution curves towards lower particle sizes. This suggests that the larger and heavier particles are found near the ground and that only the smaller particles are lifted to elevated heights meaning that they are more likely to be transported over large distances. As the particle size decreases, the height variability is gradually reduced, being neutral for $PM_{2.5}$, while for PM_{10} the percentage fraction profile indicates a larger probability for occurrence at higher levels.

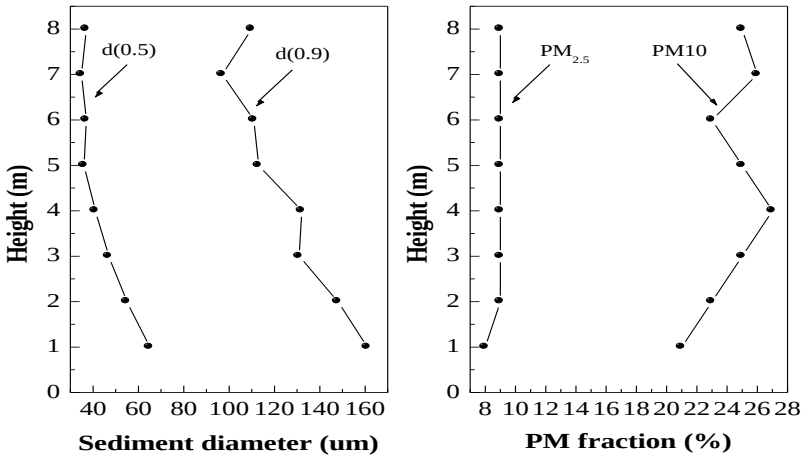

Figure 3.16: Average height variation of the grain size measured over eight days at station B for d(0.9) and (d0.5) (left panel) and $PM_{2.5}$ and PM_{10} (right panel).

3.7 Conclusions

This chapter provides analysis of the dust sediment loading and grain size distribution in the Sistan region, southeast Iran, based on first time measurements conducted at two locations that are situated close to the Hamoun basin. Hamoun is considered to be one of the most active dust source regions in Southwest Asia. Dust loading from the Hamoun basin has been found to have a significant contributing influence on the development of extreme dust storms, especially during the summer days. The influence firstly depend on the intensity and duration of dust storms, and secondarily, on the distance from the source region, the wind speed and altitude. The grain-size distribution of the dust loading was strongly influenced by the distance from the dust source, since grain sizes shifted to larger values towards station B that is closer to the Hamoun basin. Furthermore, the particle size distribution exhibited a shift towards lower values as the altitude increases, with this feature found to be more obvious amongst larger sized particles, while the frequency of particles below 2.5 μm seemed not to be affected by altitude. In general, the analysis revealed significant spatio-temporal variability of regional dust loading and characteristics. This finding necessitates more systematic observations at as many locations as possible around the Hamoun basin in order to improve the understanding of force dynamics, transport mechanisms as well as to quantify the dust amounts emitted from the Hamoun basin.

CHAPTER 4

AIRBORNE PARTICULATE MATTER CONCENTRATION OVER THE SISTAN

4.1 Introduction

Increased air pollution has recently become a major health concern in the developing countries of south Asia (e.g. Singh *et al*., 2004; Ramachandran and Rajesh, 2007). Several studies demonstrated that airborne Particulate Matter (PM) has an impact on climate (Broecker, 2000), biogeochemical cycling in ecosystems (Nriagu and Pacyna, 1988), visibility (Husar *et al*., 1997) and human health (Nriagu, 1988; Dockery *et al*., 1993; Dockery and Pope, 1996). More specifically, air pollution has an adverse effect on respiratory and cardiovascular systems (Nastos *et al*., 2010), which can result in acute reduction of lung function, aggravation of asthma, increased risk of pneumonia in the elderly, low birth weight and high death rates in newborns (Wilson *et al*., 2004). Over recent years in the public health domain the PM concentration has become a topic of considerable importance, since epidemiological studies have shown that exposure to particulates with aerodynamic diameters of < 10 µm (PM_{10}) and especially < 2.5 µm ($PM_{2.5}$) induces an increase of lung cancer, morbidity and cardiopulmonary mortality (e.g. Pope, 2000; Schwartz, 2004; Pozzi *et al*., 2005; Chakra *et al*., 2007; Brook *et al*., 2009; Sivagangabalan *et al*., 2010; Bhaskaran *et al*., 2011). Although there is still a fundamental lack of understanding of the underlying mechanisms of their toxicity to humans, one of the widely accepted hypotheses is that toxicity of PM depends not only on their size, but also on their composition, both of which depend on emissions, location, time of year, meteorological conditions and mixing processes (Akyuz and Cabuk, 2009). The national air quality standards in many countries are currently under review with the aim to include the monitoring of aerosol load in order to maintain a healthy atmospheric environment. For example, the U.S Environmental Protection Agency (USEPA) replaced the monitoring of total suspended particulate matter with PM_{10} measurements, and has recommended the monitoring of the $PM_{2.5}$ fraction of aerosols (USEPA, 2006). Based on Environmental Protection Agency (EPA) standards, the concentration of PM_{10} is regarded as an important

criterion for determining the Air Quality Index (AQI), which is a measure of quality of the ambient air at a specific location.

In addition to increased anthropogenic emissions as a result of population growth, air quality in south Asia is also affected by natural phenomena such as dust storms (Badarinath *et al.*, 2007; Alam *et al.*, 2011a, b). Dust is considered to be one of the major components of tropospheric aerosols over the globe (Mishchenko and Geogdzhayev, 2007) with global flux estimations of 1500-2600 Tg yr^{-1} (IPCC, 2007) and constitutes a key parameter in climate aerosol-forcing studies (Pandithurai *et al.*, 2007; Prasad *et al.*, 2007; Gautam *et al.*, 2009). The impact of dust on solar radiation depends mainly on its physical properties such as size, shape and mineralogy (e.g. Washington *et al.*, 2003; Kalashnikova and Kahn, 2008). These are initially determined by the terrestrial sources from which the soil sediments are entrained, although these parameters are subjected to change during dust transport (Mahowald *et al.*, 2005). Dust aerosols strongly affect visibility, atmospheric dynamics and weather, perturb the radiation balance of the earth-atmosphere system and might have a noticeable effect on ecosystems and even human health (Goudie and Middleton, 2001; Engelstaedter *et al.*, 2006; Kaskaoutis *et al.*, 2010).

Provisional studies focusing on air quality and dust over Iran have already been carried out. Amongst others, Mousavi and Nadafy (2000) performed a comparative study of air quality in Tehran during the period 1997 to 1998. The results revealed that in 1997 the air quality on 32% of the days was unhealthy, and on 5% of the days was regarded as very unhealthy, whereas in 1998 the unhealthy and very unhealthy days increased to 34% and 6%, respectively. Cheraghi (2001) studied the air quality in Tehran and Isfahan and offered solutions for its improvement using the AQI. It was found that on 329 days of the year in Tehran, and on 34 of the days in Isfahan the AQI departed beyond 100. Ardakani (2006) also studied AQI in Tehran reporting that on 273 days in 2001 the values were higher than those set for the air quality standards; 47 of the days were considered as very unhealthy and 1 was classified as dangerous.

In this Chapter the temporal variation of PM_{10} and $PM_{2.5}$ concentrations are analysed in the atmosphere above the cities of Zabol and Zahedan in southeastern Iran focusing mainly on the following five objectives: (1) establishing baseline PM_{10} and $PM_{2.5}$ concentration levels, which could be used in the future to assess the effectiveness of any

implemented emission control strategies; (2) comparing the observed PM_{10} and $PM_{2.5}$ concentration levels to the corresponding EU and USA ambient particle standards; (3) determining the relative contribution of $PM_{2.5}$ and examining the relationship between PM_{10} and $PM_{2.5}$ levels, which may be used to estimate, retrospectively, particle concentration trends, (4) revealing the role of wind speed, especially in summer, to the PM levels and, (5) revealing the fraction of days that are unhealthy for the population based on AQI values. It should be noted that such studies are lacking from this region and that this is the first that examines the seasonal evolution of PM concentrations and AQI, aiming also to relate the peak values in PM to dust exposures from the nearby Sistan desert.

4.2 Assessment of PM concentration in the city of Zahedan

4.2.1 Study area and meteorology

The measurements were carried out in the city of Zahedan located in the southeastern part of Iran (60.52° East, 29.32° North, 1384 m above mean sea level) close to the Iranian borders with Pakistan and Afghanistan (Fig. 4.1). Located just south of the Sistan desert, Zahedan is affected by frequent dust and sand storms, especially during the summer season (June to August) due to the prevailing northerly winds, commonly known as the "120 day wind" or "Levar" (Middleton, 1986; Goudie and Middleton, 2001). The city has a population of more than 800,000 and is regarded as a moderately urbanized area with several small industries and a large number of automobiles, which contribute to the production of local aerosols.

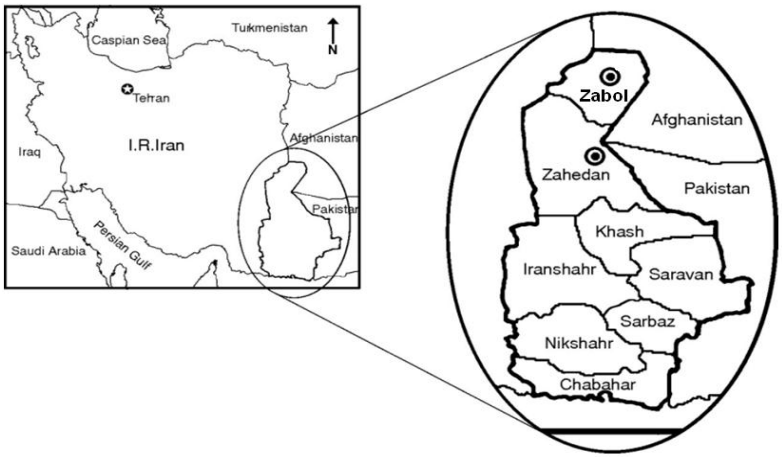

Figure 4.1: Position of the cities Zahedan and Zabol in Iran.

The climate is semi-arid to arid, with a low annual average precipitation of 84 mm occurring mainly in winter (December to February). Monthly mean values of temperature, RH, atmospheric pressure and accumulated precipitation in Zahedan during the study period (July 2008 to March 2010) are plotted in Fig. 4.2. The monthly mean temperature exhibits a clear annual pattern with low values in winter (10-13 ^{o}C) and high values (~33 ^{o}C) in summer following the common pattern found in the northern mid-latitudes. RH illustrates an inverse annual variation with larger values in winter (50 to 65%) and very low values in summer (below 20%), which are indicative of an arid environment. The atmospheric pressure is generally steady (~869 hPa) from January to April, and then decreases significantly during summer, and increases again in autumn.

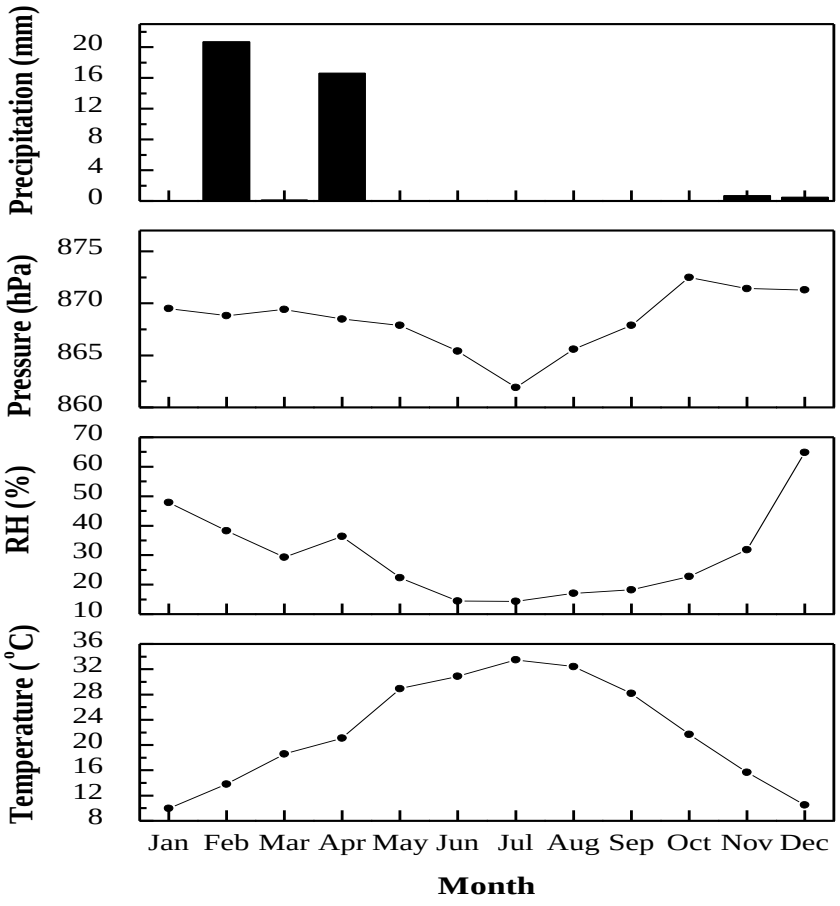

Figure 4.2: Monthly-mean variation of meteorological variables in Zahedan, Iran covering the period July 2008 to March 2010.

The summer low pressure (862 hPa in July) is attributed to the Indian thermal low that extends further to the west over the arid environments of Iran and the Middle East as a consequence of the south Asian monsoon system. These low pressure conditions are the

trigger for the development of the Levar wind. During the study period (July 2008 to March 2010) the rainfall was restricted to winter and spring, while the maximum acccumulated rainfall in February (20 mm) is indicative of the typical arid environment.

4.2.2 Particulate Matter (PM) measurements

PM concentrations at near-surface level in the city of Zahedan were systematically measured using the Environmental Dust Monitor model 180 (EDM-180). The measurements were carried out during the period July 2008 to March 2010 (total of 399 days) at the Environmental institute in Zahedan, Iran. The EDM-180 measures PM concentration (in $\mu g.m^{-3}$) for 3 particle sizes, namely PM_{10}, $PM_{2.5}$ and $PM_{1.0}$, with a relatively high temporal resolution (5-minutes) of recordings. The recording station is located at the outskirts of the city, in a sparsely-populated area without any industries or any direct influence from anthropogenic emissions. The 5-minutes measured PM data were converted to 24-hour averages (daily averages) from which the monthly and seasonal values and variations were obtained. For assessment of air quality in Zahedan, the desired data were sorted according to AQI standards and were analyzed to determine the fraction of days per month and season where air pollution was above AQI standards, or levels regarded as dangerous for public health.

4.2.3 Results and discussion

4.2.3.1 Seasonal and monthly variability in PM concentrations

Fig. 4.3 illustrates the annual variation of PM concentrations as obtained from the monthly mean EDM recordings during the period July 2008 to March 2010. The vertical bars depict one standard deviation from the monthly mean and are indicative of the day-to-day variation. On this basis, it is observed that the months with the highest PM levels also depict the largest standard deviations. This occurs mainly in summer, which is the period with the most frequent dust-storm events. One can, therefore, conclude that the intense dust storms taking place on specific days during summer are predominantly responsible for the large day-to-day variations at all PM concentrations.

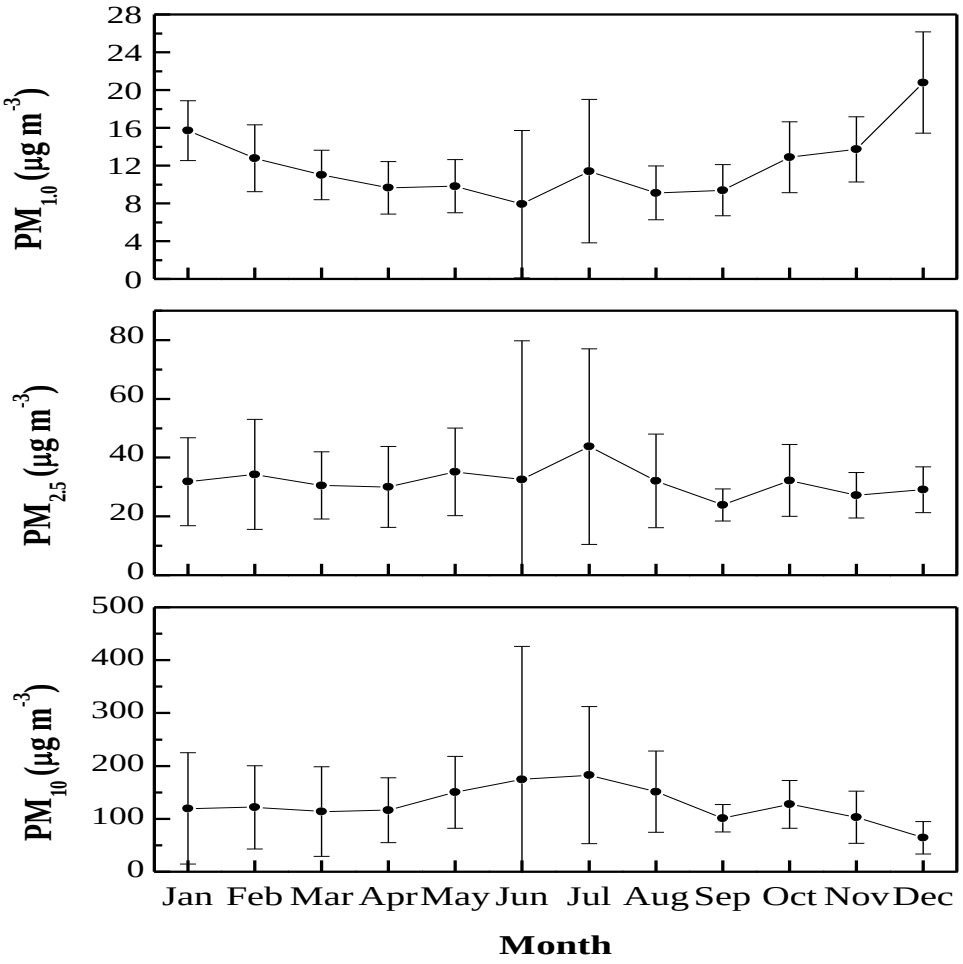

Figure 4.3: Annual variation of monthly-mean values of PM_{10}, $PM_{2.5}$ and $PM_{1.0}$ at Zahedan during the period July 2008 to March 2010.

The annual pattern of PM_{10} shows a significant increase in summer where monthly mean concentrations of up to ~170-180 µg.m^{-3} were recorded in June and July (Table 4.1). PM_{10} concentrations during winter months are significantly lower, with 64µg.m^{-3} measured in December. January and February exhibit PM_{10} concentrations of above 100µg.m^{-3}, which persist until April when PM_{10} levels increase as a result of the Levar wind. The highest PM_{10} concentration (970µg.m^{-3}) is recorded during June (Table 4.1) closely associated with a severe dust event. The annual variation of monthly mean $PM_{2.5}$ is somewhat similar (July maximum), but with a more complex pattern. In contrast, the annual variation of monthly mean $PM_{1.0}$ is reversed, since maximum values (14-20 µg.m^{-3}) are observed in winter months. A small peak is also observed in July associated with a large standard deviation. The difference in the annual variation between PM_{10} and $PM_{1.0}$ suggests differences in source regions for these aerosol sizes. The main anthropogenic

source of PM in the Zahedan urban environment can be confined to vehicular traffic, fossil-fuel combustion, central heating and industrial activities that release a large amount of near-surface anthropogenic aerosols. Similar annual variations of the anthropogenic aerosols have been observed within urban environments in India (Badarinath *et al*., 2009; Ramachandran and Kedia, 2010; Pathak *et al*., 2010). In addition, the boundary layer mixing height is lower in winter and traps the pollutants near the ground as a result of temperature inversions. All the above explain the higher concentration of small-sized particles ($PM_{1.0}$) in winter. In contrast, during summer months thermal heating at the surface and the increase of the mixing layer height favors buoyancy and the dilution of anthropogenic aerosols ($PM_{1.0}$). Apart from desert dust, a natural contribution to the total PM (mainly to $PM_{2.5}$ and PM_{10}) is also expected to originate from eolian and traffic-driven re-suspension of dust, since the scarce rainfall favors the accumulation of road dust in summer.

Table 4.1: Monthly mean, maximum and minimum PM_{10} and $PM_{2.5}$ concentrations in Zahedan during the period July 2008 to March 2010.

Month	Monthly Mean		Daily minimum		Daily maximum	
Season	PM2.5 (µgm-3)	PM10 (µgm-3)	PM2.5 (µgm-3)	PM10 (µgm-3)	PM2.5 (µgm-3)	PM10 (µgm-3)
January	32	119	14	18	84	444
February	34	121	12	38	112	428
March	28	95	17	48	44	136
April	30	116	13	41	67	242
May	35	150	15	75	89	363
June	33	174	10	42	182	970
July	43	182	16	88	178	643
August	32	151	15	78	73	320
September	24	101	12	70	31	183
October	32	127	17	73	79	297
November	27	103	13	33	53	263
December	29	64	13	23	49	139
Winter	32	107	12	18	111	444
Spring	32	121	13	41	89	363
Summer	38	172	10	42	182	970
Autumn	29	114	12	33	79	297

Some studies conducted in other urban environments, e.g. Akyuz and Cabuk (2009) in Turkey and Chaloulakou et al. (2003) in Athens, Greece found, contrary to our results, that in winter both PM concentrations were higher, which was attributed to larger use of fossil fuels in winter. Chaloulakou *et al*. (2003) reported monthly mean PM_{10}

concentrations in Athens ranging from 60.3 μg.m^{-3} (January) to 88.9 μg.m^{-3} (December), with an annual mean value of 75.5 μg.m^{-3}. In Barcelona, Spain, the ambient PM_{10} and $PM_{2.5}$ were in the range of 39 to 42 μg.m^{-3} and 25 to 29 μg.m^{-3}, respectively over the period 2003-2006 with 97 daily values exceeding 50 μg.m^{-3} (Perez et al., 2008), while the mean annual PM_{10} concentration ranges from 20 to 37 μg.m^{-3} in Rio de Janeiro, Brazil (Godoy *et al*., 2009). Comparing the present results with those of the above-mentioned studies, it is concluded that the city of Zahedan experiences much higher PM concentration levels. This is not only the case for summer, when the area is affected by natural phenomena, but also for winter. This emphasizes the fact that PM concentrations over Zahedan can be regarded as a real environmental problem that poses a serious risk to quality of life and endangers human health.

The frequency of occurrence for PM_{10} and $PM_{2.5}$ concentrations for each season is depicted in Fig. 4.4(a), (b), respectively. In spring and summer ~33% of the PM_{10} values were between 100 and 150 μg.m^{-3}, with higher frequency for lower values in spring. In summer, the frequency distribution shifts towards larger values, with values even above 500 μg.m^{-3} and negligible PM_{10} values below 50 μg.m^{-3}. On the other hand, a considerable fraction (24%) of PM_{10} values < 50 μg.m^{-3} is observed in winter. Regarding the frequency distributions of $PM_{2.5}$ in all seasons except summer, the largest frequency is observed for values between 20 and 30 μg.m^{-3}, while in summer the largest frequency shifts towards lower values (10-20 μg.m^{-3}), which is opposite to that observed for PM_{10}. However, similarly to PM_{10}, summer presents a broader distribution for $PM_{2.5}$, with values > a 100 μg.m^{-3} range. Apart from these similarities in the PM_{10} and $PM_{2.5}$ frequency distributions, some differences in winter and summer reveal a possible different source of aerosols in these seasons (natural or anthropogenic). For example, the intense dust storms during summer do not have such a pronounced signal in $PM_{2.5}$ concentrations as in PM_{10} ones, while the larger contribution of anthropogenic aerosols in winter rather increases the $PM_{2.5}$ levels. Also note that the mean $PM_{2.5}$ in winter (32 μg.m^{-3}) is similar to that of spring and larger than that of autumn, despite the fact that winter PM_{10} is the lowest (Table 4.1). However, it should be noted that dust events may also affect significantly the $PM_{2.5}$ levels, as observed during a severe dusty day in June ($PM_{2.5}$ daily value of 182 μg.m^{-3}) (Table 4.1). An important finding revealed from Fig. 4b is the absence of $PM_{2.5}$ <10 μg.m^{-3}, while

mean monthly $PM_{2.5}$ values (Table 4.1) are similar or even lower, than those reported for urban Athens (Chaloulakou *et al.*, 2003).

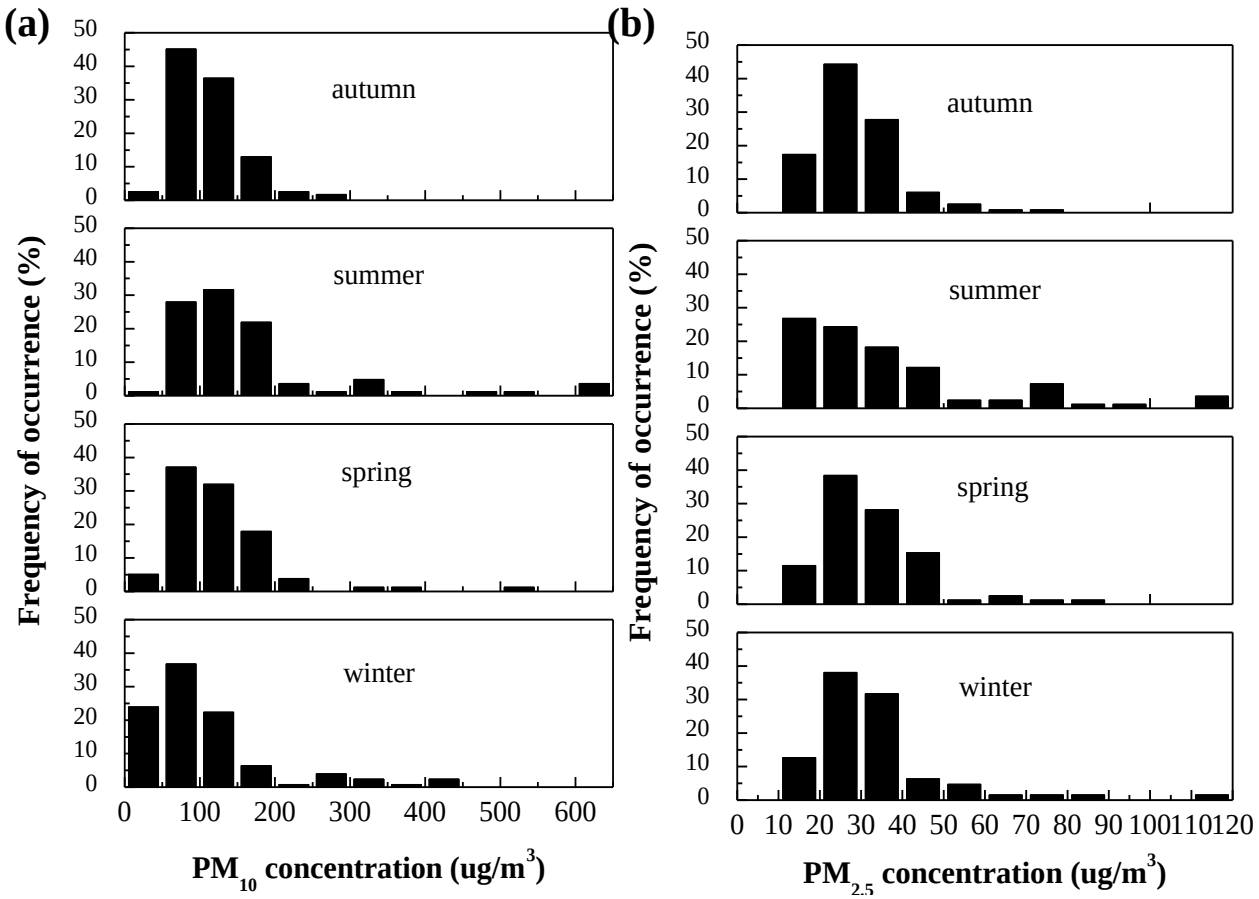

Figure 4.4: Frequency (%) distribution of (a) the daily PM_{10} and (b) $PM_{2.5}$ for each season in Zahedan.

Relationships between daily mean $PM_{2.5}$ and PM_{10} concentrations were calculated using linear regression analysis for each season (Fig. 4.5) and with the Pearson's coefficient of correlation (Table 4.2). Such correlations may reveal the consistency of the sources for PM_{10} and $PM_{2.5}$ emissions. Results indicate maximum and minimum correlations in summer ($r = 0.95$) and autumn ($r = 0.82$), respectively, implying that the sources of $PM_{2.5}$ and PM_{10} are somewhat similar. The correlation between PM_{10} and $PM_{2.5}$ for the whole dataset is associated with 81% of the variance ($R^2 = 0.81$), while poor correlation was found for PM_{10} vs $PM_{1.0}$ ($R^2 = 0.11$). It should be noted that the correlation between PM_{10} and $PM_{1.0}$ exhibited (not presented) strong seasonality with very low r values in winter and autumn and large r values in spring (0.66) and summer (0.86) (Table 4.2).

Table 4.2: Correlation coefficient (r) values between daily mean PM_{10} and $PM_{2.5}$ and PM_{10} and $PM_{1.0}$ for each season over Zahedan. [** Correlation is significant at the 0.01 level, N: number of daily values]

Season	PM_{10} vs $PM_{2.5}$	PM_{10} vs $PM_{1.0}$
Winter (N=125)	0.85**	-0.004
Spring (N=78)	0.90**	0.66**
Summer (N=81)	0.95**	0.86**
Autumn (N=115)	0.82**	0.26**
Whole (N=399)	0.9**	0.33**

This indicates that sub-micron aerosols during winter are of local anthropogenic origin, while larger aerosols have a strong natural component. In contrast, during summer, increase of PM_{10} from natural sources may also have an impact on fine aerosol concentrations ($PM_{1.0}$), since transported dust can also be of fine mode (Hess et al., 1998). The relationship between $PM_{2.5}$ and $PM_{1.0}$ reveals similar results and discussions, with high correlations in summer and spring and lower in winter and autumn (Fig. 4.6).

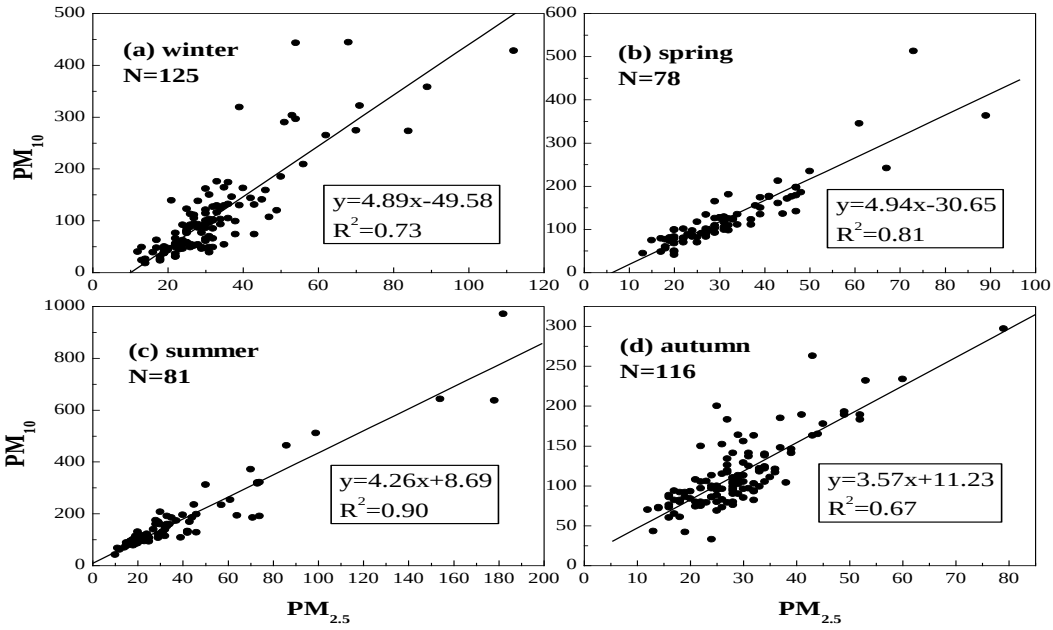

Figure 4.5: Relationship between $PM_{2.5}$ and PM_{10} for each season using the daily mean values of $PM_{2.5}$ and PM_{10} in Zahedan.

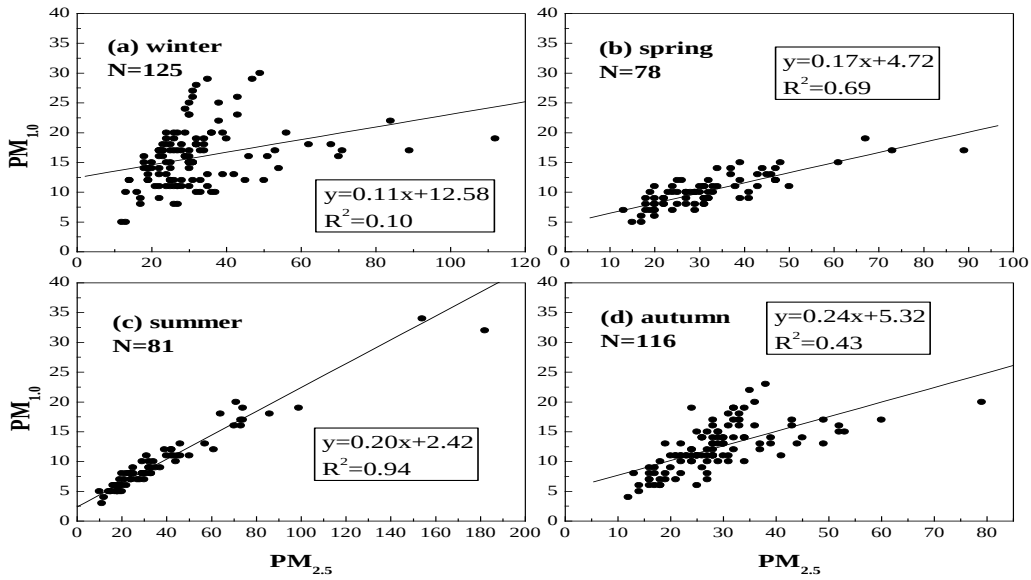

Figure 4.6: Relationship between $PM_{2.5}$ and $PM_{1.0}$ for each season using the daily mean values of $PM_{2.5}$ and $PM_{1.0}$ in Zahedan.

4.2.3.2 Diurnal variability of PM concentrations

Daily mean variations in PM concentrations at all levels during the period 2 July 2008 to 16 March 2010 are shown in Fig. 4.7. A threshold value of 400 $\mu g.m^{-3}$ was chosen for the city of Zahedan in order to identify days with severe PM_{10} levels. Such extremely high PM concentrations were observed in Athens during an intense dust storm (Kaskaoutis *et al.*, 2008) and are also considered as being very unhealthy and even hazardous for human life. Days with severe PM_{10} concentrations are observed mainly in summer (4 days), but also in winter (3 days) and spring (1 day). The maximum of daily PM_{10} and $PM_{2.5}$ concentrations was up to 970 μgm^{-3} and 182 μgm^{-3}, respectively on 29 June 2009. These values are comparable in magnitude to those observed during an intense dust storm in Beijing (Sun *et al.*, 2004; Zhao *et al.*, 2007). Despite the fact that long-range advection of dust usually takes place above the boundary layer, subsidence, fumigation and sedimentation allow for a large proportion of dust to diffuse into it (e.g. Gobbi *et al.*, 2007; Kaskaoutis *et al.*, 2008), thus strongly influencing the PM concentrations at the ground level.

Significant daily variability is observed especially for PM_{10} with several peaks and gaps attributed to the intensity of local emissions, regional meteorology, boundary layer dynamics and long-range transported aerosols. The current EU legislation employs PM_{10} concentrations as one of the reference parameters in assessing urban air quality (Chaloulakou *et al.*, 2003; Gobbi *et al.*, 2007). According to EU standards adopted from 1st January 2005 it is permissible that the daily-average threshold of 50µg.m^{-3} at any station is exceeded for a maximum of 35 times per year, while the annual average PM_{10} should not exceed 40µg.m^{-3}. These are ambitious goals considering the current levels of PM_{10} observed in Zahedan (Fig. 4.7, Table 1), since on 361 out of 399 days (90.5%) the PM_{10} levels were found to be above the daily EU threshold value of 50 µg.m^{-3}.

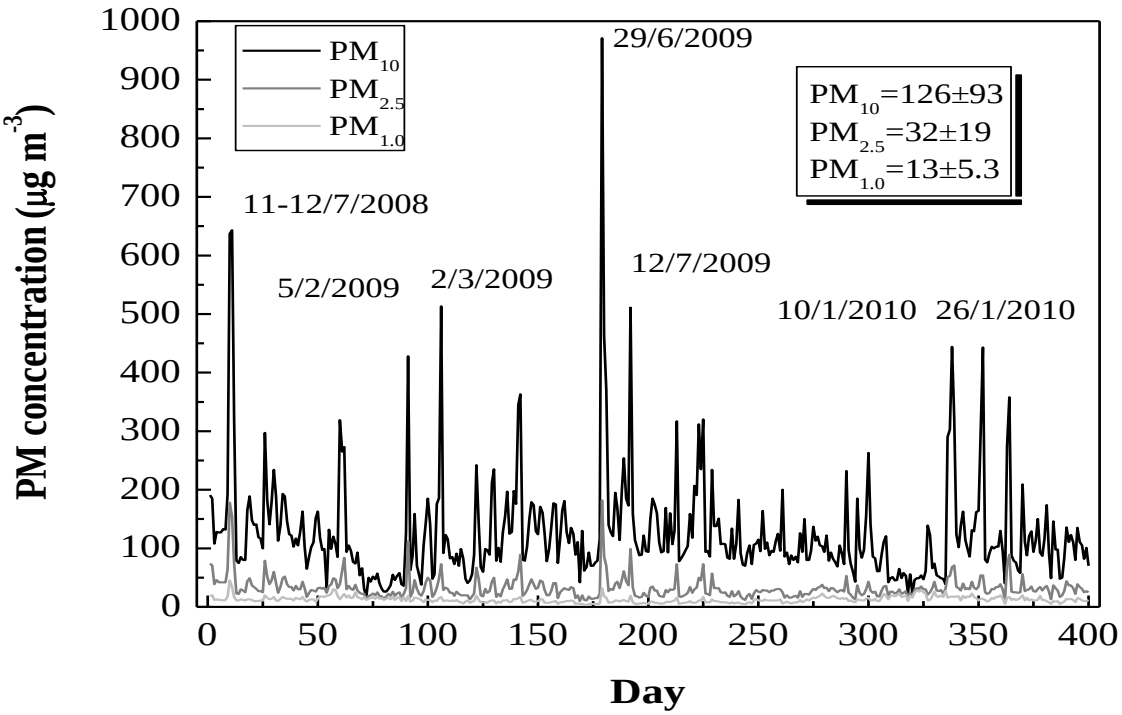

Figure 4.7: Daily particulate matter (PM) concentrations at Zahedan during the period 2/7/2008 to 16/3/2010.

In order to examine the influence of dust outbreaks on the coarse-mode aerosols in Zahedan, the daily variation in $PM_{10-2.5}$ (coarse particles) and $PM_{2.5}/PM_{10}$ was analyzed (Fig. 4.8). Comparing Figs. 4.7 and 4.8 it is observed that on 5 out of the 8 days with extreme PM_{10} values, coarse-mode concentrations of above 400 µg.m^{-3} were reached, while all these events occurred in spring and summer. In Zahedan $PM_{2.5}$ values ranged from 10 - 182 µg.m^{-3}, while coarse particles ranged from 4 to 788 µg.m^{-3} with a mean

value of 94±76 μg.m^{-3}. Although the range and mean of $PM_{2.5}$ are similar to that observed in Athens (Chaloulakou *et al.*, 2003), the coarse-mode particles and the $PM_{2.5}/PM_{10}$ ratio (29±11) in Zahedan are much higher and lower, respectively, indicating the influence of the arid environment for the latter location. Fig. 4.8 shows that the $PM_{2.5}/PM_{10}$ ratio is larger on days with low PM_{10} concentration, mainly in winter and autumn, suggesting a dominance of local anthropogenic aerosols. Daily PM_{10} concentrations during four Saharan dust outbreaks in Madrid ranged from ~80 μg.m^{-3} to ~200 μg.m^{-3} depending on the emission rates, the altitude of the dust plume and the measuring location, while dust is the second biggest contributor to PM_{10} in Madrid making up 40%, on average, of total emissions (Coz *et al.*, 2009). Our results reveal that the PM_{10} concentrations are much higher in Zahedan, while the fraction of coarse-mode particles ($PM_{10\text{-}2.5}$) ranges from 72% to 85% during dust events.

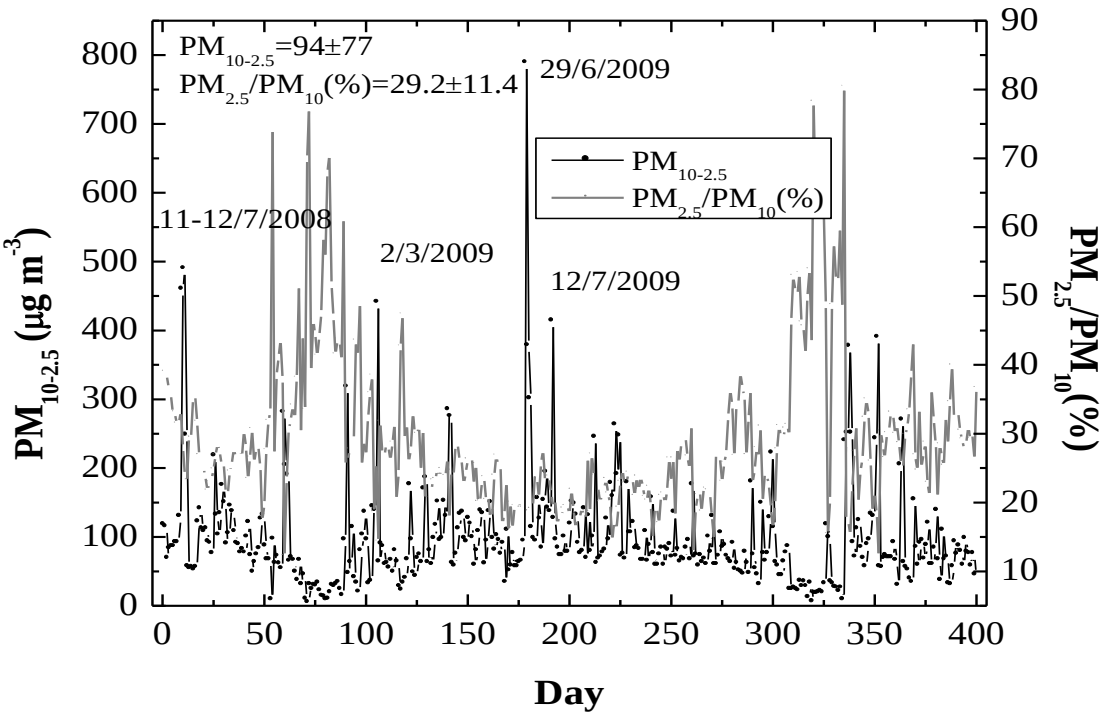

Figure 4.8: Daily concentration of the coarse-mode particular matter ($PM_{10\text{-}2.5}$) and percentage contribution of the $PM_{2.5}$ to PM_{10} at Zahedan during the period 2/7/2008 to 16/3/2010.

Fig. 4.9 depicts mean diurnal variation of PM_{10} concentrations (upper panel) for each season in Zahedan. Significant seasonal differences in the maximum of the diurnal variation are observed while in all seasons PM_{10} values reach a minimum in the early morning hours (~04:00 LST) before human activities start. In winter and autumn, maximum PM_{10} levels occur in the morning hours close to rush hour and the associated

increase of anthropogenic pollution in the city. Solar heating and vertical mixing of pollutants may be the main reasons for the reduction of PM_{10} levels at local noon and early afternoon hours, while fossil-fuel combustion and the use of thermal heating in the evening result in an increase in PM_{10} levels at these times. Similar diurnal variation was found (not presented) for $PM_{2.5}$ levels, but with more pronounced morning and evening increases in winter. The similarity between diurnal PM_{10} variations recorded in this study during autumn and winter and those recorded over several Indian cities (e.g. Madhavan *et al*., 2008; Pathak *et al*., 2010) suggests that local anthropogenic emissions and vertical mixing in the boundary layer play a major role in controlling diurnal PM concentrations. During spring no clear pattern in PM_{10} diurnal variation is observed since several peaks and gaps occur. However, there is a slight steadily increasing trend from morning till late afternoon. In further contrast, the maximum PM_{10} concentrations normally occur between 12:00 and 20:00 LST in summer, indicating that Sistan dust storms (generally originating in Sistan between 8:00 to 11:00 LST (see fig 4.9)) reach the study region after 4 to 9 hours. The diurnal PM_{10} variability in summer is closely associated with the intensity of the wind speed measured at the Zahedan meteorological station (see Fig. 4.9 right panel). This wind, being northerly in direction, carries large quantities of dust from the Sistan desert. It should be noted that the mean diurnal wind speed variation is similar for all seasons; however, the wind favors the increase of aerosol load in summer (maximum PM_{10} for higher wind speeds) and acts as a ventilation tool for the atmosphere in autumn and winter (minimum PM_{10} levels at noon and early afternoon). Studying the weekly variability of PM_{10} and $PM_{2.5}$, it was found that both PM levels were lower on Friday (mean value of 108 against 127 $\mu g.m^{-3}$ for the other days for PM_{10} and 29 against 33 $\mu g.m^{-3}$ for $PM_{2.5}$), which is the day of rest in the Muslim culture; lower PM levels were also found on weekends as against weekdays.

Days with extremely high PM_{10} concentrations (>400 $\mu g.m^{-3}$), as illustrated in Fig. 4.7, are further examined regarding diurnal variability of PM_{10}, $PM_{2.5}$ and $PM_{1.0}$ (Fig. 4.10a, b, c). More specifically, during severe pollution events in winter, PM_{10} values are much higher during the night and early morning hours. The shallow boundary layer and the strong thermal inversion that occur during cold winter nights in the arid environment of Zahedan reduce buoyancy and, therefore, “trap” pollutants near the surface. Thus, explaining the extremely large PM_{10} concentrations (up to 1000 $\mu g.m^{-3}$) sometimes found during winter nights and early morning hours. Because of the stable nocturnal boundary

layer conditions it is concluded that the larger nighttime PM_{10} concentrations in winter can be attributed to local emissions (e.g. thermal heating and fossil-fuel combustion).

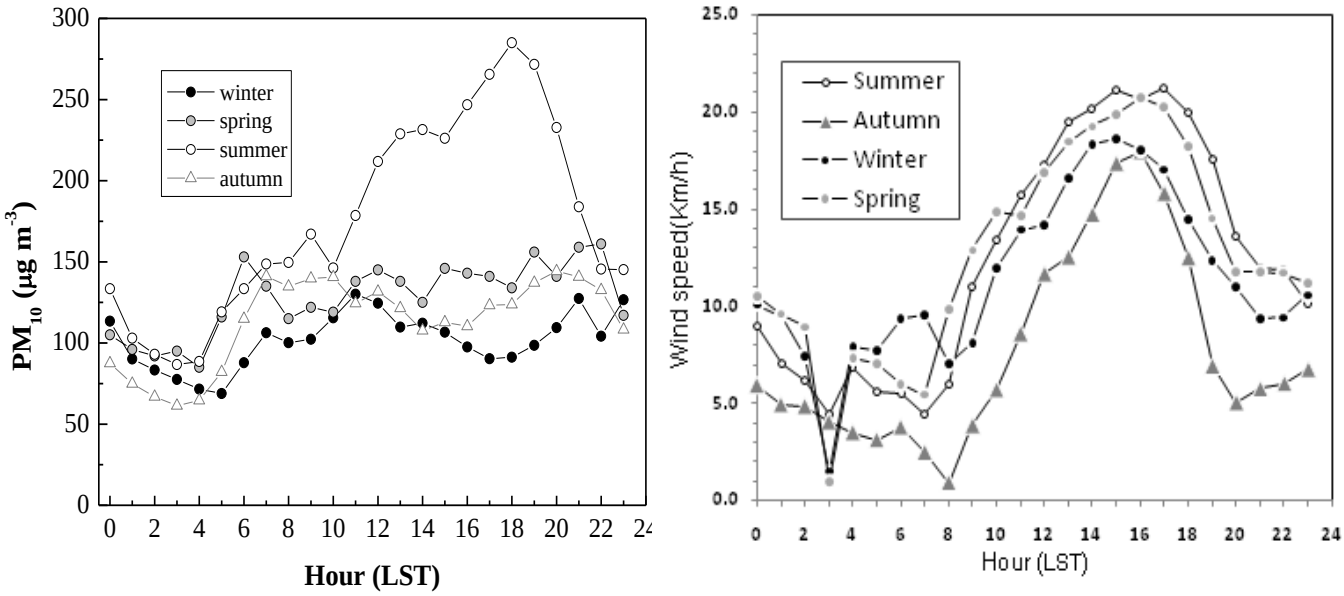

Figure 4.9: Mean hourly variation of PM_{10} (left panel) and wind speed (right panel) for each season in Zahedan.

During severely polluted days in spring, and mainly in summer, the diurnal variability in PM_{10} concentrations follows an opposite pattern with low values in the nighttime and early morning and extremely high values at noon and afternoon hours. The diurnal variation on four summer days that were influenced by intense dust storms (Fig. 4.10a) controls the summer seasonal diurnal variability (Fig. 4.9), although it was found that during most summer days PM_{10} values were high in the afternoon. This can be explained by the frequent arrival of dust storms from the Sistan desert during noon and afternoon, and the associated stronger northerly winds (18 - 20 $km.hr^{-1}$).

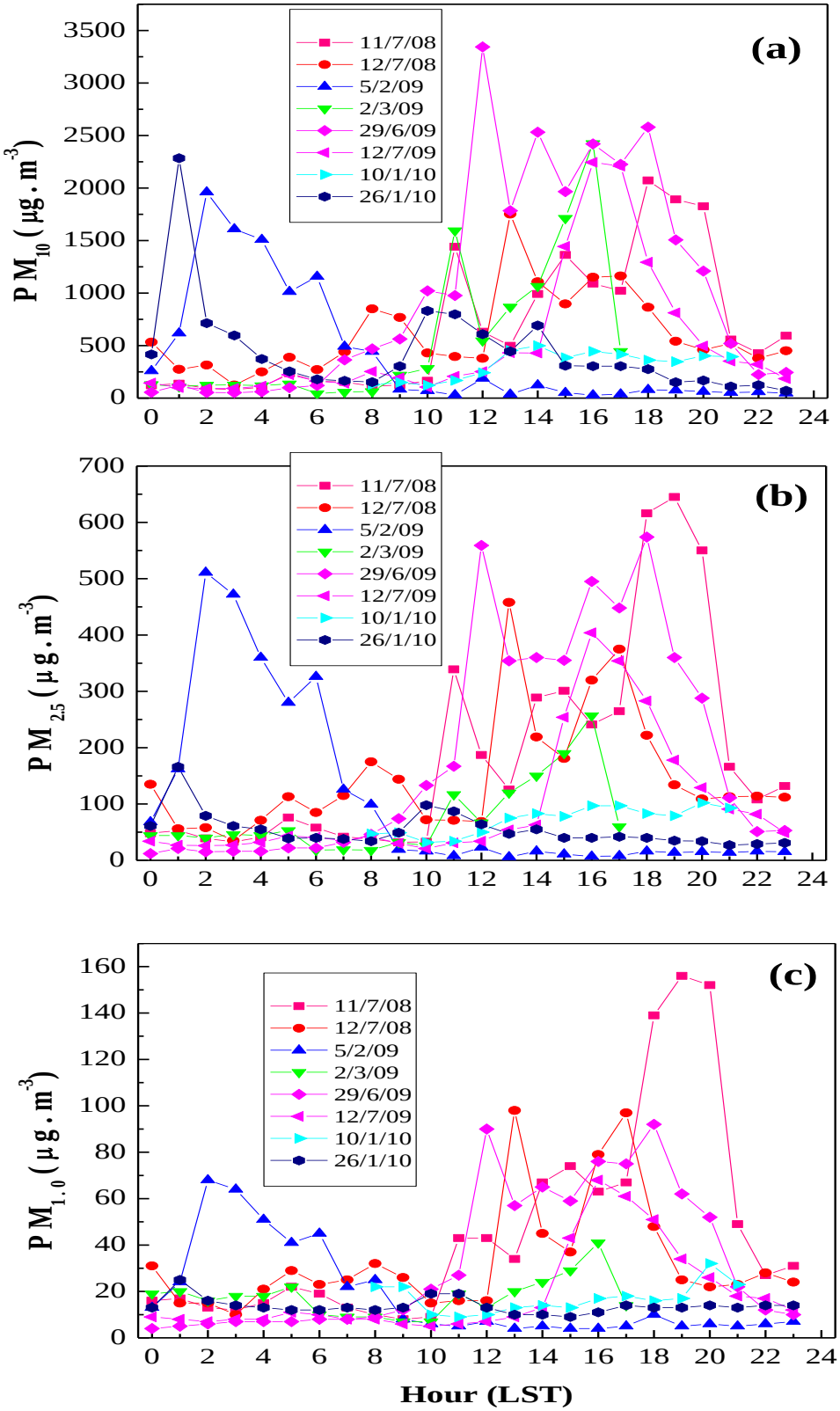

Figure 4.10: Diurnal variation of PM_{10} (a), $PM_{2.5}$ (b) and $PM_{1.0}$ (c) on selected days with severe pollution over Zahedan.

The diurnal variability in $PM_{2.5}$ and $PM_{1.0}$ on the 8 selected most polluted days is similar to that of PM_{10}. Higher $PM_{2.5}$ and $PM_{1.0}$ concentrations were also measured from noon to afternoon hours in summer, indicating that dust storms can also carry significant quantities of sub-micron particles over distances of greater than ~300 km from the source region. On the 8 polluted days the correlation between hourly PM_{10} and $PM_{2.5}$ and between hourly PM_{10} and $PM_{1.0}$ was found to be high, with R^2 =0.82 and 0.63, respectively. This clearly indicates that during severe atmospheric conditions in Zahedan, the main source region for all particle sizes is the dust transported from the Sistan desert. It should be noted that the influence of long-range transported aerosols, such as dust particles, on surface aerosol concentrations is more profound in rural or suburban areas with local background pollution levels than in downtown urban environments, as has also been found in Rome (Gobbi *et al*., 2007). Thus, apart from local emissions, dust deposition during dusty days significantly affects PM concentrations in Zahedan, thereby causing dramatic increases in all PM levels, even much higher than levels prescribed by EU standards.

4.2.3.3 Air Quality Index (AQI)

Air pollution indices are commonly used in order to define the level of impact of air pollution on human health (Cogliani, 2001; Nikolaou *et al*., 2004). As a consequence, the AQI is a powerful precautionary tool to ensure public health protection (EPA, 1999).

The AQI varies from 0 to 500, is divided into six categories, and its health indicators are mentioned in Table 4.3, each of which corresponds to a different level of health concern (EPA, 1999). All AQI categories have less or more impact on human health, and specifically the last AQI category (hazardous, >425 PM_{10} $\mu g.m^{-3}$), is associated with a serious risk of respiratory symptoms and aggravation of lung diseases, such as asthma, for sensitive groups and with respiratory effects likely in the general population (Ozer *et al*, 2006; Mohan and Kandya, 2007).

Based on the technological rules related to AQI, the following formula was used to derive the PM_{10} concentration from AQI (Triantafyllou *et al*., 2006; Larissi *et al*., 2010a):

$$I = \frac{I_{high} - I_{low}}{C_{high} - C_{low}}(C - C_{low}) + I_{low} \qquad (4.1)$$

Where I is the (Air Quality) sub-index, C is the pollutant concentration, I_{low} and I_{high} are the index breakpoints corresponding to C_{low} and C_{high}, respectively and, C_{low} and C_{high} are the concentration breakpoints that are ≤C or ≥C.

Considering air pollution standards as defined by the USEPA which specifies that AQI values can be higher than 100 on only one day of the year, the city of Zahedan did not perform well at all. It was found that AQI values exceeded 100 on 86 days out of 399 (21.5%) in Zahedan. Such severe atmospheric conditions occur mainly in summer and, as indicated before, transported or re-suspended dust plays a major role in the air pollution. An assessment of air quality during the period of investigation showed that 86 days (21.5%) had air pollution levels of above the air quality standard (> 155µg.m^{-3}). Sixty one days were regarded as unhealthy for sensitive people, 17 days were unhealthy or very unhealthy and 9 days were hazardous (Table 4.3). The accumulation of ambient air pollutants associated with enhanced values of AQI (>100) can result in an increase in hospital admissions for the treatment of cardiovascular and respiratory problems (Bartzokas *et al*., 2004; Paliatsos *et al*., 2006). More specifically, several studies have indicated that ambient air pollution is highly correlated with respiratory morbidity amongst children (Jalaludin *et al*., 2004; Schwartz, 2004).

Table 4.3: Indication of health quality with the AQI, PM_{10} and number of days with severe pollution in Zahedan during the period July 2008 to March 2010.

Health Quality	Days	(%)	PM_{10} (µg. m^{-3})	AQI
Good	50	12.5	0-54	0-50
Moderate	263	66	55-154	51-100
Unhealthy for sensitive people	61	15.3	155-254	101-150
Unhealthy	13	3.2	254-354	151-200
Very unhealthy	4	1	355-424	201-300
Hazardous	9	2	>425	301-500

Among other meteorological parameters, such as air temperature and RH, the effect of wind speed and direction on AQI levels was found to be significant. Thus, the highest AQI values are found in summer (season with the highest temperature, lowest RH, and

highest sunshine duration), and are closely associated with strong northerly winds from the Sistan desert. During the period May to August, monthly mean AQI values were above 90, reaching up to ~130 in June-July (Table 4.4). This is in contrast to findings over the Greater Athens Area (Larissi *et al.*, 2010b) where, due to complex topography and the accumulation of pollutants, the AQI was higher during calm days and days with weak sea-breeze circulation and lower when strong northeasterly winds dominate. However, the present results reveal that the wind speed over Zahedan in summer acts as an additional tool for enhanced PM levels and deteriorating air quality.

Table 4.4: Monthly and seasonal mean Air Quality Index (AQI) values in Zahedan during the period July 2008 to March 2010.

Month Season	Air Quality Index (AQI)		
	mean	min	max
January	83	17	325
February	84	35	305
March	77	44	91
April	71	38	144
May	98	61	212
June	110	39	500
July	114	67	500
August	99	62	183
September	74	58	115
October	87	60	172
November	75	31	155
December	55	21	93
Winter	77	17	235
Spring	83	38	212
Summer	109	39	500
Autumn	80	31	172

4.3 PM concentration over the city of Zabol

Zabol (Fig. 4.1) is the biggest city in the Sistan region, close to the Iranian border with Pakistan and Afghanistan, in the southeastern part of Iran. This city has a population of more than 100,000. During the summer season, the city is under the influence of the Levar northerly winds, causing frequent dust and sand storms (Goudie and Middleton, 2000; Middleton, 1996) and contributing to the deterioration of the air quality (Rashki *et al.*, 2011). The Hamoun Lakes are located about 15 km north of Zabol. Desiccation of the Hamoun lakes, especially after 1999, has caused formation of a fine layer of sediment that is easily lifted by the wind; therefore Zabol is influenced by severe dust storms. The strong

winds, especially during the summer season, blow fine sands off the exposed lake bed and deposit this detritus within residential areas in Zabol and surroundings.

4.3.1 PM_{10} measurements

In order to provide a first ever in-situ analysis of the air quality and to compare the results with those obtained at Zahedan (located about 200 km south of Zabol), PM_{10} concentration measurements were obtained by using an automatic Met One BAM 1020 beta gauge monitor (Met One, Inc.,) over Zabol (Rashki *et al*., 2011). The instrument measures PM_{10} concentrations (in $\mu g.m^{-3}$) with a temporal resolution of one hour. The measurements were carried out at the Environmental Institute in Sistan located at the outskirts of Zabol during the period September 2010 to September 2011 (total of 373 days). The recording station is close to the Hamoun basin and is placed in the main pathway of the dust storms of the Sistan region. The hourly measured PM_{10} data were daily-averaged, from which the monthly values and seasonal variations were obtained (Table 4.5). For further assessing the air quality over Zabol, the PM_{10} concentrations were used to calculate an AQI.

Table 4.5: Monthly mean, daily maximum and daily minimum PM_{10} concentrations in Zabol during the period September 2010 to July 2011.

	Monthly Mean	**Daily minimum**	**Daily maximum**
Season	PM10 (µgm-3)	PM10 (µgm-3)	PM10 (µgm-3)
January	196	29	597
February	147	13	787
March	262	21	2698
April	224	97	515
May	322	71	1276
June	627	100	1875
July	847	110	2007
August	807	155	2448
September	564	88	1046
October	531	100	2339
November	200	66	737
December	476	84	3094
Winter	273	13	3094
Spring	270	21	2698
Summer	716	100	2448
Autumn	484	66	2339

The results show extremely large PM_{10} concentrations at Zabol (see Fig. 4.11), but it should be borne in mind that the instrumentation used for the PM10 monitoring is different between Zabol and Zahedan for any comparative purposes. Even the mean values are much higher than the most risky and dangerous maximum levels provided by the USEPA (397 μgm^{-3}). During each month, and especially during the period June to October, the area suffers from severe pollution since even the lower PM_{10} values are above 100 $\mu g.\ m^{-3}$, while the maximum ones are usually above 1000 $\mu g.m^{-3}$. On the other hand, extreme PM_{10} measurements associated with severe dust events may also occur in other months, for example like December.

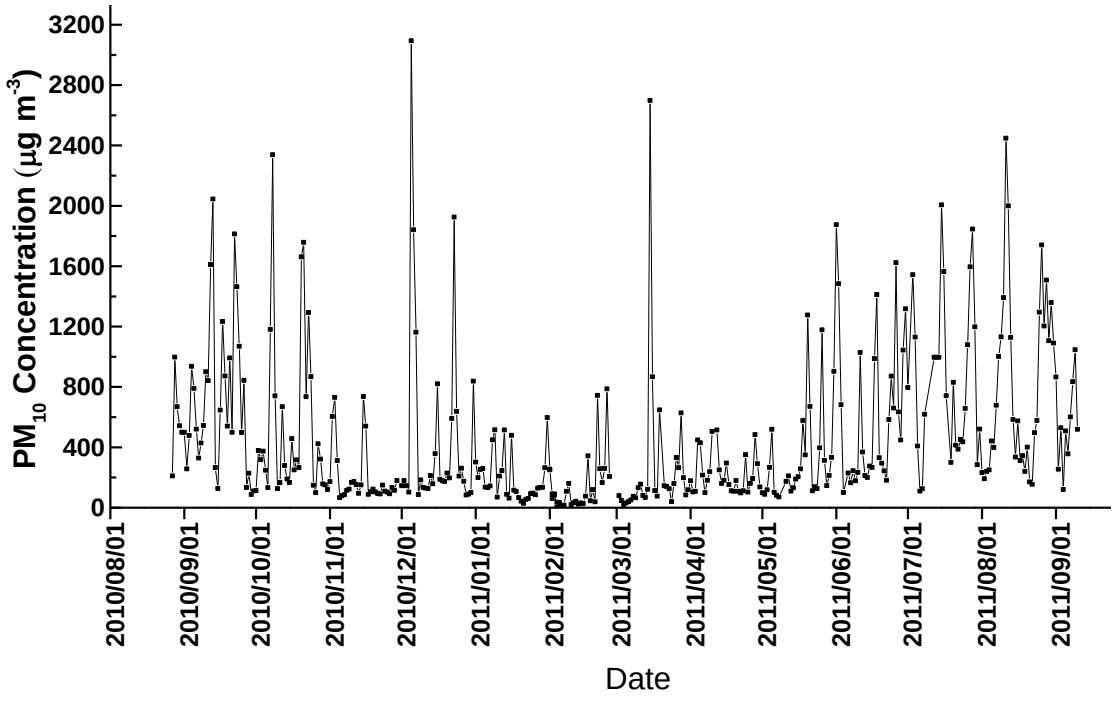

Figure 4.11: Daily PM_{10} concentrations at Zabol during the period 28/8/2010 to 10/9/2011.

Daily PM_{10} concentrations during major dust storms are about 10 to 20 times above the standard levels, and are much higher (~1000 to 2000 $\mu g.m^{-3}$) than those measured for intense dust storms at Zahedan (~400 to 600 $\mu g.m^{-3}$). Regarding the monthly mean PM_{10} concentrations, the results show extremely large values (>500 $\mu g.m^{-3}$) during the period June to October, reaching up to 743 $\mu g.m^{-3}$ in July. The annual variation of PM_{10} in Zabol is similar to that recorded at Zahedan (Rashki *et al*., 2011), but with much higher values at the former site, in the order of ~160 to 170 $\mu g.m^{-3}$ in winter and spring and ~510 $\mu g.m^{-3}$ in summer. These large differences in PM_{10} concentrations between the two neighboring (Fig. 4.1) cities are attributed to severe dust storms that directly affect Zabol, which is

located along the main pathway of intense dust plumes, while Zahedan is usually influenced by the margins of the dust storms originating from Hamoun.

The frequency of occurrence of PM_{10} concentrations for each season is depicted in Fig. 4.12. In summer ~60% of the PM_{10} values were higher than 425 $\mu g.m^{-3}$, while the lower PM_{10} values occur in winter and spring with larger frequency in the 55-154 $\mu g.m^{-3}$ interval. Autumn also presents high frequency in the >425 $\mu g.m^{-3}$ interval that might be due to continues the Levar wind in September.

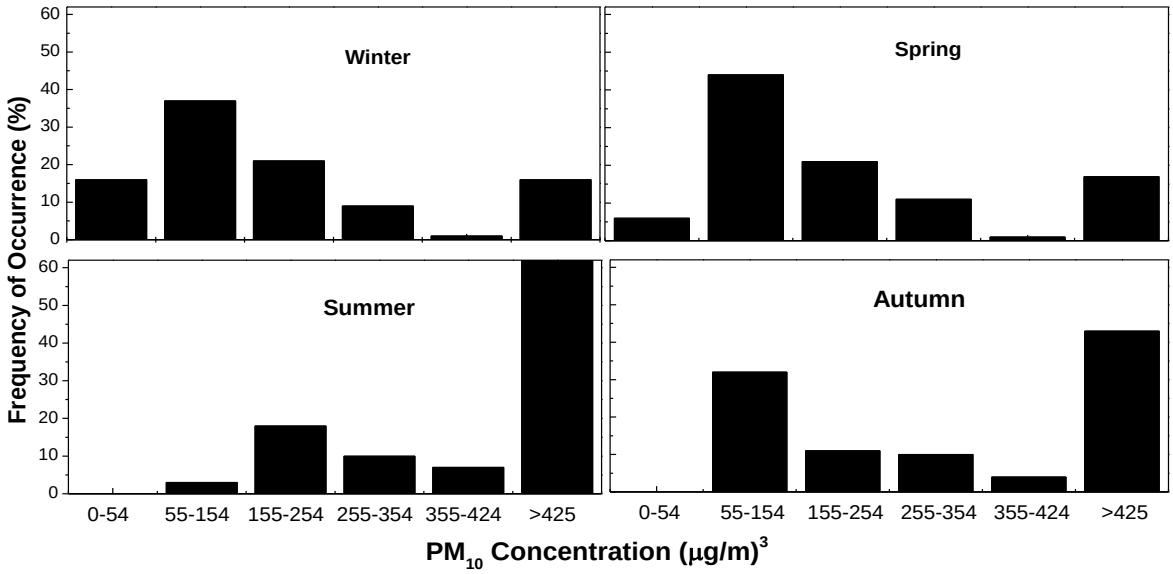

Figure 4.12: Frequency (%) distribution of the daily PM_{10} values for each season in Zabol.

4.3.2 Air quality index

In order to identify the impact of air pollution on human health, air pollution indices are commonly used, of which the AQI is the most well known (EPA, 1999; Mohan and Kandya, 2007; Larissi *et al*., 2010a). The AQI is divided into six categories, varying from 0 to 500, with different health impacts as listed in Table 4.6. The AQI for Zabol was calculated for the period September 2010 to July 2011 using the same technique as for Zahedan. This will make comparisons of air quality between the two cities possible.

Assessment of air quality in Zabol shows that 243 days out of 370 (65%) exhibit air pollution levels of above the air quality standards (>155 μgm^{-3}), a fraction that is much higher than that (26.5%) reported for Zahedan. The most significant finding is the 129 days (34.9%) that are characterized as hazardous (Table 4.6), which in combination with the adverse effects on human health, make it clear that environmental conditions in the

Sistan region are rather poor for human well-being. On the other hand, only 5.7% of the days are associated with low pollution levels when the air quality is considered satisfactory and air pollution poses little or no risk. Several studies have shown that ambient air pollution is highly correlated with respiratory morbidity, mainly amongst children (Bartzokas *et al.*, 2004; Nastos *et al.*, 2010; Samoli *et al.*, 2011).

Table 4.6: Health quality as determined by the Air Quality Index (AQI), PM_{10} and number of days with severe pollution in Zabol during the period September 2010 to July 2011

Health Quality	AQI	PM10 (µg. m-3)	Days	(%)
Good	0-50	0-54	21	5.7
Moderate	51-100	55-154	106	28.6
Unhealthy for sensitive people	101-150	155-254	66	17.8
Unhealthy	151-200	254-354	36	9.7
Very unhealthy	201-300	355-424	12	3.2
Hazardous	301-500	425<	129	34.9

The results gathered from hospitals in the Sistan region showed that during dust storms respiratory patients increased significantly, especially those affected by chronic obstructive pulmonary disease and asthma. The percentage of these diseases increases in summer (June and July) (Miri *et al.*, 2007). Apart from the dust storms, re-suspended dust within the urban environment is a strong source of PM10 concentrations, while urban-anthropogenic and industrial activities are considered to have a much lower effect on the air pollution over Zabol.

Mean diurnal variation of PM_{10} concentrations for each season in Zabol indicates a clear pattern for all seasons except winter, with the maximum of the diurnal variation being observed in the middle of the day ((~08:00 to 11 LST) while in winter PM_{10} values reach a maximum in the afternoon hours to early morning (~16:00 to 02:00 LST). Solar heating and vertical mixing of pollutants may be the main reasons for the reduction of PM_{10} levels at local noon and early afternoon hours. However, the maximum PM_{10} concentrations normally occur between 08:00 LST and 11:00 LST. The diurnal PM_{10} variability in all seasons except winter is closely associated with the intensity of the wind speed measured at the Zabol meteorological station (see Fig. 4.13). This wind, being northerly in direction, carries large quantities of dust from the Hamoun dry lake bed. The mean diurnal wind speed variation is similar for all seasons; however, the wind favors the increase of aerosol load in summer and autumn (maximum PM_{10} for higher wind speeds).

Note that the Hirmand River and some other ephemeral provide some water in winter and spring to the Hamoun lake beds. Therefore in early summer, the Hamoun lakes are wet and at the end of summer and early autumn are always completely dried out. On the other hand, the Levar wind continues also in September and so high wind speeds cause huge dust storms (Fig. 4.13).

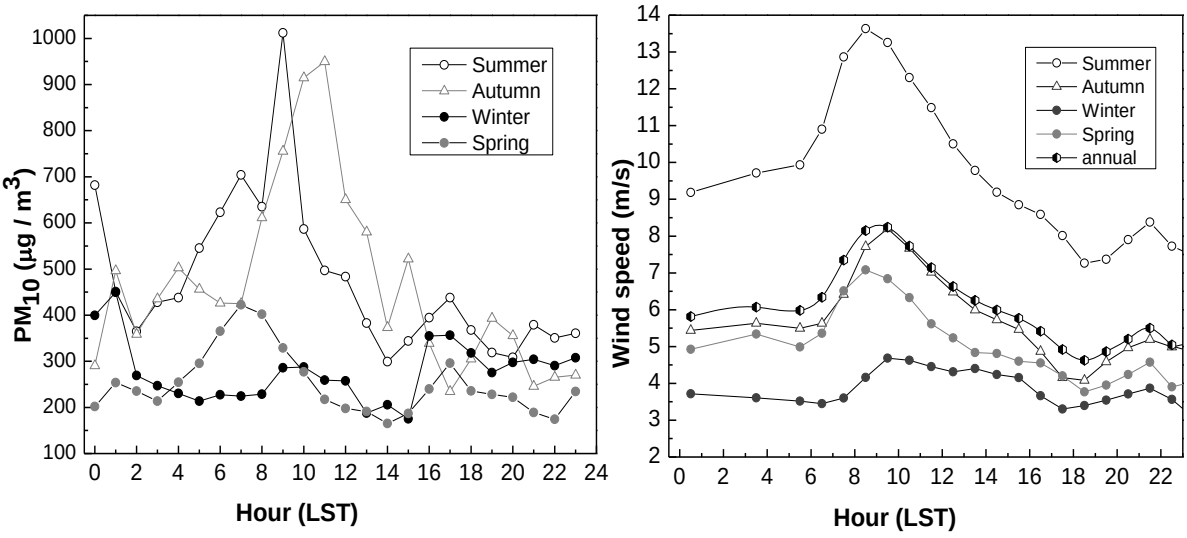

Figure 4.13: Mean hourly variation of the PM_{10} (left panel) and wind speed (right panel) for each season in Zabol.

4.4 Conclusions

Systematic PM concentrations were measured in two cities affected by the Sistan dust storms, Zabol and Zahedan, in southeast Iran covering the period September 2010 to September 2011 and July 2008 to March 2010, respectively. The present Chapter focused on analyzing the daily, monthly and seasonal variability of PM levels and to establish the role of the "Levar" wind in deteriorating the air quality.

The results show that the PM_{10} concentrations were considerably higher than the corresponding European Union air quality annual standard and the mean $PM_{2.5}$ concentration (32 μgm^{-3}) also overcame the AQI annual $PM_{2.5}$ standards. The analysis of the daily PM concentrations showed that the air quality is affected by dust storms from the Sistan desert, which may be very intense during summer.

The drainage of the Hamoun wetlands, in association with the intense Levar winds in summer, is the main factor responsible for the frequent and massive dust storms over the Sistan region. Hamoun, as an intense dust source region, caused a dramatic increase in PM_{10} concentrations and a deterioration of air quality (65% of the days were considered unhealthy for sensitive people and 34.9% as hazardous) in Zabol city.

The PM_{10} and $PM_{2.5}$ levels in Zahedan showed an annual pattern of summer high and winter low, while the $PM_{1.0}$ exhibited the opposite pattern. The maximum PM_{10} concentrations occurred between 8:00 to 11:00 LST in Zabol and between 12:00 and 20:00 LST in Zahedan, indicating that Sistan dust storms reach Zahedan after 6 to 9 hours. The strong correlation between daily $PM_{2.5}$ and PM_{10} concentrations indicated that they have similar sources and an increase of PM_{10} significantly affects $PM_{2.5}$. The strong correlation and the absence of scatter especially in summer also imply that the linear regression model can be used reliably for future predictions, especially for $PM_{2.5}$. Considering the air pollution standards defined by the U.S. Environmental Protection Agency, determining that only on one day per year may the AQI be higher than 100, it was found that the values of AQI in Zahedan overcame this level for 86 days out of 399, expressing a fraction of 21.5%. It should be noted that on 25 days (6.3%) the atmospheric conditions were very unhealthy or hazardous for the whole population and this requires more attention by officials, managers and urban planners.

CHAPTER 5

CHEMICAL AND MINERALOGICAL CHARACTERISTICS OF AIRBORNE DUST

5.1 Introduction

Mineral dust plays an important role in the optical, physical and chemical processes in the atmosphere (Xi and Sokolik, 2012), while dust deposition adds exogenous mineral and organic material to terrestrial surfaces having a significant impact on the Earth's ecosystems and biogeochemical cycles (Jickels *et al.*, 2005; Lawrence and Neff, 2009). Dust particles are fine airborne soil and/or weathered or transported rock particles removed from the Earth's surface as a result of wind erosion under certain climatic, meteorological and soil conditions. The Earth's surface is composed of a large number of minerals, which occur in heterogeneous mixtures within rocks and weathering mantles. Analysis of the physical properties and chemical composition of dust aerosols is, therefore, important to determine aerosol sources, mixing processes and transport pathways (Bergametti *et al.*, 1989; McConnell *et al.*, 2008; Mishra and Tripathi, 2008). It is estimated that 1000 to 3000 Tg of mineral aerosols are emitted annually into the atmosphere over the globe (d'Almeida, 1987; Jones *et al.*, 1995), which can be transported over long distances (e.g., Prospero, 1999). The role of dust aerosols in atmospheric processes (i.e. Earth's radiation balance, cloud microphysics, etc) strongly depends on a variety of physico-chemical parameters, size distribution, dust sources, atmospheric lifetime and mixing processes in the atmosphere (Charlson *et al.*, 1992; Tegen and Fung, 1994; Andreae, 1996; Frank *et al.*, 1996; Sokolik *et al.*, 1998; Rosenfeld *et al.*, 2008).

Some dust contaminants (soluble and chelatable metallic salts, pesticides, etc) affect human health when they are transported over densely populated areas (Larney *et al.*, 1999), retained in residences and other occupied structures (Lioy *et al.*, 2002), and they also impact the nutrient loading of waters flowing from adjacent watersheds (Wood and Sanford, 1995) and terminal bodies of water by direct and indirect deposition (Ganor *et al.*, 2003; Lawrence and Neff, 2009). PM is a complex mixture of substances suspended in

the atmosphere in solid or liquid state with different properties (e.g. variable size distribution or chemical composition amongst others) and origins (anthropogenic and natural). Owing to this mixture of substances, the chemical composition of PM may vary widely as a function of emission sources and the subsequent chemical reactions which take place in the atmosphere (Chow *et al*., 2003; Engelbrecht *et al*., 2009; Mishra *et al*., 2010). Therefore, it is important to determine temporal variations in aerosol concentrations to assess health exposure effects and to improve correlations between source emission rates and ground-based measurements (Christopher *et al*., 2004; Kidwell and Ondov, 2004; Nastos *et al*., 2010). The chemical mass balance is the most commonly used method for assessing PM source contributions (Wilson *et al*., 2002), while statistical methods, such as factor analysis and multi-linear regression (Thurston and Spengler, 1985), have also produced interesting results regarding dust source identification. Elemental and mineralogical analyses have also been used to identify the source regions of dust deposited in Arctic ice caps (Biscaye and Grousset, 1998) and on other depositional surfaces (Shaw, 1980; Lawrence and Neff, 2009).

The Sistan region located in southeastern Iran is a major dust source in southwest Asia (Goudie and Middleton, 2000), often producing intense dust storms that cover Sistan and the southwest of Afghanistan and Pakistan (Alam *et al*., 2011; Rashki *et al*., 2012). Particles from dust storms might also cover farm and grasslands resulting in damage to crops and fill the rivers and water channels with aeolian material. After the extreme drought of 1999, the dust activity over Sistan appears to be increasing in both frequency and severity. Over recent years, ten thousands of people have suffered from respiratory diseases and asthma during months of devastating dust storms in the Sistan basin, especially in the cities of Zabol and Zahak and the surrounding villages (Miri *et al*., 2007). According to the Asthma Mortality Map of Iran, the rate of asthma in Sistan is, in general, higher than in other regions (Selinus *et al*., 2010).

In order to understand the influence of dust on the atmospheric environment, climatic system and health and to establish effective remedial policies and strategies, it is regarded as necessary to investigate the chemical (composition and mineralogy) characteristics of airborne and soil dust over Sistan. To the best of our knowledge there are currently no published studies about the geochemical characteristics and dust mineralogy, and only few about the geology and potential impact of airborne dust on human health in

this region, such as the first PM analysis over Zahedan city (Rashki *et al*., 2011), the investigation of the sediment loading during major dust events over the Hamoun basin (Jadidoleslamir *et al*., 2011; Rashki *et al*., 2012) and the effects of droughts and winds on desertification (Ranjbar and Iranmanesh, 2008; Hosseini *et al*., 2010). Moreover, nearby locations, Bagram and Khowst in Afghanistan, were selected for analyzing the mineralogical dust composition, major and trace elements whitin the framework of the Enhanced Particulate Matter Surveillance Program (EPMSP) campaign (Engelbrecht *et al*., 2009). Furthermore, mineralogical and geochemical characteristics of dust were recently examined at Khuzestan province in southwestern Iran (Zarasvandi *et al*., 2011).

In this thesis, an overview of the geological-geochemical characteristics of airborne and soil dust in the Sistan region is given for airborne and soil samples collected during the period August 2009 to August 2010. The chemical constituents during major dust storms over the region are analyzed at two locations, also investigating the relationship between the chemical constituents of the dust storms and those of the inferred (Hamoun) source soils.

5.2 Methods, data and material samples

The amount of sediment loading during major dust storms was measured using passive dust samplers fixed on two monitoring towers (at four and eight meters from ground), with one meter distance between the traps (Fig 3.9), during the period August 2009 to August 2010 (Rashki *et al*., 2012). The towers were installed in two opens locations near Hamoun (31.10^{o}N, 61.51^{o}E and 31.20^{o} N, 61.61^{o}E), and sufficiently far away from any obstacles, so that undisturbed wind flow was entering the samplers (stations A and B in Fig. 3.8). After each measurement, the samplers were evacuated to be ready for measuring the next dust event. The most commonly used passive sampling techniques collect dust using a non-reactive collection pan filled with glass marbles, which serves as the depositional surface (Goossens and Offer, 1994; Reheis and Kihl, 1995). Furthermore, during the summer of 2009, topsoil samples at depths of 0 to 5 cm were collected from different land-use areas in Hamoun and Sistan. These samples were selected and analyzed as they are good indicators of the atmospheric deposition of geochemical elements in the Sistan region.

5.2.1 Chemical and mineralogical analysis

Analyses of the chemical and physical characteristics of dust particles are regarded as essential in studies on the environmental impact of dust storms (Zarasvandi, 2009). Determination of the chemical composition of airborne dust is also necessary for clarifying the likely sources of dust and is important for quantitative climate modeling and understanding the possible effects of dust on health, soils, precipitation, ocean-biogeochemistry and weathering phenomena (Goudie and Middleton, 2006). During the dust-storm days in 2009 and 2010, 132 samples of airborne dust were collected at the two stations in the Sistan region. These samples were analyzed at the University of Pretoria, South Africa, in the Stoneman Laboratory (Geology Department) for major and trace elements, and for minerals by X-Ray Fluorescence (XRF) and X-Ray Diffraction (XRD) techniques, respectively.

The samples were prepared for XRD analysis using a back loading preparation method. They were analyzed using a PANalytical X'Pert Pro powder diffractometer with X'Celerator detector and variable divergence and receiving slits with Fe filtered Co-Kα radiation. The phases were identified using X'Pert High score plus software. The relative phase amounts (weights %) were estimated using the Rietveld method (Autoquan Program). Mineral analysis by XRD is the single most important nondestructive technique for the characterization of minerals such as quartz, feldspars, calcite, dolomite, clay, silt and iron oxides in fine dust. Mineral phase analysis by XRD is one of few techniques that is phase sensitive, rather than chemically sensitive, as is the case with XRF spectrometry. Quantitative mineralogical analyses using XRD technique have been performed by a number of scientists over the globe (e.g., Rietveld, 1969; Sturges *et al*., 1989; Caquineau *et al*., 1997; Engelbrecht *et al*., 2009; Zarasvandi, 2009).

The sample preparation for XRF is made up of two methods, pressed powders and fusions. The former samples were prepared for trace element analyses and the latter for major element analyses. Each milled sample (<75µm) was combined with a polyvinyl alcohol, transferred into an aluminum cup and manually pressed to ten tons. The pressed powders were dried at 100°C for at least 30 minutes and stored in a desiccator before analyses were conducted. For the fusion method, each milled sample (<75µm) was weighed out in a 1/6 sample to flux (Lithium tetraborate) ratio. These samples were then

transferred into mouldable Pt/Au crucibles fused at 1050°C in a muffle furnace. Aluminum cooling caps were treated with an iodine-ethanol mixture (releasing agent) and placed on top of the crucibles as they cooled. Some samples needed to be treated with an extra 3g of flux if they continued to crack.

Finally, all geochemical samples were analyzed using the Thermo Fisher ARL 9400 XP+ Sequential XRF. The Quantas software package was used for the major element analyses and the WinXRF software package was used for the trace element analyses. The concentrations of the major elements are reported as oxides in weight percentages, while the trace element concentrations are reported as elements in parts per million (ppm). All the dust samples, airborne and soil, were subjected to microscopic imaging, while Scanning Electron Microscopy (SEM) images were performed for the airborne dust samples at stations A and B.

5.2.2 Enrichment factor analysis

The calculation of Enrichment Factors (EFs) relative to the Earth's upper crust composition can be used to discriminate between the origins of elements from crustal or non-crustal sources (Zhang et al., 2004). EFs of elements in different particle fractions were determined by comparing the concentration of each element against the concentration of a reference (crustal) element to obtain a preliminary idea about possible origin sources, i.e crustal or anthropogenic. Usually silicon (Si), Aluminum (Al) or Iron (Fe) is used as the reference element, but there is no universally accepted rule for its choice. In this study, Si was used as the reference element, as done previously by many investigators (Lee and Hu, 1995; Bilos et al., 2001; Manoli et al., 2002; Choi and Bang, 1999; Han et al., 2005; Wang et al., 2007). Estimates of EF aid in (a) differentiating between element concentrations that originate from human activities and those from natural sources and, in (b) assessing degree of anthropogenic influence (Cong et al., 2007). The appropriateness of choosing Si is attributed to its more significant distribution in coarse particles (83% on average) than other elements, with very low contribution from non-crustal inputs (Wang et al., 2006). The abundance ([E/R] Crust values) of elements in the Earth's crust was taken from Wang et al. (2006). The EFs for crustal material (EF_{crust}) were calculated as follows:

$$EF_{Crust} = [E/R]_{Air} / [E/R]_{Crust} \quad (5.1)$$

Where E is the elemental concentration, R is a reference element (R = Si in this thesis) of crustal material and $[E/R]_{Air}$ is the concentration ratio of E to R in a collected aerosol sample, and $[E/R]_{Crust}$ is the concentration ratio of E to R in the Earth's crust. Si was used as reference element because it is abundant in the crustal materials, it is usually not of anthropogenic origin and, consequently, values of EF_{Si} are close to one. If EF_{Crust} approaches unity, then crustal soils are most likely the predominant source of element E. In practical terms, if the EF_{Crust} value is above 10, then the element is considered to be of non-crustal origin, possibly anthropogenic (Scheff and Wadden, 1997; Gao *et al*., 2002; Wang *et al*., 2006). EF_{Crust} values in the range of 1 to 5 suggest no significant contribution of anthropogenic sources to the ambient level of these elements. In general, as the EF_{Crust} value increases, the non-crustal source contribution also increases.

5.3 Results and discussion

5.3.1 Mineralogical characteristics of dust

Although the optical and physical properties of dust are well-defined, less knowledge is available about the spatio-temporal variations of the chemical composition of dust. The mineralogical characteristics of dust samples at stations A and B (Fig 5.1a, b) were obtained by means of XRD analysis. The mineralogy percentage composition averaged at all heights for each day is shown in Fig. 5.1a, b for stations A and B, respectively. The chemical formulas of the main mineralogical components are given in Usher *et al*. (2003), as well as the chemical reactions of dust with atmospheric constituents and trace gases during the dust life cycle. The mineralogical composition corresponds to screened samples with diameter <75 μm and can constitute an indication of both regional geology and wind transported dust that is deposited in local soils (Engelbrecht *et al*., 2009). Furthermore, dust mineralogy has been used for the identification of different source regions over the globe (Claquin *et al*., 1999; Krueger *et al*., 2005).

Emphasizing the dust mineralogy at station A, it is seen that the airborne dust is mainly composed of quartz, which is the dominant component (26-40%) for all the days of observations. Calcareous particles, mainly consisting of calcite, is the second dominant mineralogical component over the site with average mass percentage of 22%, while micas (muscovite) contribute 13% and plagioclase (albite), 11%. The remaining components

contribute much less to the dust mass, while chlorite (6.3%) is apparent in all dust samples for all days. The others, i.e. dolomite, enstatite, gypsum, halite, etc are present only at some samples with various percentages. It is quite interesting to note that quartz is much more common over Sistan than the feldspars (plagioclase, microcline and orthoclase).

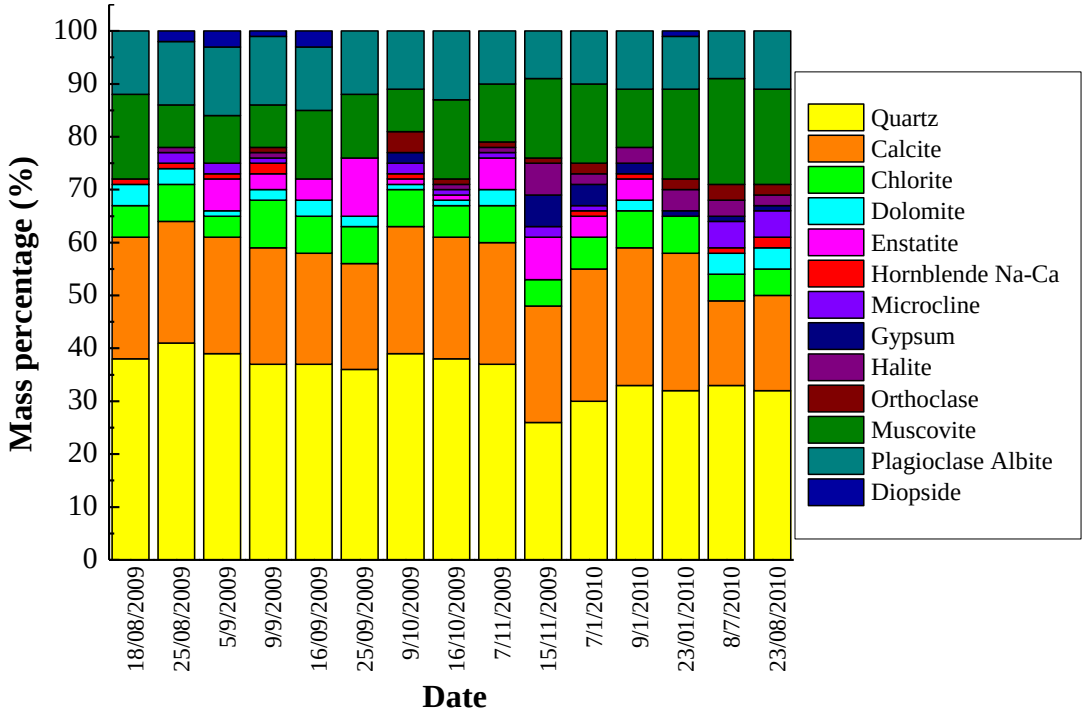

Figure 5.1a: Mineralogical composition as obtained from X-Ray Diffraction (XRD) analysis for airborne dust samples collected on different days at station A (Fig. 3.8).

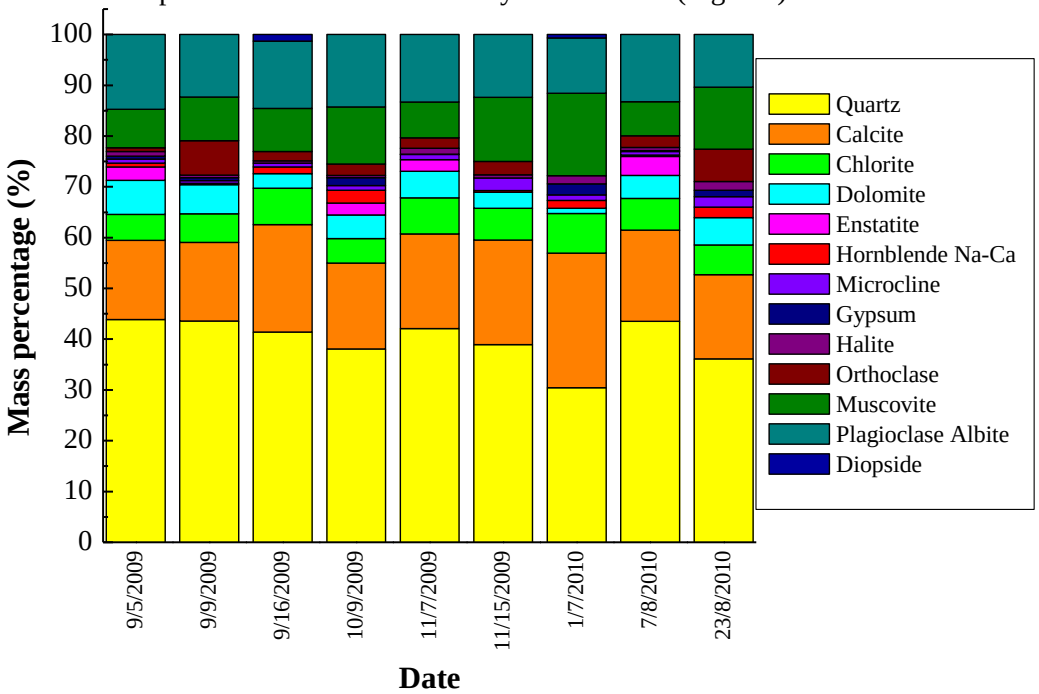

Figure 5.1b: Same as in Figure 3a, but for station B.

The mineralogical analysis for the nine days recorded data at station B (Fig. 5.1b) shows more or less similar results to those obtained for station A and, therefore, any discussion will be given on their comparison (Fig. 5.3). The mineralogical composition has the same descending order as in station A, i.e. quartz (39.8±4.4%), calcite (18.8±3.5%), plagioclase (albite) (12.7±1.4%) and muscovite (10.1±3.2%). On the other hand, dust deposition may influence biogeochemical cycling in terrestrial ecosystems, while dust accumulation in soils can influence texture, element composition and acid neutralizing capacity (Larssen and Carmichael, 2000; Muhs and Benedict, 2006). Furthermore, the chemical and mineralogical composition of soil dust provides useful information about its provenance (Yang *et al.*, 2007), radiative forcing implications (Sokolik and Toon, 1999) and human health effects (Erel *et al.*, 2006). For these reasons, in addition to the airborne dust samples, soil samples were collected at 16 locations around Sistan and Hamoun, at depths ranging from 0 to 5 cm from the soil crust. The results of soil sample mineralogy are summarized in Fig. 5.2.

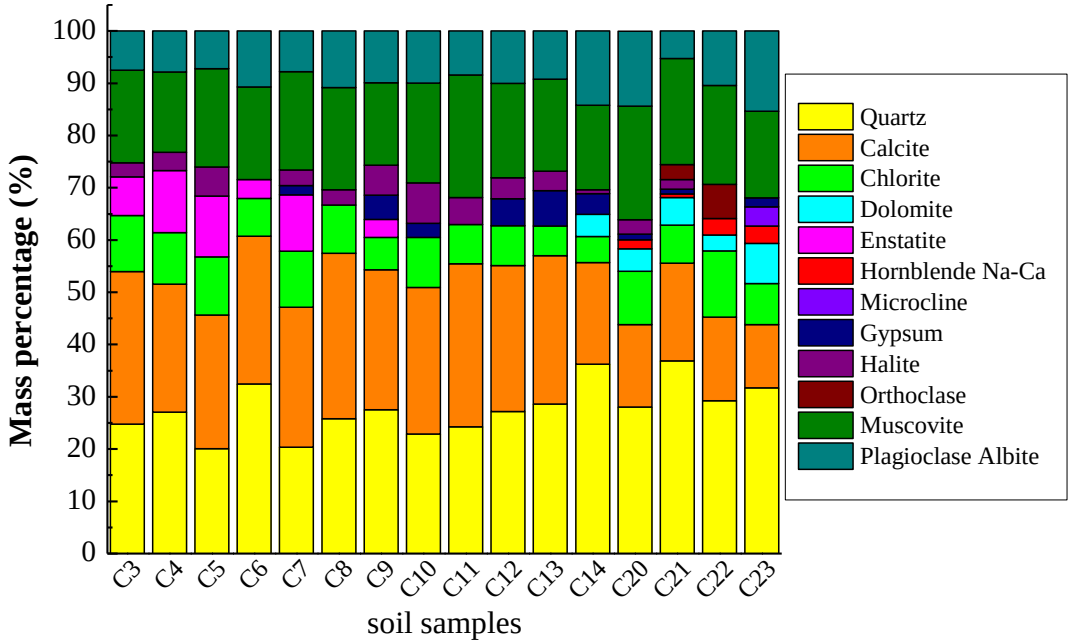

Figure 5.2: Mineralogical composition as obtained from X-Ray Diffraction (XRD) analysis for soil samples collected at various locations in the Hamoun Basin.

From an initial consideration of these results, it is established that the soil samples exhibit similar mineralogy to the airborne dust at both stations, thus suggesting similarity in sources for both airborne and soil dust. On the other hand, some soils in the Sistan region have been primarily formed from dust transported from the Hamoun lakes,

presenting large similarities in mineralogy and chemical composition to airborne dust. However, atmospheric chemical reactions involving dust and aerosols of other types can alter the chemical characteristics of dust before its deposition (Dentener *et al*., 1996). Therefore, the mineralogy of the soil samples may differ significantly in comparison to the results obtained for airborne dust at stations A and B, since some of the soil samples (11 samples) were collected in the Hamoun dried lakes and others (four samples) around stations A and B.

Figure 5.3 summarizes the results from the mineralogical analysis of samples taken at the two stations and from the soil samples, allowing a quantitative comparison between them. The vertical bars correspond to one standard deviation from the mean for both airborne and soil samples. The distance from the source region from whence dust is deposited also influences the particle size distribution, mineralogy and chemical composition of dust. Therefore, generally speaking, at local scales quartz clearly dominates with fractions up to ~50%, while as the distance from the dust source increases, feldspars (plagioclase, microcline) and phyllosilicate minerals (illite and kaolinite) present increased fractions (Arnold et al., 1998; Lawrence and Neff, 2009). However, in our study the dust samples were all obtained within the same area, and therefore are mineralogically similar. Nevertheless, station B, which is located closer to the Hamoun basin, the source of dust exposures, exhibits higher percentages of quartz, while station A (near to Zabol city) exhibits higher concentrations of calcite and muscovite compared to station B. On the other hand, the soil samples exhibit a lower mean percentage for quartz (27.7±4.7) and higher percentages for calcite, chlorite, halite and muscovite compared to the airborne samples.

These mineralogical airborne dust and soil compositions, derived essentially from the Hamoun source region, reflect the composition of the material available from this provenance as well as the relevant grain size characteristics, enabling the wind storms to entrain this material into the lower atmosphere. While most of the minerals (quartz, feldspars of various types, muscovite) can easily be tied to basement-type lithology of generally gneissic-granitic character, others (chlorite, pyroxenes and hornblende) rather suggest mafic parent rocks, as can be inferred from basic mineralogical analysis (e.g., Deer *et al*., 1966).

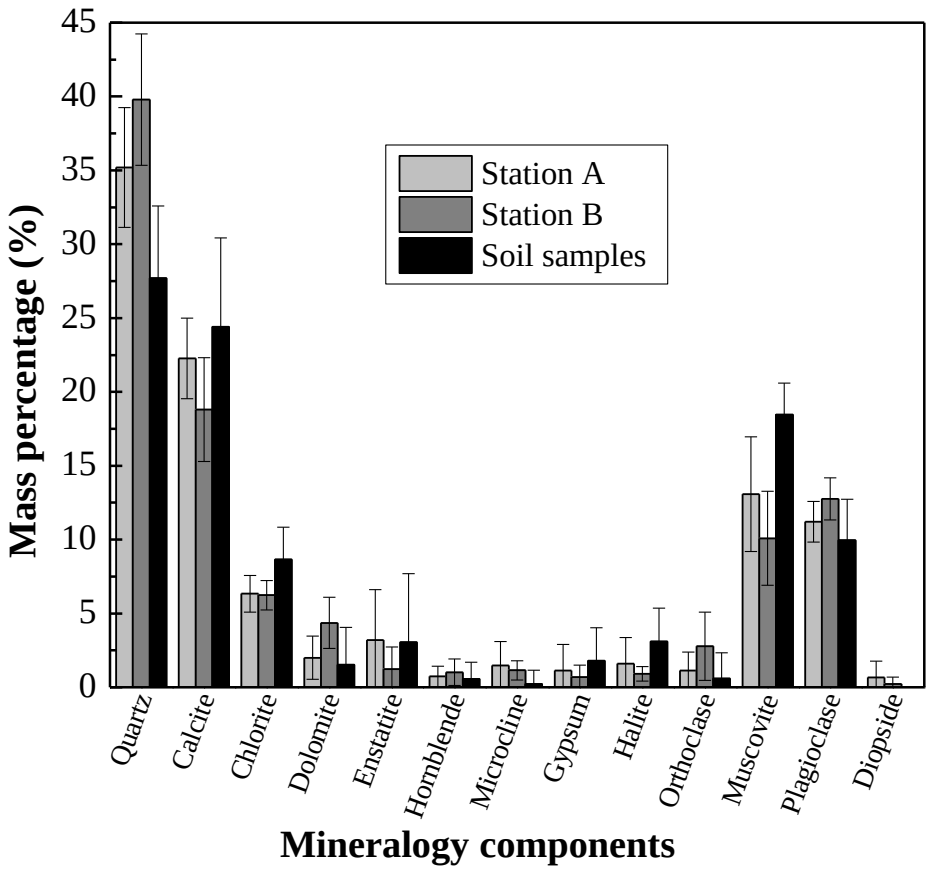

Figure 5.3: Average mineralogy components for airborne dust samples at stations A and B and for soil samples obtained at various locations in the Hamoun Basin. The vertical bars express one standard deviation from the mean.

However, the calcite, dolomite, halite and gypsum suggest evaporite minerals, although both calcite and dolomite can also reflect alteration products of primary acid or mafic rock constituents. The inferred evaporite minerals reflect local derivation of salt from desiccating water bodies in the Hamoun lakes, originally formed from altered transported components via the Hirmand river system. Thus, the semi-quantitative mineral determinations for the airborne dust over the Sistan region support derivation of the particles from well weathered and well eroded (transported) argillaceous alluvium from the extensive Hirmand river system draining Afghanistan and terminating in the Hamoun Basin. The general geology of Afghanistan encompasses extensive terrains of both acidic and mafic rocks, while similar mineralogical composition of dust (i.e. dominance of quartz, but lower percentage of calcite) was found at the Bagram and Khowst sites located in eastern Afghanistan (Engelbrecht et al., 2009). More specifically, they found that these

sites are underlain by loess (wind deposited silt), sand, clay and alluvium containing gravel. As shown in Fig. 2.6 and 3.8, as well as in other studies (Engelbrecht et al. 2009; Alam et al., 2011; Rashki et al., 2012 a, b), nearly the whole of Afghanistan is affected by the dust storms originating from Hamoun, since the dust plume usually follows a counter-clockwise direction, carrying wind-blown dust towards eastern Afghanistan. Similarly to our findings, the airborne dust at selected locations in southwestern Iran was found to be composed mainly from quartz and calcite, suggesting detrital sedimentary origin, followed by kaolinite and a minor percentage of gypsum (Zarasvandi, 2009). Furthermore, Engelbrecht et al. (2009) found that airborne dust samples derived from poorly drained rivers and lakes in central and southern Iraq contain substantial calcite (33– 48%), quartz, and feldspar with minor chlorite and clay minerals. Previous studies (Schütz and Sebert, 1987; Reheis and Kihl, 1995) have shown that silicate minerals (quartz, feldspars) and phyllosilicates (illite, kaolinite, smectite/montmorillonite clays, chlorite) dominate eolian dust. Dust samples may also contain substantial amounts of carbonates, oxides, gypsum, halite and soluble salts, but the quantity and percentage of these minerals are quite variable from site to site.

Fig. 5.4 shows the altitude variation of the dust mineralogy for dust samples collected during 9 dust-storm days at 8 heights from station B. The mass percentages correspond to the average values during the dust storms over the region. The results show no clear tendency in the altitude variation of the dust mineralogy, at least within the first eight meters from the ground, suggesting that dust is regionally transported within the lower boundary layer. The surface winds over Sistan control the dust erosion and emission rates (Rashki *et al*., 2012), thus determining the quantity, chemical and mineralogical composition of dust emitted over the region.

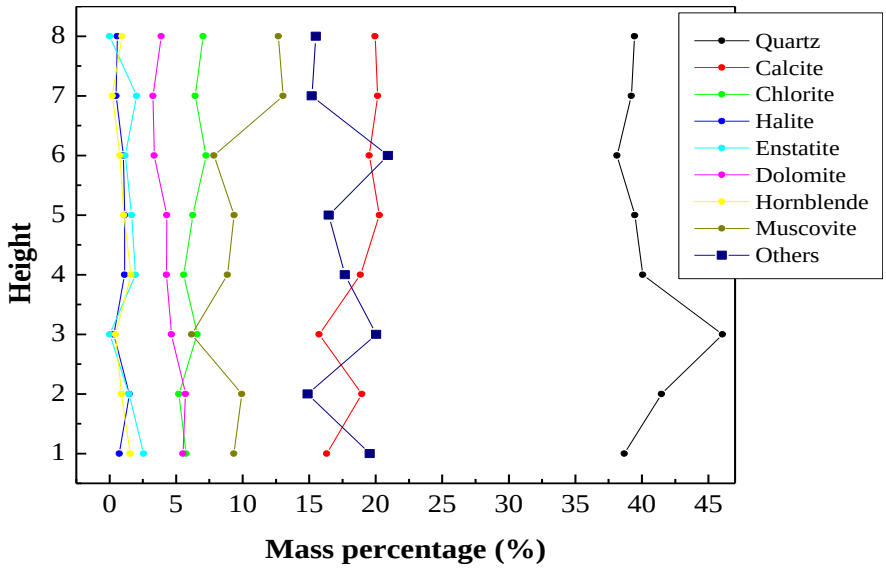

Figure 5.4. Mean altitude variation of dust mineralogy components at station B. *[others: Plagioclase, Orthoclase, Microcline, Gypsum, Bloedite, Diopside, Hornblende Na-Ca]*

5.3.2 Elemental composition of dust

Knowledge of the chemical composition of airborne dust is necessary for clarifying the likely source regions and is important for quantitative climate modeling, in understanding possible effects on human health, precipitation, ocean biogeochemistry and weathering phenomena (Goudie and Middleton, 2006). Chemical analysis of dust provides valuable information about potentially harmful trace elements such as lead, arsenic and heavy metals (Cobalt (Co), Chrome (Cr), Copper (Cu), Nickel (Ni), lead (Pb)). On the other hand, the major-element and ion-chemistry analyses provide estimates of mineral components (Figs. 5.1-5.3), which themselves may be hazardous to human health and ecosystems and which can act as carriers of other toxic substances. The chemical analysis of dust samples at both stations was performed via XRF analysis for the major oxides (Figs. 5.5a, b).

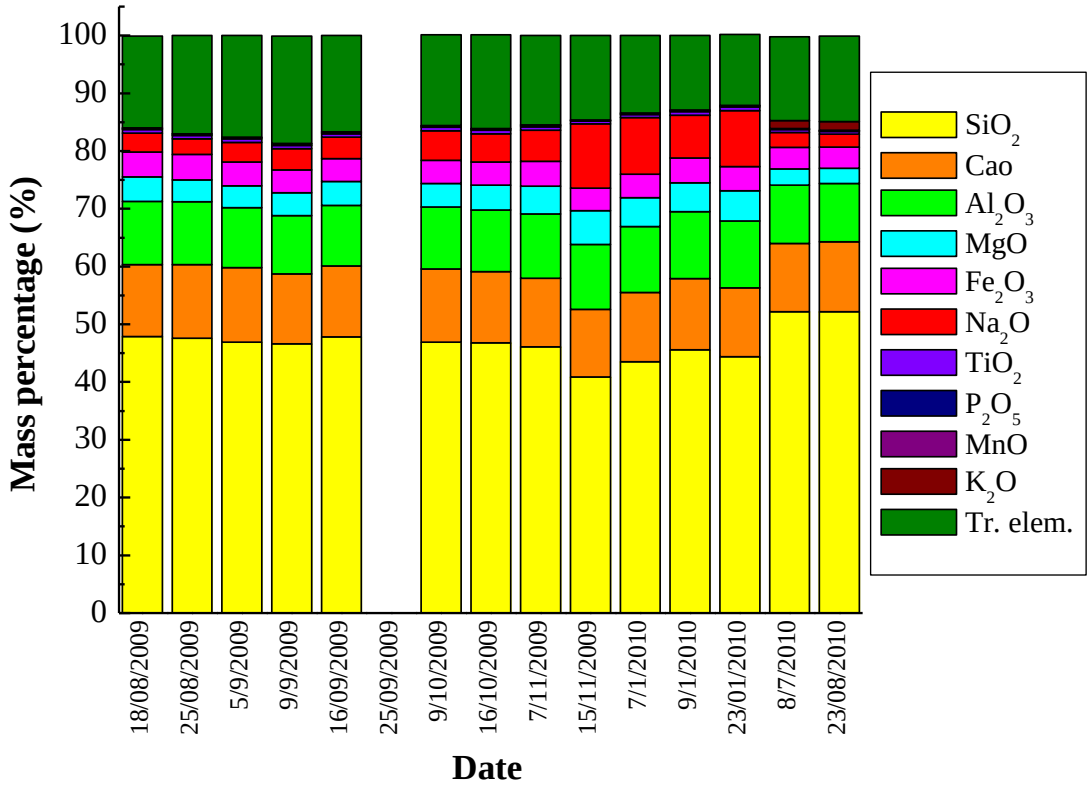

Figure 5.5a: Major elements (oxides) for airborne dust samples obtained on different days at Station A by means of the X-Ray Fluorescence (XRF) analysis.

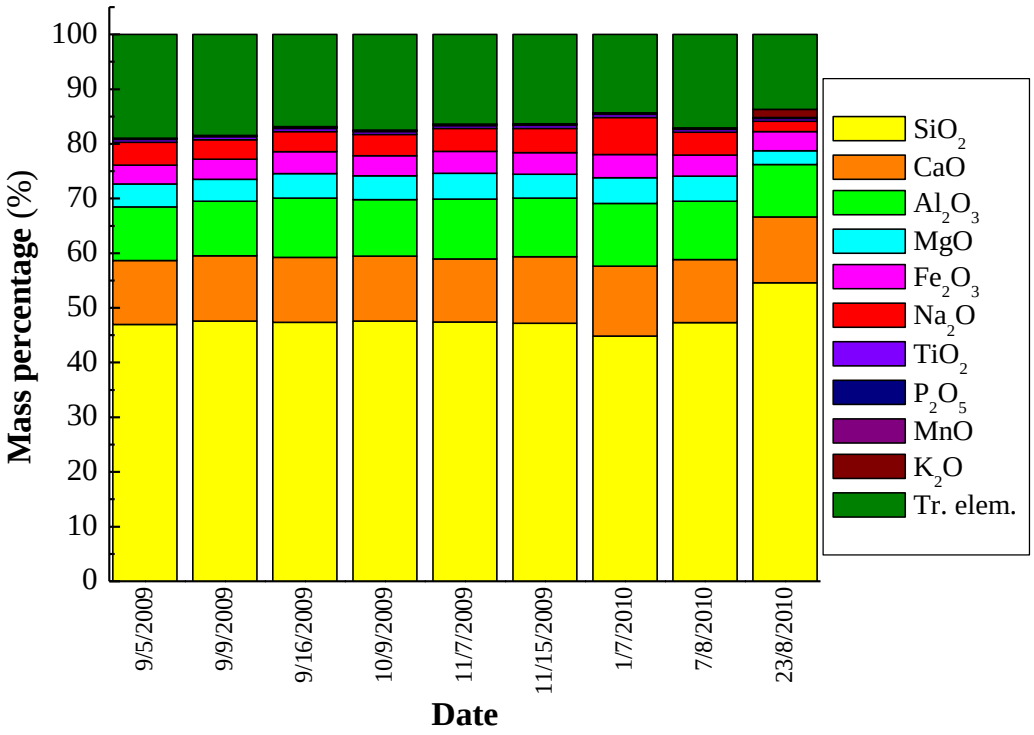

Figure 5.5b: Same as in Figure 5.5a, but at station B.

In general, the analysis reveals that all samples at both stations A and B contain major amounts of Silicon dioxide (SiO_2), mainly in the mineral quartz, variable amounts of Calcium oxide (CaO) in the mineral calcite, plagioclase feldspar and to a limited extent in dolomite, as well as substantial Aluminum oxide (Al_2O_3) concentrations. More specifically, average major elements of airborne dust at both stations indicate a predominant SiO_2 mass component (46.8 – 47.8%) with significant CaO (12-12.2%) and Al_2O_3 (10.4-10.8%) contributions; a few percent of Sodium oxide (Na_2O) (4.2-5.4%), Magnesium Oxide (MgO) (4.3%) and total iron as Iron (III) Oxide (Fe_2O_3) (3.8-4.1%), as well as trace amounts (<1%) of Titanium dioxide (TiO_2), Potassium oxide (K_2O), Phosphorus pentoxide (P_2O_5) and Manganese oxide (MnO), while the remaining major elements (dichromium trioxide (Cr_2O_3), Nickel Oxide (NiO), vanadium pentoxide (V_2O_5), Zirconium oxide (ZrO_2)) were not detected by XRF analysis (Figs. 5.5a, b). When compared to various average shale analyses in the literature (Geosynclinal Average Shale and Platform Average Shale from Wedepohl, 1971; Average Shale from Clarke, 1924; North American Shale Composite from Gromet *et al.*, 1984), the Sistan dust is significantly depleted in SiO_2, Al_2O_3, K_2O and total Fe and significantly enriched in CaO, Na_2O and MgO. The MgO is largely contained in dolomite and, to a lesser extent, in clay minerals such as palygorskite and montmorillonite (Goudie and Middleton, 2001; Engelbrecht et al., 2009). These components can be ascribed to the importance of evaporite minerals such as calcite, dolomite, halite and gypsum (as also suggested by the mineralogical analysis) inferred to have come from the desiccation taking place in the Hamoun dust source region. Furthermore, the elevated values for the trace elements Cl, F and S (Table 5.1) support the latter postulate as it would be expected from an evaporite-rich source for deflation of dust (e.g., Talbot and Allen, 1996). Similar to the present findings, Engelbrecht et al. (2009) determined a high fraction of SiO_2 in silt, less CaO in calcite and slightly more Al_2O_3 in clay minerals at the Khowst site. At both Afghanistan sites (Bagram and Khowst), the SiO_2 was dominant with fractions of about 50 to 55%, followed by Al_2O_3, CaO and MgO.

By comparing the major elements of different dust storms, some interesting relationships are revealed. More specifically, on days (e.g. 15/11/2009, 7/1/2010, 23/1/2010) (Fig. 5.5a) when airborne dust was relatively depleted in SiO_2, enhanced MgO and, particularly Na_2O values were recorded. Conversely, when SiO_2 values were higher

(e.g. 8/7/2010, 23/8/2010), both MgO and Na_2O contributions dropped. This suggests that certain intense dust storms were richer in evaporite source material (i.e., elevated MgO and Na_2O) coming from Hamoun dried lake beds, while others had more silica, reflecting weathered rock detritus from the Hirmand river and Afghanistan mountains. An explanation of these variable chemical compositions of dust samples is a real challenge, but it is postulated here that they may reflect local desiccation cycles and, possibly, even micro-climatic changes in the Hamoun-lakes dust source region. Excessive desiccation of the lakes would enhance potential evaporite minerals for deflation in drier periods, while in wetter periods, airborne dust would logically have been derived more from weathered fluvial detritus rich in SiO_2.

Fig. 5.6 summarizes the results of the elemental compositions determined by XRF analysis at both stations. For comparison reasons, the mean elemental composition found for several sites in southwestern Iran (Khuzestan province) (Zarasvandi *et al.*, 2009) is also shown. The vertical bars express one standard deviation from the mean. Concerning the major elemental oxides over Sistan, both stations exhibit similar results, well within the standard deviations, suggesting that the transported dust over Sistan is locally or regionally produced with similarity in source region. In contrast, the mean elemental composition of airborne dust over Khuzestan province exhibits remarkable differences from that over Sistan, revealing various source regions and dust mineralogy. More specifically, the SiO_2 percentage is significantly lower and highly variable over Khuzestan, which is also characterized by higher contributions of Na_2O, MgO and K_2O compared to Sistan. The dust storms over southwestern Iran may originate from local sources as well as being transported over medium- and long-ranges from different sources located in Iraq as well as in the Arabian Peninsula. A comparative study of the mineralogy and elemental composition of airborne dust at several locations in Iraq, Kuwait and the Arabian Peninsula (Engelbrecht *et al.*, 2009) has shown significantly variable contributions, suggesting differences in overall geology, lithology and mineralogy of these regions. In further contrast, airborne dust over Sistan seems to have its individual characteristics originating from local and well-defined sources.

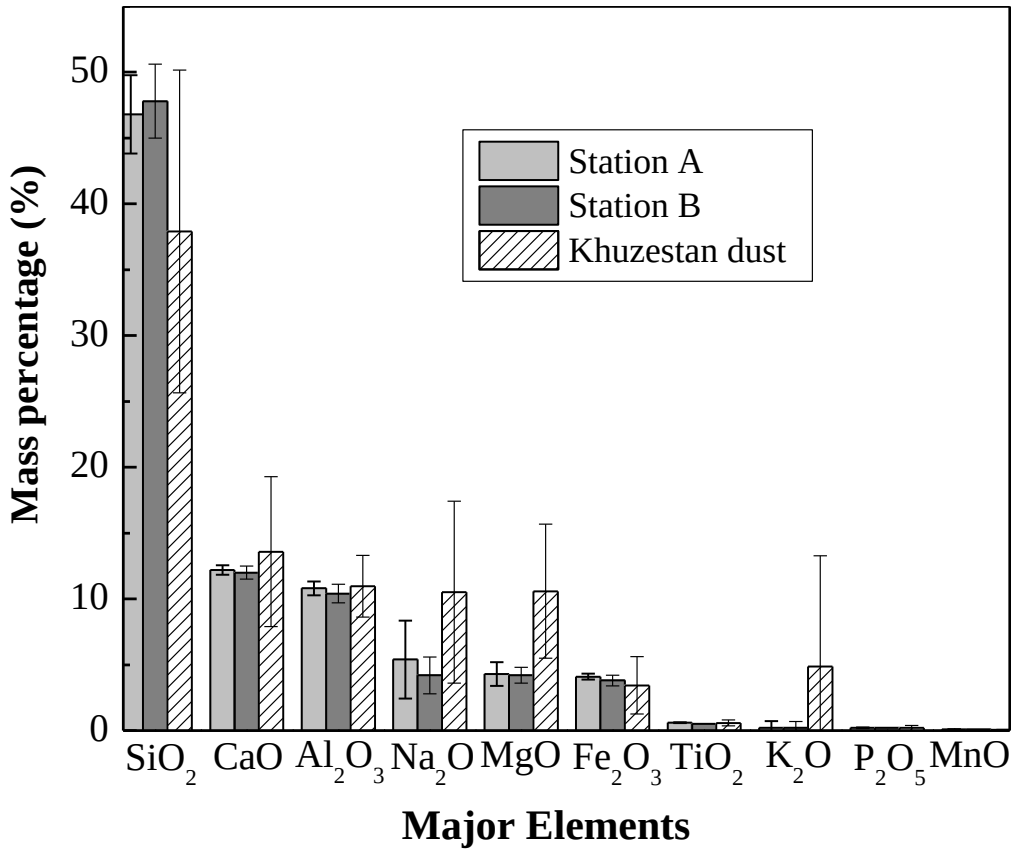

Figure 5.6: Average XRF results for major dust elements at stations A and B. Similar results obtained in Khuzestan Province, southwestern Iran (Zarasvandi *et al.*, 2009) are also shown for comparison reasons.

The Earth's crust is dominated by silicon and aluminum oxides. Numerous studies (Goudie and Middleton, 2001, 2006 and references therein) reviewing the elemental composition of airborne dust over the globe report that mineral dust is composed of ~60% SiO_2 and 10-15% Al_2O_3. The contribution of other oxides, i.e. Fe_2O_3 (~7%), MgO (~2.5%) and CaO (~4%), are, in general, more variable depending on source location. Furthermore, the review study of Usher *et al.* (2003) showed that airborne dust samples collected over the globe have fairly small variations in elemental composition. The CaO concentrations over Sistan are found to be much higher than those (5.5%) summarized in Usher *et al.* (2003).

5.3.3 Trace elements

The average concentrations of trace elements (in ppm) in dust samples collected during major dust storms at stations A and B are summarized in Table 5.1, as obtained from XRF analysis. The results show that the dominant trace elements over Sistan are F and Cl, with the former being dominant in the vast majority of the dust events at station A. However, on two days (8/7/2010 and 23/8/2010) the Cl concentrations were extremely large, thus controlling the average value. There is a lack of observations at station B on 23/8/2010, thus the lower overall Cl concentration. Note that on both these days, the SiO_2 component is large, while MgO and Na_2O are low (Fig. 5.5a). The dominance of chlorine indicates soil salinization in the Hamoun basin and along the Hirmand river and its tributaries. Furthermore, S exhibits higher concentration at station A, while for the other elements the concentrations between the two stations are more or less similar. The concentrations of potentially harmful and toxic elements, like Cesium (Cs), lead(Pb) and Arsenic (As) are, in general, low at both stations; however, Barium (Ba), Chrome (Cr) and Zinc (Zn) present moderate concentrations.

Table 5.1: Average X-ray fluorescence (XRF) values for trace elements of airborne dust at stations A and B

Trace Elements		
Parts per million (ppm)	**Station A**	**Station B**
Cl	28670	15047
F	13938	13456
S	4445	2506
Ba	210	253
Sr	154	125
Zr	83	76
Cr	70	84
V	69	69
Zn	57	51
La	30	32
Rb	24	19
Ni	18	16
Ce	17	16
Cs	14	13
Sc	11	11
Cu	11	11
Pb	10	10

The analysis of the major element ratios provides essential knowledge of the dust chemical composition and source region. The ratios of Si/Al at stations A and B are similar (7.8±0.8 and 8.3±0.9, respectively), due to the presence of silicate and aluminosilicate minerals in most dust samples. The ratios of Mg/Al (0.90±0.16,

0.92±0.12), Ca/Al (3.09±0.19, 3.12±0.19) and Fe/Al (0.51±0.02, 0.49±0.01) at the two stations suggest contributions of clays and Ca-rich (calcite) minerals to the chemical compositions of airborne dusts. In contrast, the Fe/Al ratio is low over Sistan and is nearly half of that found for airborne dust over southwestern Iran and several locations over the globe (Zarasvandi, 2009), but is comparable to that found over central Asia (Kreutz and Sholkovitz, 2000). It should be noted that this ratio remains nearly invariant, ranging from 0.47 to 0.54, for all the collected dust samples at both stations and can be a good surrogate for the dust source region, since any variation in Fe/Al mainly corresponds to variations in clay minerals and not to coating during dust transportation (Goudie and Middleton, 2006). In contrast, the Ca/Al ratio exhibits the highest variations from sample to sample (2.80-3.46), since it is influenced by particle size, with higher values as particle-size increases (Zarasvandi *et al*., 2009). Synoptically, all the ratio values and the low standard deviations suggest similarity in geochemical characteristics over Sistan and a uniform source of airborne dust.

5.3.4 Enrichment factor analysis

The EFs for major and trace elements were calculated via the procedure described in section 3.2 for all the airborne dust samples at both stations (Table 5.2). The results show that the EF values of the main elements Al, Ca and Fe are close to unity, indicating that these elements have not been enriched yet and are composed from natural soil materials. The EF values of elements Sulfur (S), Zn and Arsenic (As) are well below unity suggesting that these elements were not affected by human activities. The overall analysis reveals that the elements found in the dust originate from natural sources and that they are not affected by human activities when they are transported over Sistan. The EF values for the major and trace elements shown in Table 5.2 are more or less similar to those reported by Lawrence and Neff (2009) summarizing the results of several studies over the globe. In contrast, Zarasvandi *et al*. (2009) found that the trace elements Na, Ni, Co, Ba and Cr, are of anthropogenic origin (EF>10) in southwestern Iran. The main reason for this discrepancy is that the above-mentioned trace elements, and particularly the Ba, are associated with anthropogenic and industrial (oil and gas drilling) activities, which are absent in the Sistan region.

Table 5.2: Enrichment Factors (EFs) for the major and trace elements, averaged at stations A and B.

EF(Si)crust					
	A	B		A	B
Ba	2.08	2.41	**F**	0.53	0.50
La	1.53	1.56	**Zn**	0.51	0.44
Cr	1.53	1.92	**Mo**	0.50	0.49
P	1.38	1.28	**W**	0.43	0.50
V	1.33	1.27	**Ga**	0.43	0.37
Co	1.29	1.20	**Cu**	0.43	0.37
Ti	1.26	1.17	**S**	0.41	0.23
Fe	1.13	1.05	**Zr**	0.41	0.37
Mn	1.07	0.99	**Th**	0.38	0.37
Ce	1.05	0.89	**Ni**	0.37	0.30
Si	1.00	1.00	**K**	0.34	0.28
Sc	0.95	0.93	**Pb**	0.33	0.29
Ca	0.92	0.88	**Sr**	0.24	0.18
Cs	0.88	0.82	**Y**	0.24	0.18
Al	0.78	0.74	**Nb**	0.23	0.20
As	0.63	0.64	**Rb**	0.21	0.16
U	0.61	0.60	**Cl**	0.10	0.05
Mg	0.54	0.52	**Na**	0.07	0.05

5.3.5 Scanning Electron Microscopy (SEM) analysis

Fig. 5.7 summarizes some microscope images as well as the respective Scanning Electron Microscopy (SEM) images for both airborne and soil dust samples collected over the Sistan study area (see Fig. 5.7 caption for details). The microscope images reveal various shapes and colors of airborne and soil dust over the region which were selected for this summary figure. Note the larger dust particles, associated with higher quartz and dolomite and lower calcite mass percentages, having prismatic and crystalline shapes (second row, left in Fig 5.7). On the other hand, the microscope images corresponding to airborne dust taken at stations A and B at heights 4m and 8m, respectively (first and third rows in fig. 5.7) show much smaller dust particle sizes and somewhat of a coating between the particles. Both these samples have a lower quantity of quartz and plagioclase (albite) and higher percentages of calcite, chlorite and muscovite than the previous case (larger particles). The two soil samples collected from the Sistan agricultural lands and in the Hamoun Basin (last row) present remarkable differences in the mineralogy and chemical composition, suggesting that the soil in Hamoun is mainly composed of evaporite minerals with high concentrations of Na_2O. Furthermore, the similar mineralogy and chemical dust composition of the soil sample from Hamoun and the airborne dust sample taken at Zabol during a major dust storm on 9 January 2010 must be emphasized, suggesting not only that

the source region of this particular dust outflow was the Hamoun basin but that the alluvial and lacustrine material from Hamoun is deposited widely over the whole Sistan region. In general, higher SiO_2 values in soil crust samples are accompanied by elevated CaO and total Fe values, while there is a strong inverse relationship (r = -0.87) between SiO_2 and Na_2O values. Moreover, SiO_2 is inversely correlated with both MgO (r = -0.96) and Al_2O_3 (r = -0.73), while all the above correlations are statistically significant at 95% confidence level. These results clearly indicate that soil-forming processes downwind of the airborne sampling stations have radically altered the chemistry of the deposited air-transported dust; particularly, sodium and silica components are subject to rapid fluctuations from one sample locality to another. Taking into account that silica will essentially be related to fine air-transported quartz and silt particles while sodium reflects evaporitic material as well as some mica and feldspar minerals, the role of dynamic sorting processes during sedimentation may have played an important role in coating samples. On the other hand, the influence of rain may also be important in altering soil crust compositions (Zarasvandi *et al*., 2009).

In general, all SEM images show that the dust samples have non-spherical, irregular, crystalline prismatic and rhombic shapes, as do those observed over Khuzestan province, southwestern Iran (Zarasvandi *et al*., 2009). The dust size is, in the vast majority of the cases, much larger than 10 μm. Previous study analyzing the dust particle size at stations A and B (Rashki *et al*., 2012) showed that the dust mode size was ~30 μm at station A and ~70 μm at station B, due to closer proximity of the latter to the dust source region (Hamoun basin). However, in some cases the airborne dust is composed of smaller particles with mean diameters of about 1-3 μm. In general, the smaller particles, that are composed mainly from clay minerals, seem to be more spherical, while the larger prismatic and irregular shapes are composed mainly of gypsum and quartz, respectively, as also shown in southwestern Iran (Zarasvandi *et al*., 2009).

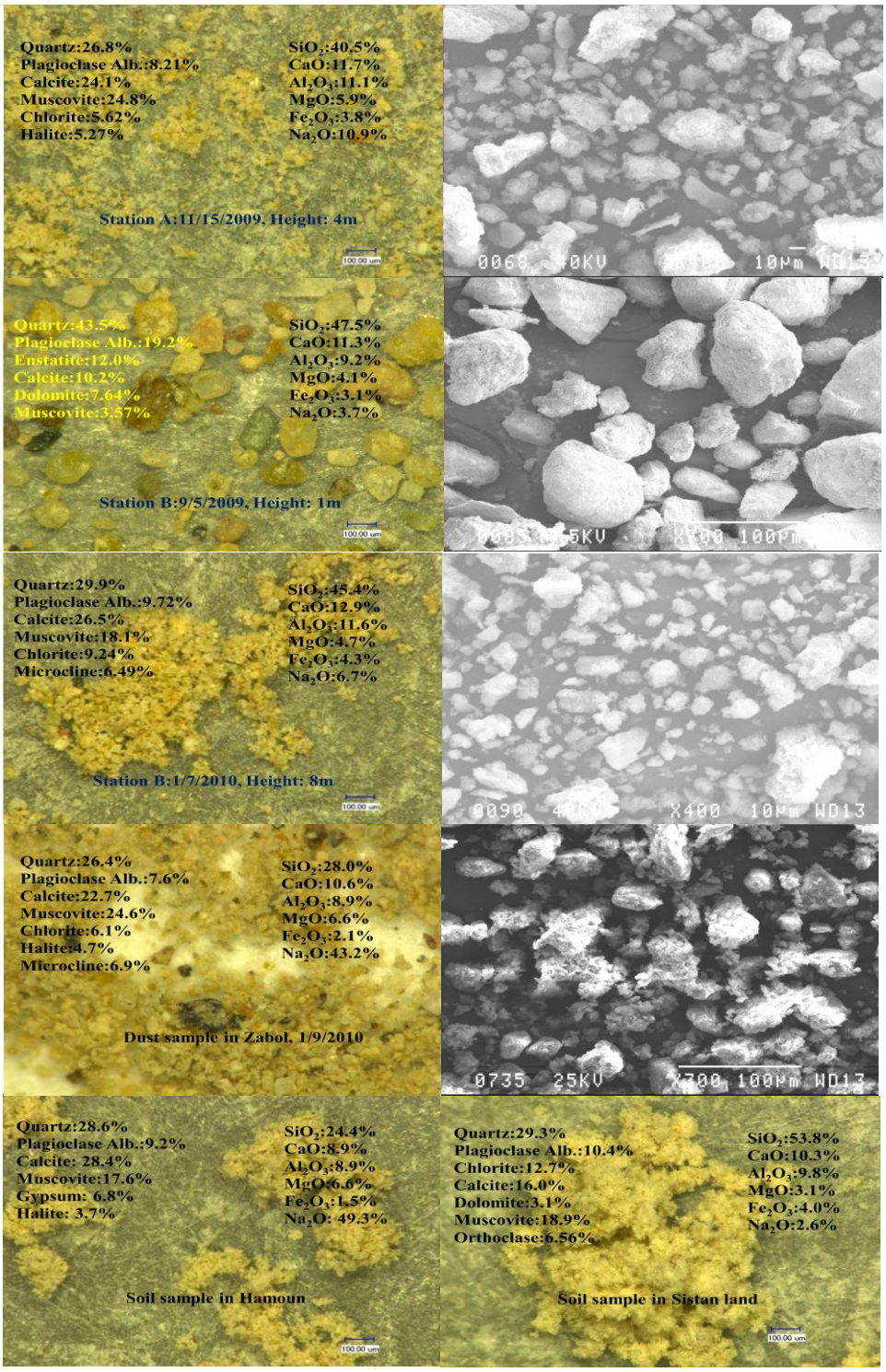

Figure 5.7: Microscope images (left column) and SEM images (right column) for airborne and soil dust samples over Sistan; there are no SEM images for soil samples (last row). The location and the height for the airborne dust samples are given, while the soil samples were collected in Sistan agriculture land and in Hamoun dry-lakes basin. The dust sample in Zabol was collected on the roof of a building during a dust event on 9 January, 2010. For each case, the mineralogy and major elements percentage contribution are given for the main dust components. The scale bar in each image defines the particle size.

5.4 Conclusions

To fully understand mineral dust characteristics and the potential impact on human health, dust mineralogy and geochemical properties were examined in Sistan region, southeastern Iran by collecting airborne and soil samples at two stations and several locations over Sistan and Hamoun basin. The Sistan region is an ideal site to study the nature of dust storms as it receives large amounts of fine alluvial material from the extended Hirmand river system draining much of the Afghanistan highlands, which comprise crystalline basement rocks, Phanerozoic sediments and extensive flood basalts. As a result, large quantities of quartz-rich, feldspar- and mica-bearing silt, as well as mafic material from flood basalt sources and carbonate minerals from dolomites, are transported to the Hamoun wetlands in northern Sistan. Due to droughts at Hamoun and large irrigation projects upstream on the river catchment, extensive desiccation has occurred in the wetlands resulting in large dry lake environments. These have produced large quantities of evaporate minerals to add to the alluvial silts and the combination of these materials provides the provenance for the airborne dust.

Dust aerosol characterization included chemical analysis of major and trace elements by XRF and mineral analysis by XRD. The results showed that quartz, calcite, muscovite, plagioclase and chlorite are the main mineralogy components of dust, in descending order, over Sistan that were present in all the selected airborne dust samples. In contrast, significantly lower percentages for enstatite, halite, dolomite, microcline, gypsum, diopside, orthoclase and hornblende were found, since these elements occurred only in some of the samples at both stations. On the other hand, SiO_2, CaO, Al_2O_3, Na_2O, MgO and Fe_2O_3 were the major elements of dust, while large amounts of F, Cl and S were also found as trace elements. The mineralogy and chemical composition of airborne dust at both stations were nearly the same and quite similar to the soil samples collected at several locations downwind. This suggests that the dust over Sistan is locally emitted, i.e. from the Hamoun Basin, and in few cases can be long-range transported. On the other hand, individual dust storms showed significant differences between either evaporate-dominated aerosols or those characterized by deflation from alluvial silts. These possibly reflect either localized climatic cyclicity or desiccation cycles. However, in some cases the soil samples showed poor comparisons with aerosol compositions, suggesting that dynamic sorting, soil-forming processes and climatic influences, such as rainfall, altered the

mineralogy and chemistry in these partially Aeolian deposits. Sistan is also an ideal site for studying dust storms and enrichment factors relative to crustal norms, suggesting that the dust is essentially of crustal rather than anthropogenic origin. SEM analyses of the samples indicated that airborne dust has rounded irregular, prismatic and rhombic shapes and only the finer particles and in few cases can be assumed as spherical.

CHAPTER 6
SPATIO-TEMPORAL PATTERNS OF AEROSOL BASED ON SATELLITE OBSERVATORY

6.1 Introduction

The physical, optical and radiative properties of dust aerosols are of great importance over the globe, especially over the desert areas and regions affected by frequent and intense dust outflows, for the attenuation of solar radiation, mixing processes in the atmosphere, interaction between dust aerosols and clouds and thermal heating of the troposphere (e.g. Rosenfeld *et al*., 2001; Dey *et al*., 2004; Prasad *et al*., 2009; Gautam *et al*., 2009a; Anton *et al*., 2011; Christopher *et al*., 2011). The characterization of aerosol optical and microphysical properties is crucial to the understanding of their effect on the Earth-atmosphere radiation budget and climate (e.g. Haywood *et al*., 1999; Meloni *et al*., 2005; Marey *et al*., 2011). Thus, it is necessary to analyze the seasonality of dust aerosols, particularly over regions with frequent and intense dust storm events, which affects solar radiation, ecosystems and human health (Singh *et al*., 2008; Nastos *et al*., 2010; Maghrabi *et al*., 2011). Assessment of the aerosol properties is necessary for understanding the aerosol radiative effects on climate using remote sensing techniques and in-situ measurements. Furthermore, changes in the vertical structure of the atmospheric aerosols due to formation of distinct aerosol layers aloft may significantly alter the radiative forcing in to the atmosphere (Guan *et al*., 2010; Lemaître *et al*., 2010). These elevated aerosol layers mainly consist of dust plumes transported thousands of kilometers away from their sources causing severe affects on air quality and public health (e.g. Torres *et al*., 2002; Marey *et al*., 2011; Rashki *et al*., 2012).

Atmospheric aerosols affect the incoming and outgoing solar radiation directly by scattering and absorbing the solar and terrestrial radiation and indirectly by modifying the physical and radiative properties of clouds (Charlson *et al*., 1992; Rosenfeld *et al*., 2008). AOD is one of the most important optical properties of aerosols, which is directly related to the magnitude of attenuation of direct solar radiation by scattering and absorption

processes. Assessment of the aerosol properties is necessary for understanding the aerosol radiative effects on climate and retrieving the aerosol optical properties using remote-sensing techniques. Changes in the atmospheric aerosol load and land surface properties alter the energy balance of earth's atmosphere (Wild *et al*., 2012).

Satellite monitoring of aerosols over the desert areas and downwind regions over the globe has been increasingly available via observations of Total Ozone Mapping Spectrometer (TOMS) and Ozone Monitoring Instrument (OMI) (e.g. Hsu *et al*., 1999; Alpert *et al*., 2004; Engelstaedter *et al*., 2006; Kaskaoutis *et al*., 2010), Moderate Resolution Imaging Spectroradiometer (MODIS) Deep Blue algorithm (e.g. Hsu *et al*., 2004; Gautam et al., 2011), Multi-angle Imaging Spectro-Radiometer (MISR) (Kalashnikova *et al*., 2005; Kahn *et al*., 2009), SEVIRI (e.g. Bou Karam *et al*., 2010; Haywood *et al*., 2011) and Cloud-Aerosol Lidar and Infrared Pathfinder Satellite Observation (CALIPSO) (e.g. Generoso *et al*., 2008; Liu *et al*., 2008a, b). Individual ground-based observations represent point measurements and do not have coverage required to map regional or global distributions of aerosols. Thus, satellite remote sensing has made tremendous progress within the last 10-15 years; recently, MODIS (Chu et al., 2003; Wang and Christopher, 2003), MISR (Liu et al., 2007). Despite the larger uncertainties compared to ground-based observations, satellite remote sensing allows the spatial distribution and properties of aerosols to be assessed, and it also has the major benefit of allowing complete and synoptic mapping of a large area in a single snapshot (Kosmopoulos *et al*., 2008).

This Chapter focuses on dust-aerosol monitoring over the arid environment of Sistan and surroundings mainly aiming to present the first climatology of dust-aerosol patterns, i.e. multi-year, seasonal and monthly variations of spatial and vertical extend of aerosols by means of multiple satellite observations. A large database of remotely sensed aerosol loading have been compiled in order to analyze its spatio-temporal variability, and how this load interacts with different variables that characterize the dynamic and thermodynamic states of the environment. More specifically, the TOMS-AI and OMI-AI values are utilized along with AOD retrievals from MODIS Deep Blue algorithm and MISR over desert regions. The diversity of this database relies on the different satellite product retrieval techniques and calibration procedures that provide a synergistic approach to complement the analysis.

6.2 Satellite data sets

Aerosol datasets used in this Chapter correspond to TOMS-Nimbus 7(N7T, 1978-1992), TOMS-Earth Probe (EP, 1996-2005), Aura-OMI (2005-2011), Terra-MISR (2000-2010), Aqua-MODIS (2002-2011) and Terra-MODIS (2000-2010) (Table 6.1). For all the above-mentioned sensors the AI and AOD values are analyzed over Sistan and surrounding regions both temporally and spatially in order to reveal the annual variability as well as the trend in aerosol loading during the different periods. It should be noted that it's the first time that aerosols are systematically monitored over the region via satellite remote sensing. Although, TOMS-Earth Probe AI data are available till 2005 due to calibration issues associated with sensor degradation, trend analysis of the data after 2001 is not recommended as per the NASA TOMS science team and other available documentation (Kiss *et al*., 2007; Gautam *et al*., 2009). Hence, we restrict the trend analysis of AI data till 2001. In the following, each sensor used for aerosol retrievals over the region is described.

Table 6.1: Satellite datasets used in this thesis

Satellite sensor	Period	Product	Spectral resolution	Spectral band
TOMS Nimbus-7	11/1978- 4/1992	AI Daily level-2	1.25° x 1°	UV
Earth Probe	8/1997- 12/2001	AI Daily level-2	1.25° x 1°	UV
OMI	01/2005- 12/2011	AI Daily level-2	0.25° x 0.25°	UV
MISR Terra	3/2000- 12/2010	AOD Daily level-3	0.5^{o} x 0.5°	558 nm
Aqua-MODIS **(Deep Blue)**	08/2002- 12/2011	AOD Daily level-3	1^{o} x 1^{o}	550 nm
Terra-MODIS **(Deep Blue)**	03/2000- 12/2007	AOD Daily level-3	1^{o}x1^{o}	550 nm

6.2.1 TOMS, OMI sensors

The TOMS Aerosol Index (AI) is the longest available aerosol database on board several satellites (Nimbus-7, Meteor-3, Earth Probe, Aura) from 1978 to present. For about four decades, the TOMS sensors have been providing useful global data on the long-range transport of dust plumes (McPeters *et al*, 1996, Griffi *et al*, 2001; Badarinath *et al*., 2010). TOMS was designed to provide global estimates of total ozone column using

backscattered UV radiance measured at six bands (313, 318, 331, 340, 360 and 380 nm). Aerosol measurements are made in the three longest wavelengths, where gaseous absorption is weak and where the backscattered radiation is primarily controlled by molecular and aerosol scattering, surface reflection and scattering by clouds.

OMI is on board the Finnish–Dutch Aura satellite launched in July 2004. OMI was designed to replace TOMS to continue recording total ozone and other atmospheric parameters related to ozone chemistry and climate. OMI has a spatial resolution of 13 × 24 km at nadir and uses the same retrieval algorithm as TOMS (Torres *et al.*, 1998). It measures back scattered radiances in the near UV region, and using these measurements, the retrieval algorithm computes an absorbing AI, which is a qualitative measure of the presence of UV-absorbing aerosols over all terrestrial surfaces, including deserts and snow-ice covered areas.

The AI has been established as a powerful tool in determining the sources of dust aerosols (Prospero *et al.*, 2002; Alpert *et al.*, 2004; Engelstaedter *et al.*, 2006). The AI is a measure of the wavelength-dependent change in Rayleigh-scattered irradiance from aerosol absorption and is especially suitable for detecting the presence of UV-absorbing aerosols (desert dust, soot, volcanic ash) above high reflecting surfaces, such as deserts and snow/ice areas. These aerosol types are also detected intermingled with clouds and above cloud decks. This is the great advantage between AI and AOD derived from other satellite sensors, like MODIS. The AI can differentiate very well the absorbing and non-absorbing aerosols, by providing a measure of absorption of the UV radiation by smoke and desert dust. The absorbing AI is defined as the difference between the measured (includes aerosol effects) spectral contrast at the 360 nm and 331nm wavelength radiances and the contrast calculated from the radiative transfer theory for a pure molecular (Rayleigh) atmosphere (Ahmad *et al.*, 2003). AI is mathematically defined as:

$$AI = -100[\log_{10}(I_{360}/I_{331})_{meas} - \log_{10}(I_{360}/I_{331})_{calc}] \quad (6.1)$$

where I is the radiance. Since I_{360} calculation uses reflectivity derived from the I_{331} measurements, the AI definition essentially simplifies to:

$$AI = 100 \log_{10} (I_{360\_meas}/I_{360\_calc}) \quad (6.2)$$

The method for the AI retrievals via Eq. (6.1) is based on the principle that for a fixed 360-nm radiance the I_{331}/I_{360} spectral contrast is larger for non-absorbing aerosols and clouds and decreases with increasing absorption. Thus, UV-absorbing aerosols (e.g. dust, smoke and volcanic ash) produce smaller contrast than predicted by the pure Rayleigh scattering atmospheric model; consequently they yield positive values. On the other hand, the non-absorbing aerosols (e.g. sea-salt and sulfate particles from both natural and anthropogenic sources) produce greater contrast and negative values (Torres *et al.*, 1998; Kaskaoutis *et al.*, 2010c). Nevertheless, negative AI values can also be caused by features other than non-absorbing aerosols. Amongst these features are elevated clouds and spectral slopes in the surface albedo between the two wavelengths used for the AI detection. Moreover AI<0 indicates absence of elevated absorbing aerosols, since the AI increases with altitude for the same aerosol load (Prospero *et al.*, 2002). This is the main disadvantage in the AI use as a measure of the aerosol load in the atmosphere. Nevertheless, desert dust has a direct effect on AI because of its strong dependence on the imagery part of the refractive index in the UV wavelengths (Sinyuk *et al.*, 2003; De Graaf et al., 2005), and due to the fact that it is usually transported at elevated layers into the atmosphere. On the other hand, the presence of clouds results in near-zero values for the AI (Hsu *et al.*, 1999).

In interpreting the results, care has to be taken that some surface effects, such as sea glint and ocean color, can also enhance the AI. The advantage of the AI is that it can be applied over both oceans and land, thus improving the knowledge about the distribution of dust sources and transport pathways over the globe (Middleton and Goudie, 2001; Israelevich *et al.*, 2002; Prospero *et al.*, 2002; Alpert *et al.*, 2004). However, there are several factors that complicate the interpretation of the TOMS and OMI AI values. The detection of absorbing aerosols is based on the perturbation of the backscattered UV flux that originates below the aerosol layer. Because the albedo of land and water surfaces in the UV is typically low (Herman and Celarier, 1997), essentially all of the UV upwelling flux originates from backscatter from the gaseous constituents in the atmosphere. Consequently, for any given total column aerosol concentration, aerosol at the top of the atmosphere will yield a larger value of AI than an equal amount of aerosol at a lower altitude. Hsu *et al.* (1999) showed that the altitude dependence of aerosols is almost linear. Thus, TOMS and OMI sensors are more sensitive to aerosols in the middle and upper

troposphere and in the stratosphere; aerosols lofted to these altitudes are most likely to be carried over larger distances. On the other hand, both sensors are least sensitive to aerosols in the boundary layer, where aerosol residence times are short. In fact, aerosols below 500-1000 m are unlikely to be detected by TOMS and OMI (Torres *et al*., 1998; 2002; Kaskaoutis *et al*., 2012b). For these reasons, one cannot simply use the AI values to compare the relative strengths of dust sources in different climate and meteorological regimes. Nonetheless, within specific regions and in specific seasons, the AI should provide a rough measure of relative dust concentrations and, hence, relative source strength. Moreover, TOMS and OMI can retrieve AI in partially clouded pixels, but not in regions covered with clouds except for aerosol above the cloud deck (Herman *et al*., 1997; Torres *et al*., 1998). Nevertheless, TOMS should yield relatively unbiased distributions over arid regions because of the sparse cloud cover. The discrimination between UV-absorbing and non-absorbing aerosols via satellites can find application in the identification of such particles as well as their source regions. Thus, the detection and mapping of dust events and dust transport pathways have benefited greatly from the use of remote sensing.

The TOMS-OMI data used in this Chapter is the most recently re-classified and re-calculated version (Version 8). The dataset is composed of an ensemble of daily records from three satellite mission retrievals namely: (1) Nimbus 7 (N7T, 1978-1993), (2) Earth Probe (EP, 1996-2005) and (3) OMI satellite (2004 to 2011). Periods of data from 2000 to 2005 for EP and 2008 to 2009 for OMI were removed from the AI records. Data was removed because EP present a calibration drift produced by sensor degradation affecting the retrieval (Kiss *et al*. 2007; Bollasina *et al*., 2008) and because OMI presents an obstruction in the sensors field of view causing stripes of bad data (see *http://macuv.gsfc.nasa.gov/*, 2010 for details). In addition, AI values less than 0.5 are treated as missing values because contamination of the variable by sea-glint and water-leaving radiances (Courier *et al*., 2008). The entire compilation of TOMS-OMI AI was obtained from the Giovanni website (*http://giovanni.gsfc.nasa.gov/*) covering the south west Asia bounded from 20 to 34^{o}N and 52 to 72^{o}E in a 1° x 1.25° spatial resolution for TOMS and 0.25^{o}x0.25^{o} for OMI.

6.2.2 MODIS sensors

The MODIS sensors onboard NASA's Terra (launched in December 1999) and Aqua (launched in May 2002) satellites have been acquiring nearly daily global coverage data in 36 spectral bands from visible to thermal infrared (29 spectral bands with 1-km, 5 spectral bands with 500-m, and 2 spectral bands with 250-m, nadir pixel dimensions). The MODIS sensor is on board the polar-orbiting NASA-EOS Terra and Aqua spacecrafts with equator crossing times of 10:30 and 13:30 Local Solar Time, respectively (Levy *et al*., 2007). A nearly global image is produced due to the large swath widths of MODIS and instrument-scanning angle of 110° (Levy *et al*., 2003). Numerous parameters describing various properties over land and ocean surfaces as well as in the atmosphere are retrieved operationally from MODIS data at different spatial and temporal resolutions (daily, weekly and monthly). Aerosol retrievals from MODIS observations are performed over land and ocean surfaces by means of two separate algorithms described in literature (Kaufman and Tanrè, 1998). As discussed in validation studies (e.g. Chu *et al*., 2002; Remer *et al*., 2002) a different expected uncertainty is applied over ocean (±0.03±0.05AOD) and over land (±0.05±0.2AOD) for the previous Collection 4 (C004) retrievals. Over land, even larger errors can be found in coastal zones due to sub-pixel water contamination. Similarly, a significant watercolor contribution can reduce the ocean AOD retrieval quality in coastal areas. In dust aerosol regimes, the retrieved AOD values have greater error due to non-spherical effects (Remer *et al*., 2002; Chu *et al*. 2002; Levy *et al*., 2003).

The retrieval of AOD from MODIS sensor is done with three independent algorithms using seven of the sensor spectral bands between 0.47 and 2.130 µm that are sensitive to aerosol content in the atmospheric column. The first two algorithms are based on the "dark target" approach and were designed to retrieve AOD over ocean and non-bright land surfaces (Kaufman *et al*. 1997; Tanre *et al*. 1997). The latter, called "Deep Blue", is able to retrieve AOD over bright land surfaces (Hsu *et al*. 2004, 2006). Whereas TOMS and OMI AI is only capable of retrieving absorbing aerosols, MODIS AOD measurements are sensitive to both absorbing and non-absorbing aerosols. In addition, MODIS sensors are capable of providing additional and much more accurate aerosol properties (i.e., scattering angle, Angstrom exponent, etc) because it uses a multiple wavelength retrieval technique and cloud masking procedures (Remer *et al*., 2005). The aerosol properties are derived by

the inversion of the MODIS-observed reflectance using pre-computed radiative transfer tables based on aerosol models (Remer *et al*., 2005; Levy *et al*., 2007). The initial versions of the MODIS algorithms have been under continual development, and have recently received an improved aerosol determination, via processing to Collection 5 (C005) (Levy *et al*., 2007, 2010). In general, OMI-AI and MODIS-AOD are somewhat complementary; the first is ideal for initial dust detection and the second can be used to both identify plumes and sources at higher spatial resolution.

The "dark target" approach is unable to provide any aerosol retrievals above arid and desert surfaces, as in the Sistan region, due to high surface albedo, which is similar to the radiation reflected by the aerosol layers. Thus, only the "Deep Blue" algorithm is able to provide such aerosol retrievals over the region, which is used in the present analysis. An alternative method for the dust-plume identification as well as its source region and spatial extent is the land-surface temperature observations from the satellite sensors using the infrared channels. This method has become increasingly available in recent years and is assumed quite accurate, since the temperature variation between the dust plume and the underlying surface can be very large and easily detected by the satellite sensors. Two characteristic cases for the dust identification via the infrared satellite channels are presented in the following images (Fig. 6.1).

A heavy dust plume was observed over Sistan region, southern Afghanistan and northern Pakistan on June 14, 2004. The dust appears to be blowing out of the Sistan basin. In this MODIS image, the dust is masking the arid deserts of Afghanistan and Pakistan and is sweeping around the Chagai Hills, the dark land in the center of the storm. The crescent of the Siahan mountain range in Pakistan is preventing the dust from blowing further south. Once airborne, the dust cools considerably, which makes it stand out in this surface temperature image. The dust is about 40 ^{o}C cooler than the ground-land temperature, which reaches up to 57 ^{o}C in pockets where the land is darker, and therefore, absorbs more sunlight. Patches of clouds also show up as extremely cold blue regions in the temperature image. Though the dust is easy to be detected in the true color image, surface temperature images can make dust storms easier to be detected in cases when the dust plume has the same color with the ground.

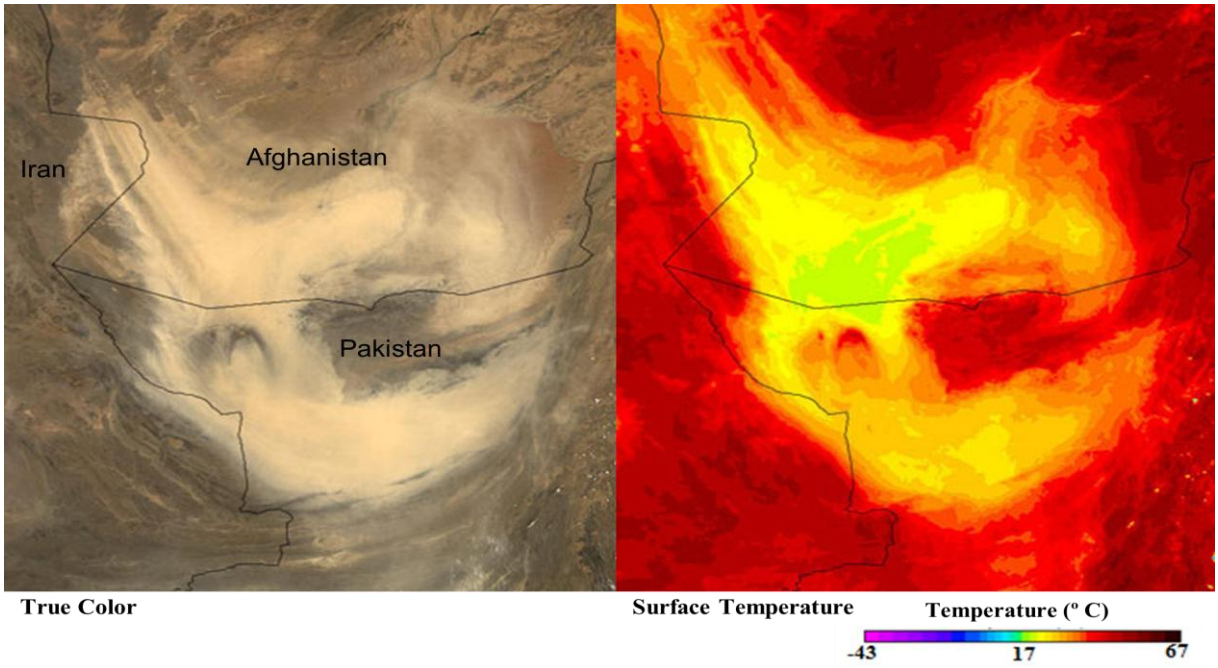

Figure 6.1: Terra-MODIS satellite true color and infrared (temperature) images captured on June 14, 2004 over Iran, Afghanistan and Pakistan.[Source*: http://earthobservatory.nasa.gov/IOTD/view.php?id=4574*]

In this analysis a set of MODIS data downloaded from the NASA Atmosphere Archive and Distribution System (LAADS, *http://ladsweb.nascom.nasa.gov/*) was used. Daily and monthly AOD data at 550 nm were obtained during the period July 2002 to December 2011 from the Aqua platform and from Terra platform in the period March 2000 to December 2010 by means of the Deep Blue algorithm. The data covers the section of south west Asia that includes the Sistan region at an equal-angle latitude-longitude grid with a horizontal resolution of 1° x 1°.

6.2.3 Multi-angle Imaging SpectroRadiometer (MISR) sensor

The Multi-angle Imaging SpectroRadiometer (MISR) was launched into polar Earth orbit aboard NASA's Terra satellite on December 18, 1999. The instrument contains 9 push broom cameras pointed at nadir and along-track view angles of 70.5º, 60º, 46.1º, 26.1º forward and backward of nadir, with spectral bands at 446, 558, 672, and 866 nm. Surface and atmospheric targets within the observed swath (~400 km) are viewed at all 9 angles over a span of 7 minutes with an intrinsic spatial resolution of 275 m. No instrument that combines MISR's attributes—multi angle imaging at moderately high spatial resolution with near-simultaneous temporal sampling; stable and accurate on-board

calibration suitable for climate quality science; and global coverage had not flown in space prior to Terra launch, nor is there is a similar capability currently available on any other satellite platform (Kahn *et al*. 2009; Diner *et al*., 2010). Due to multi-angle viewing MISR is able to obtain aerosol retrievals over desert and arid surfaces of high reflectance.

Thus, additionally to MODIS and OMI, AOD data was retrieved from the MISR sensor mounted on the EOS-Terra satellite to complement the analysis. The aerosol retrievals are based on prescribed tables of forward radioactive calculations that are then compared with the MISR observations to determine AOD and other properties (Diner *et al*. 1998). While MODIS provides information on aerosol concentrations with approximately 1-2 day global coverage, MISR repeats coverage every 7 to 9 days due to the much smaller swath (~400 km against ~2300 km). This lengthy cycle limits the use of MISR data for high temporal analysis, but the high accuracy of the retrieved data over bright deserts provides the necessary additional synergistic information to supplement the study. The MISR AOD dataset is obtained from Giovanni website (*http://giovanni.gsfc.nasa.gov//)* over southwest Asia containing Sistan region at a 0.5° x 0.5° spatial resolution from February 2000 to December 2010.

6.2.4 Giovanni data base

From Giovanni online data visualization tool one can easily obtain several atmospheric, hydrological, land and surface variables by selecting the desired variables via the satellite sensors or via models and re-analysis on a global scale. The user has the ability to select the study region by inserting in the system the geographical coordinates (Lat, Long) as well as the study period. The user may have the data as lat-long maps, as dataseries, as scatter plots, etc… There is also the possibility to download the dataset in different formats (ASCII files) and then to analyze them through statistical software. Giovanni online visualization tool has been increasingly available during the last years, mainly due to its simplicity to provide accurate satellite datasets for specific regions and periods. However, it cannot provide observations of high resolution, i.e. MODIS Level 2 retrievals (10 x 10 km) or the original Level 1 satellite observations.

6.3. Multi-year variation of aerosol properties over Sistan

This section analyzes the multi-year fluctuation of the aerosol properties, AOD and AI, over Sistan region as obtained from satellite observations. In addition, the satellite observations, although some of them correspond to different periods, are compared to each other and the trend in aerosols is examined via linear regression analysis in order to reveal the tendency in aerosol loading over Sistan region. The AI and AOD time series from the multiple satellite sensors are shown in Fig. 6.2, while the lower panel concentrates on the 2000s. In general, the results show considerable inter-annual and intra-seasonal variability for all aerosol characteristics, revealing a pronounced seasonally-dependent aerosol field over Sistan.

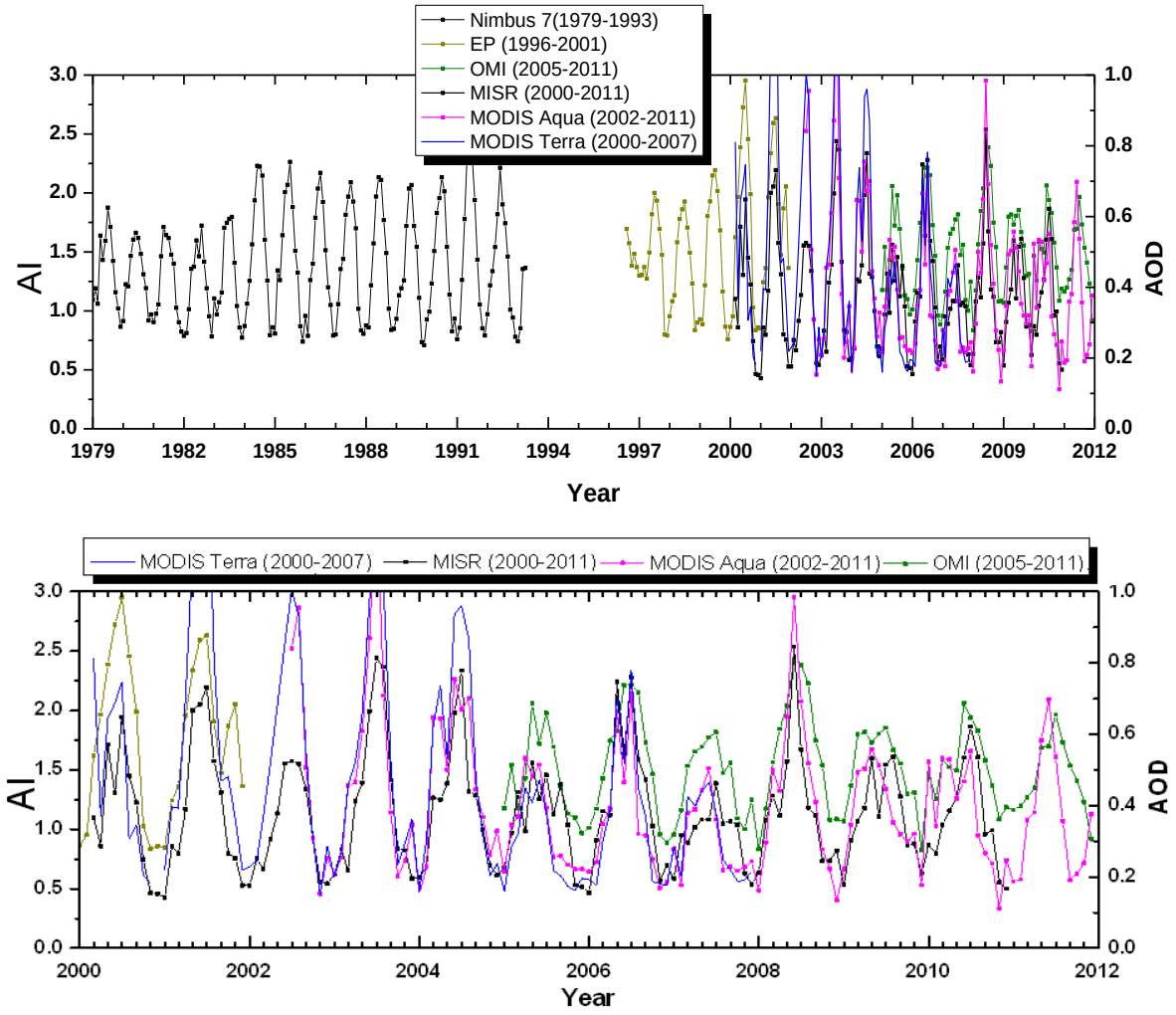

Figure 6.2: Data series of Aerosol Index (AI) values from Nimbus 7, Earth Probe and Ozone Monitoring Instrument (OMI), as well as aerosol optical depth (AOD) values from MISR and Terra/Aqua-MODIS over Sistan region.

Dust outbreaks originating from the Hamoun Basin during summer provide the necessary amount of aerosols in order to enhance the AI and AOD values at levels above ~2.0 and ~0.7, respectively on monthly basis, which are considered very high and characteristic of desert environments (Kim *et al*., 2011; Marey *et al*., 2011). Figure 6.2 shows enhanced AI values from Nimbus 7 after 2004 compared to the previous years, while both AOD and AI values are very high during early 2000s, especially in 2001. The large increase in AOD during 2000-2003 is mainly defined at the summer maximum values, while the winter ones are nearly similar for all years.

The AI and AOD data series during the common periods, i.e. after 2000, show a similar monthly and yearly variation for all sensors. Their relationships show significant correlation between Terra and Aqua MODIS AODs (R^2=0.96), as well as between MISR and Terra MODIS (R^2=0.79) and MISR vs Aqua-MODIS (R^2=0.79). This suggests that the satellite sensors reveal similar aerosol load and variability over Sistan giving credit to the present results, which, however, need comparison and extra validation with ground-based instrumentation, i.e. sun photometers, which, however, are lacking over Sistan region. The correlation coefficients from the comparison between the monthly values of AOD and AI from the different sensors are summarized in Table 6.2. The results show that all the correlations are statistically significant at 95% confidence level.

This research is the first that examines the aerosol variations and trends over Sistan region by means of multiple satellite platforms in the absence of long-term ground-based data series. Previous studies examining aerosol variations and trends over southwest Asia have been conducted by Yoon *et al*. (2011) for selected AERONET locations in the Middle East, by Dey and di Girolamo (2011) and Kaskaoutis *et al*. (2011) over the Indian sub-continent and adjoining oceanic region using MISR and MODIS data, respectively during the last decade. These studies agree that there is a general increase in aerosol loading over southwest Asia, which is mainly attributed to significant increase in anthropogenic emissions. In contrast, aerosols over the Sistan region are mainly composed of soil and dust particles, whereas the anthropogenic component is rather low due to absence of major industries and urban centers over the region. Note also that southeastern Iran, southern Afghanistan and western Pakistan are very sparsely populated areas. Thus, the variability in aerosol emissions and atmospheric lifetime is strongly influenced by natural phenomena (i.e. dryness of Hamoun lakes, land use land cover changes, soil

moisture, frequency and intensity of dust storms) and meteorological conditions, i.e. wind speed and direction, variability in precipitation, etc.

Table 6.2: Coefficient of determination (R^2) values from the correlations between the monthly values of the multiple satellite sensors over Sistan region. *[N: number of data; a.: lack of common period for the correlations; **: The correlation is significant at the 0.05 level]*

		Earth Probe	OMI	MISR	Terra MODIS	Aqua MODIS
Earth Probe	Correlation	1				
	N	65				
OMI	Correlation	a.	1			
	N	0	84			
MISR	Correlation	0.839**	0.819**	1		
	N	22	72	130		
Terra MODIS	Correlation	0.654**	0.783**	0.791**	1	
	N	22	36	94	94	
Aqua MODIS	Correlation	a.	0.763**	0.790**	0.963**	1
	N	0	84	102	66	114

The data series of the aerosol properties from the different sensors reveal different trends over the time period of each sensor. More specifically, Nimbus 7 and Earth Probe AI values show an increasing trend for the periods 1979 to 1992 and 1997 to 2001, respectively, which is statistically significant for Earth Probe (+29.65%). These trends are strongly controlled by the considerable increase in aerosol loading during early 2000s following the extreme droughts after 1999 that modified the Land Use Land Cover (LULC) conditions over Hamoun Basin causing the dryness of the lakes. With the exception of the three shallow freshwater lakes (see Fig. 2.4), the wetlands dried completely, leaving deposits of alluvial silt, which is easily lifted by the wind. As a consequence, the dust erosion becomes easier causing more frequent and massive dust storms, especially during summer when the Levar winds are more intense.

Several previous studies (see Engelstaedter *et al*., 2006, and references therein) have shown an association between dust erosion, source regions and intensity in dust storms with rainfall amount over the desert areas. Such an association was also examined over Sistan region by using the rainfall data from the Zabol meteorological station during the period 1979 to 2011*(http://www.irimo.ir/english/province/systan.asp*). In general, the results reveal an inverse relationship between aerosol loading and precipitation (Fig. 6.3)

over Sistan, since the periods with increased precipitation are associated with lower AOD and AI and vice versa. More specifically, during 1979 to 1981 the precipitation was higher and associated with lower AI values compared to the flowing years; AI is relatively high between 1985-1990 due to decrease in precipitation. The most characteristic period is after 1999 when the lowest precipitation amounts and the highest values for both AOD and AI are shown.

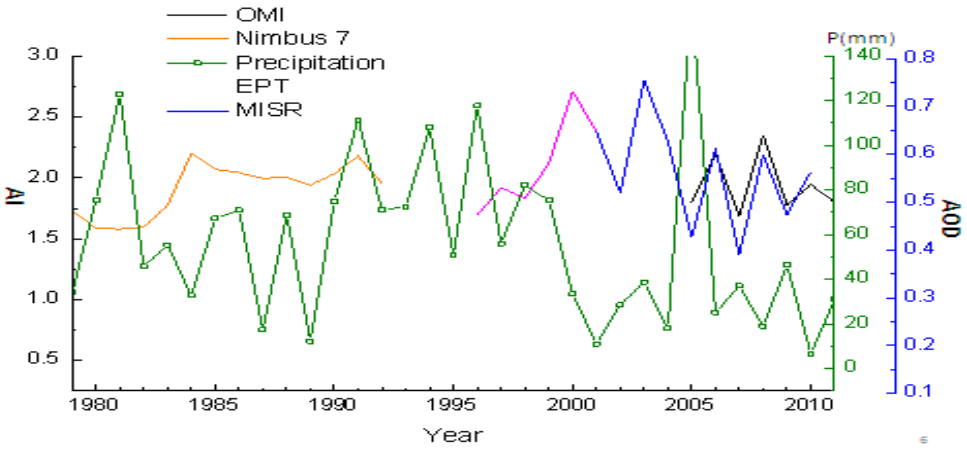

Figure 6.3: Annual average of Aerosol Index (AI) and aerosol optical depth (AOD) with annual average of precipitation at the Zabol meteorological station during 1979 to 2011.

Especially in 2001, the accumulated rainfall over Zabol was 11 mm against the annual average of 55 mm. This resulted in late spring and summer seasons of 2001, increasing the EP-AI to ~2.6, the MISR-AOD to 0.6-0.7 and the Terra-MODIS AOD to 1.5-1.9 in June-July of 2001. On the other hand, the abnormal precipitation (~130 mm) in 2005 (Fig. 6.4) has a direct signal in the low AOD values during this year (Fig. 6.3). The multi-year variation of the precipitation amount over Zabol on both annual and monthly basis during the period 1979 to 2011 is shown in Fig. 6.4. In general, the results establish a close relation between aerosol loading and precipitation over Sistan. Thus, the soil moisture and the amount of water surface in Hamoun lakes affect the frequency and intensity of dust storms, similarly to that found over Thar desert, where the amount of suspended aerosols was very different between two contrasting monsoon years (Gautam *et al.*, 2009b). However, it should be noted that the water surface in Hamoun lakes depends on several other factors including temperature, number of rainy days, and rainfall amounts in Afghanistan from where rivers and tributes bring water to Hamoun lakes. In the recent

years, due to saving of water in two reservoir dams (Arghandab dam and Kajaki dam), the volume of water to Hamoun Basin has been significantly reduced, while the regression analysis showed a pronounced declining trend in precipitation of ~-1 mm/yr or -58.4% during the period 1979-2011 over Zabol.

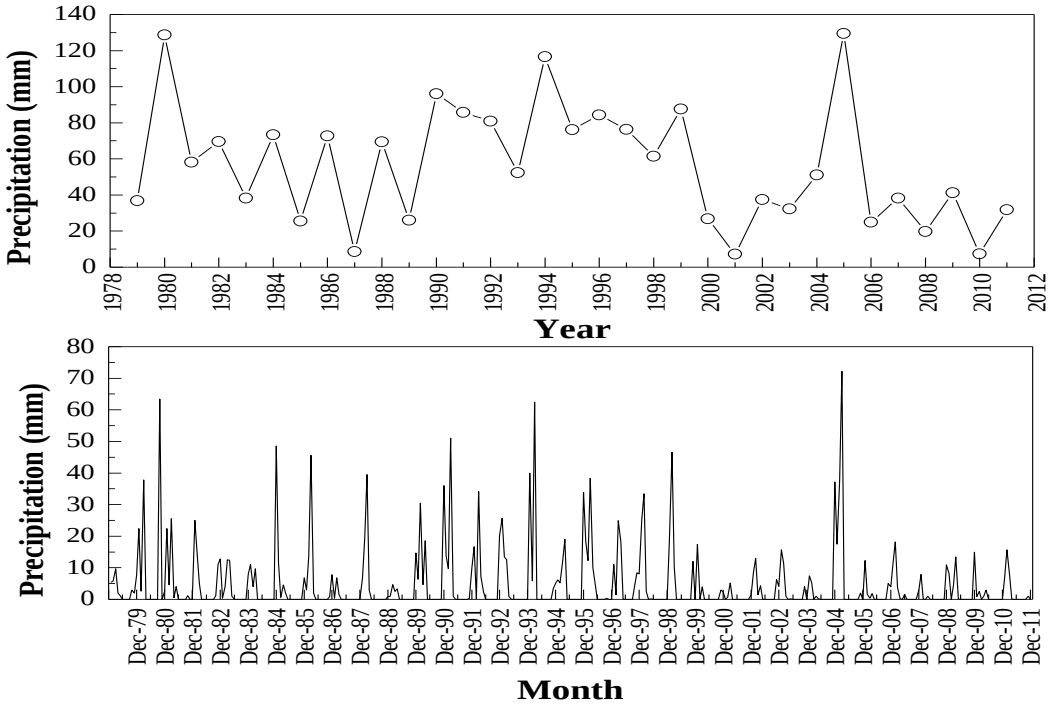

Figure 6.4: Multi-year variation of the annual accumulated rainfall values at the Zabol meteorological station during 1979 to 2011.

The annual mean variation of the OMI and AOD values from the various sensors is shown in a common diagram in Fig. 6.5. All sensors agree to a clear-defined annual variation of summer maximum and winter minimum values, without any significant discrepancies from this pattern. This pattern is similar to those found over sites in the Arabian Peninsula and Persian Gulf (Smirnov *et al.*, 2002; Kambezidis and Kaskaoutis 2008; Kim *et al.*, 2011) as well as over the Thar desert (Dey and di Girolamo, 2010), indicating maximum aerosol loading during the summer season due to more frequent and intense dust events, longer aerosol lifetime and absence of precipitation. The AODs from MISR and Aqua MODIS seem to be similar during the months September to February, while MISR underestimates MODIS during the rest of the year. On the other hand, Terra-MODIS exhibits significantly higher AODs from May to August due to the extreme AODs of these months in 2001 (Fig. 6.5). For the same reason, the EP-AI values are much higher than those of Nimbus 7 and OMI during this period (May to August).

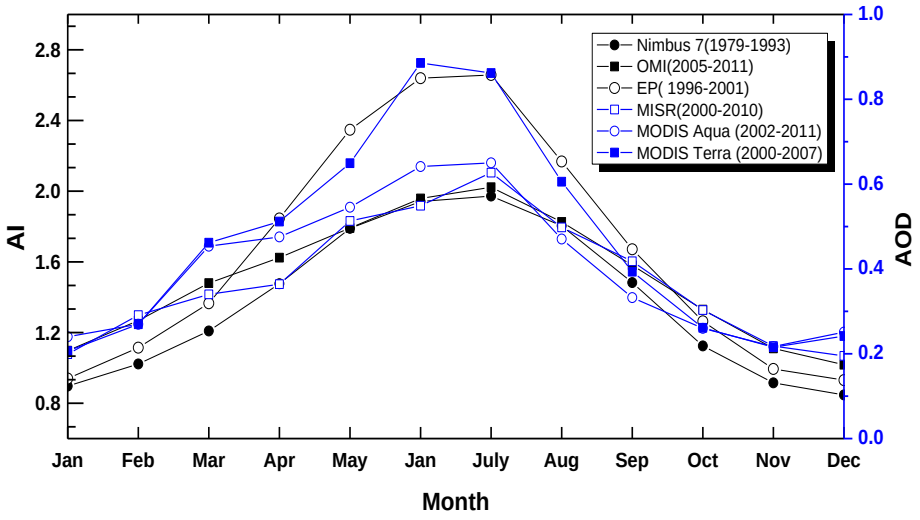

Figure 6.5: Annual mean variation of AOD and AI for different satellite sensors and time periods over Sistan region.

The mean, median as well as the distribution of AI and AOD values from the different sensors are presented in a common diagram (Fig. 6.6) in box charts view (see Figure caption for details). Concerning AI, Earth Probe exhibits the higher mean value and standard deviation (1.55±0.54) compared to Nimbus 7 (1.36±0.44) and OMI (1.51±0.38) due to AI peaks in 2001, a period that does not exist in Nimbus 7 and OMI data sets. These values of AI are lower than those reported over the Sahara (Alpert *et al*., 2004; Engelstaedter et al., 2006), but similar to those found over the Thar desert (Gautam *et al*., 2009b, c). On the other hand, MISR AOD (0.38±0.16) is similar to that of Aqua MODIS (0.39±0.20), although different procedures and algorithms are used for the aerosol retrievals over land from the two sensors (Chin *et al*., 2006; Kahn *et al*., 2010). However, due to the enhanced 2001 values, Terra MODIS exhibits higher AOD over Sistan (0.47±0.32). This much higher value is also influenced by the lower time period of Terra-MODIS Deep Blue retrievals (2000-2007) compared to the other sensors.

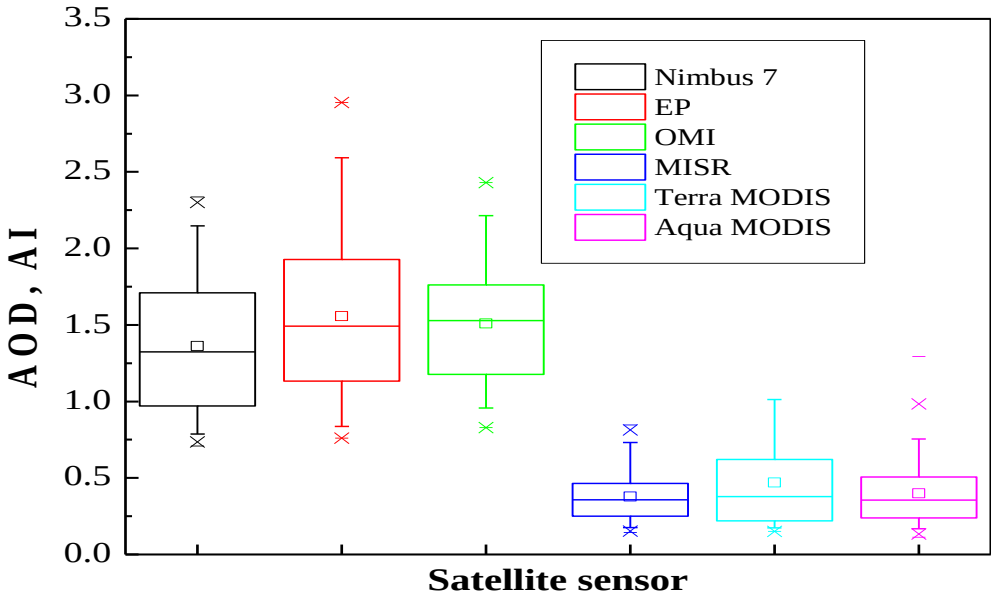

Figure 6.6: Box charts view of the Aerosol Index (AI) and Aerosol Optical Depth (AOD) values for different satellite sensors over Sistan region. Each box contains 50% of the values (25% to 75%). The line is the median and the small square the mean value. The standard deviations are defined by the vertical bars, while 1% and 99% of the data donate by the symbol∗; the maximum and minimum values are defined by the symbol - .

Since the aerosol loading exhibits a pronounced seasonal variability over Sistan as shown in Fig. 6.5, the multi-year variability of AI and AOD is also analyzed on a seasonal basis (Fig. 6.7). Winter exhibits the lowest values of both AI and AOD without any significant yearly variation, except the declining trend observed by EP-AI. In spring, the AI and AOD values start to increase, with the Nimbus 7 AI showing an increasing trend, while the maximum AI is shown for EP during 2000 to 2001. The AOD values during 2000s exhibit a rather neutral or even slight decreasing trend for all sensors indicating a decrease in dust-aerosol loading or even dust activity over Sistan region, as also found over northern India via MISR (Dey and di Girolamo, 2011) and MODIS (Kaskaoutis *et al.*, 2011) observations as well as over south Asia via GOCART simulations (Kaskaoutis *et al.*, 2011). Both AOD and AI values increase further in summer, when the multi-year variability and trends are similar to those found in spring, but are even more intense, i.e. increasing for Nimbus 7 and EP and decreasing for the other sensors. In autumn, the AI and AOD values are significantly reduced and the pattern seems to be similar to that observed in winter.

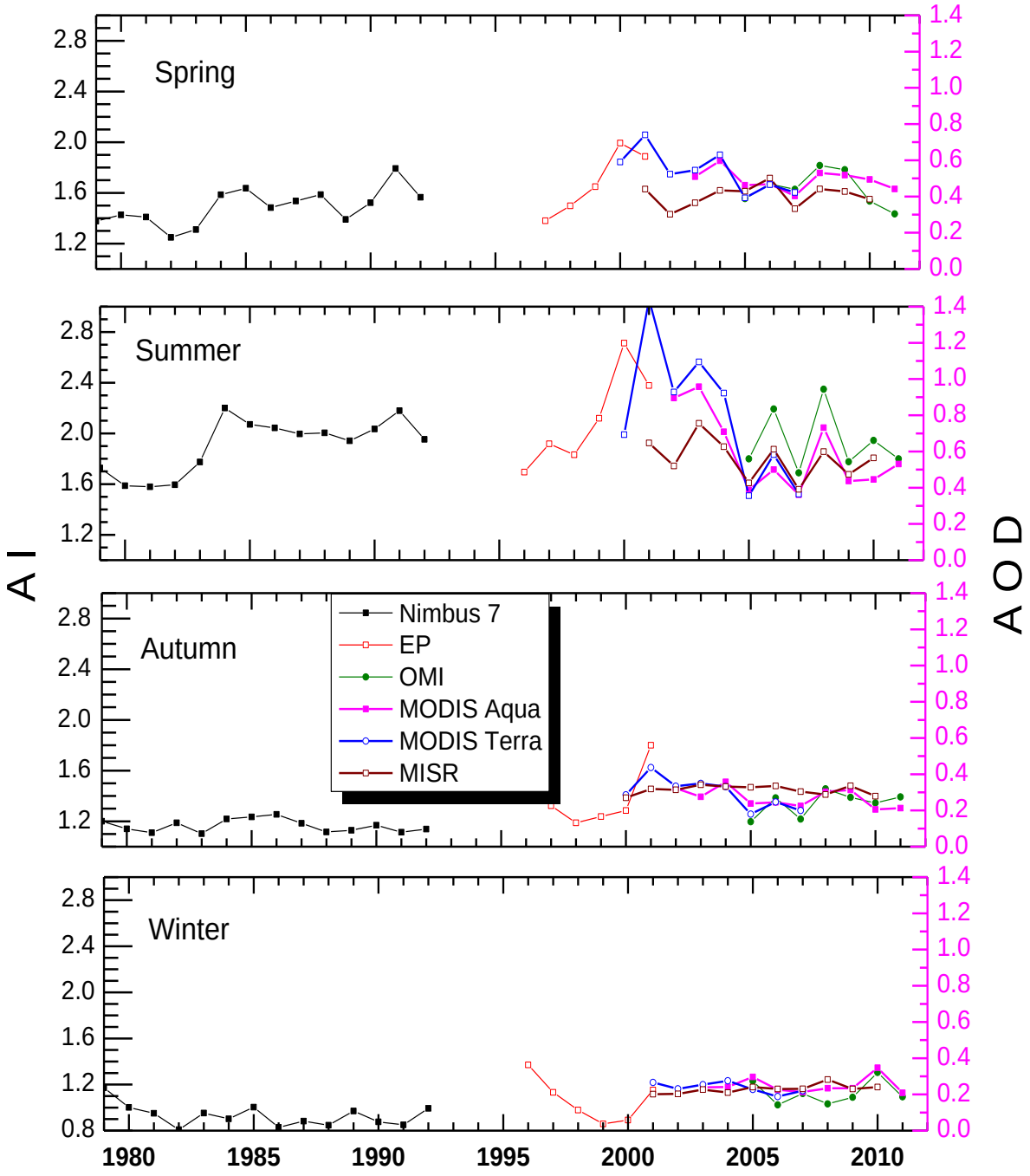

Figure 6.7: Multi-year seasonal variation of Aerosol Index (AI) and Aerosol Optical depth (AOD) values from different sensors over the Sistan region.

The monthly and seasonal mean values of AI and AOD from multiple satellite sensors over Sistan region (Latitude, Longitude) during different time periods are summarized in Tables 6.3, 6.4 and 6.5.

Table 6.3: Monthly and seasonal variability of Nimbus 7 TOMS (N7T), Earth Probe TOMS (EP), OMI AI and MISR AOD over the Sistan region.

	Nimbus 7	EP	OMI	MISR
January	0.897	0.940	1.097	0.199
February	1.022	1.115	1.268	0.291
March	1.209	1.366	1.480	0.340
April	1.476	1.845	1.624	0.364
May	1.789	2.347	1.792	0.513
June	1.942	2.639	1.959	0.549
July	1.972	2.658	2.022	0.627
August	1.804	2.168	1.826	0.498
September	1.483	1.671	1.580	0.418
October	1.124	1.263	1.330	0.303
November	0.915	0.994	1.110	0.218
December	0.847	0.931	1.018	0.195
Spring	1.555	1.670	1.628	1.816
Summer	1.799	2.193	1.689	2.349
Autumn	1.197	1.384	1.218	1.456
Winter	1.230	1.023	1.122	1.032
Annual	**1.445**	**1.568**	**1.414**	**1.663**

Table 6.4: AOD_{550} over Sistan region based on Terra-MODIS Deep Blue retrievals during the period 2000-2007.

Year	**2000**	**2001**	**2002**	**2003**	**2004**	**2005**	**2006**	**2007**	**annual**
Month									
Jan		0.22	0.229	0.2	0.16	0.16	0.193	0.284	0.207
Feb		0.397	0.245	0.276	0.306	0.285	0.176	0.202	0.270
Mar	0.811	0.392	0.368	0.457	0.621	0.319	0.301	0.425	0.462
Apr	0.37	0.708	0.521	0.521	0.738	0.45	0.386	0.4	0.512
May	0.645	1.12	0.681	0.658	0.531	0.409	0.709	0.441	0.649
Jun	0.688	1.979	0.85	0.975	0.939	0.472	0.519	0.466	0.886
Jul	0.747	1.52	1.006	1.296	0.96	0.379	0.782	0.379	0.862
Aug	0.307	0.816	0.929	1.013	0.868	0.217	0.447	0.248	0.606
Sep	0.345	0.469	0.547	0.518	0.474	0.203	0.372	0.22	0.394
Oct	0.205	0.482	0.305	0.234	0.315	0.174	0.187	0.188	0.261
Nov	0.181	0.36	0.15	0.296	0.204	0.162	0.181	0.19	0.215
Dec		0.219	0.287	0.361	0.238	0.196	0.176	0.215	0.242
Winter	0.194	0.160	0.210	0.187	0.140	0.105	0.116	0.079	0.149
Spring	0.275	0.383	0.338	0.373	0.415	0.146	0.204	0.194	0.291
Summer	0.256	0.434	0.479	0.518	0.402	0.106	0.251	0.134	0.323
Autumn	0.122	0.245	0.192	0.189	0.188	0.065	0.123	0.074	0.150

Table 6.5: AOD_{550} over Sistan region based on Aqua-MODIS Deep Blue retrievals during the period 2002 to 2011.

Year	2002	2003	2004	2005	2006	2007	2008	2009	2010	2011	Annual
Month											
Jan		0.209	0.149	0.216	0.214	0.279	0.162	0.222	0.523	0.187	0.240
Feb		0.254	0.229	0.345	0.241	0.177	0.297	0.347	0.342	0.194	0.270
Mar		0.455	0.647	0.369	0.348	0.378	0.5	0.493	0.534	0.359	0.454
Apr		0.465	0.644	0.534	0.392	0.39	0.441	0.504	0.529	0.381	0.476
May		0.609	0.501	0.483	0.665	0.442	0.649	0.557	0.42	0.584	0.546
Jun		0.871	0.755	0.515	0.465	0.505	0.984	0.512	0.468	0.698	0.641
Jul	0.842	1.294	0.671	0.393	0.714	0.361	0.692	0.445	0.552	0.537	0.650
Aug	0.955	0.709	0.7	0.256	0.321	0.218	0.519	0.353	0.317	0.357	0.471
Sep	0.506	0.381	0.445	0.259	0.315	0.229	0.41	0.32	0.267	0.191	0.332
Oct	0.309	0.201	0.368	0.234	0.25	0.217	0.277	0.298	0.237	0.209	0.260
Nov	0.153	0.245	0.261	0.221	0.169	0.228	0.223	0.321	0.112	0.238	0.217
Dec	0.253	0.346	0.328	0.222	0.184	0.244	0.134	0.177	0.246	0.376	0.251
Winter		0.239	0.241	0.296	0.226	0.213	0.234	0.234	0.347	0.209	0.249
Spring		0.510	0.597	0.462	0.468	0.403	0.530	0.518	0.494	0.441	0.492
Summer	0.895	0.958	0.709	0.388	0.500	0.361	0.732	0.437	0.446	0.531	0.596
Autumn	0.323	0.276	0.358	0.238	0.245	0.225	0.303	0.313	0.205	0.213	0.270

6.4. Spatial distribution of aerosols over southwest Asia and Sistan

In this section the spatial distribution of aerosols over southwest Asia, in general, and Sistan region, in particular, is analyzed on seasonal basis by means of different satellite sensors in order to compute and compare the annual aerosol cycle over a wide area surrounding Sistan. Figure 6.11 summarizes the spatial distribution maps of the seasonally averaged values of AI from Nimbus 7 and OMI and of AOD values from MISR and Aqua MODIS. Both variables (AI and AOD) present a pronounced seasonal variability over southwest Asia with winter minima and summer maxima similar to that found for the Sistan region (Fig. 6.8). As far as the AI is concerned the results exhibit similar spatial distribution for Nimbus 7 and OMI over the whole area and for each season. More specifically, during spring the hot-spot AI areas are defined in the Sistan region and Hamoun Basin, eastern Pakistan and in the Arabian Peninsula without influencing significantly the Arabian Sea. During summer the AI values are higher over the whole area compared to those in spring with the most important increases to be defined over the major dust sources in southwest Asia, i.e. Hamoun Basin, eastern Pakistan and southeastern Arabian Peninsula. In this season significant amount of UV-absorbing aerosols at higher altitudes corresponding to dust, mainly originated from Arabian Peninsula, is transported

over the Arabian Sea from westerlies at higher altitudes (>700 hPa) as shown in Lawrence and Lelieveld (2010). Furthermore, the northernmost part of Arabian Sea is also strongly influenced by the dust storms that originated from the Hamoun Basin and the arid areas of Iran, Pakistan and Afghanistan since the Arabian Sea is in the downwind direction of the Levar winds. By the end of summer the dust activity over the region is significantly reduced as well as the dust-aerosol lifetime in the atmosphere due to increased precipitation mainly over the oceanic areas. However, over land, some limited areas of increased AI still exist (autumn and winter), such as Hamoun Basin and southern Afghanistan and some areas in the Arabian Peninsula. The increased AI observed in autumn over northeastern Pakistan corresponds mainly to biomass burning aerosols, and not to dust, since this is the season of crop-residue burning over the Punjab (Badarinath *et al*., 2009; Sharma et al., 2010).

The AOD spatial distributions both from MISR and Aqua MODIS are rather similar to each other and with those observed for AI. However, the deep blue algorithm over land applied to Aqua MODIS observations overestimates the AOD compared to MISR at least over hot spot areas or over the dust source regions as shown for Sistan and eastern Pakistan for spring and summer. This inconsistency is mainly attributed to the different algorithm and procedures used for aerosol retrievals from the two sensors as well as to the fact that MODIS provides nearly daily observations over the area, while MISR one per week, approximately. Thus, some intense dust storms, mainly in summer, may not be detected by MISR, thus the lower AODs over the dust source regions and downwind areas. Note also that the sampling period is different for the two sensors, i.e. 2000 t0 2010 for MISR and 2002 to 2011 for Aqua-MODIS. In contrast, MISR exhibits higher values in autumn and winter over the arid regions of Arabian Peninsula, while both sensors highlight the enhanced AOD over northeastern Pakistan during late autumn and winter caused by smoke aerosols from crop residue burning over the area.

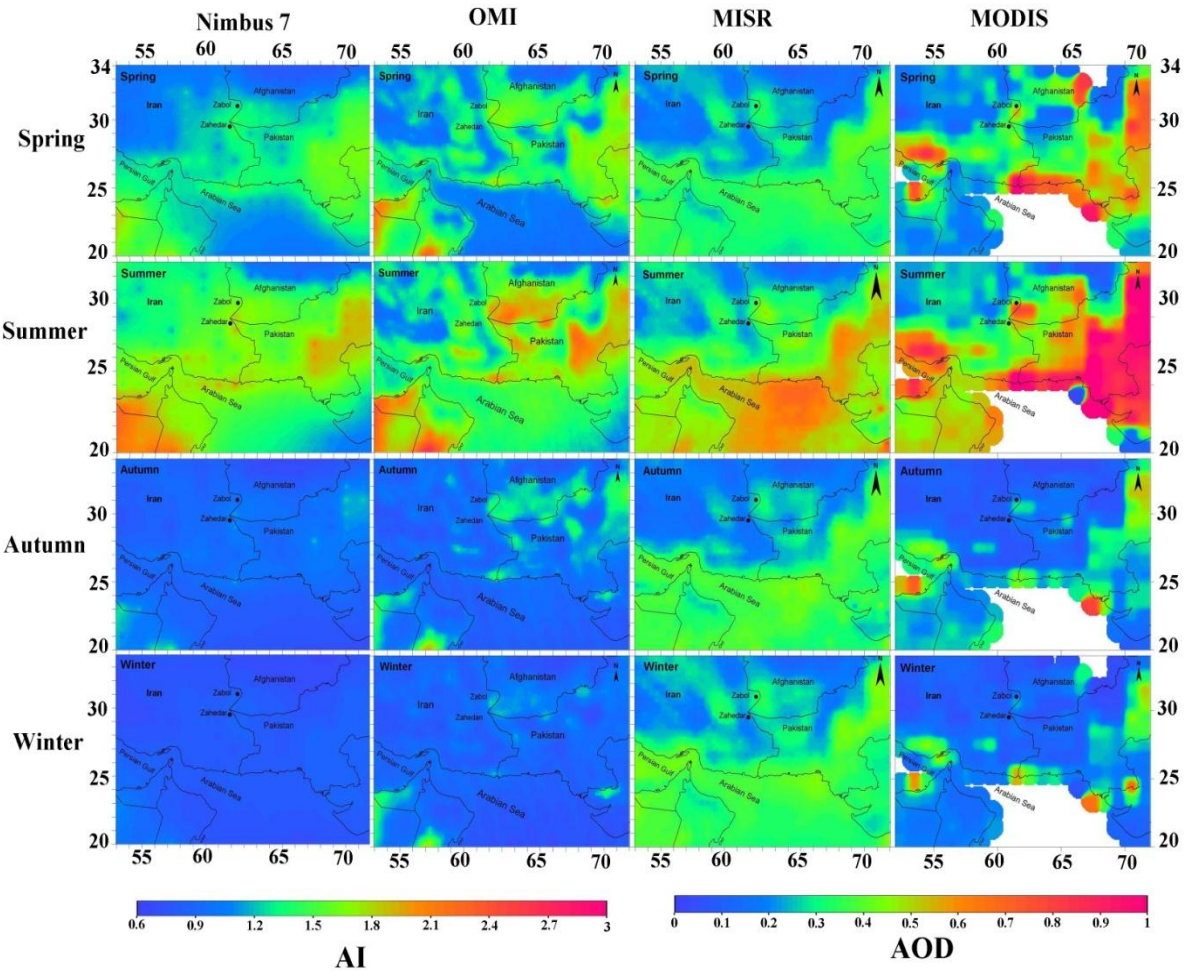

Figure 6.8: Seasonal maps of the spatial distribution of AI (Nimbus 7 and OMI) and AOD (MISR and MODIS) values over southwest Asia. The period of measurements are: for Nimbus 7 (1979 to 1992), for OMI (2005 to 2011), for MISR (2000 to 2010) and for Aqua-MODIS (2002 to 2011).

The use of TOMS and OMI AI satellite data presents some promising results for the identification of dust source regions, although they have a larger spatial resolution compared to MODIS (Baddock *et al*., 2009). Therefore, the use of OMI-AI satellite data for the identification of major dust sources over southwest Asia allows one to focus on critical regions and to characterize emission rates in response to environmental conditions. Apart from the seasonal spatial distribution of AI (Fig. 6.8), the OMI-AI over southwest Asia bounded from 20 to 34^{o}N and 52 to 72^{o}E is also examined on monthly basis during the period 2005 to 2011 (Fig. 6.9). The AI concern data via the Aura-OMI Level-2G (Version 003) with a spatial resolution of 0.25^{o} x 0.25^{o} obtained from Giovanni.

The spatial distribution of AI values reveals a considerable annual variation in aerosol load, in general, and in dust occurrence, in particular. During the winter season (December to February) the AI is generally low, except for some hotspot regions with values of above 1.5, e.g. Hamoun Basin. From March onwards high AI values start to spread over a wider area, covering southern Afghanistan (near to Hamoun), as well as the Arabian and Thar deserts. The AI continuously increases until May, with the highest increase over the Thar desert influencing the aerosol load in northern India (Gautam *et al.*, 2009; Dey and di Girolamo, 2010). During the summer period (June to August) the AI significantly increases over the northern Arabian Sea due to the large influence of dust coming from Arabia as well as from Iran and Pakistan due to strong northern Levar winds. This is also the period with the highest AI over Sistan which is closely associated with a reduction in visibility and stronger winds. From September to November the high AI is limited over Sistan, as well as over some hotspots in Arabia and northeastern Pakistan. From the AI spatial distribution one may put emphasis on the large regional differences between Zabol (near to Hamoun basin) and the city of Zahedan, located about 200 km south. The AI at Zabol is significantly higher during all months, suggesting a larger presence of dust compared to the adjacent southern areas. This is consistent with the large differences in PM_{10} concentrations found between Zabol and Zahedan (See chapter 4).

In synopsis, the spatial distribution of AI identified the Hamoun basin as one of the most active dust source regions in southwest Asia. In general, the dust sources, regardless of size or wind strength, are usually associated with topographic lows in close proximity to mountains and highlands with annual rainfall of less than 200 to 250 mm (Prospero *et al.*, 2002; Engelstaedter *et al.*, 2006). The topography and meteorological conditions in Hamoun favor such a dust outflow. As mentioned in the previous Chapters, this region is associated with drainage features and extensive alluvial deposits, exhibiting some similarities with the lowlands south of the Atlas Mountains in northwest Sahara (Kahn *et al.*, 2009) and Lake Eyre in Australia (Baddock *et al.*, 2009). The accumulation of recent and ancient sediments in such areas, often with salt, which enhances the weathering of sediments, makes them good sources of fine-grained mineral particles (Middleton, 1986) which might be transported potentially thousands of kilometers downwind.

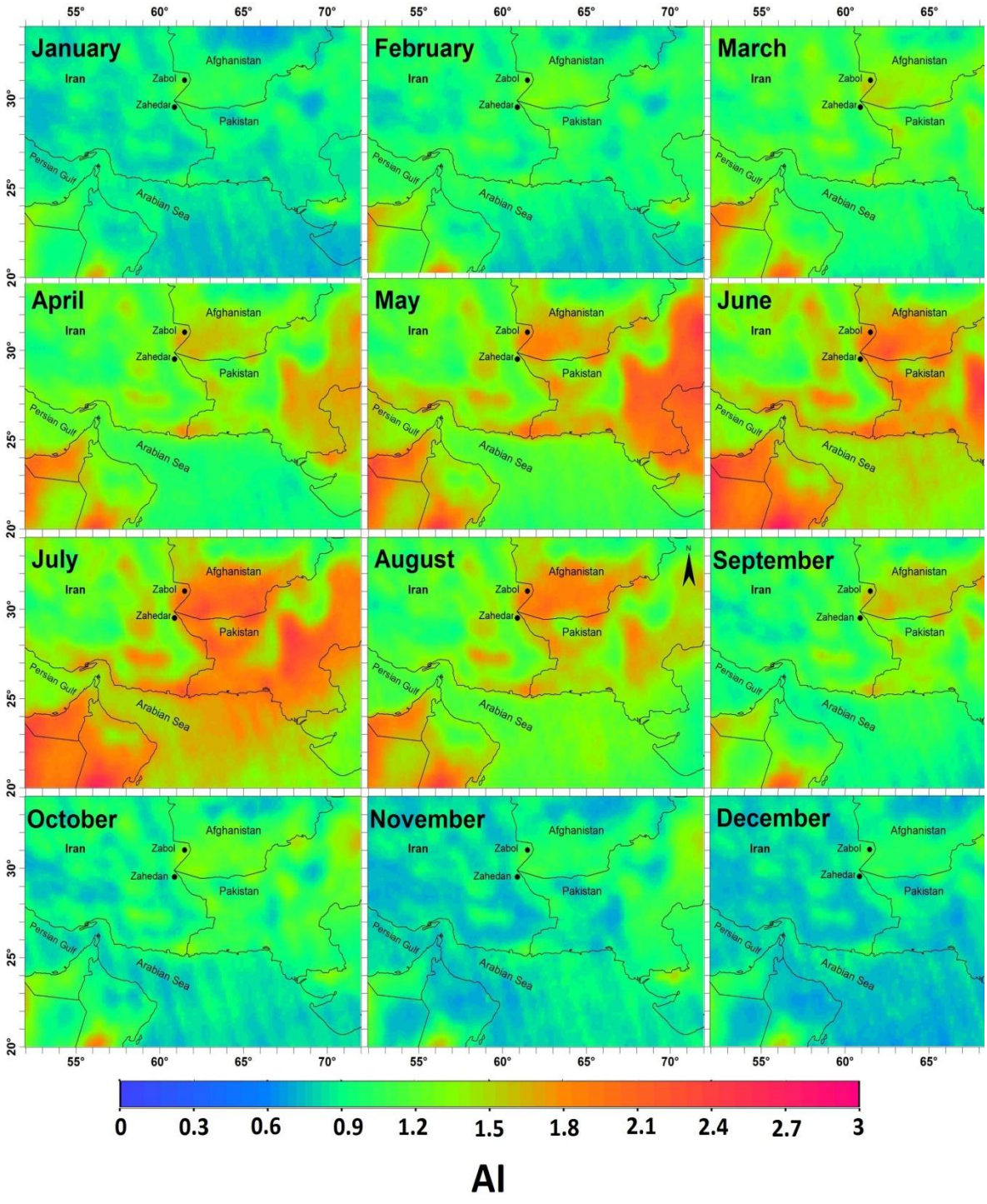

Figure 6.9: Monthly mean spatial distribution of Ozone Monitoring Instruments (OMI) satellite observations over southwest Asia during the period 2005 to 2011.

Intense dust storms originated from Hamoun are responsible for the dramatic increase in AOD over the downwind areas. Alam et al. (2011) reported that such an intense dust plume , which occurred on 21 July 2007 affected coastal AS to such an extent that the AOD increased in Karachi to 1.36. The monthly mean spatial AOD variation via MISR (2000-2010) over southwest Asia is shown in Fig. 6.10. The AOD monthly mean spatial distribution over southwest Asia is similar to that observed for OMI-AI for the reasons discussed above. Once again, the AOD values increase considerably in late spring and summer months, especially in Hamoun, eastern Pakistan, Arabia and Arabian Sea. On the other hand, during winter months high AOD values are observed only over the Indus basin in Pakistan and in some areas in the Arabian Peninsula and Sistan. The former is attributed mainly to anthropogenic aerosols during this period over the densely populated Indus Basin and not to dust presence, since dust activity is low during the winter season in southwest Asia (note the very low AOD values over nearly the whole Iran and Afghanistan during the period November to February suggesting absence of anthropogenic aerosols and very low dust activity).

Finally, the AOD spatial distribution from Aqua MODIS deep blue algorithm over land during the period 2002 to 2010 is shown in Fig. 6.11. In these graphs the ocean pixels have been removed as the aerosol retrievals over sea are obtained with a different algorithm. Also, larger uncertainties in the AOD retrievals exist in the coastal areas due to ocean-land sub-pixel contamination. For this reason there are pockets of very high AODs near to coastal areas which seem to be unreal taking into account the neighboring pixels. Furthermore, the Sistan region is defined in the graph as the annual AOD variation (see section 6.3) and the AOD trends (see next section) are examined in more detail over this area.

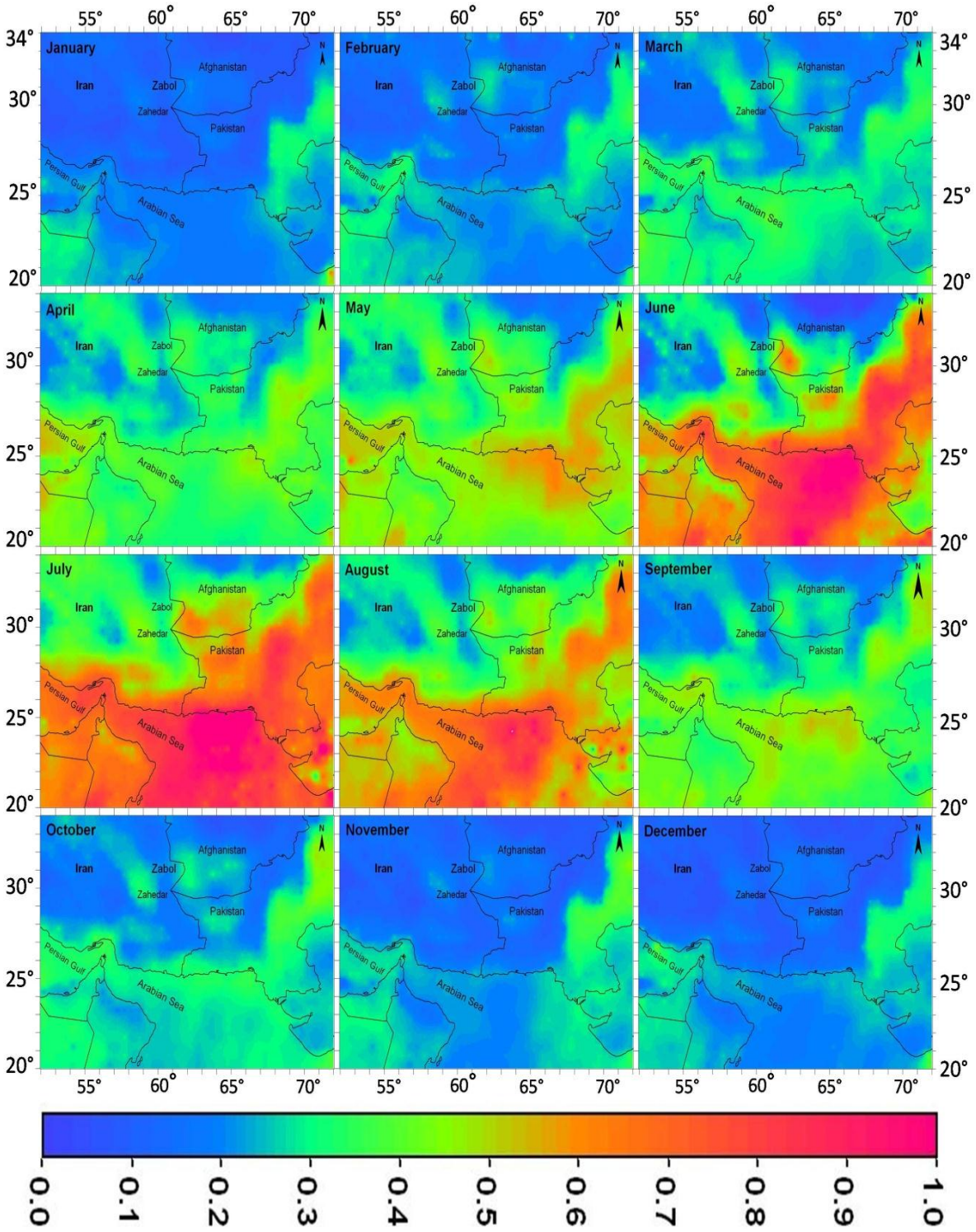

Figure 6.10: Monthly mean spatial distribution of MISR Aerosol Index (AOD) over southwest Asia during the period 2000 to 2010.

Fig. 6.11 reveals a similar spatial and monthly distribution of AOD over southwest Asia from Aqua-MODIS as that found from MISR over the same region (Fig. 6.10). So, any new discussion about the annual variation of the AOD spatial distribution and the reason influencing it is avoided. It is characteristic that both Aqua MODIS and MISR exhibit similar values over Sistan region as also shown in Fig. 6.5.

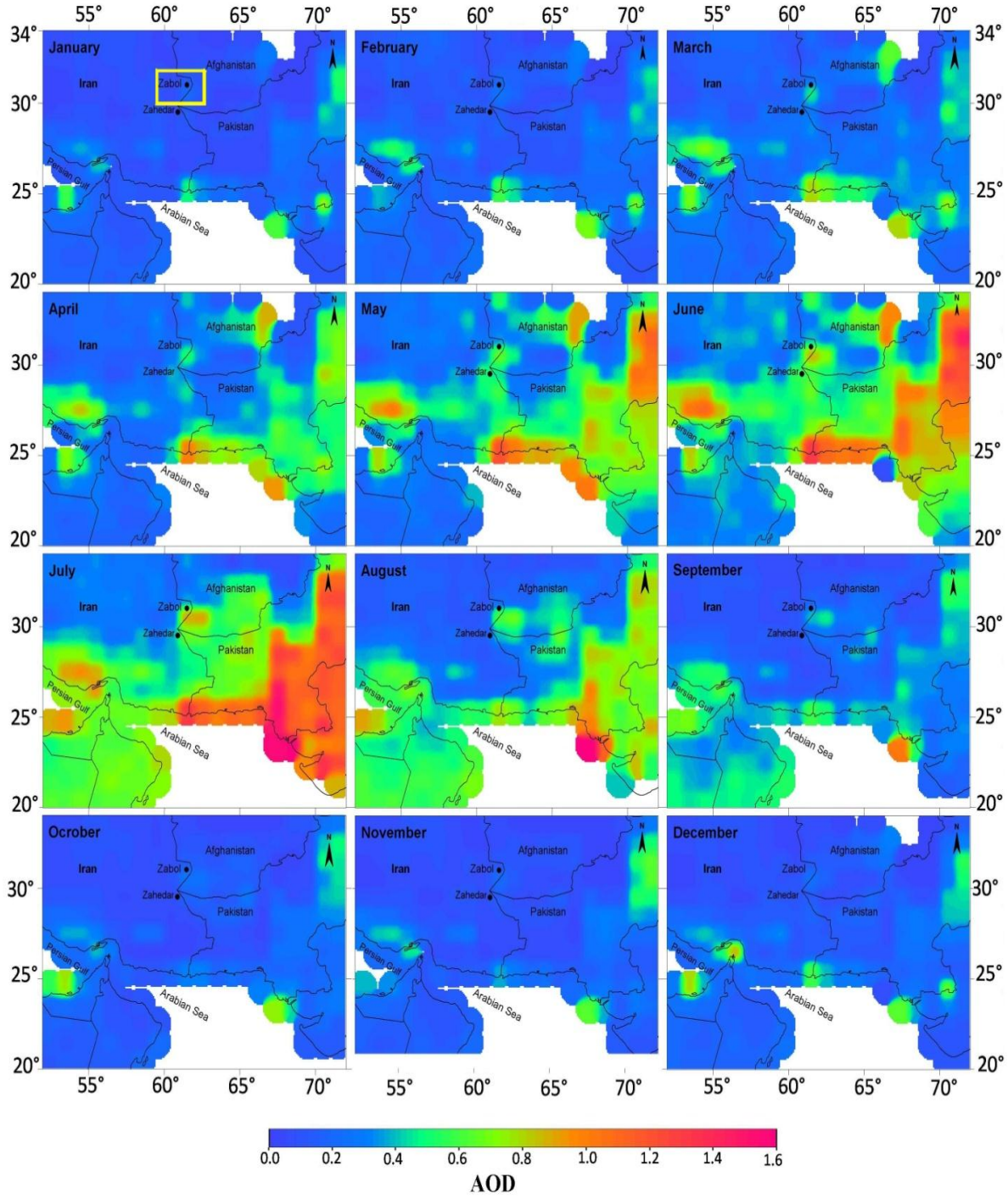

Figure 6.11: Monthly mean spatial distribution of Aqua MODIS satellite observations over southwest Asia during 2000 to 2010.

6.5 Aerosol trends over southwest Asia detected from satellites

Recently, the investigation of the aerosol trends over an extended area via satellite remote sensing has created great scientific interest with respect to the view of the accuracy of the computed trends as compared to aerosol trends obtained from AERONET stations (Prasad and Singh, 2007; Dey and di Girolamo, 2011; Kharol *et al*., 2011). On the other hand, the large spatial coverage of the satellite sensors and ad up to ten years of recordings establish them as a useful tool for the monitoring of the aerosol trends from space (Mishchenko *et al*., 2009; Zhang and Reid, 2010; Kaskaoutis *et al*., 2011). Southwest Asia, as shown in this Chapter, has not received a great attention from satellite remote sensing or ground-based instrumentation such as the neighboring Indian subcontinent and adjoining oceanic regions. With the increase in population, urbanization, industrialization and demands for energy, the aerosol load over south Asia is gradually increasing and having a significant impact on the continuation of solar dimming (Ohmura, 2009; Badarinath *et al*., 2010). The increasing aerosol emissions, mainly from anthropogenic activities, are responsible for the presence of the atmospheric brown clouds (Ramanathan *et al*., 2007), which have significant climate implications in view of heating of the middle and upper troposphere (Gautam *et al*., 2010). However, the arid environments of southwest Asia are sparsely populated without any significant industrial and anthropogenic activity except for the Indus basin in Pakistan. Thus, the spatial distribution and trends of aerosols over this region are mainly affected by the natural variability of aerosols and dust activity.

Fig. 6.15 shows, the monthly % variation of the AOD values obtained from MISR during the period 2000-2010. Similar research, i.e. analysis of the MISR AODs trend over Indian sub-continent and adjoining oceanic areas was recently performed by Dey and Di Girolamo (2011). It should be noted that the % AOD variations were estimated via the formula $\Delta AOD = a*N/\overline{AOD}*100$, where a is the slope value computed from the linear regression of the monthly mean values during 2000 to 2010 for each pixel, N the number of years, and $\overline{AOD}$ the mean AOD for each pixel during 2000 to 2010. The results reveal a considerable spatial distribution of the AOD % variations during the last decade, which also exhibits pronounced seasonal and monthly differences. In general, the western part of the study area exhibits positive values corresponding to AOD increasing trends, while the eastern rather neutral or even negative AOD trends during the months February to

October. This declining trend is especially pronounced over the Thar desert and the northeastern part of the Arabian Sea during June to August was also found by Dey and Di Girolamo (2011) using MISR data and Kaskaoutis *et al*. (2011) using MODIS observations. A more recent study over the region (Kaskaoutis *et al*., 2012) has shown that this declining trend is mainly attributed to the extremely large values during these months in years 2002 and 2003 favored by absence of precipitation and longer aerosol lifetime in the atmosphere. This is strong evidence that the AOD trends observed over southwestern Asia, an area without significant anthropogenic emissions and industrial activities, are mainly controlled by the dust annual variability, which in turn is under the influence of the intensity and onset of the monsoon and larger-scale synoptic weather conditions (Gautam et al., 2009). On the other hand, the AOD % variation seems to be positive over Sistan region during the winter period (December to March). However, the calculated trends using the monthly mean AOD values are strongly influenced by the studied period and the intra-annual variation of AOD over a specific area. In cases when month during the beginning or the end of the examining period has extreme low or high AOD value, this value may influence considerably the linear regression trend analysis. Thus, the results of Fig. 6.12 as well as those of Fig. 6.13 corresponding to Aqua MODIS must be considered qualitatively and not quantitatively.

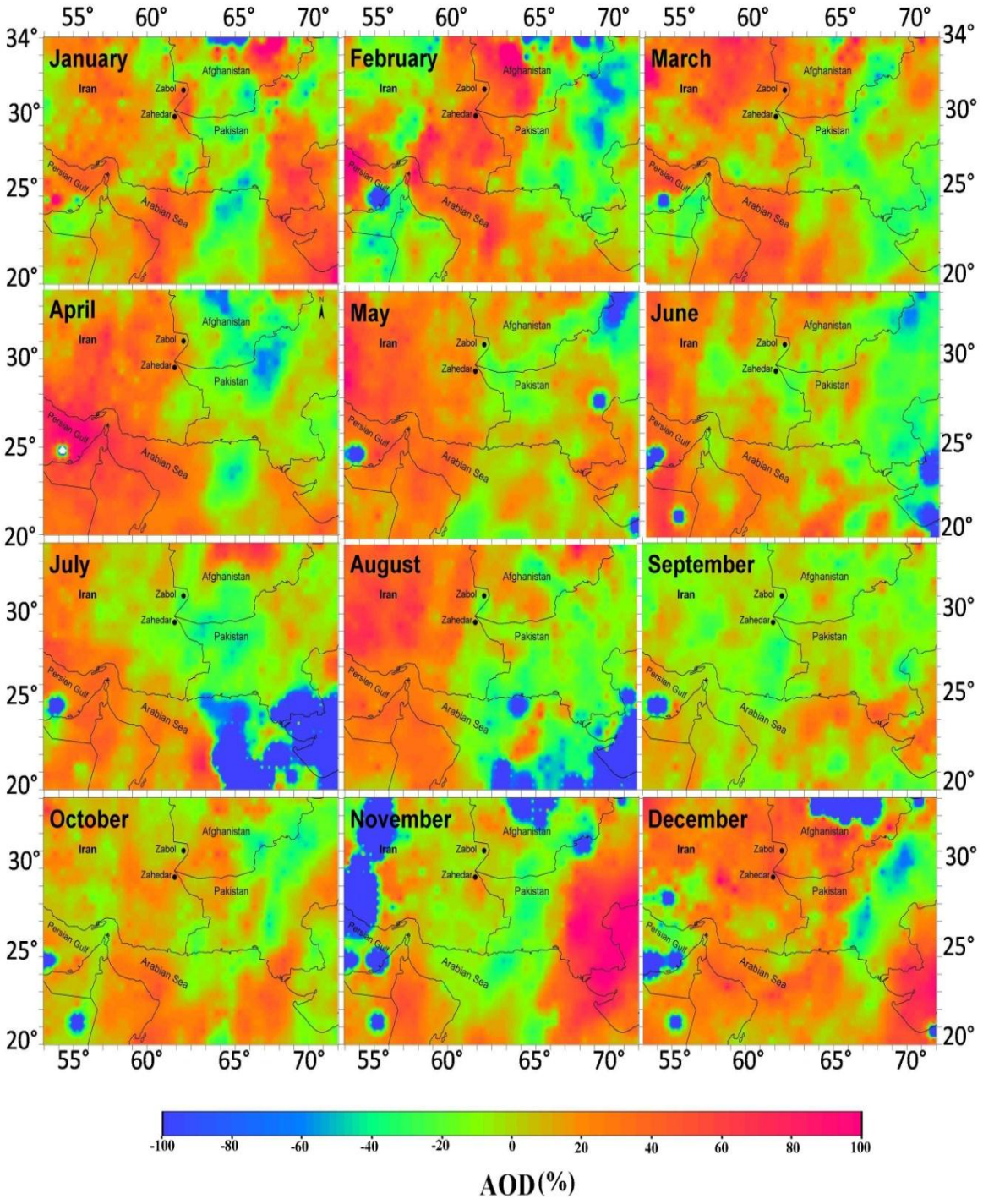

Figure 6.12: Spatial distribution of the Aerosol Optical Depth (AOD) % variation obtained from MISR sensor during the period 2000 to 2010 over southwest Asia.

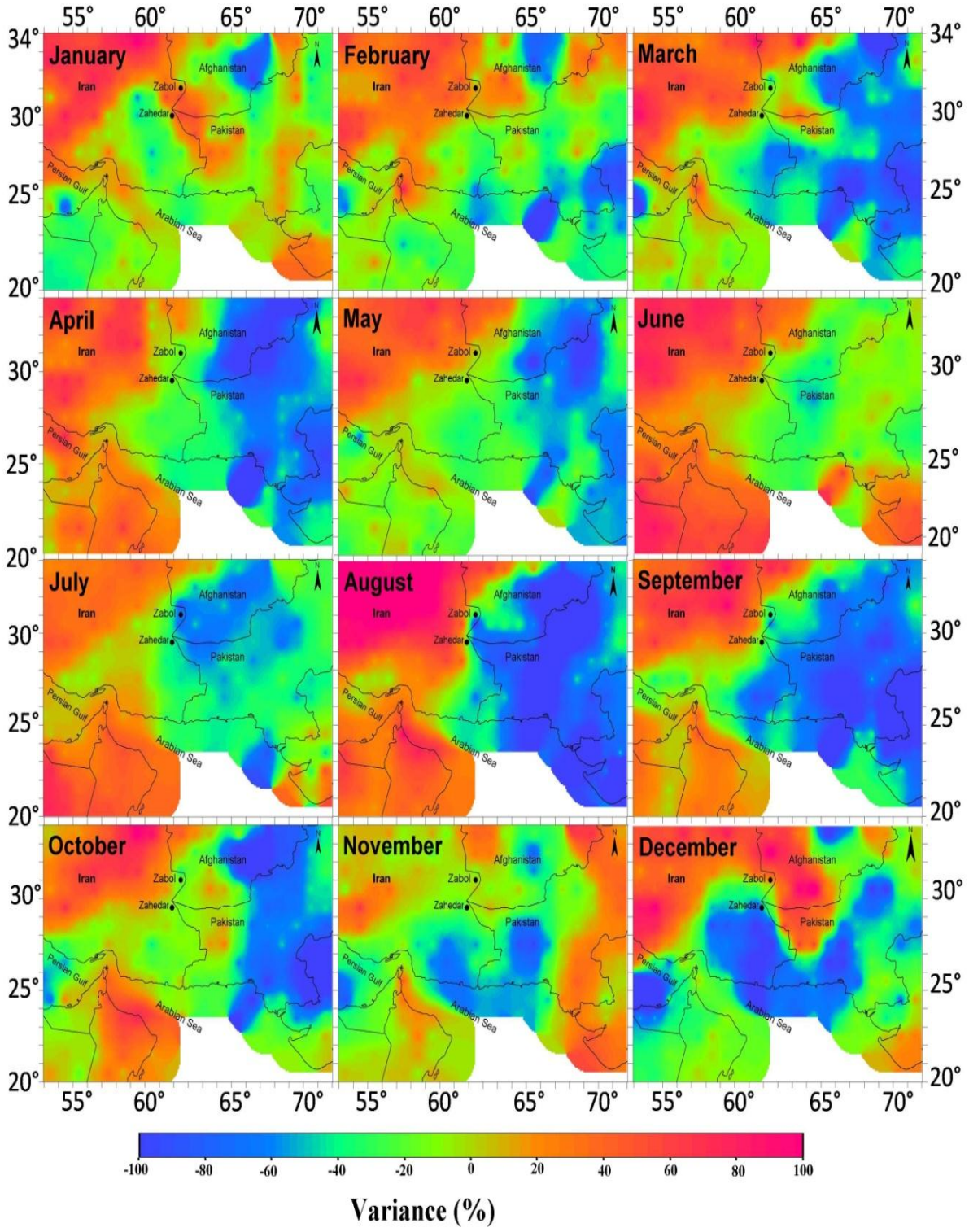

Figure 6.13: Spatial distribution of the Aerosol Optical depth (AOD) % variation obtained from Aqua-MODIS sensor (deep blue algorithm) during the period 2000 to 2010 over southwest Asia.

The above statement is justified by comparing the results of the AOD % trends as obtained from the two sensors. In general, the western part of the study area exhibits positive AOD trends for Aqua MODIS as for MISR, and the eastern part negative trends. However, the AOD % variations as well as the spatial distributions exhibit large differences for the two sensors justifying that the length of the study period plays the main role in the AOD trend estimations, which are strongly affected by the intra-annual AOD variation for each month over a specific region (Kaskaoutis *et al*., 2011). Finally, Table 6.6 summarizes the results of the slope values, as obtained from the AOD linear regression analysis, as well as the AOD % variation for both MISR and Aqua-MODIS sensors.

Table 6.6: Slope values and % variations of Aerosol Optical depth (AOD) over Sistan region as obtained from MISR and Aqua-MODIS satellite sensors.

	Slope MODIS Aqua (2002-2011)	**Slope MISR (2000-2010)**	**AOD% MODIS Aqua (2002-2011)**	**AOD% MISR (2000-2010)**
Jan	0.01657	0.00778	62.1	39.2
Feb	0.00265	0.00510	8.8	17.5
Mar	-0.00538	0.00907	-10.7	29.3
Apr	-0.01153	0.00474	-21.8	14.3
May	-0.00352	-0.00698	-5.8	-15.0
Jun	-0.01733	-0.00457	-24.3	-9.2
Jul	-0.05167	-0.01469	-79.5	-25.8
Aug	-0.05561	-0.00770	-118.2	-17.0
Sep	-0.02358	-0.00809	-71.0	-21.3
Oct	-0.00547	0.00414	-21.0	15.0
Nov	0.00121	0.00290	5.6	14.6
Dec	-0.00443	0.00436	-15.9	24.6
Spring	-0.00681	-0.00227	-12.8	-3.3
summer	-0.04154	-0.01016	-74.0	-21.4
Autumn	-0.00928	0.00380	-28.8	18.1
Winter	0.00866	0.00575	18.3	27.1
Annual	-0.01224	-0.00033	-24.3	-5.2

Even though the slope values are of similar magnitude for both sensors in a specific month, the AOD % variations may differ significantly, thus highlighting the significant role of the examined period for such retrievals. Despite the large differences in the monthly % variations, both sensors exhibit a positive trend in AOD (increasing values during the last decade) in winter, except for December as obtained from Aqua-MODIS, and a negative trend (declining in AOD) during late spring and summer months (May to

September). The decreasing in AOD during these months, which are characterized by the higher AOD values and the more frequent and intense dust storms, may suggest a declining trend in the dust activity over Sistan region and Hamoun Basin during more recent years, after the extreme droughts in the beginning of the 2000s. Such a decreasing trend on days with visibility below 2km during recent years has also been shown in Zabol (Fig. 2.11). However, more years must be taken into consideration in order for these mentioned trends to be confirmed. On the other hand, the significant differences revealed by the two sensors require the use of ground-based instrumentation to be compared for such retrievals, which must be compared with satellite sensors in order to stablish the sensors accuracy over this arid environment.

6.6. Conclusions

For monitoring dust production and effects of regional-scale atmospheric processes on dust emission and transport over the Sistan, satellite remote sensing data was used to provid observational constraints over the region. The aerosol patterns were analyzed by means of multiple satellite platforms aiming to reveal the spatio-temporal and vertical distribution of dust aerosols. The main focus is to determine similarities and differences in dust climatology provided by these sensors over the Sistan region and surroundings. AI and AOD were used as measures of the atmospheric aerosol load. The analysis used the strength of each data set separately to provide a general picture on how the aerosols vary across different regions of southwest Asia and how this variability relates to the atmospheric environment. The results show a marked seasonal cycle with high aerosol loading during summer and lower in winter, while MISR, MODIS Deep Blue and OMI climatologies agree in both terms of monthly and seasonally mean spatial and temporal AOD patterns revealing similar seasonal behavior over the region. Comparisons of the distribution of the aerosol load between AI and AOD, find similar characteristics in the representation of the main sources of aerosol on Hamoun lakes. Both products are able to represent the maximum values of aerosols, especially for those regions affected by dust aerosols. After prolonged drought conditions in 1999 at Hamoun lakes (northern of Sistan) the dust-aerosol load over the area increased. The higher aerosol concentrations during summer are interpreted as a result of the Levar northerly winds and the drying of Hamoun lakes.

CHAPTER 7

CONCLUSIONS AND RECOMMENDATIONS

7.1 Conclusions

The thesis focused on shedding light on the dust loading, PM concentrations, physical and optical properties as well as chemical composition of dust for the first time over the Sistan region of southeastern Iran. The Sistan region is a closed topographic low basin surrounded by arid and rocky mountains and constitutes a major dust source region in south west Asia, while its northern part drains the Hilmand river, thus constituting a wetland area known as Hamoun Basin. Hamoun lakes complex have an area of about 4500 Km^2 with a water volumes of 13025 million m^3 and play the role of a "water cooler" for the region when they are full of water as the severe winds blow across the lakes. The Sistan depression at the end of basin is covered by Quaternary sediments with a maximum thickness of about 500 m in the central part of the plain that have been eroded by fluvial processes. The major portion of this sediment is made up of clay and silt. Therefore, fine-grained soils including silt and clay are the main surface cover the Sistan depression. Sistan has a population of about 400,000, of which half work in agricultural and animal domesticated fields. The economy is strongly dependent on agriculture and the goods and services provided by the wetlands.

Severe droughts over the past decades, especially after 1999, have caused desiccation of the Hamoun lakes, leaving a fine layer of sediment that is easily lifted by the wind and, therefore, making the basin one of the most active sources of dust in southwest Asia. The strong "Levar", especially during the summer season, blows fine sands off the exposed lake bed and deposits this detritus within huge dune bed forms that may cover a hundred or more villages along the former lakeshore. The drainage of the Hamoun wetlands, in association with the intense Levar winds in summer, is the main factor responsible for the frequent and massive dust storms over the Sistan region. Analysis of water surface in

combination with dust storms showed that the Hamoun dried beds have a strong effect on dust storms as sources of aerosols.

Systematic PM concentrations were measured in Zabol city, affected by the Sistan dust storms, covering the period September 2010 to August 2011. The results show that the PM_{10} concentrations were considerably higher than the corresponding European Union air quality annual standard. The air quality is affected by dust storms from the Sistan desert, which are very intense during summer. Hamoun dried beds cause a dramatic increase in PM_{10} concentrations and a deterioration of air quality (65% of the days were considered unhealthy for sensitive people and 34.9% as hazardous).

Dust loading from the Hamoun basin was found to have a significant contributing influence on the development of extreme dust storms, especially during the summer days. This influence, firstly was found to depend on the intensity and duration of dust storms, and secondly, on the distance from the source region, the wind speed and altitude. The grain-size distribution of the dust loading was strongly influenced by the distance from the dust source. Furthermore, the particle size distribution exhibited a shift towards lower values as the altitude increases, with this feature to be more obvious amongst larger size particles, while the frequency of particles below 2.5 μm seemed not to be affected by the altitude. In general, the regional dust loading and characteristics are subject to significant spatio-temporal variability. This finding necessitates more systematic observations at as many locations as possible around the Hamoun basin in order to improve the understanding of forcing dynamics, transport mechanisms as well as to quantify the dust amounts emitted from the Hamoun basin.

Dust mineralogy and geochemical properties were examined in the Sistan region by collecting airborne samples at two stations and soil samples from several locations around Sistan and Hamoun basin in order to understand their characteristics and the potential impact on human health. The Sistan region is an ideal site to study the nature of dust storms as it receives large amounts of fine alluvial material from extended rivers system draining much of the Afghanistan highlands, which comprise crystalline basement rocks, Phanerozoic sediments and extensive flood basalts. As a result, large quantities of quartz-rich, feldspar- and mica-bearing silt, as well as mafic material from flood basalt sources and carbonate minerals from dolomites are transported to the Hamoun wetlands in

northern Sistan. Due to droughts at Hamoun and large irrigation projects upstream on the river catchment, extensive desiccation has occurred in the wetlands resulting in large dry lake environments. These have produced large quantities of evaporate minerals to add to the alluvial silts, and the combination of these materials provides the provenance for the airborne dust.

Dust aerosol characterization included chemical analysis of major and trace elements by XRF and mineral analysis by XRD. The results showed that quartz, calcite, muscovite, plagioclase and chlorite are the main mineralogical components of the dust, in descending order, over Sistan, and were present in all the selected airborne dust samples. In contrast, significantly lower percentages for enstatite, halite, dolomite, microcline, gypsum, diopside, orthoclase and hornblende were found, since these minerals occurred only in some of the samples at both stations. On the other hand, SiO2, CaO, Al2O3, Na2O, MgO and Fe2O3 were the major elements characterising the dust, while large amounts of F, Cl and S were also found as trace elements. The mineralogy and chemical composition of airborne dust were nearly the same and quite similar to the soil samples collected at several locations downwind. This suggests that the dust over Sistan is locally emitted, i.e. from the Hamoun basin, and in a few cases can also be long-range transported. On the other hand, individual dust storms showed significant differences between either evaporite-dominated aerosols or those characterized by deflation from alluvial silts. These possibly reflect either localized climatic cyclicity or desiccation cycles. However, in some cases the soil samples showed poor comparisons with aerosol compositions, suggesting that dynamic sorting, soil-forming processes and climatic influences, such as rainfall, altered the mineralogy and chemistry in these partially Aeolian deposits. Sistan is also an ideal site for studying dust storms and enrichment factors relative to crustal norms; the latter factors suggest that the dust is essentially of crustal rather than anthropogenic origin.

For monitoring dust production and effects of regional-scale atmospheric processes on dust emission and transport over the Sistan, satellite remote sensing provided observational constraints. The aerosol patterns were analysed by means of multiple satellite platforms aiming to reveal the spatio-temporal and vertical distribution of dust aerosols. The main focus is to determine similarities and differences in dust climatology provided by these sensors over the Sistan region and surroundings. AI and AOD were used as measures of the atmospheric aerosol load. The analysis used the strength of each

data set separately to provide a general picture on how the aerosols vary across different regions of southwest Asia and how this variability relates with the atmospheric conditions. The results showed a marked seasonal cycle with high aerosol loading during summer and lower in winter, while MISR, MODIS Deep Blue and OMI climatologies agree in both terms of monthly and seasonally mean spatial and temporal aerosol patterns revealing similar seasonal behavior over the region. After prolonged drought conditions in 1999 at Hamoun lakes (northern of Sistan) the dust-aerosol load over the area has increased. The higher aerosol concentrations during summer are interpreted as a result of the Levar northerly winds and the drying of Hamoun lakes. The satellite monitoring highlights Sistan and Hamoun basin as major dust source regions in south Asia, spreading dust aerosols over Afghanistan, Pakistan and Arabian Sea.

7.2 Future work

The unique research and finding in this thesis, over Sistan region needs to be continued and expended with the aim of examining dust storms in the regions and their influence on human health, ecosystems, ocean color and phytoplankton as well as examining the optical and physical properties of dust in a more comprehensive way by means of new established ground-based instrumentation, such as sun photometers, lidars, etc.

Dust storms over Sistan basin are a challenging issue for the region. There are no meteorological stations in the Afghanistan part of Hamoun and only a few in Iran and Pakistan. To fully understand the issues mentioned above, co-operative work with the governments of Afghanistan, Iran and Pakistan is recommend to stablish a network of ground-based data measurements, which have to be integrated and compared with satellite observatory data. Future work needs to also focus on the dried lakes of Hamoun Jazourian between Sistan and Arabian Sea. The methodology of this dissertation can be applied to provide regional dust characterization, and seasonal and interannual variability.

The dust flux loading, mineral and chemical characterizations were analyzed using samples only at the ground surface up to 8 m height and at two stations, due to remote region and lack of established towers and measurement samplers as well as financial aid

for the study period. The characterization of physical, chemical and mineralogy characteristics of dust over a more extended area around Sistan would better reveal the modification of dust properties as it is transported from the source region to downwind areas. Systematic monitoring of the vertical profiles of dust would also be benefical for mode studies over the region.

This research demonstrated that the behavior of dust outbreaks over Sistan depend strongly on the Hamoun dried beds as source regions. Systematic monitoring of dust from satellites and ground-based observations would also anable constitute the basis for model simulations of dust storms over Sistan and Hamoun basin. Furthermore, the chemical and mineralogy composition of dust can be used in radiative transfer models for obtaining the radiative forcing of dust over the whole region.

Measurements for $PM_{2.5}$ and $PM_{1.0}$ concentrations were restricted to Zahedan city, 200 km far away from Hamoun lakes. It is recommended that more systematic observations of particulate matter are necessary over the whole of the Sistan region and, especially in Zabol city and Hamoun dried lakes, in order to compare air quality standards as well as health effects of $PM_{2.5}$ and PM_{10} over Sistan. It is also recommended that the PM_{10} and $PM_{2.5}$ samples collected over Sistan be analyzed using XRF and XRD techniques in order to reveal the chemical and mineralogy composition of the particulate matter (coarse and fine particles).

In addition to TOMS, OMI, MODIS, MISR satellite monitoring over Sistan regions. CALIPSO observations may provide important information about the optical properties of aerosol and its vertical distribution over both the dust sources and downwind regions. By using of CALIPSO data in combination with other aerosol monitoring from space, a more accurate assessment of the impact of dust aerosols on the radiative energy balance and climate over the Sistan Basin can be achieved. With respect to the Sistan climate, implementation of CALIPSO profiles used with regional transport models can be used to improve understanding of how the aerosol's vertical distribution affects the temperature profile, atmospheric heating and stability over the region.

REFERENCES

Abel, S.J., E.J. Highwood, J.M. Haywood, and M.A. Stringer, 2005. The direct radiative effect of biomass burning aerosol over southern Africa. Atmos. Chem. Phys. Discuss., 5, 1165–1211.

Acker, J.G. and Leptoukh, G., 2007. Online analysis enhances use of NASA Earth Science Data. Transactions of the American Geophysical Union, 88(2): 14-17.

Ackerman, A.S., Toon, O.B. Stevens, D.E. Heymsfield, A.J. Ramanathan, V. and Welton. E.J. 2000. Reduction of tropical cloudiness by soot, Science, 288, 1042–1047.

Adamopoulos, A.D., Kambezidis, H.D., Kaskaoutis, D.G., Giavis, G., 2007. A study of particle size in the atmosphere of Athens, Greece retrieved from solar spectral measurements. Atmos. Res. 86, 194-206.

Akyuz, M., Cabuk, H., 2009. Meteorological variations of PM2.5/PM10 concentrations and particle-associated polycyclic aromatic hydrocarbons in the atmospheric environment of Zonguldak,Turkey. Journal of Hazardous Materials 170: 13–21

Alam, K., Qureshi, S., Blaschke, T., 2011b. Monitoring Spatio-temporal aerosol patterns over Pakistan based on MODIS, TOMS and MISR satellite data and a HYSPLIT model. Atmos. Environ., 45, 4641-4651.

Alam, K., Trautmann, T., Blaschke, T., 2011a. Aerosol optical properties and radiative forcing over mega-city Karachi. Atmos. Res., 101, 773-782.

Albrecht, B.A. 1989. Aerosols, cloud microphysics, and fractional cloudiness, Science, 245(4923), 1227–1230.

Alpert, P., Kaufman, Y., Shay-El, Y., Tanrè, D., da Silva, A., Schubert, S., Joseph, J., 1998. Quantification of dust-forced heating of the lower troposphere. Nature 395, 367-370.

Alpert, P., Kishcha, P., Shtivelman, A., Krichak, S.O., Joseph, J.H., 2004. Vertical distribution of Saharan dust based on 2.5-year model predictions. Atmos. Res. 70, 109–130.

Andreae, M.O., 1996. Raising dust in the greenhouse. Nature 380, 389–390.

Ant´on, M., Loyola, D., Clerbaux, C., L´opez, M., Vilaplana, J. M.., Ba˜n´on, M., Hadji-Lazaro, J., Valks, P., Hao, N., Zimmer,W., Coheur, P. F., Hurtmans, D., and Alados-Arboledas, L. 2011. Validation of the Metop-A total ozone data from GOME-2 and IASI using reference ground-based measurements at the Iberian Peninsula, Remote Sens. Environ., 115, 1380–1386,

Ardakani, S.Q., 2006. Determine the air quality in Iran in (2004).Journals of Environmental Science and Technology, Volume 8, Number 4, winter, p. 38-33(In Persian)

Arnold, E., Merrill, J., Leinen, M., and King, J. 1998. The effect of source area and atmospheric transport on mineral aerosol collected over the north pacific ocean, Global Planet Change, 18, 137–159

Asian Development Bank .2005. Establishment of a regional monitoring and early warning network for dust and sandstorms in northeast Asia, volume 2. Asian Development Bank, Manila

Badarinath , K.V.S., Kharol, S.K., Kaskaoutis, D.G. Kambezidis H.D., 2007. Influence of atmospheric aerosols on solar spectral irradiance in an urban area, J. Atmos. Solar Terr. Phys., 69, pp. 589–599

Badarinath, K.V., Kharol, S., Kaskaoutis, D.G., Sharma, A.R., Ramaswamy, V., and Kambezidis, H.D. 2010. Long range transport of dust aerosols over Arabian Sea and Indian region – A case study using satellite data and ground-based measurements, Global Planet. Change 72 164–181.

Badarinath, K.V.S., Kharol, S.K., Reddy, R.R., Rama Gopal, K., Narasimhulu, K., Siva Sankara Reddy, L., Raghavendra Kumar, K., 2009. Black carbon aerosol mass concentration variation in urban and rural environments of India - A case study. Atmospheric Science Letters, 10, 29-33.

Baddock, M.C., Bullard, J.E., Bryant, R.G., 2009. Dust source identification using MODIS: A comparison of techniques applied to the Lake Eyre Basin, Australia. Rem. Sens. Environ. 113, 1511-1528.

Bagnold, R.A. 1941. The physics of blown sand and desert dunes. Methuen, London

Balis, D.S., Amiridis, V., Nickovic, S., Papayannis, A., Zerefos, C.S. 2004. Optical properties of Saharan dust layers as detected by a Raman lidar at Thessaloniki, Greece. Geophys. Res. Lett. 31: LI3104, doi:101029/2004GL019881.

Barlow, M., Cullen, H., and Lyon, B., 2002, Drought in central and southwest Asia: La Niña, the warm pool, and Indian Ocean precipitation: Journal of Climate, v. 15, p. 697–701.

Barnaba, F., Gobbi, G.P. 2004: Modeling the aerosol extinction versus backscatter relationship for lidar applications: maritime and continental conditions, J. Atmos. Oc., 21, 428–442,.

Bartzokas, A., Kassomenos, P., Petrakis, M., Celessides, C., 2004. The effect of meteorological and pollution parameters on the frequency of hospital admissions for cardiovascular and respiratory problems in Athens. Indoor and Built Environ. 13, 271-275.

Bar-Ziv, J., Goldberg, G.M. 1974. Simple siliceous pneumoconiosis in Negev Bedouins. Arch Environ Health 29:121–126

Bergametti, G., Gomes, L., Coude-Gaussen, G., Rognon, P., Le Coustumer, M.-N., 1989. African dust observed over Canary islands: Source-regions identification and transport pattern for some summer situations. J. Geophys. Res., 94, D12, 14855-14864.

Berrick, S., Gregory Leptoukh, John Farley, Hualan Rui, 2008. Giovanni: A Web Services Workflow-Based Data Visualization and Analysis System, IEEE Trans. on Geos. & RS,

Bhaskaran , k., Wilkinson, p., and smeeth, L. 2011. Cardiovascular consequences of air pollution: what are the mechanisms? Heart, 97, 519-520.

Bilos, C., Colombo, J.C., Skorupka, C.N., Presa, M.J.R., 2001. Sources, distribution and variability of airborne trace metals in La Plata City area, Argentina. Environ. Pollut. 111, 149–158.

Biscaye, P. E., Grousset, F.E. 1998. Ice-core and deep-sea records of atmospheric dust. In A. Busacca (Ed.), Dust aerosols, loess soils, and global change (pp. 101–103). College Agric. Home Econ. Misc. Publ. MISC0190 (1998). Pullman, WA: Washington State Univ.

Bollasina, M., Nigam, S., and Lau, K.-M. 2008. Absorbing aerosols and summer monsoon evolution over South Asia: An observational portrayal, J. Climate, 21, 3221–3239.

Bou Karam, D., Flamant, C., Cuesta, J., Pelon, J and Williams, E., 2010. Dust emission and transport associated with a Saharan depression: February 2007 case. Journal of Geophysical Research, vol. 115, d00h27, doi:10.1029/2009jd012390, 2010

Brazel, A., Hsu, S. 1981. The climatology of hazardous Arizona dust storms. In: Péwé TL (ed) 1981 Desert dust. Geol Soc Am Spec Pap 186:293–303

British Geological Survey, http://bgs.ac.uk/

Broecker, W.S., 2000. Abrupt climate change: causal constraints provided by the paleoclimate record. Earth Science Reviews 51, 137–154.

Brown, J.K.M., Hovmøller, M.S. 2002 Aerial dispersal of pathogens on the global and continental scales and its impact on plant disease. Science 297:537–541

Bücher, A., 1986. Recherches sur les poussières minérales d'originesaharienne. PhD thesis, Université de Reims-Champagne-Arddenne,France.

Bullard, J.E., McTainsh, G.H., Pudmenky, C. 2004. Aeolian abrasion and modes of fine particle production from natural red dune sands: an experimental study. Sedimentology 51:1103–1125

Bullard, J.E., White, K. 2005. Dust production and the release of iron oxides resulting from the Aeolian abrasion of natural dune sands. Earth Surf Process Landforms 30:95–106

Burritt, B., Hyers, A.D. 1981 Evaluation of Arizona's dust warning system. In: Péwé TL (ed) Desert dust. Geol Soc Am Spec Pap 186:281–292

Caquineau, S., Magonthier, M.C., Gaudichet , A., Gomes, L. 1997. An improved procedure for the X-ray diffraction analysis of low-mass atmospheric dust samples. Eur. J. Mineral. 9: 157–166.

Carlson, T. N., and J. M. Prospero, 1972. The Large-Scale Movement of Saharan Air Outbreaks over the Northern Equatorial Atlantic. J. Appl. Meteor., 11(2), 283-297.

Chakra, O.R.A., Joyeux, M., Nerriere, E., Strub, M.P., Zmirou-Navier, D., 2007. Genotoxicity of organic extracts of urban airborne particulatematter: an assessment within a personal exposure study, Chemosphere 66:1375–1381.

Chaloulakou, A., Kassomenos, P., Spyrelis, N., Demokritou, P., Koutrakis, P., 2003. Measurements of PM10 and PM2.5 particle concentrations in Athens, Greece. Atmos. Envir. 37, 649-660.

Charlson, R. J., S. E. Schwartz, J. M. Hales, R. D. Cess, J. A. Coakley, Jr., J. E. Hansen, and D. J. Hofmann, 1992: Climate forcing by anthropogenic aerosols. Science, 255, 423–430.

Charlson, R. J., Schwartz, S. E. Hales, J. M. Cess, R. D. Coakley, J. A. Hansen, J. R. and Hofmann, D. J. 1992. Climate forcing by anthropogenic aerosols, Science, 255, 423-430, 1992.

Chen, Y.S., Sheen, P.C., Chen, E.R., Liu, Y.K., Wu, T.N., Yang, C.Y. 2004. Effects of Asian dust storm events on daily mortality in Taipeh, Taiwan. Environ Res 95:151–155

Cheraghi, M., 2001. Evaluation and comparison of air quality in Tehran and Isfahan in 1999 and offering solutions to improve It, MSc thesis of Environment, Natural Resources Faculty of Tehran University, 150 Pages (In Persian)

Choi, M. S., & Bang, E. J. 1999. Trace metals in airborne particulate collected at Cheju Island, Korea. Journal of Korean Society for Atmospheric Environment, 15, 727–738.

Chow, J. C., Watson, J. G., Ashbaugh, L. L., Magliano, K. L. 2003. Similarities and differences in PM10 chemical source profiles for geological dust from the San Joaquin Valley, California. Atmospheric Environment, 37, 1317– 1340.

Christopher SA, Gupta P, Johnson B, Brindley H, Haywood J, Hsu C. 2011. Multi-sensor satellite remote sensing of dust aerosols overNorth Africa during GERBILS. Q. J. R. Meteorol. Soc. 137: 1168–1178, DOI: 10.1002/qj.863

Christopher, B.K., John M. O. 2004. Elemental Analysis of Sub-Hourly Ambient Aerosol Collections, Aerosol Science and Technology , Volume 38, Issue 3, 205-218

Christopher, S. A., Zhang , J., 2002. Shortwave aerosol radiative forcing from MODIS and CERES observations over the oceans, Geophys. Res. Lett., 29(18), 1859, doi:10.1029/2002GL014803.

Chu, D. A., Kaufman, Y. J. Zibordi, G. Chern, J. D. Mao, J. Li, C. and Holben, B. N. 2003: Global monitoring of air pollution over land from EOS- Terra MODIS. J. Geophys. Res, 108 (D21), 4661, doi: 10.1029/2002JD003179.

Claquin, T., Schulz, M., Balkanski, Y., Boucher, O., 1998. Uncertainties in assessing radiative forcing by mineral dust. TellusB 50, 491-505.

Claquin, T., Schulz, M., Balkanski, Y.J., 1999. Modeling the mineralogy of atmospheric dust sources. Journal of Geophysical Research-Atmospheres 104 (D18), 22243–22256.

Clarke, F. W., 1924. Bull. U.S. geol. Surv., 700, p. 29.

Clements, T., Stone, R.O., Mann, J.F., Eyman, J.L., 1963. A study of windborne sand and dust in desert areas. U.S. Army, Natick Laboratories Mass., Earth Science Division, Technical Report ES- 8, Project Ref. 7x83-01-008.

Clough, W.S., 1975. The deposition of particles on moss and grasssurfaces. Atmospheric Environment 9, 1113–1119.

Cogliani, E., 2001. Air pollution forecast in cities by an air pollution index highly correlated with meteorological variables. Atmospheric Environment, 35, 2871-2877.

Cong, Z., Kang, S., Liu, X., Wang, G., 2007. Elemental composition of aerosol in the Nam Co region, Tibetan Plateau, during summer monsoon season. Atmospheric Environment 41, 1180–1187.

Coudé-Gaussen, G. 1984. Le cycle des poussières éoliennes désertiques actuelles et la sedimentation des loess péridesertiques quaternaries. Bull Cent Rech Explor Prod Elf Aquitaine 8:167–182

Coz, E., Gómez-Moreno, F.J., Pujadas, M., Casuccio, G.S., Lersch, T.L. and Artinano, B. 2009. Individual particle characteristics of North African dust under different long-range transport scenarios. Atmospheric Environment 43(11):1850-1863.

Crooks, G.A., Cowan, G.R.C. 1993. Duststorm, South Australia, November 7th, 1988. Bull Aust Meteorol Oceanogr Soc 6:68–72

d'Almeida, G.A., 1987. On the variability of desert aerosol radiative characteristics. Journal of Geophysical Resarch 92, 3017–3026.

Dalmeida, G.A., 1987. On the variability of desert aerosol radiative characteristics. Journal of Geophysical Resarch 92, 3017–3026.

Darmenova, K., Sokolik, I. N., Darmenov, A. 2005, Characterization of east Asian dust outbreaks in the spring of 2001 using ground-based and satellite data, J. Geophys. Res., 110, D02204, doi:10.1029/2004JD004842

De Graaf, M., Stammes, P., Torres, O., Koelemeijer, R.B.A., 2005. Absorbing Aerosol Index: Sensitivity Analysis, application to GOME and comparison with TOMS. J. Geophys. Res. 110, D01201, doi: 10.1029/2004JD005178.

Deer, W. A., Howie, R. A. and Zussman, J. 1966. An Introduction to the Rock Forming Minerals, Longmans, pp. 528.

Dentener, F.J., Carmichael, G.R., Zhang, Y., Lelieveld, J., Crutzen P.J. 1996, Role of mineral aerosol as a reactive surface in the global troposphere, Journal of Geophysical Research-Atmospheres, 101 (D17) pp. 22869–22889

Derbyshire, E. 2001. Geological hazards in loess terrain, with particular reference to the loess regions of China. Earth Sci Rev 54:231–260

Dey, S., and di Girolamo, L., 2010. A climatology of aerosol optical and microphysical properties over the Indian subcontinent from 9 years (2000-2008) of Multiangle Imaging Spectroradiometer (MISR) data. J. Geophys. Res., 115, D15204, doi:10.1029/2009JD013395.

Dey, S., and Di Girolamo, L., 2011 A decade of change in aerosol properties over the Indian subcontinent Geophys. Res. Lett. 38 L14811

Dey, S., Tripathi, S. N., Singh, R. P., and Holben, B. N. 2004: Influence of dust storms on the aerosol optical properties over the Indo–Gangetic Basin, J. Geophys. Res., 109, D20, 211, doi:10.1029/2004JD004924,. 2870

Di Sarra, A., Cacciani, M., Chamard, P., Cornwall, C., DeLuisi, J. J., Di Iorio, T., Disterhoft, P., Fiocco, G., Fua`, D., and Monteleone. F. 2002. Effects of desert dust and ozone on the ultraviolet irradiance the Mediterranean island of Lampedusa during PAUR II, J. Geophys.

Di Sarra, A., M. Caccian, M. Campanelli, P. Chamard, C. Cornwal, J. Deluici, L. De Silverteri, T., Di Iorio, P. DISTERHOFT, G. FIOCCO, D. FUÀ, P. Grigioni, W.

Junkermann, F. Marenco, D. Meloni, F. Monteleone and B. Olivieri, B., 2001. Radiation, ozone, and aerosol measurements at Lampedusa during the PAUR II Campaign, in IRS 2000: Current Problems in Atmospheric Radiation, edited by W.L. Smith and YU. M. Timofeyev (A. Deepak Publishing, Hampton,Virginia), 1193-1196.

Dickerson, R.R., Kondragunta, S., Stenchikov, G., Civerolo, K.L., Doddridge, B.G., Holben, B.N. 1997. The impact of aerosols on solar ultraviolet radiation and photochemical smog. Science 278, 827-830.

Diner, D. J., T. P. Ackerman, A. J. Braverman, C. J. Bruegge, M. J. Chopping, E. E. Clothiaux, R. Davies, L. Di Girolamo, R. A. Kahn, Y. Knyazikhin, Y. Liu, R. Marchand, J. V. Martonchik, J-P. Muller, A. W. Nolin, B. Pinty, M. M. Verstraete, D. L. Wu, M. J. Garay, O. V. Kalashnikova, A. B. Davis, E. S. Davis, R. A. Chipman, 2010.Ten years of MISR observations from TERRA: Looking back, ahead and in between, Proceedings of the 2010 IEEE International Geoscience and Remote Sensing Symposium, Honolulu, HI, 2010.

Diner, D.J., Beckert, J.C., Reilly, T. HBruegge, C.J., Conel, J.E., Kahn, R.A., Martonchik, J., VAckerman, T.P., Davies, R., Gerstl, S.A.W., Gordon, H.R., Muller, J.-P., Myneni, R.B., Sellers, P.J., Pinty, B., Verstraete, M.M. 1998. Multi-angle imaging spectroradiometer (MISR) instrument description and experiment overview. IEEE Trans. Geosci. Rem. Sens. 36, 1072-1087, 1998

Dockery D, Pope A. Epidemiology of acute health effects: summary of time-series studies. In: Particles in Our Air: Concentrations and Health Effects (Wilson R, SpenglerJD, eds). Cambridge, MA:Harvard University Press, 1996,123-147.

Dockery, D., Pope, C.A., Xiping, X., Spengler, J., Ware, J., Fay, M., Ferris, B., Spiezer, F., 1993. An association between air pollution and mortality in six US cities. New England Journal of Medicine 329 (24), 1753–1759.

Dong, Z., Man, D., Luo, W., Qian, Q., Wang, J., Zhao, M., Liu, Sh., Zhu, G., Zhu, Sh. 2010. Horizontal aeolian sediment flux in the Minqin area, a major source of Chinese dust storms, Geomorphology 116 58–66

Dunion, J., Velden, C., 2004. The impact of the Saharan air layer on Atlantic tropical cyclone activity. Bull. Amer. Meteor. Soc. 85, 353-365.

Ekhtesasi, M.R., 2009. National project of monitoring of wind erosion and sand storm in Iran, forests and range and watershed organization of Iran (Persian language)

Ekhtesasi, M.R., Daneshvar, M.R., Abolghasemi, M., Feiznia, S., and Saremi Naeini, M.A. Measurement and Mapping of Aeolian Sand Flowthrough Sediment Trap Method (Case Study: Yazd-Ardakan Plain), Journal of the Iranian Natural Res., Vol. 59, No. 4, 2007, pp. 773-781

El-Askary, H., Gautam, R., Singh, R.P., Kafatos, M , 2006. Dust storms detection over the Indo-Gangetic basin using multi sensor data. Adv Space Res, Volume 37, Issue 4, 728–733

Engelbrecht, J.P., McDonald, E.V., Gillies, J.A., Jayanty RKM, Casuccio, G., Gertler, A.W. 2009, Characterizing mineral dusts and other aerosols from the Middle East—Part 1: Ambient sampling.Inhalation Toxicology 21:297 -326

Engelstaedter, S., Tegen, I., Washington, R., 2006. North African dust emissions and transport. Earth-Science Reviews 79, 73-100.

Environmental Protection Agency (EPA), 1999. Guideline for reporting the daily air quality-air quality index (AQI). EPA-1999-454/R-99-010.

Erel,Y., Dayan,U., Rabi, R., Rudich,Y., Stein,M., 2006. Trans boundary transport of pollutants by atmospheric mineral dust. Environmental Science & Technology 40 (9), 2996–3005.

Esmaili, O and Tajrishy, M, 2006, Results of the 50 year ground-based measurements in comparison with satellite remote sensing of two prominent dust emission sources located in Iran, Proc. SPIE 6362, 636209, http://dx.doi.org/10.1117/12.692989

Fahey, B. 1985. Salt weathering as a mechanism of rock breakup in cold climates: an experimental approach. Zeitschr Geomorphol 29:99–111

Falkowski, P.G., Barber, R.T., Smetacek, V. 1998. Biogeochemical controls and feedbacks on ocean, primary production. Science 281, 200-206.

Folk, R.L. 1975. Geological urban hindplanning, an example from a Hellenistic Byzantian city, Stobi, Jugoslavian Macedonia. Environ Geol 1:5–22

Frank, J.D., Gregory, R.C., Yang, Z., et al., 1996. Role of mineral aerosol as a reactive surface in the global troposphere. Journal of Geophysical Research 101 (D17), 22,869–22,889.

Franzen, L.G., Mattson, J.O., Martensson, U. 1994. Yellow snow over the Alps and sub-Arctic from dust storm in Africa, March 1991. Ambio 23, 233-235.

Fung, I.Y., Meyn, S.K., Tegen, I., Doney, S.C., John, J.G., Bishop, J.K.B. 2000. Iron supply and demand in the upper ocean. Global Biogeochemical Cycles 14, 281-295.

Gabriel, A.P., Martínez-Ordaz, V.A., Velasco-Rodreguez, V.M., Lazo-Sáenz, J.G., Cicero, R 1999. Prevalence of skin reactivity to coccidioidin and associated risks factors in subjects living in a northern city of Mexico. Arch Med Res 30:388392

Ganji, M.H., 1968, The climate of Iran, in Fisher, W.B., ed., The land of Iran—The Cambridge history of Iran, I: Cambridge, University Press, p. 212–245.

Ganor, E., 1975. Atmospheric dust in Israel. Sedimentological and Meteorological Analysis of Dust Deposition. PhD thesis, Hebrew University of Jerusalem, Israel.

Ganor, E., Foner, H.A., & Gravenshorst, G. 2003. The amount and nature of the dust on Lake Kinneret (the Sea of Galilee), Israel: flux and fractionation. Atmospheric Environment, 37, 4301–4315.

Gao, X. J., Zhao, Z. C. and Giorgi, F. 2002, Changes of extreme events in regional climate simulations over East Asia, Adv. Atmos. Sci., 19(5), 927– 942.

Garrison V.H., E.A. Shinn, W.T. Foreman, D.W. Griffin, C.W. Holmes, C.A. Kellogg, M.S. Majewski, L.L. Richardson, K.B. Ritchie, and G.W. Smith. 2003. African and Asian dust: From desert soils to coral reefs. BioScience 53: 469-480.

Gautam, R., Hsu, N. C., and Lau, K.-M. 2010. Premonsoon aerosol characterization and radiative effects over the Indo-Gangetic Plains: Implications for regional climate warming, J. Geophys. Res., 115, D17208, doi:10.1029/2010JD013819.

Gautam, R., Liu, Z., Singh, R. P., Hsu, N.C., 2009. Two contrasting dust-dominant periods over India observed from MODIS and CALIPSO data. Geophys. Res. Lett., 36, L06813, doi:10.1029/2008GL036967.

Gautam, R.. Hsu, N. C, Tsay, S. C. , Lau, K. M. , Holben, B., Bell, S 2011 Accumulation of aerosols over the Indo-Gangetic plains and southern slopes of the Himalayas: distribution, properties and radiative effects during the 2009 pre-monsoon season Atmos. Chem. Phys. 11 12841–63

Generoso, S., I. Bey, M. Labonne, 2008, Aerosol vertical distribution in dust outflow over the Atlantic: Comparisons between GEOS-Chem and Cloud-Aerosol Lidar and Infrared Pathfinder Satellite Observation (CALIPSO), J. Geophys. Res., 113, D24209, doi:10.1029/2008JD010154.

Giles, J. 2005. The dustiest place on Earth. Nature 434:816–819

Ginoux, P., Chin, M., Tegen, I., Prospero, J., Holben, B.N., Dubovik, O., Lin, S.J. 2001. Sources and distributions of dust aerosols simulated with the GOCART model. J. Geophys. Res. 106, 20255–20273.

Gobbi, G.P., Barnaba, F., Ammannato, L., 2007. Estimating the impact of Saharan dust on the year 2001 PM10 record of Rome, Italy. Atmos. Environ. 41, 261-275.

Godoy, L., Godoy, J. L. A., Roldão, L., 2009. Coarse and fine aerosol source apportionment in Rio de Janeiro, Brazil, Atmospheric Environment Volume 43, Issue 14, May 2009, Pages 2366-2374

Goldsmid, S., 1876, Eastern Persia: London, Macmillan and Co., 2 volumes.

Goodman, G.T., Inskip, M.J., Smith, S., Parry, G.D.R., Burton, M.A. S., 1979. The use of moss-bags in aerosol monitoring. In: Morales, C. (Ed.), Saharan Dust. Mobilization, Transport, Deposition. Wiley, New York, pp. 211–232.

Goossens, D., 2005. Quantification of the dry aeolian deposition of dust on horizontal surfaces: an experimental omparison of theory and measurements. Sedimentology 52:859–873

Goossens, D., Offer, Z.Y., 1990. A wind tunnel simulation and fieldverification of desert dust deposition (Avdat Experimental Station, Negev Desert). Sedimentology 37, 7–22.

Goossens, D., Offer, Z.Y., 1993. Eolian deposition of dust over symmetrical hills: an evaluation of wind tunnel data by means of terrain measurements. Zeitschrift für Geomorphologie 37, 103–111.

Goossens, D., Offer, Z.Y., 1994. An evaluation of the efficiency of some eolian dust collectors. Soil Technology 7 (1), 25–35.

Goudie , A.S., Day, M.J. 1980. Dinsintegration of fan sediments in Death Valley, California, by salt weathering. Phys Geogr 1:126–137

Goudie, A.S., Cooke, R.U,, Doornkamp, J,C .1979. The formulation of silt from quartz dune sand by salt weathering processes in deserts. J Arid Environ 2:105–112

Goudie, A. S., and Middleton.N.J., 2001. Saharan dust storms: nature and consequences. Earth-Science Reviews 56: 179–204.

Goudie, A.S., 1983. Dust storms in space and time. Progress in Physical Geography 7, 502-530.

Goudie, A.S., Middleton, N.J., 1992. The changing frequency of dust storms through time. Climate Change 20, 197-223.

Goudie, A.S., Middleton, N.J., 2000. Dust storms in south west Asia. Acta Universitatis Carolinae, Supplement 73-83.

Goudie, A.S., Middleton, N.J., 2006. Desert dust in the global system, Springer. 2006.

Goudie, A.S., Stokes, S., Livingstone, I., Bailiff, I.K., Allison, R.J. 1993. Post-depositional modification of the linear sand ridges of the West Kimberley area of north-west Australia. Geogr J 159:306–317

Goudie. A.S., Viles, H. 1995. The nature and pattern of debris liberation by salt weathering: a laboratory study. Earth Surf. Processes Landforms 20, 437-449

Griffin, D.W., Garrison, V.H., Herman, J.R., Shinn, E.A. 2001. African desert dust in the Caribbean atmosphere: microbiology and public health. Aerobiologia 17:203–213

Griffin, D.W., Kellogg, C. A., Garrison, V. H., Lisle, J. T., Borden, T. C., Shinn, E. A. 2003. Atmospheric microbiology in the northern Caribbean during African dust events. Aerobiologia 19, 143–157.

Gromet, L. P., Dymek, R.F., Haskin, L.A., and Korotev, R.L. 1984. The "North American shale composite": Its compilation, major and trace element characteristicsG. eochimica et CosmochimicaA cta, 48,2469- 2482

Guan, H., Esswein, R., Lopez, J., Bergstrom, R., Warnock, A., Follette-Cook, M., Fromm, M., Iraci, L., 2010. A multi-decadal history of biomass burning plume heights identified using aerosol index measurements. Atmospheric Chemistry and Physics Discussion 10, 1e25.

Gyan, K., Henry, W., Lacaille, S., Laloo, A., Lamsee-Ebanks, C., McKay, S., Antoine, R.M., Monteil, M.A. 2005. African dust clouds are associated with increased paediatric asthma accident and emergency admissions on the Caribbean island of Trinidad. Int J Biometeorol 49:371–376

Hall, D.J., Upton, S.L., 1988. A wind tunnel study of the particle collection efficiency of an inverted frisbee used as a dust collector. Atmospheric Environment 22, 1383–1394.

Hall, D.J., Waters, R.A., 1986. An improved, readily available dust gauge. Atmospheric Environment 20, 219–222.

Han, J. S., Moon, K. J., Ryu, S. Y., Kim, Y. J., & Perry, D. 2005. Source estimation of anthropogenic aerosols collected by a DRUM sampler during spring of 2002 at Gosan, Korea. Atmospheric Environment, 39, 3113–3125. doi:10.1016/j.atmosenv.2005.01.047.

Haywood, J. M., Ramaswamy, V. and Soden, B. J. 1999. Tropospheric aerosol climate forcing in clear-sky satellite observations over the oceans, Science, 283, 1299–1305,.

Haywood, J.M. and Boucher, O., 2000: Estimates of the direct and indirect radiative forcing due to tropospheric aerosols: a review. Revs. Geophys., 38, 513-543.

Haywood, J.M., Johnson, B.T., Osborne, S.R., Baran, A.J., Brooks, M., Milton, S.F., Mulcahy, J., Walters, D., Allan, R.P., Klave,r A., Formenti, P., Brindley, H.E., Christopher, S., Gupta, P. 2011. Motivation, rationale and key results from the GERBILS Saharan dust measurement campaign. Q. J. R. Meteorol. Soc. 137: 1106–1116. DOI:10.1002/qj.797

Herman, B.M., Celarier, E. 1997. Earth surface climatology at 340 nm and 380 nm from TOMS data. J. Geophys. Res. 102, 12059-12076.

Hess, A. M., Koepke, P., and Schult, I., 1998. Optical properties of aerosol and clouds: the software package OPAC, Bull. Am. Meteorol. Soc., 79, 831-844.

Hobbs, P.V. 1993. Aerosol-Cloud-Climate Interactions. San Diego, Academic Press

Hoseini, S. M., Ekhtesasi, M.R., Bazi, KH. R., 2010. Study of types and intensity of effective factors in desertification of the Sistan (Case study Natak region), Iranian journal of Geografic Space, 10(31):119-136.

Hsu, N. C., Tsay, S.-C., King, M. D., and Herman, J. R. 2004: Aerosol properties over bright-reflecting source regions, IEEE Trans. Geosci. Remote Sens., 42, 557–569,.

Hsu, N. C., Tsay, S.-C., King, M. D., and Herman, J. R. 2006: Deep Blue retrievals of Asian aerosol properties during ACE-Asia, IEEE Trans. Geosci. Remote Sens., 44, 3180–3195.

Hsu, N.C., Herman, J.R., Torres, O., Holben, B.N., Tanre, D., Eck., T.F., Smirnov, A., Chatenet, B., Lavenu, F., 1999. Comparisons of the TOMS aerosol index with sun photometer aerosol optical thickness: results and applications. J. Geophys. Res. 104, 6269-6279.

Husar, R.B., Prospero, J.M., Stowe, L.L., 1997. Characterization of tropospheric aerosols over the oceans with the NOAA advanced very high resolution radiometer optical thickness operational product. Journal of Geophysical Research 102, 16,889–16,909.

Hussain A, Mir H, Afzal M , 2005. Analysis of dust storms frequency over Pakistan during 1961–2000. Pak J Meteorol 2:49–68

Immerzeel, W.W., Droogers, P., de Jong, S. M., and Bierkens, M. F.P. 2009. Large-scale monitoring of snow cover and runoff simulation in Himalayan river basins using remote sensing, Remote 5 Sens. Environ., 113, 40–49, doi:10.1016/j.rse.2008.08.010,.

IPCC, (Intergovernmental Panel on Climate Change), 2001. Climate Change 2001: The Scientific Basis. In Contribution of Working Group I to the Third Assessment Report of the Intergovernmental Panel on Climate. J.T. Houghton et al., Eds, Cambridge Univ. Press, New York, USA.

IPCC, 2007. Climate Change 2007: Synthesis Report. Contribution of Working Groups I, II and III to the Fourth Assessment Report of the Intergovernmental Panel on Climate Change. In: Core Writing Team, Pachauri, R.K., Reisinger, A. (Eds.), Geneva, Switzerland, p. 104.

Israelevich, P.L., Levin, Z., Joseph, J.H., Ganor, E. 2002. Desert aerosol transport in the Mediterranean region as inferred from the TOMS aerosol index. J. Geophys. Res. 107, D21, doi:10.1029/2001JD002011.

Jadidoleslami, M., Rahanama Rad, J., Basirani N., 2011. The origin of Aeolian sediments in the Chahnimeh of Zabol. Appl. Geology, 7(1), 9-16.

Jalaludin, B.B., O'Toole, B.I., Leeder, S.R., 2004. Acute effects of urban ambient air pollution on respiratory symptoms, asthma medication use, and doctor visits for asthma in a cohort of Austalian children. Environmental Research, 95, 32-42.

Janssen, W. and Tetzlaff, G., 1991. Entwicklung und Eichung einer registrierenden Suspensionsfalle. Zeitschrift für Kulturtechnik und Landesentwicklung 32, 167–180.

Jones, P., Charlson, R., Rodhe, H., 1995. In: Houghton, J.T., et al. (Eds.), Aerosols in Climate Change 1994. Cambridge University Press, New York

Kahn, R. A., Gaitley, B. J., Garay, M. J., Diner, D. J., Eck, T. F., Smirnov, A., and Holben, B. N., 2010. Multiangle Imaging SpectroRadiometer global aerosol product assessment by comparison with the Aerosol Robotic Network, J. Geophys. Res., 115, D23209, doi:10.1029/2010JD014601.

Kahn, R., B. Gaitley, J. Martonchik, D. Diner, K. Crean, and B. Holben, 2005. MISR global aerosol optical depth validation based on two years of coincident AERONET observations, J. Geophys. Res., doi:10:1029/2004JD004706.

Kahn, R., Petzold, A., Wendisch, M., Bierwirth, E., Dinter, T., Esselborn, M., Fiebig, M., Heese, B., Knippertz, P., Muller, D., Schladitz, A., Von Hoyningen-Huene, W., 2009. Desert dust aerosol air mass mapping in the western Sahara, using particle properties derived from space-based multi-angle imaging. TellusB, 61, 239-251.

Kalashnikova O. V. and I. N. Sokolik , 2002. Importance of shapes and compositions of wind-blown dust particles for remote sensing at solar wavelengths, GRL, 29, N. 10, 10.1029/2002GL014947

Kalashnikova, O. V., R. Kahn, I. N. Sokolik, and W.-H. Li 2005, Ability of multiangle remote sensing observations to identify and distinguish mineral dust types: Part 1. Optical models and retrievals of optically thick plumes, J. Geophys. Res., 110, D18S14, doi:10.1029/2004JD004550

Kalashnikova, O.V., and Kahn, R.A., 2008. Mineral dust plume evolution over the Atlantic from MISR and MODIS aerosol retrievals. J. Geophys. Res., 113, D24204, doi:10.1029/2008JD010083.

Kambezidis H.D., Katevatis E.M., Petrakis M., Lykoudis S. and Asimakopoulos D.N. (1998) Estimation of the Linke and Unsworth-Monteith turbidity factors in the visible spectrum: application for Athens, Greece. Solar Energy 62 (1), 39-50.

Kandler, K., Schütz, L., Deutscher, C., Ebert, M., Hofmann, H., Jäckel, S., Jaenicke, R., Knippertz, P., Lieke, K., Massling, A., Petzold, A., Schladitz, A., Weinzierl, B., Wiedensohler, A., Zorn, S., Weinbruch, S. 2009. Size distribution, mass concentration, chemical and mineralogical composition and derived optical parameters of the boundary layer aerosol at Tinfou, Morocco, during SAMUM 2006. TellusB, 61, 32–50.

Kaskaoutis, D. G., Gautam, R., Singh, P., Houssos, E., Goto, D., Singh, S., Bartzokas, A., Kosmopoulos, P.G., Sharma, M., Hsu, N., Holben, B.N. 2012 Influence of anomalous dry conditions on aerosols over India: transport, distribution and properties J. Geophys. Res. at press (doi:10.1029/2011JD017314)

Kaskaoutis, D. G., Kambezidis, H. D.,Nastos, P. T., and Kosmopoulos, P. G., 2008. Study on an intense dust storm over Greece. Atmospheric Environment, 42, 6884-6896.

Kaskaoutis, D. G., Kharol, S. K., Sinha, P. R., Singh, R. P., Badarinath, K. V. S., Mehdi, W., and Sharma, M., 2011. Contrasting aerosol trends over South Asia during the last decade based on MODIS observations Atmos. Meas. Tech. Discuss. 4 5275–323

Kaskaoutis, D.G., Kambezidis, H.D., Badarinath, K.V.S., Kumar Kharol, S., 2010. Dust storm identification via satellite remote sensing, ISBN: 978-1-60876-906-3,

Kaskaoutis, D.G., 2008. A study on the optical properies and on the type of aerosols over various land uses, by using satellite and AERONET data, PhD Thesis, University of Ioannina, Greece 2008

Kaskaoutis, D.G., Kalapureddy, M.C.R., Krishna Moorthy, K., Devara, P.C.S., Nastos, P.T., Kosmopoulos, P.G., Kambezidis, H.D., 2010b. Heterogeneity in pre-monsoon aerosol types over the Arabian Sea deduced from shipboard measurements of spectral AODs. Atmos. Chem. Phys. 10, 4893-4908.

Kaskaoutis, D.G., Kambezidis, H.D., Badarinath, K.V.S., Kumar Kharol, S., 2010a. Dust storm identification via satellite remote sensing. In: Dust Storms: Elemental Composition, Causes and Environmental Impacts. Eds: Siniša Brstilo and Quentin Madunic, Nova Science Publishers, ISBN-13: 978-1608769063, pp. 1-59.

Kaskaoutis, D.G., Nastos, P.T., Kosmopoulos, P.G., Kambezidis, H.D., Kumar Kharol, S., Badarinath, K.V.S., 2010c. The Aura-OMI Aerosol Index distribution over Greece. Atmos. Res. 98, 28-39.

Kaufman, Y. J., D. Tanre, and O. Boucher ,.2002. A satellite view of aerosols in the climate system, Nature, 419, 215– 223.

Kaufman, Y. J., Tanre´, D. Remer, L. Vermote, E. F. Chu, A. and Holben B. N., 1997, Operational remote sensing of tropospheric aerosol over the land from EOS-MODIS, J. Geophys. Res., 102, 17,051– 17,068.

Kellogg CA, Griffin DW, Garrison VH, Peak HK, Royall N, Smith RM, Shinn EA (2004) Characterization of aerosolized bacteria and fungi from desert dust events in Mali, West Africa. Aerobiologia 20:99–110

Kendrew, W.G., 1961, The climate of the continents: New York, Oxford University Press, 5th ed., 608 p.

Kharol, S. K., Badarinath, K. V. S., Sharma, A. R., Kaskaoutis, D. G., and Kambezidis, H. D. 2011. Multiyear analysis of Terra/Aqua MODIS aerosol optical depth and ground observations over tropical urban region of Hyderabad, India, Atmos. Environ., 45, 1532–1542,.

Kidwell, C. B. and Ondov, J. M. 2001. Development and Evaluation of a Prototype System for Collecting Sub-Hourly Ambient Aerosol for Chemical Analysis. Aerosol Sci. Technol., 35: 596–6

Kim, D., Chin, M., Yu, H., Eck, T.F., Sinyuk, A., Smirnov, A., Holben, B.N., 2011. Dust optical properties over North Africa and Arabian Peninsula derived from the AERONET dataset. Atmos. Chem. Phys. Discuss. 11, 20181–20201.

Kim, S. B., Yumimoto, K., Uno, I., and Chun, Y. 2011: Dust model intercomparison between ADAM and CFORS/Dust for Asian dust case in 2007 (March 28 – April 3), SOLA, 7A, 025–028,

Kinne, S., Pueschel, R., 2001. Aerosol radiative forcing for Asian continental outflow. Atmos. Environ. 35, 5019–5028.

Kirkland, T.M., Fierer, J., (1996) Coccidioidomycosis: a reemerging infectious disease. Emerg Infect Dis 2:192–199

Kiss, P., Janosi, I. M., and Torres, O. 2007: Early calibration problems detected in TOMS Earth-Probe aerosol signal, Geophys. Res. Lett., 34, L07803, doi:10.1029/2006GL028108,.

Knippertz, P., Ansmann, A., Althausen, D., et al., 2009. Dust mobilization and transport in the northern Sahara during SAMUM 2006 - A meteorological overview. Tellus B 61, 12-31.

Kohfeld, K., E., Le Que´re´ C., Harrison, S. P., and Anderson R. F. 2005. Role of marine biology in glacial-interglacial CO2 cycles. Science 308, 74–78.

Kohfeld, K.E., Harrison, S.P. 2001. DIRTMAP: The geological record of dust. Earth-Science Reviews 54, 81-114.

Köhler, A., Fleck, U.W., 1963. Untersuchungen zur Festlegung eines Standardmessgerätes für Staubniederschlag. Inst. Meteorol. Abschlussber. No. J., vol. 84, p. 2.

Koren, I, Kaufman, Y. J., Remer, L. A., and Martins, J. V., 2004, Measurement of the effect of Amazon smoke on inhibition of cloud formation Science 303 1342–5

Koren, I., Y. J. Kaufman, R. Washington, M. C. Todd, Y. Rudich, J. V. Martins, and D. Rosenfeld 2006, The Bodele depression: a single spot in the Sahara that provides most of the mineral dust to the Amazon forest, Environmental Research Letters, 1(1).

Kosmopoulos, P.G., Kaskaoutis, D.G., Nastos, P.T., Kambezidis, H.D., 2008. Seasonal variation of columnar aerosol optical properties over Athens, Greece, based on MODIS data. Remote Sensing of Environment 112, 2354e2366.

Kreutz, K. and Sholkovitz, E. 2000. Major element, rare earth element, and sulfur isotopic composition of a high-elevation firn core: Sources and transport of mineral dust in central Asia. Geochemistry, Geophysics, Geosystems 1(11).1525-2027.

Krueger, B.J., Grassian, V.H., Cowin, J.P., Laskin, A., 2005. Heterogeneous chemistry of individual mineral dust particles fromdifferent dust source regions: the importance of particle mineralogy. Atmospheric Environment 39 (2), 395-395.

Kuenen PH (1960) Experimental abrasion 4: eolian action. J Geol 68:427–449

Kulmala M. 2003. How particles nucleate and grow. Science, 302, 1000-1001

Kulmala M., Pirjola L., and M¨akel ¨a J. M, 2000. Stable sulphate clusters as a source of new atmospheric

Kwaasi AAA, Parhar RS, Al-Mohanna FAA (1998) Aeroallergens and viable microbes in sandstorm dust – potential triggers of allergic and non-allergic respiratory ailments. Allergy 53:255–265

Kwon HJ, Cho SH, ChunY, Lagarde F, Pershagen G (2002) Effects of the Asian dust events on daily mortality in Seoul, Korea. Environ Res 90:1–5

Larissi, I.K., Antoniou, A., Nastos, P.T., Paliatsos, A.G., 2010a. The role of wind in the configuration of the ambient air quality in Athens, Greece. Fres. Environ. Bull. 19, 1989-1996.

Larissi, I.K., Koukouletsos, K.V., Moustris, K.P., Antoniou, A., Paliatsos, A.G., 2010b. PM10 concentration levels in the greater Athens area, Greece. Fresen Environ Bull. 19:226–231

Larney, F. J., Leys, J. F., Muller, J. F., & McTainsh, G. H. 1999. Dust and endosulfan deposition in cotton-growing area of Northern New South Wales, Australia. Journal of Environmental Quality, 28, 692–701.

Larssen, T., Carmichael, G.R., 2000. Acid rain and acidification in china: the importance of base cation deposition. Environmental Pollution 110 (1), 89–102.

Lashkaripour, G.R. and Soloki, H.R. (2003) Study of Dispersive Soils in Sistan Plain in the East of Iran, Proceeding of 12th Asian Regional Conference, Singapore.

Lawrence, C.R. and Neff, J.C. 2009. The contemporary physical and chemical flux of aeolian dust: A synthesis of direct measurements of dust deposition. Chemical Geology 267: 46-63.

Lawrence, M.G., Lelieveld, J., 2010. Atmospheric pollutant outflow from southern Asia: a review. Atmospheric Chemistry and Physics 10, 11017e11096

Leathers, C.R., 1981. Plant components of desert dust in Arizona and their significance

Lee, K. H., Hu, C. G. 1995.. A study on chemical composition of dustfall sampled in Cheju area: 2. Identification of source. Journal of Korean Society for Atmospheric Environment, 15, 101–111.

Legrand, M., Plana-Fattori, A., N'Doume, C. 2001. Satellite detection of dust using the IR imagery of Meteosat, 1. Infrared difference dust index. J. Geophys. Res. 106 (D16), 18251-18274.

Lemaître, C., Flamant, C., Cuesta, J., Raut, J-C., Chazette, P., Formenti, P., Pelon, J. 2010. Radiative heating rates profiles associated with a springtime case of Bodélé and Sudan dust transport over West Africa. Atmos Chem Phys 10:8131–8150. doi:10.5194/acp-10- 8131

Lenes, J. M., Darrow, B. P., Cattrall, C., Heil, C. A., Callahan, M., Vargo, G. A., Byrne, R. H., Prospero, J.M., Bates, D.E., Fanning, K.A., Walsh, J. J. 2001. Iron fertilization and the Trichodesmium response on the West Florida shelf. Limnology and Oceanography 46 (6), 1261–1277.

Léon JF, LeGrand M , 2003. Mineral dust sources in the surroundings of the North Indian Ocean. Geophys Res Lett 30:1309

Levin, Z. and Cotton, W. 2009: Aerosol Pollution impact on Precipitation: A Scientific Review. Springer, Netherlands, ISBN 140208689X.

Levin, Z., Ganor, E., Gladstein, V. 1996. The effects of desert particles coated with sulphate on rain formation in the eastern Mediterranean. J. Appl. Meteorol. 35, 1511-1523.

Levy, R. C., Remer, L. A., Kleidman, R. G., Mattoo, S., Ichoku, C., Kahn, R., and Eck, T. F. 2010. Global evaluation of the Collection 5 MODIS dark-target aerosol products over land, Atmos. Chem. Phys., 10, 10399–10420, doi:10.5194/acp-10-10399-2010,

Levy, R.C., Remer, L.A., Dubovik, O. 2007. Global aerosol optical properties and application to Moderate Resolution Imaging spectroradiometer aerosol retrieval over land. J. Geophys. Res. 112, D13210, doi:10.1029/2006JD007815

Levy, R.C., Remer, L.A., Tanre, D., Kaufman, Y.J., Ichoku, C., Holben, B., Livingston, J.,Russell, P., Mating, H. 2003. Evaluation of the MODIS retrievals of dust aerosol over the ocean during PRIDE. J. Geophys. Res. 108, doi:10.1029/2002JD002460.

Lioy, P. J., Freeman, N. C. G., & Millette, J. R. 2002. Dust: A metric for use in residential and building exposure assessment and source characterization. Environmental Health Perspectives, 110, 969–983.

Littmann, T., 1997. Atmospheric input of dust and nitrogen into the Nizzana sand dune ecosystem, north-western Negev, Israel. Journal of Arid Environments 36, 433–457.

Liu, Y., Franklin, M., Kahn, R., Koutrakis, P., 2007. Using aerosol optical thickness to predict ground-level PM concentrations in the St. Louis area: a comparison between MISR and MODIS. Remote Sensing of Environment 107, 33e44.

Liu, Z. Liu, D. Huang, J. 2008a: Airborne dust distributions over the Tibetan Plateau and surrounding areas derived from the first year of CALIPSO lidar observations. Atmos. Chem. Phys. Discuss., 8, 5957–5977.

Liu, Z. Liu, D. Huang, J. 2008b: CALIPSO lidar observations of the optical properties of Saharan dust: A case study of long-range transport. J. Geophys. Res., 113, D07207, doi:10.1029/ 2007JD008878

Lohmann, U. and Feichter, J. 2005. Global Indirect Aerosols Effects: A Review. Atmos. Chem. Phys. 5: 715–737.

Madhavan, B.L., Niranjan, K., Sreekanth, V., Sarin, M.M., Sudheer, A.K., 2008. Aerosol characterization during the summer monsoon period over a tropical coastal Indian station, Visakhapatnam. J. Geophys. Res. 113, D21208, doi:10.1029/2008JD010272.

Maghrabi, A., Alharbi, B., Tapper, N., 2011. Impact of the March 2009 dust event in Saudi Arabia on aerosol optical properties, meteorological parameters, sky temperature and emissivity. Atmos. Environ. 45, 2164-2173.

Mahowald, N., Baker, A., Bergametti, G., Brooks, N., Duce, R., Jickells, T., Kubilay, N., Prospero, J., Tegen, I., 2005. Atmospheric global dust cycle and iron inputs to the ocean. Global Biogeoch. Cycles 19, GB4025, doi: 10.1029/2004GB002402.

Manoli, E., Voutsa, D., Samara, C., 2002. Chemical characterization and source identification apportionment of fine and coarse air particles in Thessaloniki, Greece. Atmos. Environ. 36, 949–961.

Marey, H. S. , Gille, J. C. El-Askary, H. M., Shalaby E. A., and El-Raey M. E.2011, Aerosol climatology over Nile Delta based on MODIS, MISR and OMI satellite data, Atmos. Chem. Phys., 11, 10637–10648

Masmoudi M, Chaabane M, Medhioub K, Elleuch F., 2003. Variability of aerosol optical thickness and atmospheric turbidity in Tunisia. Atmos Res 66:175–188

McCauley, J.F., Grolier, M.J., and Breed, C.S., 1977, Yardangs, in Doehring, D.O., ed., Geomorphology in arid regions: Proceedings, 8th Annual Geomorphology Symposium, Binghamton, State University of New York, p. 233–269.

McConnell, C.L., Highwood, E.J., Coe, H., Formenti, P., Anderson, B., Osborne, S., Nava, S., Desboeufs, K., Chen, G., Harrison, M.A.J., 2008. Seasonal variations of the physical and optical characteristics of Saharan dust: Results from the Dust Outflow and Deposition to the Ocean (DODO) experiment. J. Geophys. Res., 113, D14S05, doi:10.1029/2007JD009606.

McKendry IG, Hacker JP, Stull R, Sakiyama S, Mignacca D, Reid K , 2001. Long-range transport of Asian dust to the Lower Fraser Valley, British Columbia, Canada. J Geophys Res 106:18361–18370

McMahon, H. 1906. Recent survey and exploration in Seistan: Journal of the Royal Geographical Society, v. 28, p. 209–228 and 333–352.

McPeters, R. D., 1996: Nimbus-7 Total Ozone Mapping Spectrometer (TOMS) data products user's guide. NASA Ref. Publ. 1384, 73 pp.

McTainsh, G.H. and Pitblado, J.R. (1987), Dust storms and related phenomena measured from meteorological records in Australia. Earth Surface Processes and Landforms 12: 415-424.

Meloni, D., di Sarra, A., di Iorio, T., and Fiocco, G. 2005: Influence of the vertical profile of Saharan dust on the visible direct radiative forcing, J. Quant. Spectrosc. Ra., 93, 347–413,

Meloni, D., di Sarra, A., Di Iorio, T., Fiocco, G. 2004. Direct radiative forcing of Saharan dust in the Mediterranean from measurements at Lampedusa Island and MISR space-borne observations. J. Geophys. Res. 109, D08206, doi:10.1029/2003JD003960.

Middleton, N. J. 1986. 'Dust storms in the Middle East', Journal of Arid Environments, 10, 83-96

Middleton, N. J., 1986. Dust storms in the Middle East. J. Arid Environ. 10, 83-96.

Miri, A., Ahmadi, H., Ghanbari, A., Moghaddamnia, A., 2007. Dust Storms Impacts on Air Pollution and Public Health under Hot and Dry Climate. Int. J. Energy and Environ. 2, 1.

Miri, A., Moghaddamnia, A., Pahlavanravi, A., Panjehkeh, N. 2010. Dust storm frequency after the 1999 drought in the Sistan region, Iran. Clim Res 41:83-90

Mishchenko M I et al 2009 Toward unified satellite climatology of aerosol properties: what do fully compatible MODIS and MISR aerosol pixels tell us? J. Quant. Spectrosc. Radiat. Transfer 110 402–8

Mishchenko, M.I., and I.V. Geogdzhayev. 2007. Satellite remote sensing reveals regional tropospheric aerosol trends. Optics Express 15:7423-7438

Mishra, S.K., Tripathi, S.N., 2008. Modeling optical properties of mineral dust over the Indian Desert. J. Geophys. Res., 113, D23201, doi:10.1029/2008JD010048.

Moghadamnia, A., Ghafari, M.B., Piri, J., Amin.S., Han. D., 2009. Evaporation estimation using artificial neural networks and adaptive neuro-fuzzy inference system techniques. Adv. Water Resources 32, 88–97.

Mohan, M., Kandya, A., 2007. An analysis of the annual and seasonal trends of Air Quality Index of Delhi. Environ. Monit. Assess. 131, 267–277.

Molesworth, A.M., Cuevas, L.E., Morse, A.P. 2002. Dust clouds and spread of infection. Lancet 359:81–82

Monteil, M.A. 2002. Dust clouds and spread of infection. Lancet 359:81

Morales, A.F. 1946. El Sahara Español. Alta Comisaria de España en Marruecos, Madrid

Mottershead, D.N, Pye, K. 1994. Tafoni on coastal slopes, South Devon, UK. Earth Surf Process Landforms 19:543–563

Mousavi, G., Nadafy, R.K., 2000. Comparative study of air quality in Tehran in 1997 and 1998, The third National Conference on Environmental Health. Kerman. 47-50(In Persian)

Muhs, D.R., Benedict, J.B., 2006. Eolian additions to late quaternary alpine soils, Indian Peaks Wilderness Area, Colorado Front Range. Arctic Antarctic and Alpine Research 38 (1), 120–130.

Myhre, G., Grini, A., Haywood, J.M., Stordal, F., Chatenet, B., Tanre, D., Sundet, J.K., Isaksen, I.S.A. 2003. Modeling the radiative impact of mineral dust during the Saharan Dust Experiment (SHADE) campaign. J. Geophys. Res. 108, D18, art. no. 8579.

Nahon D, Trompette R (1982) Origin of siltstones: glacial grinding versus weathering. Sedimentology 29:29–35

Nastos, T., Athanasios. G., Michael, B., Eleftheria, S.R., Kostas, N.P., 2010. Outdoor particulate matter and childhood asthma admissions in Athens, Greece: a time-series study. Environmental Health , 9:45, 1-9.

Nickling WG, Gillies JA (1993) Dust emission and transport in Mali, West Africa. Sedimentology 40:859–868

Nikolaou, K., Basbas, S. i Taxiltaris, C. 2004. Assessment of air pollution indicators in an urban area using the DPSIR model. Fresenius. Environmental Bulletin, 13: 820-830

Nriagu, J.O., 1988. A salient epidemic of environmental metal poisoning? Environmental Pollution 50, 139–161.

Nriagu, J.O., and Pacyna, J.M. 1988. Quantitative assessment of worldwide contamination of air, water and soils with trace metals. Nature, 333: 134–139

O'Hara S, Wiggs G, Mamedov B, Davidson G, Hubbard RB (2000) Exposure to airborne dust contaminated with pesticide in the Aral Sea region. Lancet 355:627–628

O'Leary, D.W., and Whitney, J.W., 2005a, Geological map of quadrangles 3062 and 2962, Charbuiak (609), Khannesin (610), Gawdezereh (615) and Galach (616), Afghanistan: U.S. Geological Survey Open-File Report 2005–1122A, scale 1:250,000.

O'Leary, D.W., and Whitney, J.W., 2005b, Geological map of quadrangles 3164, Lashkargah (605) and Kandahar (606), Afghanistan: U.S. Geological Survey Open-File Report 2005–1119A, scale 1:250,000.

Offer, Z.Y., Goossens, D. 2001. Airborne particle accumulation and composition at different locations in the Negev desert, Zeitschrift für Geomorphologie, 45 (2001), pp. 101–120

Ohmura, A. (2009), Observed decadal variations in surface solar radiation and their causes, J. Geophys. Res., 114, D00D05, doi:10.1029/ 2008JD011290.

Orange, D., Gac, J.-Y., Probst, J.-L., Tanre, D., 1990. Mesure du depot au sol des aérosols désertiques. Une méthode simple de prélèvement: le capteur pyramidal. Comptes Rendus de l'Académie des Sciences Paris 311, 167–172.

Ozer, P., 2001. Les lithometeores en region sahelienne. International Journal of Tropical Ecology and Geography 24, 1–317.

Ozer, P., Bechir, M., Laghdaf, O.M., Gassani, J., 2006. Estimation of air quality degradation due to Saharan dust at Nouakchott, Mauritania, from horizontal visibility data. Water Air Soil Pollut, 178:79–87

Paliatsos, A.G., Priftis, K.N., Ziomas, I.C., Panagiotopoulou-Gartagani, P., Nikolaou-Panagiotou, A., Tapratzi-Potamianou, P., Zachariadi-Xypolita, A., Nicolaidou, P., Saxoni-Papageorgiou, P: Association between ambient air pollution and childhood asthma in Athens, Greece. Fresen Environ Bull 2006 , 15:614-618

Pandithurai, G., R.T. Pinker, P.C.S., Devara, T., Takamura, K.K., 2007. Seasonal asymmetry in diurnal variation of aerosol optical characteristics over Pune, western India. J. Geophys. Res., 112, D08208, doi:10.1029/2006JD007803.

Partow, Hassan, 2003, Sistan oasis parched by droughts, in Atlas of global change: United Nations Environmental Programme, Oxford University Press, p. 144–145.

Patadia, F., Yang, E.-S., Christopher, S.A., 2009. Does dust change the clear sky top of atmosphere shortwave flux over high surface reflectance regions? Geophys. Res. Lett., 36, L15825, doi:10.1029/2009GL039092.

Pathak, B., G. Kalita, K.., Bhuyan, P.K., Bhuyan, K., 2010. Aerosol temporal characteristics and its impact on shortwave radiative forcing at a location in the northeast of India. J. Geophys. Res., 115, D19204, doi: 10.1029/2009JD013462.

Pauley PM, Baker NL, Barker EH (1996) An observational study of the “Interstate 5” dust storm case. Bull Am Meteorol Soc 77:693–720

Penner, J. E., M. Andreae, H. Annegarn, L. Barrie, J. Feichter, D. Hegg, A. Jayaraman, R. Leaitch, D. Murphy, J. Nganga and G. Pitari (2001). Aerosols, Their Direct and Indirect Effects. Climate Change 2001: The Scientific Basis. Contribution of Working Group I to the Third Assessment Report of the Intergovernmental Panel on Climate Change. C. A. Johnson. Cambridge, New York, Cambridge University Press: 289-348.

Pérez, N., Pey, J., Querol, X., Alastuey, A., López, J. M., Viana, M., 2008. Partitioning of major and trace components in PM10–PM2.5–PM1 at an urban site in . Southern Europe. Atmospheric Environment, 42, 1677– 1691

Piechota, T., van, J., Batista, J., Stave, K., James, D., 2002. Potential Environmental Impacts of Dust Suppressants: “Avoiding Another Times Beach”. An Expert Panel Summary. U.S. EPA and University of Nevada, Las Vegas

Pope, C. A., 2000. Epidemiology of fine particulate air pollution and human health: Biologic mechanisms and who's at risk?, Environmental Health Perspectives, 108, 713-723.

Pozzi, R., B.D. Berardis, B.D., Paoletti, L., Guastadisegni, C., 2005. Winter urban air particles from Rome (Italy): effects on the monocytic–macrophagic RAW264.7 cell line, Environ. Res. 99: 344–354.

Prados, A.I, Leptoukh, G., Johnson, J., Rui, H., Lynnes, C., Chen, A., Husar, R.B. 2010. Access, visualization, and interoperability of air quality remote sensing data sets via the Giovanni online tool. IEEE J Selected Topics in Earth Observations and Remote Sensing.

Prasad, A. K. Singh, R. P. Kafatos, M. 2006, Influence of coal based thermal power plants on aerosol optical properties in the Indo-Gangetic basin, Geophysical Research Letters, 33(5).

Prasad, A.K., Singh, S., Chauhan, S.S., Srivastava, M.K., Singh, R.P., Singh, R., 2007. Aerosol radiative forcing over the Indo-Gangetic Plains during major dust storms. Atmos. Environ. 41, 6289-6301.

Prasad, A.K., Yang, K.-H.S., El-Askary, H.M., Kafatos, M., 2009. Melting of major glaciers in the western Himalayas: evidence of climatic changes from long term MSU derived tropospheric temperature trend (1979-2008). Ann. Geophys. 27, 4505-4519.

Prospero, J. M. 1999. Long term measurements of the transport of African mineral dust to the south-eastern United States: Implications for regional air quality. Journal Geophysical Research, 104, 15917–15927.

Prospero, J.M. 2004. Interhemispheric transport of viable fungi and bacteria from Africa to the Caribbean with soil dust. In: Werner D (ed) Biological resources and their migration. Springer, Berlin Heidelberg New York, pp. 127–132

Prospero, J.M., Ginoux, P., Torres, O., Nicholson, S.E., Gill, T.E., 2002. Environmental characterization of global sources of atmospheric soil dust identified with the Nimbus 7 total ozone mapping spectrometer absorbing aerosol product. Reviews of Geophys. 40, 2–31.

Psenner, R. 1999. Living in a dusty world: airborne dust as a key factor for alpine lakes. Water, Air and Soil Pollution 112, 217-227.

Pye, K., Sperling, C.H.B. 1983. Experimental investigation of silt formation by static breakage processes: the effect of temperature, moisture and salt on quartz dune sand and granitic regolith. Sedimentology 30:49–62

Pye, K. 1987. Aeolian dust and dust deposits. Academic Press, London

Pye, K., 1992. Aeolian dust transport and deposition over Crete and adjacent parts of the Mediterranean Sea. Earth Surface Processes and Landforms 17, 271–288.

Querol, X., Alastuey, A., Rodriguez, S., Viana, M. M., Artinano, B., Salvador, P., Mantilla, E., Garcia do Santos, S., Fernandez Patier, R., Rosa, J. de la, Sanchez de la Campa, A., Menendez, M., Gil, J. J (2004) Levels of particulate matter in rural, urban and industrial sites in Spain. Sci Total Environ 334/335:359–376

Quijano, A., Sokolik, I.N., Toon, O.B. 2000. Radiative heating rates and direct radiative forcing by mineral dust in cloudy atmospheric conditions. J. Geophys. Res. 105, 12207-12219.

Rahn KA, Borys RA, Shaw GE .1977. The Asian source of Arctic haze bands. Nature 268:712–714

Raloff, J. 2001. Ill winds. Sci News 160:218–220

Ralph, M.O., Barrett, C.F., 1976. Awind-tunnel study of the efficiencyof deposit gauges—interim report. Report LR 235 (AP). Warren Spring Laboratory, Stevenage, UK.

Ramachandran, S., Kedia, S., 2010. Black carbon aerosols over an urban region: Radiative forcing and climate impact. J. Geophys. Res., 115, D10202, doi:10.1029/2009JD013560.

Ramachandran, S., Rajesh, T.A., 2007. Black carbon aerosol mass concentrations over Ahmedabad, an urban location in western India: Comparison with urban sites in Asia, Europe, Canada and USA. J. Geophys. Res., 112, D06211, doi:10.1029/2006JD007488.

Ramanathan, V., Crutzen, P. J., Kiehl, J. T., and Rosenfeld, D., 2001, Aerosols climate and the hydrological cycle Science 294 2119–24

Ramanathan, V., Ramana, M. V., Roberts, G., Kim, D., Corriganm, C., Chung, C., andWinker, D. 2007. Warming trends in Asia amplified by brown cloud solar absorption, Nature, 448, 575–578,.

Ranjbar, M., and Iranmanesh, F. 2008. Effects of "Drought" on "Wind Eroding and Erosion" in Sistan Region with use of Satellite Multiple Images. WSEAS, ISSN: 1792-4294.

Rashki, A., Kaskaoutis, D.G., Rautenbach, C.J.deW., Eriksson, P.G.,Giang, M, Gupta, P., 2012. Dust storms and their horizontal dust loading in the Sistan region, Iran. Aeolian Research, vol 5, p 51-62

Rashki, A., Rautenbach, C.J.deW., Eriksson, P.G., Kaskaoutis, D.G., Gupta, P., 2011. Temporal changes of particulate concentration in the ambient air over the city of Zahedan, Iran. Air Quality, Atmosphere & Health. DOI: 10.1007/s11869-011-0152-5

Rea, D.K. 1994. The paleoclimatic record provided by Eolian deposition in the deep sea: The geologic history of wind. Reviews of Geophysics 32, 159-195.

Reheis, M.C., Kihl, R., 1995. Dust deposition in southern Nevada and California, 1984–1989—relations to climate, source area, and source lithology. Journal of Geophysical Research-Atmospheres 100 (D5), 8893–8918.

Remer, L.A. , et al. 2005. The MODIS aerosol algorithm, products, and validation. J. Atmos. Sci. 62, 947-973.

Remer, L.A., Tanre, D., Kaufman, Y.J., Ichoku, C., Matoo, S., Levy, R., Chu, D.A., Holben, B., Dubovik, O., Ahmad, Z., Smirnov, A., Martins, J.V., Li, R.R. 2002. Validation of MODIS aerosol retrieval over ocean. Geophys. Res. Lett. 29, doi:10.1029/2001GL013204.

Rietveld H.M. 1969. A profile refinement method for nuclear and magnetic structures. J. ppl. Crystallogr.2:65–71.

Rodriguez, S., Querol, X., Alastuey, A., Kallos, G., Kakaliagou, O. 2001. Saharan dust contributions to PM_{10} and TSP levels in Southern and Eastern Spain. Atmos. Environ. 35, 2433-2447.

Rosenfeld, D., Lohmann, U., Raga, G. B., O'Dowd, C. D., Kulmala, M., Fuzzi, S., Reissell, A., Andreae, M. O., 2008. Flood or Drought: How do aerosols affect precipitation?. Science, 321, 1309, DOI: 10.1126/science.1160606.

Rosenfeld, D., Rudich, Y., and Lahav, R.: Desert dust suppressing precipitation: A possible desertification feedback loop, P. Natl. Acad. Sci. USA, 98, 5975–5980, 2001.

Rutherford S, Clark E, McTainsh GH, Simpson R, Mitchell C (1999) Characteristics of rural dust events shown to impact on asthma severity in Brisbane, Australia. Int J Biometeorol 42:217–225

Samoli, E., Kougea, E., Kassomenos, P., Analitis, A., Katsouyanni, K., 2011. Does the presence of desert dust modify the effect of PM10 on mortality in Athens, Greece? Sci. Total Environ. 409, 2049-2054.

Satheesh, S.K., Krishna Moorthy, K. 2005. Radiative effects of natural aerosols: A review. Atmos. Environ. 35, 2089-2110.

Satheesh, S.K., Moorthy, K.K., Kaufman, Y.J., Takemura, T., 2006. Aerosol optical depth, physical properties and radiative forcing over the Arabian Sea. Meteorol. Atmos. Phys. 91, 45–62.

Scheff, P.A., Wadden, R.A., Ticho, K.K.L., Nakonechniy, J.J., Prodanchuk. M., and Hryhorczuk, D.O., 1997, Toxic air pollutants in chernivtsi, Ukraine. Environmental International, 23 3, 273–290,

Schütz, L., Sebert,M., 1987, Mineral aerosols and source identification, Journal of Aerosol Science, 18 (1) , pp. 1–10

Schwartz J. 2004. Air pollution and children's health. Pediatrics 113:1037-1043.

Selinus, O., Finkelman, R.B., Centeno, J.A, 2010, Medical Geology: A regional synthesis, springer. pp: 391

Shao, Y. 2001. A model for mineral dust emission. J Geophys Res 106: 20,239–20,254

Shao, Y. 2010. Physics and modelling of wind erosion, springer

Shao, Y., Li, A. 1999. Numerical modelling of saltation in atmospheric surface layer. Boundary-Layer Meteorol 91: 199–225

Shao, Y., McTainsh, G.H., Leys, J.F., Raupach, M.R. 1993. Efficiency of sediment samplers for wind erosion measurement. Aust J Soil Res 31: 519–532

Sharma, A. R., Kharol, S. K., Badarinath, K. V. S., and Singh, D. 2010: Impact of agriculture crop residue burning on atmospheric aerosol loading – a study over Punjab State, India, Ann. Geophysicae, 28, 367–379,.

Shaw, G. E. 1980. Transport of Asian desert aerosol to the Hawaiian Islands. Journal of Applied Meteorology, 19, 1254–1259.

Shinn, E. A., Smith, G. W., Prospero, J. M., Betzer, P., Hayes, M. L., Garrison, V., Barber, R.T. 2000. African dust and the demise of Caribbean coral reefs. Geophys. Res. Lett. 27 (19), 3029–3032.

Singh, R.P., Prasad, A.K., Kayetha, V.K., Kafatos, M., 2008. Enhancement of oceanic parameters associated with dust storms using satellite data. J. Geophys. Res., 113, C11008, doi:10.1029/2008JC004815.

Singh, R.P., S. Dey, S.N. Tripathi, V. Tare, B. Holben 2004. Variability of aerosol parameters over Kanpur, northern India. J. Geophys. Res., 109, D23206, doi:10.1029/2004JD004966.

Sinyuk, A., Torres, O., Dubovik, O. 2003. Combined use of satellite and surface observations to infer the imaginary part of the refractive index of Saharan dust. Geophys. Res. Lett. 30, 201081, doi:10.1029/2002GL016189

Sivagangabalan, G., Spears, D., Masse, S., Urch, B., Brook, R.D., Silverman, F., Gold, D.R., Lukic, K.Z., , Speck, M., Kusha, M., Farid, T., Poku, K., Shi, E., Floras, J., Nanthakumar, K., 2010. Mechanisms of Increased Arrhythmic Risk Associated With Exposure to Urban Air Pollution. Circulation, 122, A17901

Sivall, T.R., 1977, Synoptic-climatological study of the Asian summer monsoon in Afghanistan: Geografiska Annaler, v. 59, p. 67–87.

Skärby, L., 1977. Correlation of moss analysis to direct measurement by deposit gauge of cadmium, lead, and copper. Swedish Water and Air Pollution Research Laboratory, Publ. B377a.

Smalley IJ (1966) The properties of glacial loess and the formation of loess deposits. J Sediment Petrol 36:669–676

Smalley IJ, Vita-Finzi C (1968) The formation of fine particles in sandy deserts and the nature of 'desert' loess. J Sediment Petrol 38:766–774

Smalley, I.J., Kumar, R., O'Hara Dhand, K., Jefferson, I.E., Evans, R.D., 2005. The formation of silt material for terrestrial sediments: particularly loess and dust. Sediment Geol 179:321–328

Smirnov, A., Holben, B.N., Dubovic, O., O'Neill, N.T., Eck, T.F., Westphal, D.L., Goroth, A.K., Pietras, C., Slutsker, I., 2002. Atmospheric aerosol optical properties in the Persian Gulf. J. Atmos. Sci. 59, 620-634.

Smith, B.J., McGreevy, J.P., Whalley, W.B. 1987. The production of silt-size quartz by experimental salt weathering of a sandstone. J Arid Environ 12:199–214

Smith, B.J., Wright, J,S,, Whalley, W.B. 2002. Sources of non-glacial, loess-size quartz silt and the origins of "desert loess". Earth Sci Rev 59:1–26

Sokolik I., Winker D., Bergametti G., Gillette D., Carmichael G., Kaufman Y., Gomes L., Schuetz L., and Penner J. 2001. Introduction to special section: outstanding problems in quantifying the radiative impacts of mineral dust.

Sokolik, I. N., Toon, O. B., 1999. Incorporation of mineralogical composition into models of the radiative properties of mineral aerosol from UV to IR wavelengths. J. Geophys. Res., 104(D8), 9423-9444.

Sokolik, I.N., Toon, O.B., Bergstrom, R.W., 1998. Modeling the radiative characteristics of airborne mineral aerosols at infraredwavelengths. Journal of Geophysical Research- Atmospheres 103 (D8), 8813–8826

Sturges, W.T., Harrison, R.M. , Barrie L.A., 1989. Semi-quantitative XRD analysis of size fractionated atmospheric particles, Atmospheric Environment, 23 , 1083–1098

Sultan, B., Labadi, K., Guegan, J.F., Janicot, S. 2005. Climate drives the meningitis epidemics onset in West Africa. Plos Medicine 2, 43-49.

Sun, J., M. Zhang, and T. Liu, 2001: Spatial and temporal characteristics of dust storms in China and its surrounding regions, 1960–1999: Relations to source area and climate. J. Geophys. Res., 106, 10 325–10 333

Sun, Y., Zhuang, G., Yun, H., Zhang, X., Guo, J., 2004. Characteristics and sources of 2002 super dust storm in. Beijing. China Science Bulletin 49, 698–705

Ta, W., Wang, T., Xiao, H., Zhu, X., Xiao, Z. 2004. Gaseous and particulate air pollution in the Lanzhou Valley, China. Sci Total Environ 320:163–176

Takahashi, Koichiro, and Arakawa, H., ed., 1981, Climates of southern and western Asia: Elsevier Publishing Company (World Survey of Climatology, v. 9), 333 p.

Talbot M.R. and Allen P.A. 1996. Lakes. in Sedimentary Environments: Reading H.G. (ed), Processes, Facies and Stratigraphy, Blackwell: Oxford, 83–124.

Tanaka TY, Kurosaki Y, Chiba M, Matsumura T, Nagai T, Yamazaki A, Uchiyama A, Tsunematsu N, Kai K (2005) Possible transcontinental dust transport from North Africa and the Middle East to East Asia. Atmos Environ 39:3901–3909.

Tanre´, D., Kaufman, Y. J., Herman, M., and Mattoo, S. 1997. Remote sensing of aerosol properties over oceans using the MODIS/EOS spectral radiances., J. Geophys. Res., 102, 16,971– 16,988.

Tate, G.P., 1910–12, Seistan, A memoir on the topography, ruins, and people: Calcutta, Superintendent of Printing, 4 volumes, 374 p.

Tegen, I., Fung, I., 1994. Modeling of mineral dust in the atmosphere: sources, transport, and optical thickness. J. Geophys. Res. 99, 22897–22914.

Tegen, I., Lacis, A.A., Fung, I., 1996. The influence on climate forcing of mineral aerosols from disturbed soils. Nature, 380, 419-422.

Thurston, G.D., Spengler, J.D., 1985, A quantitative assessment of source contributions to inhalable particulate matter pollution in metropolitan Boston. Atmospheric Environment, 19, 9–25.

Tirrul, R., Bell, I. R., Griftis, R. J., Camp, V. E., 1983. The Sistan suture zone of eastern Iran. Bull. of Geological Soc. of America, 94, 134-150.

Torres, O., Bhartia, P.K., Herman, J.R., Ahmad, Z., Gleason, J. 1998. Derivation of aerosol properties from satellite measurements of backscattered ultraviolet radiation: Theoretical basis. J. Geophys. Res. 103, 17099–17110.

Torres, O., Bhartia, P.K., Herman, J.R., Sinyuk, A., Ginoux, P., Holben, B. 2002. A long-term record of aerosol optical depth from TOMS observations and comparison to AERONET measurements. J. Atmos. Sci. 59: 398-413

Tosi, M., 1973, L'industria litica e italiana, lavorazione degli element, di collana a Shahr-i-Sokhta (Iran): Geo-Archeologia, v. 1, p. 23–29.

Tosi, M., 1976, A topographical and stratigraphical periplus of Sahr-e Suxteh, in Bagherzadeh, F., ed.: Proceedings of the 4th Annual Symposium an Archeological Research in Iran, 3−8 November, Tehran, 1975, p. 130–158.

Triantafyllou, A.G., Evagelopoulos, V., Zoras, S., 2006. Design of a web-based information system for ambient environmental data. Journal of Environmental Management, 80, 230-236.

Twomey, S.A. 1959. The Nuclei of Natural Cloud Formation. Part II: The Supersaturation in Natural Clouds and the Variation of Cloud Droplet Concentrations. Geofis. Pure Appl. 43, 227-242.

U.S. Agency for International Development, 1976, Helmand River Basin—Soil and water survey study report: Open File Report in Kabul, 180 p.

United Nations Environment Programme (UNEP). 2006. History of Environmental Change in the Sistan Basin Based on Satellite Image Analysis:1976 – 2005. P: 60

USEPA, 2006.Guideline for Reporting of Daily Air Quality: Air Quality Index, Environmental Protection Agency, Washington, DC. P. 17.

Usher, C.R., Michel, A.E., VH Grassian, V.H. 2003. Reactions on mineral dust, Chemical Review, 103 (12) , 4883–4940

Wang, J., Christopher, S.A., 2003. Intercomparison between satellite-derived aerosol optical thickness and PM2.5 mass: implications for air quality studies.Geophysical Research Letters 30. doi:10.1029/2003GL018174.

Wang, Y., Guoshun, Z., Xingying, Z., Kan, H., Chang, X., Aohan, Jianmin, C. and Zhisheng, A. 2006. The Ion Chemistry, Seasonal Cycle, and Sources of PM2.5 and TSP Aerosol in Shanghai. Atmos. Environ. 40: 2935– 2952

Wang, Y., Zhuang, G., Tang, A., Zhang, W., Sun, Y., Wang, Z., et al. 2007. The evolution of chemical components of aerosols at five monitoring sites of China during dust storms. Atmospheric Environment, 41, 1091–1106. doi:10. 1016/j.atmosenv.2006.09.015.

Washington, R., Todd, M.C., Middleton, N.J., Goudie, A.S., 2003. Dust-storm source areas determined by the total ozone monitoring spectrometer and surface observations. Annals of the Association of American Geographers 93, 297-313.

Wedepohl, K.H., 1971. Environmental influences on the chemical composition of shales and clays. In: Ahrens, L.H., Press, F., Runcorn, S.K., Urey, H.C. (Eds.), Physics and Chemistry of the Earth. Pergamon, Oxford, UK, pp. 307–331

Wedepohl, K.H., 1971. Environmental influences on the chemical composition of shales and clays. In: Ahrens, L.H., Press, F., Runcorn, S.K., Urey, H.C. (Eds.), Physics and Chemistry of the Earth. Pergamon, Oxford, UK, pp. 307–331

Wentworth CK (1922)A scale of grade and class terms for clastic sediments. J Geol 30:377–392

Whitney, J. W., 2006. Geology, Water, and Wind in the Lower Helmand Basin, Southern Afghanistan U.S. Geological Survey, Reston, Virginia, Retrieved 2010-08-31

Whitney, J.W., and Trousdale, W., 1982, Catastrophic floods, wind erosion, and historical occupation on the Helmand River delta, southwest Afghanistan: American Quaternary Association, 7th biennial conference, June 28–30, Seattle, Wash., p. 180.

Whitney, J.W., and Trousdale, W., 1984, Man versus sand in southwest Afghanistan: Geological Society of America Abstracts with Programs, v. 16, no. 7, p. 693.

WHO, 2003. Health aspects of air pollution with particulate matter, ozone and nitrogen dioxide. World Health Organization, 98 pp

Wild, M. 2012. enlightening global dimming and brightening. bull. american meteor. soc. doi:10.1175/bams-d-11-00074.1, pp. 27-37

Williams P, Young M (1999) Costing dust. (CSIRO Land and Water, Policy and Economic Research Unit, Final Report). CSIRO, Canberra, 36 pp

Wilson, A. M., Salloway, J. C., Wake, C. P., Kelly, T., 2004. Air pollution and demand for hospital services: A review. Environ. Int., 30, 1109-1018

Wilson, W.E., Chow, J.C. Claiborn, C. Fusheng, W. Engelbrecht, J. and Watson, J.G., 2002, Monitoring of particulate matter outdoors. Chemosphere, 49, 1009–1043

Wittekindt, Hans, and Weippert, D., compilers, 1973, Geologische Karte von Zentral-und Sudafghanistan: Hannover, Bundesanstalt fur Bodenforschung, 4 sheets, scale 1:500,000

Wood, W. W., & Sanford, W. E. 1995. Eolian transport, saline lake basins and groundwater solutes. Water Resources Research, 31, 3121–3129.

Wright, J. 2002. Granitoid weathering profiles as a source of loessic silt. Trans Jpn Geomorphol Union 23/25:769–793

Wright, J. 2001a. Making loess-sized silt: data from laboratory simulations and implications for sediment transport pathways and the formation of 'desert' loess deposits associated with the Sahara. Quat Int 76/77:7–19

Wright, J. 2001b. "Desert" loess versus "glacial" loess: quartz silt formation, source areas and sediment pathways in the formation of loess deposits. Geomorphology 36:231–256

Wu, P.C., Tsai, J.C., Li, F.C., Lung, S.C., Su, H.J. (2004) Increased levels of ambient fungal spores in Taiwan are associated with dust events from China. Atmos Environ 38:4879–4886

Xi, X., and Sokolik, I.N. 2012. Impact of Asian dust aerosol and surface albedo on photosynthetically active radiation and surface radiative balance in dryland ecosystems. Advances in Meteorology, (in press)

Yang, C.Y., Chen, Y.S, Chiu, H.F., Goggins, W.B, 2005. Effects of Asian dust storm events on daily stroke admissions in Taipei, Taiwan. Environ Res 99:79–84

Yang, G., Xiao, H., Tuo, W. 2001. Black windstorms in northwest China: a case study of thre strong sand-dust storm of May 5th 1993. In: Yang Y, Squires V, Qi L (eds) Global alarm: dust and sandstorms in the world's drylands. UNESCO, Bangkok, pp. 49–73

Yang, X.P., Zhu, B.Q., White, P.D. 2007, Provenance of aeolian sediment in the Taklamakan Desert of western China, inferred from REE and major-elemental data. Quaternary International 175, 71–85.

Yoon, J., von Hoyningen-Huene, W., Vountas, M., and Burrows, J. P. 2011. Analysis of linear longterm trend of Aerosol Optical Thickness derived from SeaWiFS using BAER over Europe and South China, Atmos. Chem. Phys. Discuss., 11, 20757–20792, doi:10.5194/acpd-11- 20757-2011,.

Yung, Y.L., Lee, T., Wang, C.-H., Shieh, Y.-T. 1996. Dust: A diagnostic of the hydrologic cycle during the Last Glacial Maximum, Science, 271, 962–963,

Zarasvandi, A., 2009, Environmental impacts of dust storms in the Khuzestan province, Environmental Protection Agency (EPA) of Khuzestan province, Internal Report, 375p

Zawar-Reza P, Kingham S, Pearce J. Evaluation of a year-long dispersion modelling of PM_{10} using the mesoscale model TAPM for Christchurch. New Zealand Sci Total Environ 2006,349: 249–59.

Zender, C.S., Miller, R.L., Tegen, I., 2004. Quantifying mineral dust mass budgets: terminology, constraints, and current estimates. EOS, Transactions, American Geophysical Union 85 (48), 509–512.

Zhang J., J. Reid, D. Westphal, E. Hyer, N. Baker, J. Campbell,. 2010. multi-sensor aerosol data assimilation, Aerosol Observability Workship, Monterey, CA, April, 2010

Zhang, D. D., Peart, M., Jim, C. Y., He, Y. Q., Li, B. S., & Chen, J. A. 2003. Precipitation chemistry of Lhasa and other remote towns, Tibet. Atmospheric Environment, 37, 231–240.

Zhang, D.E., 1985. Meteorological characteristics of dust fall in China since the historic times. In: Liu, T.S. (Ed.), Quaternary Geology and Environment of China. China Ocean Press, Beijing, pp. 45–56

Zhao, X., Zhuang, G., Wang, Z., Sun, Y., Wang, Y., Yuan, H., 2007. Variation of sources and mixing mechanism of mineral dust with pollution aerosol in a super dust storm —revealed by the two peaks of a super dust storm in Beijing, Atmospheric Research 84, 265-279